University of Massachusetts Amherst

Ion Mobility Studies of Functional Polymeric Materials for Fuel Cells and Lithium Ion Batteries

Item Type	dissertation
Authors	Sanghi, Shilpi
DOI	10.7275/2396255
Download date	2024-11-29 09:15:26
Link to Item	https://hdl.handle.net/20.500.14394/38919

ION MOBILITY STUDIES OF FUNCTIONAL POLYMERIC MATERIALS FOR FUEL CELLS AND LITHIUM ION BATTERIES

A Dissertation Presented

by

SHILPI SANGHI

Submitted to the Graduate School of the
University of Massachusetts Amherst in partial fulfillment
of the requirements for the degree of

DOCTOR OF PHILOSOPHY

SEPTEMBER 2011

Polymer Science and Engineering

© Copyright by Shilpi Sanghi, 2011

All Rights Reserved

ION MOBILITY STUDIES OF FUNCTIONAL POLYMERIC MATERIALS FOR FUEL CELLS AND LITHIUM ION BATTERIES

A Dissertation Presented

by

SHILPI SANGHI

Approved as to style and content by:

_____
E. Bryan Coughlin, Chair

_____
Ryan C. Hayward, Member

_____
Mark T. Tuominen, Member

_____
David A. Hoagland, Department Head
Polymer Science and Engineering

DEDICATION

To my beloved family

ACKNOWLEDGMENTS

I express my gratitude to my advisor Prof. E. Bryan Coughlin for his unwavering support and guidance, countless discussions, and above all, being my mentor. He has helped me, more than he knows, to learn how to be successful both in academia and in life. Thanks to Prof. Mark Tuominen for providing thoughtful suggestions in designing conductivity experiments and interpreting the impedance spectroscopy data. I would like to acknowledge Prof. Ryan Hayward for serving on my committee and providing constructive criticism during defenses.

I would like to thank Craig Versek and Michael Thorn for all their efforts in developing customized instrumentation for conductivity measurements and helping to interpret the impedance data. Thanks to Birgit Fassbender for her collaboration on solid state NMR experiments. It was a privilege to work with two undergraduate students: Erik Willett and Mike Tylenski. Mike cheered up the office with his curiosity about science, graduate school and Amherst. I appreciate the help of Chelsea Davis and Dr. Sekar Dhanasekaran with nanoindentation. I acknowledge Jimmy Lawrence and Prof. Alejandro Briseno for their valuable suggestions on cyclic voltammetry. I would like to thank Dr. Stephen Eyles for performing mass spectroscopy experiments. I would also like to thank Dr. Weiguo Hu for doing solid state NMR experiments and for helping me as a NMR teaching assistant and NMR czar. I appreciate the helpful discussions with Ian Henderson and Prof. Alejandro Briseno for ORP.

I thank all past and present members of Coughlin group. Sergio taught me the lab techniques and helped me to get started with the fuel cell project. Gunjan and Ying have been awesome friends and mentors throughout the graduate career. I also want to thank Yoan for teaching me scientific writing and improving my presentation skills. Special thanks to Liz for proof reading my writings. Tsung Han has been a great pal to work with on fuel cell project. It has been fun being around Katherine, Mufide, Chris, Sahas, WenXu and Brian.

I cherish the good times that I had with all my friends in Amherst and I would like to thank all of them. I am lucky to have a friend like Naveen who has always been there to help me, ensuring a smooth journey through graduate school.

I would like to express my gratitude to my family. My parents, my brother, Varun, and my fiancé, Atri, have always been there for me. I would not have been here, writing this thesis without the love, support and motivation of my parents.

ABSTRACT

ION MOBILITY STUDIES OF FUNCTIONAL POLYMERIC MATERIALS FOR FUEL CELLS AND LITHIUM ION BATTERIES

SEPTEMBER 2011

SHILPI SANGHI

B.Tech., INSTITUTE OF CHEMICAL TECHNOLOGY (Formerly UDCT), INDIA

M.S., UNIVERSITY OF MASSACHUSETTS AMHERST

Ph.D., UNIVERSITY OF MASSACHUSETTS AMHERST

Directed by: Professor E. Bryan Coughlin

The research presented in this thesis focuses on developing new functional polymeric materials that can conduct ions, H^+, or OH^- or Li^+. The motivation behind this work was to understand the similarities and/or differences in the structure property relationships between polymer membranes and the conductivity of H^+ and OH^- ions, and between polymer membranes and the anhydrous conductivity of H^+ and Li^+ ions. This understanding is critical to developing durable polymer membranes with high H^+, OH^- and Li^+ ion conductivity for proton exchange membrane fuel cells (PEMFCs), alkaline anion exchange membrane fuel cells (AAEMFCs) and lithium ion batteries respectively. Chapter 1 describes the basic functioning of PEMFCs, AAEMFCs and lithium ion batteries, the challenges associated with each research topic, and the fundamental mechanisms of ion transport.

The proton conducting properties of poly(4-vinyl-1*H*-1,2,3-triazole) were investigated on a macroscopic scale by impedance spectroscopy and microscopic scale by solid state MAS NMR. It was found that proton conductivity is independent of molecular weight of the polymer, but influenced by orders of magnitude by the presence of residual dimethylformamide. To improve the mechanical properties of otherwise liquid-like 1*H*-1,2,3-triazole functionalized polysiloxane homopolymers, hybrid inorganic-organic proton exchange membranes (PEMs) containing 1*H*-

1,2,3-triazole grafted alkoxy silanes were synthesized, using sol-gel chemistry. This method enabled self-supporting membranes having proton conductivity comparable to uncrosslinked homopolymers.

One of the biggest challenges with AEMs for use in AAEMFCs is finding a cationic polyelectrolyte that is chemically stable at elevated temperatures in high pH environment. Novel triazolium ionic salts were developed, having greater chemical stability under alkaline conditions compared to existing imidazolium ionic salts. However, the chemical stability of triazolium cations was not sufficient for AAEMFC applications. Excellent chemical stability of $(C_5H_5)_2Co^+$ in 2 M NaOH at 80 °C over 30 days was demonstrated and polymerizable vinyl functionalized cobaltocenium monomers were synthesized. This work paves the way for future development of AEMs containing cobaltocenium moieties to facilitate hydroxide ion transport.

Polymers containing covalently attached cyclic carbonates were synthesized and doped with lithium triflate and their lithium ion conductivities were investigated. The findings highlight the importance of high charge carrier density and flexibility of the polymer matrix to achieve high lithium ion conductivity. These results are similar to the key factors influencing anhydrous proton transport.

TABLE OF CONTENTS

Page

ACKNOWLEDGMENTS v

ABSTRACT vii

LIST OF TABLES xiv

LIST OF FIGURES xv

LIST OF SCHEMES xix

LIST OF ABBREVIATIONS xx

CHAPTER

1. INTRODUCTION 1

1.1 Motivation 2
1.2 Background 4

1.2.1 PEMFCs 4

1.2.1.1 Proton transport mechanism 5
1.2.1.2 Hydrated PEMFCs 6
1.2.1.3 Anhydrous PEMFCs 8

1.2.2 AAEMFCs 9
1.2.3 Lithium ion batteries 13

1.3 Objectives 15

1.3.1 Proton and hydroxide ion mobility 16
1.3.2 Proton and lithium ion mobility 17

1.4 Outline of the dissertation 18
1.5 References 19

2. PROTON CONDUCTIVITY OF POLY(4-VINYL-1*H*-1,2,3-TRIAZOLE) 25

2.1 Introduction 25
2.2 Experimental 26

2.2.1 Materials 26
2.2.2 Instrumentation 26

2.3 Poly(4-vinyl-1*H*-1,2,3-trizole) 27

2.3.1 Synthesis 27

2.3.1.1 Monomer synthesis 27
2.3.1.2 Polymerization of 4-vinyl-1*H*-1,2,3-triazole 28

2.3.1 FT-IR studies 29
2.3.3 Thermal properties 30

2.4 Proton transport 31

2.4.1 Impedance spectroscopy 31
2.4.2 Solid state NMR 33

2.4.2.1 ^{1}H MAS NMR 33
2.4.2.2 ^{13}C CP MAS NMR 33
2.4.2.3 Variable temperature ^{1}H MAS NMR 34
2.4.2.4 ^{1}H-^{1}H SQ-DQ 2D MAS NMR 35

2.4.2.4.1 Description of 2D ^{1}H-^{1}H SQ-DQ NMR 35
2.4.2.4.2 ^{1}H-^{1}H SQ-DQ MAS NMR of pristine PVTz 37

2.4.3. Comparison of macroscopic and microscopic proton conductivity 39

2.5 Conclusions 40
2.6 References 42

3. HYBRID INORGANIC-ORGANIC PROTON EXCHANGE MEMBRANES CONTAINING 1*H*-1,2,3-TRIAZOLE MOIETIES 45

3.1 Introduction 45
3.2 Experimental 46

3.2.1 Materials 46
3.2.2 Instrumentation 46

3.3 1*H*-1,2,3-triazole functionalized polysiloxane crosslinked membranes 47

3.3.1 Synthesis 47
3.3.2 Preparation of membranes 49
3.3.3 FT-IR study 50
3.3.4 Appearance of hybrid inorganic-organic membranes 51
3.3.5 Thermal properties 51

3.4 Proton conductivity 53

3.4.1 Proton conductivity of 1*H*-1, 2, 3-triazole grafted condensed organosilicon precursor 53
3.4.2 Proton conductivity of hybrid inorganic-organic membranes 55

3.5 Mechanical properties 56

3.6 Conclusions 58
3.7 References 60

4. SYNTHESIS AND CHARACTERIZATION OF 1,2,3-TRIAZOLIUM IONIC LIQUIDS 63

4.1 Introduction 63
4.2 Experimental 65

4.2.1 Materials 65
4.2.2 Instrumentation 65

4.3 Synthesis 67
4.4 Characterization 72

4.4.1 ESI-MS 72
4.4.2 Thermal stability 73
4.4.3 Phase behavior, melting point and glass transition temperatures 74
4.4.4 Chemical stability towards hydroxide ion 76
4.4.5 Conductivity 77
4.4.6 Electrochemical stability 79

4.5 Conclusions 82
4.6 References 84

5. HYDROXIDE CONDUCTING POLYELECTROLYTES COMPOSED OF COBALTOCENIUM DERIVATIVES 87

5.1 Introduction 87
5.2 Experimental 88

5.2.1 Materials 88
5.2.2 Instrumentation 89

5.3 Chemical stability of cobaltocenium salts 89
5.4 Monomer synthesis 93

5.4.1 Monosubstituted cobaltocenium salt 94
5.4.2 Disubstituted cobaltocenium salt 96

5.5 Polymerization 98

5.5.1 ADMET 99
5.5.2 Thiol-ene coupling 100
5.5.3 Hydrosilylation 101

5.6 Conclusions 104
5.7 References 106

6. POLYMERS BEARING CYCLIC CARBONATES FOR LITHIUM ION BATTERIES 108

6.1 Introduction 108
6.2 Experimental 110

6.2.1 Materials 110
6.2.2 Instrumentation 111

6.3 Carbonate functionalized norbornene polymers 111

6.3.1 Synthesis of PNbC 112
6.3.2 Synthesis of PNb3C 114
6.3.3 Synthesis of PNbdi3C 117
6.3.4 Preparation of polymer electrolytes 118

6.4 Thermal analysis 118
6.5 Conductivity 120

6.5.1 Effect of weight fraction 121
6.5.2 Coordination with lithium salts by solid state NMR 122
6.5.3 Crystallinity 123
6.5.4 Mobility 124

6.6 Conclusions 125
6.7 References 126

7. SUMMARY AND FUTURE WORK 128

7.1 Dissertation summary 128
7.2 Future directions 131

7.2.1 PS-PVTz block copolymer 131
7.2.2 Cobaltocenium containing polymers 135
7.2.3 Hydrogenation of carbonate functionalized polynorbornenes 136

7.3 References 138

APPENDICES

A. ELECTROCHEMICAL IMPEDANCE SPECTROSCOPY 140

B. SUPPORTING NMR SPECTRA AND CONDUCTIVITY PLOTS FOR CHAPTER 2 149

C. SUPPORTING NMR SPECTRA FOR CHAPTER 3 151

D. SUPPORTING NMR SPECTRA FOR CHAPTER 4 153

E. SUPPORTING NMR SPECTRA FOR CHAPTER 5 164

F. SUPPORTING NMR SPECTRA FOR CHAPTER 6 166

BIBLIOGRAPHY 169

LIST OF TABLES

Table Page

2.1. Thermal properties of the polymers studied. 30

3.1. Thermal properties of the materials studied..... 53

3.2. Reduced modulus and hardness from nanoindentation..... 58

4.1. Thermal properties of the salts investigated. 75

4.2. Cathodic and anodic limits ($E_{cathodic}$ and E_{anodic} vs. Ag/Ag^+ are set at a threshold of 1.0 mA/cm^2) and electrochemical window (EW) for the ionic salts at room temperature. 81

6.1. Thermal properties of the carbonate functionalized materials..... 120

LIST OF FIGURES

Figure Page

1.1. Schematic of different types of fuel cells..... 3

1.2. Ion conduction in polymer membranes of fuel cells and lithium ion batteries 4

1.3. Schematic of PEMFC 5

1.4. General structure of commercially available poly(perfluorosulfonic acid) 6

1.5. a) Gierke Model b) Schmidt-Rohr model 7

1.6. Structures of nitrogen containing heterocycles 8

1.7. Schematic of AAEMFC. 10

1.8. Degradation mechanisms of benzyltrimethylammonium group by OH^- ion in AEM. 11

1.9. Structures of cation containing polymers for AEMs a) Benzylmethyl-containing poly(sulfone)s with pendant quaternary trimethylamine group b) Cross-linked tetraalkylammonium-functionalized polyethylene c) tris(2,4,6-trimethoxyphenyl) polysulfone-methylene quaternary phosphonium hydroxide d) poly(arylene ether sulfone) containing guanidium hydroxide. 12

1.10. Schematic of a discharging lithium ion battery. 13

1.11. Model of lithium ion coordination to pendant cyclic carbonates of a polymer. 15

1.12. Grotthuss transport of a) protons and b) hydroxide ions in monopolar water wires. 16

1.13. a) Schematic of hydrogen bonding in 1*H*-1,2,3-triazole. b) Representation of diffusion of Li^+ ion in PEO matrix. 17

2.1. FT-IR spectra of monomer VTz, pristine PVTz and wet PVTz. a) full spectra b) expanded view 29

2.2. TGA traces of PVTz with varying residual DMF content. 30

2.3. Heat flow vs. temperature curves for PVTz with varying residual DMF content..... 31

2.4. Proton conductivity of PVTz samples along with poly(4-vinylimidazole) and poly(4-vinyl-1*H*-1,2,3-triazole) from literature for comparison..... 32

2.5. ^{1}H MAS NMR of PVTz at 260 K..... 33

2.6. ^{13}C {1H} CP-MAS NMR @ 25 kHz (126 MHz) at 320 K..... 34

2.7. ^{1}H VT MAS NMR spectra of PVTz at 29762 Hz MAS (700.1 MHz) 35

2.8. Experimental scheme for DQ NMR..... 36

2.9. a) ^{1}H MAS NMR of *cis*-polybutadiene. b) 2D ^{1}H-^{1}H SQ-DQ MAS NMR spectrum of *cis*-polybutadiene. 37

2.10. ^{1}H-^{1}H SQ-DQ MAS NMR spectra at 700.1 MHz and 29762 Hz MAS at a) 324 K and b) 410 K..... 38

2.11. a) Arrhenius plot of temperature dependent relaxation behavior of mobile protons, obtained from the ^{1}H-NMR resonance linewidth b) Arrhenius plot of macroscopic conductivity from impedance spectroscopy. 40

3.1. FT-IR spectra of condensed Tz5TrS..... 50

3.2. Appearance of membranes a) 1PEG-1TEOS -1Tz5TrS-1TFA b) 1PEG-1TEOS - 1Tz5TrS-2.5P..... 51

3.3. TGA traces of the membranes studied..... 52

3.4. DSC traces of the membranes studied 53

3.5. Proton conductivity of condensed Tz5TrS, Tz5TrS-1TFA and Tz5TrS-2.5P along with Tz5Si for comparison..... 55

3.6. Proton conductivity of 1PEG-1TEOS-1Tz5TrS-1TFA and 1PEG-1TEOS-1Tz5TrS-2.5P along with Tz5Si for comparison..... 56

3.7. Load vs. displacement curves a) Nafion-112 b) 1PEG-1TEOS-1Tz5TrS-2.5P c) 1PEG-1TEOS-1Tz5TrS-1TFA 57

4.1. Structures and abbreviations of cations and anions studied..... 68

4.2. Relative abundance in ESI mass spectra a) tosylate series b) triflate series 72

4.3. TGA traces a) tosylate series b) triflate series 74

4.4. Degradation of cations in 0.05 M NaOH/D_2O at 80 °C..... 76

4.5. Hydrogen for deuterium exchange in solutions of Tz2Tos and Tz3Tos in 0.05 M NaOH/D_2O at 80 °C..... 77

4.6. Ionic conductivity a) tosylate series b) triflate series..... 78

4.7. Comparison of ionic conductivity between two salts with same cation and different anion a) Tz1Tos vs. Tz1OTf b) Tz2Tos vs. Tz2OTf c) Tz3Tos vs. Tz3OTf d) ImTos vs. ImOTf..... 79

4.8. Cyclic voltammograms a) toslyate series b) triflate series..... 80

4.9. Discharge effect 82

5.1. ^{1}H-NMR of 0.01 M $[Cp_2Co]^+$ PF_6^- in 2 M NaOH/D_2O with sodium tosylate (0.025 M) as an internal standard a) initial NMR b) after heating at 80 °C for 40 days 91

5.2. ^{13}C-NMR of 0.01 M $[Cp_2Co]^+$ PF_6^- in 2M NaOH/D_2O with sodium tosylate (0.025 M) as an internal standard a) initial NMR b) after heating at 80 °C for 40 days 91

5.3. Stability of $[C_5H_5]_2Co^+$ PF_6^- compared to the stability of $[BnMe_3N]^+$ $[OH]^-$ 92

5.4. UV-Vis spectra of $[C_5H_5]_2Co^+$ PF_6^- 93

5.5. ESI-MS plots of 0.01 M $[Cp_2Co]^+$ PF_6^- in 2 M NaOH/D_2O a) before and b) after heating at 80 °C for 40 days. 93

5.6. Stabilization of negative charge at α position of cobaltocenium nucleus. 94

5.7. ^{1}H-NMR of crude intermediate **5.3** 96

5.8. Mass spectrum of product obtained by ADMET polymerization of monomer **5.6a** 100

5.9. ^{1}H-NMR of a) reaction mixture after proposed polymerization of monomer **5.6a** with diethylsilane b) product from hydrosilylation reaction of monomer **5.6a** with triethylsilane. 102

5.10. FT-IR spectrum of crosslinked network obtained by hydrosilylation reaction between monomer **5.6a** and tetramethylcyclotetrasiloxane. 103

5.11. TGA plot of crosslinked network obtained by hydrosilylation reaction between monomer **5.6a** and tetramethylcyclotetrasiloxane. 104

6.1. Structures of carbonate functionalized polymers studied. 110

6.2. Degradation mechanism of vinylene carbonate in the presence of Lewis acids 113

6.3. ^{1}H-NMR spectra of a) monomer b) PNbC 114

6.4. FT-IR spectra of monomer **6.1** and **6.2** 117

6.5. TGA traces of carbonate functionalized polymers 119

6.6. DSC traces of carbonate functionalized polymers 119

6.7. Conductivity of carbonate functionalized polymer electrolytes 121

6.8. ^{13}C CP MAS NMR spectra a) PNbC-LiOTf b) PNbC-LiOTf spectrum obtained by dipolar dephasing experiment 123

6.9. WAXS data for pure LiOTf, pristine PVIC and PVIC-LiOTf 124

6.10. Restricted mobility around backbone in PNbC and PNb3C compared to PVIC. 125

7.1. GPC traces a) homopolymer PS b) PS-PVTz (**7.1**) 133

7.2. ^{1}H-NMR of block copolymer **7.1** 133

7 3. DSC trace of block copolymer **7.1** 134

7.4. SAXS data for block copolymer **7.1** 135

A.1. Representation of applied sinusoidal voltage, resulting current and phase angle 140

A.2. Graphical representation of a resistor *R* and capacitor *C* in complex impedance plane 142

A.3. Cell for polymer electrolyte sandwiched between two blocking electrodes and its equivalent circuit 143

A.4. Image of the hardware used for AC impedance measurements 145

A.5. a) Sample holder used for AC impedance measurements. b) electrode used for measuring conductivity of films under anhydrous conditions c) electrode assembly for liquids under anhydrous conditions d) electrode for measuring conductivity of films under humidified environment. 146

A.6. Representative data obtained from AC impedance measurements 147

LIST OF SCHEMES

Scheme Page

2.1 Synthesis of poly(4-vinyl-1*H*-1,2,3-triazole) 28

3.1. Synthetic route to 2,2-dimethyl-propionic acid-4-(3-triethoxysilylpropyloxymethyl)-[1,2,3]triazol-1-ylmethyl ester (Tz5TrS). 48

3.2. Preparation of hybrid inorganic-organic copolymer 48

4.1. Synthesis of ionic liquids studied 68

5.1. Synthetic route to monosubstituted cobaltocenium functionalized styrene 95

5.2. Synthesis of disubstituted cobaltocenium monomers 97

5.3. ADMET polymerization of monomer **5.6a** 99

5.4. Step-growth photopolymerization using thiol-ene coupling 101

5.5. Thiol-ene reaction of monomer **5.6a** with propanethiol 101

5.6. Step-growth polymerization using hydrosilylation 102

5.7. Hydrosilylation reaction of monomer **5.6a** with triethylsilane 102

5.8. Hydrosilylation of monomer **5.6a** with tetramethylcyclotetrasiloxane 103

6.1. Synthesis of polymer PNbC 112

6.2. Synthetic route to norbornene monomer containing pendant carbonate 115

6.3. Proposed mechanism for degradation of carbonates during synthesis of norbornene containing pendant carbonate. 115

6.4. Synthesis of PNb3C 116

6.5. Synthetic route to PNbdi3C 118

7.1. Synthesis of sPS-*b*-PVTz copolymer (Pivaloxymethyl group is abbreviated as POM) 131

7.2. Step-growth polymerization using Huisgen 1,3-dipolar cycloaddition reaction 136

7.3. Proposed synthetic route for cobaltocenium containing polymers 136

7.4. Hydrogenation of carbonate functionalized polynorbornenes 137

LIST OF ABBREVIATIONS

AAEMFC	Alkaline anion exchange membrane fuel cell
AC	Alternating current
ADMET	Acyclic diene metathesis polymerization
AEM	Anion exchange membrane
AFC	Alkaline fuel cell
AIBN	Azobisisobutyronitrile
$CDCl_3$	Chloroform
CP	Cross polarization
Cp	Cyclopentadiene
DC	Direct current
DEC	Diethyl carbonate
DMA	Dynamic mechanical analyzer
DMC	Dimethyl carbonate
DMF	Dimethylformamide
DMPA	Dimethoxyphenyl acetophenone
DMSO	Dimethyl sulfoxide
DSC	Differential scanning calorimetry
E_a	Activation energy
EC	Ethylene carbonate
EIS	Electrochemical impedance spectroscopy
FID	Free induction decay
FTIR	Fourier transform infrared
GPC	Gel permeation chromatography
H_3PO_4	Phosphoric acid

k	Boltzmann constant
LiOTf	Lithium triflate
M	Molar (mol/dm^3)
MAS	Magic angle spinning
MCFC	Molten carbonate fuel cell
M_n	Number average molecular weight
NMP	N-methylpyrrolidone
NMR	Nuclear magnetic resonance
OTf	Triflate
PAFC	Phosphoric acid fuel cell
PC	Propylene carbonate
PEEK	Polyether ether ketone
PEG	Polyethylene glycol
PEM	Proton exchange membrane
PEMFC	Proton exchange membrane fuel cell
PEO	Polyethylene oxide
PFSA	Poly(perfluorosulfonic acid)
PNbC	Poly(5-norbornene-2,3-ylene ester)
POM	Pivaloxymethyl
PS	Polystyrene
PTFE	Polytetrafluoroethylene
PVIC	Poly(vinylene carbonate)
PVTz	Poly(4-vinyl-1*H*-1,2,3-triazole)
q	Scattering wave vector
RAFT	Reversible addition-fragmentation chain transfer

RCM	Ring-closing metathesis
ROMP	Ring-opening metathesis polymerization
SAXS	Small angle X-ray scattering
SEI	Solid electrolyte interphase
SOFC	Solid oxide fuel cell
SPE	Solid polymer electrolyte
SQ-DQ	Single-quantum double-quantum
t-BuOH	t-butanol
T_d	Decomposition temperature
TEOS	Tetraethoxy silane
TFA	Trifluoroacetic acid
T_g	Glass transition temperature
TGA	Thermogravimetric analysis
THF	Tetrahydrofuran
T_m	Melting point
Tos	Tosylate
UV-Vis	Ultraviolet visible spectroscopy
VT	Variable temperature
WAXS	Wide angle X-ray scattering
Z*	Complex impedance
Z’	The real component of complex impedance
Z”	The imaginary component of complex impedance
Đ	Dispersity
δ	Chemical shift in NMR
η	Efficiency

σ	Conductivity
ω	frequency
ε	Extinction coefficient

CHAPTER 1

INTRODUCTION

Society is dependent on the steady supply of fossil fuels including oil, natural gas and coal. Fossil fuels are a crucial economic input for the success of modern day life. However, the supply of fossil fuels is limited and the demand for energy is growing rapidly around the world. The world's heavy reliance on fossil fuels has increased the emission of greenhouse gases, adversely affecting the environment. Economic dependence on oil is a threat to national security of all countries that rely upon oil imports. These environmental and political issues make the development of alternative energy sources an absolute must.

Renewable energy is a resolution for the global issues related to the use of fossil fuels. Renewable energy comes from sources such as sunshine, running water, wind and biological processes. These forms of renewable energy have the benefit of far less pollution than conventional energy resources and they will not be exhausted. The financial cost of using these alternative energy resources may not be cheap, but if the environmental cost of using fossil fuels and the indirect cost of health expenditures due to the resultant pollution are considered, renewable energy can be an economic winner. Currently, these clean energy resources are being used to varying extents. They all have their own advantages and disadvantages. For example, solar power comes from the sun, a virtually endless source of energy, but it has a significant geographic dependence. Wind is free and can be captured efficiently with modern technology, but the wind turbines required to harness the wind are large, expensive and loud. Most of the renewable energy technologies are limited by cost and location. If you live in a valley, there may not be enough sun or wind but there might be a year round stream that can power a water wheel. On the other hand, if you live in a desert area, hydro power most likely is not an option, but solar or wind might be viable energy sources. The best form of renewable energy depends on where you live and what your needs are for energy.

At present, with increasing gasoline prices, there is a huge demand to shift from internal combustion powered vehicles to alternative energy vehicles in the transportation sector. The last 15 years have seen an unprecedented growth in the field of portable devices like mobile phones, lap tops etc. which need safe and light weight power supplies. Overall, our mobile world needs reliable, affordable power solutions with longer run times and off-grid availability. Fuel cells and lithium ion batteries have the potential to meet many of the demands for these applications. At present, high capacity lithium ion batteries compete with fuel cells for transportation applications and backup power, while fuel cells may become competitors of batteries in portable applications.

1.1 Motivation

Both batteries and fuel cells deliver electrical energy from a chemical reduction/oxidation (redox) reaction, but they differ in the location of energy storage and conversion. Batteries convert stored energy into electrical energy and stop working when the stored reactants are exhausted. This represents a thermodynamically closed system. A fuel cell is an open system and continues to work as long as the fuel is delivered from outside the cell. The thermodynamic efficiency (η) of batteries (η = 90%) and fuel cells (η = 80%) is much higher than that of combustion engines (max. η = 50% for steam turbines), as they are not subjected to Carnot cycle limitations.[1-3]

There are several types of fuel cells classified by the type of electrolyte used, which determines their operating temperature, figure 1.1.[4] The major types of fuel cells are solid oxide fuel cell (SOFC), molten carbonate fuel cell (MCFC), alkaline fuel cell (AFC), phosphoric acid fuel cell (PAFC) and proton exchange membrane fuel cell (PEMFC). The application of a fuel cell is mainly determined by the working temperature and the type of fuel utilized. Of all these different types of fuel cells, PEMFCs and AFCs can best operate at, or near, room temperature. The low operating temperature of PEMFCs and AFCs allows for fast start-up at low temperature

and quick response to power demand making them attractive for application in fields of transportation and portable devices.[5] Polymer electrolyte membrane fuel cells (PEMFCs), also called proton exchange membrane fuel cells, use hydrogen as a fuel, a solid polymer as an electrolyte and have high energy density with an operating temperature range of room temperature to 200 °C. Alkaline fuel cells (AFCs), one of the oldest type of fuel cell, operate between ambient temperature and 90 °C with an electrical efficiency higher than the other fuel cells.[1] Recently there has been interest in alkaline anion exchange membrane fuel cells (AAEMFCs) which are functionally similar to AFCs, the difference being AAEMFCs employ a solid polymer electrolyte while AFCs use aqueous KOH as an electrolyte. The advantages and challenges of AAEMFCs compared to AFCs are discussed in section 1.2.2.

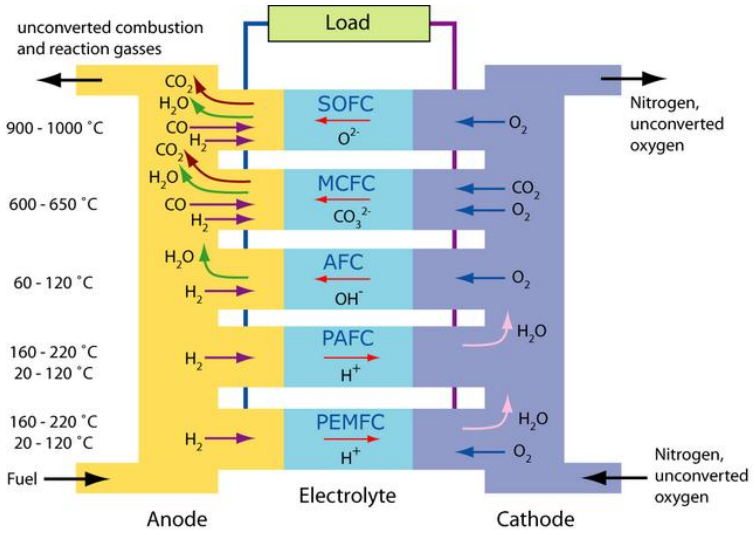

Figure 1.1. Schematic of different types of fuel cells.[4]

PEMFCs, AAEMFCs and lithium ion batteries have a few things in common, figure 1.2. They all involve an ion moving from one electrode to the other through an electrolyte and electrons passing through an external circuit. They all need an electrolyte to conduct ions and a separator between the two electrodes. Polymer membranes being able to act as an electrolye and

an electrical insulator between the two electrodes become a principal choice. Polymeric materials have an added advantage of being light weight, flexible and easy processability.

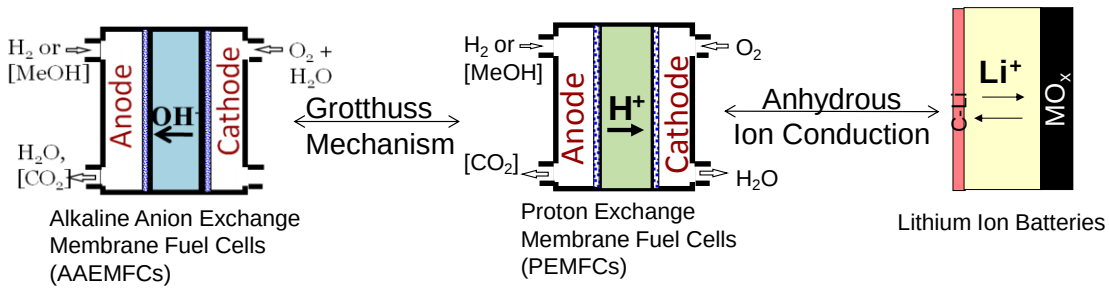

Figure 1.2. Ion conduction in polymer membranes of fuel cells and lithium ion batteries.

The performance of a polymeric membrane is critical to the overall functioning of these devices. For all of them, a membrane must be mechanically robust, thermally and electrochemically stable under the operating conditions. It should have high H^+, OH^- and Li^+ ion conductivity for PEMFC, AAEMFC and lithium ion battery respectively. The conduction mechanism of these ions bears some similarities. The transport mechanism of both H^+ and OH^- ions involves hydrogen bond making/breaking steps along chains of water molecules, as described in section 1.3.1. Under anhydrous conditions, the mechanism of H^+ transport in PEMFCs has parallels with Li^+ ion transport in lithium ion batteries, as discussed in section 1.3.2. The goal of this thesis is to understand the similarities and/or differences in the structure property relationships of polymer membranes and conductivity of different ions.

1.2 Background

1.2.1 PEMFCs

In a PEMFC, a polymer membrane is placed between two porous, catalyst containing electrodes and hydrogen or methanol is fed to the anode as fuel, while oxygen, from air, is supplied to the cathode. The fuel is oxidized at the anode producing electrons that go through the external circuit and H^+ ions, which pass through the membrane to the cathode side and react with

oxygen, producing water as the byproduct.[2] A schematic of a PEMFC is shown in figure 1.3. The PEMFCs operate at ~ 1 A/cm^2 at 0.7 V.[1] For efficient functioning of a PEMFC, its central component, the proton exchange membrane (PEM) should have high ionic conductivity, minimum permeability to fuel and oxidant, mechanical and electrochemical stability and chemical stability in the oxidative fuel cell environment.[6]

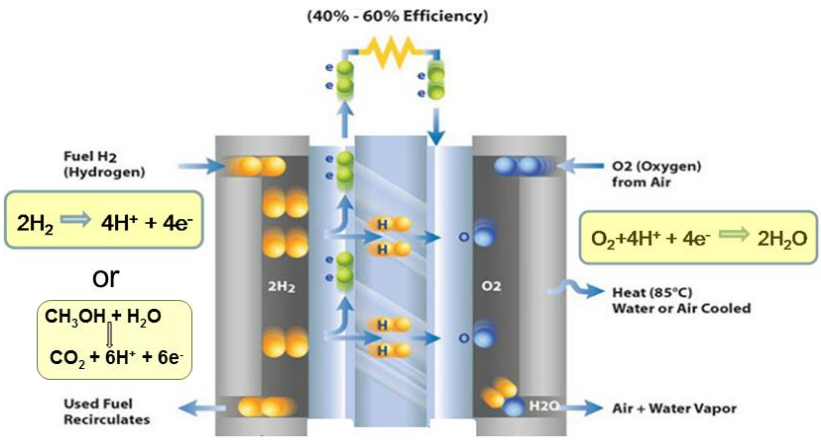

Figure 1.3. Schematic of PEMFC (adapted from CCI Research to Innovation poster).

1.2.1.1 Proton transport mechanism

Proton transport can take place by two mechanisms, the so-called vehicular mechanism and Grotthuss mechanism (structural diffusion). In the vehicular mechanism, proton diffuses through the medium along with the vehicle, water. Net proton transport depends on the rate of vehicle/solvent diffusion.[7] A point to be noted is that a bare proton does not exist, but is bound to water molecules in aqueous solution, forming hydrated hydronium ions, e.g. $H_5O_2^+$or $H_9O_4^+$.[8] The structural diffusion mechanism, suggested by Grotthuss over two centuries ago,[9] involves diffusion of an excess proton, or a protonic defect, through the hydrogen bonded network of water molecules through rapid formation/cleavage of covalent bonds. In water mediated "proton wires", water molecules reside on their site and are involved in local molecular rearrangement, a rotation which allows for next proton jump between the water molecules.[10-11] Net proton transport is governed by dynamic hydrogen bonding and rate of solvent reorientation. Depending upon the

availability of free solvent/vehicles and level of hydration, one or the other mechanism dominates the proton transport in PEMs.[12-13]

1.2.1.2 Hydrated PEMFCs

The present state-of-the-art membrane materials are based on sulfonated tetrafluoroethylene based fluoropolymers, such as Nafion®. Nafion®, (structure shown in figure 1.4) is a current standard against which performance of all other membranes are compared. Nafion® conducts protons in the hydrated environment by a vehicular mechanism and its conductivity is critically dependent on the degree of hydration.[14-15] Similar to Nafion®, a large number of fluorinated/non-fluorinated polymers with aromatic and aliphatic backbones having sulfonic acid as an anionic site have been developed.[6, 16-18] The typical proton conductivity of these membranes is 10^{-2} -10^{-1} S/cm in the fully hydrated state. Gierke *et al*. proposed a model for Nafion® as a cluster network consisting of inverted micelles, connected by narrow channels of about 1 nm in diameter, figure 1.5a.[14] A more recent model, proposed by Schmidt-Rohr, on the basis of new calculations of previously reported SAXS data, describes Nafion® as consisting of long parallel randomly packed water channels surrounded by partially hydrophilic side branches forming inverted micelles, figure 1.5b.[15] This model helps explain the observed fast diffusion of protons and water in Nafion® and persistence of proton conductivity below the freezing point of water.[15]

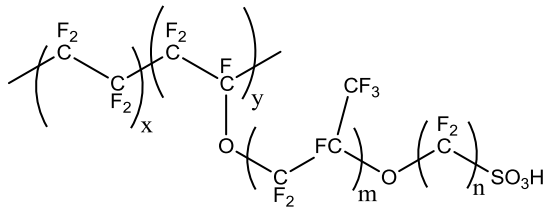

Nafion®: m>1, n=2, x=5-13.5, y=1000

Flemion®: m=0 or 1, n=1-5, y=1000

Aciplex®: m=0 or 3, n=2-5, x=1.5-14, y=1000

Figure 1.4. General structure of commercially available poly(perfluorosulfonic acid).

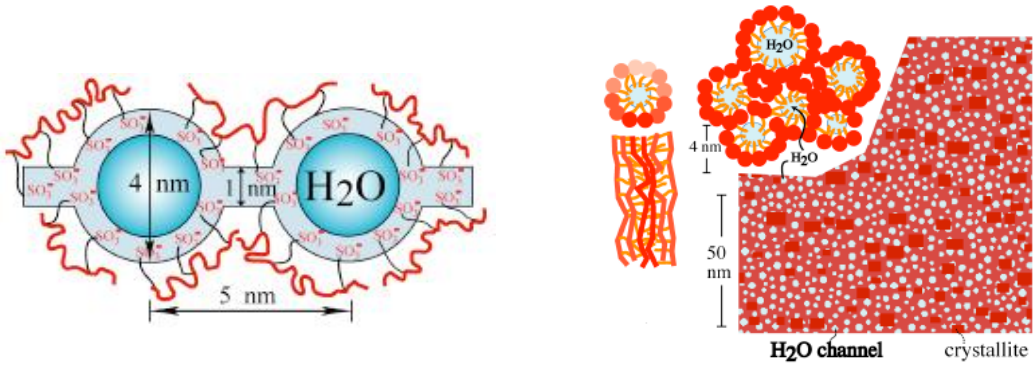

(a) (b)

Figure 1.5. a) Gierke Model[14] b) Schmidt-Rohr model[15]

The heavy reliance of proton conductivity of poly(perfluorosulfonic acid) (PFSA) membranes on water as a medium leads to two severe problems relevant to their use in fuel cells: maximum operating temperature of the fuel cell is limited to lower than 100 °C, the boiling point of water, and there is severe electro osmotic drag leading to decrease in cell potential.[17, 19-20] Maximum operating temperature of ~ 100 °C limits the activity and CO tolerance of the platinum electro catalyst. This necessitates the use of hydrogen of very high purity.[21] Methanol being a liquid fuel is a good substitute for hydrogen gas and direct methanol fuel cells have high energy densities. However, their key limitation is permeation of methanol from anode to cathode, where its catalytic reaction competes with oxygen reduction reaction leading to lower overall cell potential.[22-23] Hydrocarbon polymers suffer from oxidative radical degradation in acidic environment,[24-26] and though perfluorinated polymers show satisfactory performance; their large scale commercialization is limited by cost. Operating a fuel cell at temperatures above 120 °C has the advantages of reduced platinum catalyst loading and its improved CO tolerance, enhanced electrochemical reactions and simplified water and thermal management design.[21, 27] This has led to research efforts towards systems that transport protons at high temperature and in a low humidity environment.

1.2.1.3 Anhydrous PEMFCs

Two fundamental approaches towards anhydrous proton conduction have been adopted. One is simple substitution of water with another proton solvent, e.g., phosphoric acid or amphoteric nitrogen containing heterocycles. Similar to water, certain nitrogen containing heterocycles are amphoteric, and can form hydrogen bonded network and undergo autoprotolysis.[27] The boiling points of heterocyles such as imidazole, triazole and benzimidazole are above 200 °C. Structures of heterocycles studied for proton conduction are shown in figure 1.6. Phosphoric acid based membranes; especially polybenzimidazole-phosphoric acid (PBI-PA) system show proton conduction up to 200 °C along with other desired properties and are poised for commercialization.[28-29] However, at temperatures below 100 °C, the phosphoric acid can get washed out by reaction with water during long term PEMFC operation. In PFSA membranes, substitution of water with imidazole and other derivatives have helped retain good conductivity up to 200 °C.[30-31] However, free solvent molecules tend to leach out of the membrane and thereby cause gradual performance deterioration. This can be overcome by immobilization of protogenic moieties.

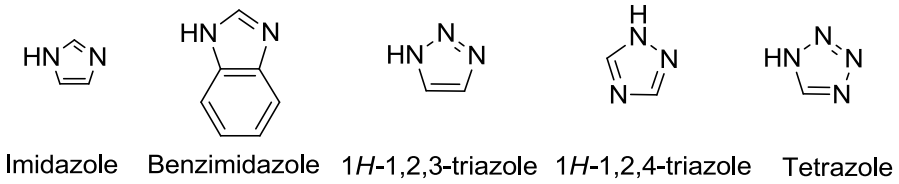

Figure 1.6. Structures of nitrogen containing heterocycles.

The other approach to achieve anhydrous proton conduction is focused towards fully polymeric materials that exhibit proton conductivity as an intrinsic property.[27] In these materials, the proton "solvent" is immobilized on to the polymer backbone via a flexible spacer and proton transport takes place through a hydrogen bonded network.[10] Immobilization prevents vehicular diffusion of protons and hence the proton mobility relies solely on a Grotthuss-type mechanism (structural diffusion). There are several reports on the use of proton conducting motifs such as

imidazole,[32-35] benzimidazole[36-39] and triazole,[40-43] attached as a pendant group to the polymer chain for anhydrous proton conduction. Studies on these heterocycle functionalized polymers have revealed that proton conductivity depends on local mobility of the heterocycle, determined by the spacer length and effective concentration of charge carriers.[34-36, 42] Fine tuning of polymer properties is critical towards the development of an "all solid state" conducting membrane.

1.2.2 AAEMFCs

In an AAEMFC, the fuel, hydrogen or methanol, is supplied at the anode and oxygen through air, and water are supplied at cathode. The schematic of an AAEMFC is shown in figure 1.7. Hydroxide ions (OH^-), generated from electrochemical oxygen reduction at the cathode, migrate to the anode where they react with the fuel to produce water and electrons.[44-45] The most significant advantage of AAEMFCs is that under alkaline conditions, electrode reaction kinetics are much more facile, allowing use of inexpensive, non-noble metal catalysts such as nickel for the fuel electrode[46] and silver, iron phthalocyanines etc. for the oxygen electrode.[47] Corrosion problems are also substantially reduced under alkaline conditions. An alkaline medium accelerates oxidation of methanol making it an attractive fuel to be used. Methanol has an advantage of easier storage and transportation and has higher volumetric energy density compared to hydrogen. Also, methanol crossover from anode to cathode is reduced in AAEMFCs compared to PEMFCs, due to the opposite direction of ion transport in the membrane, from cathode to anode.[44] In addition, use of higher alcohols such as ethanol and propanol is possible in AAEMFCs, since anode potential in AAEMFCs is sufficient to oxidize C-C bonds present in alcohols.[44]

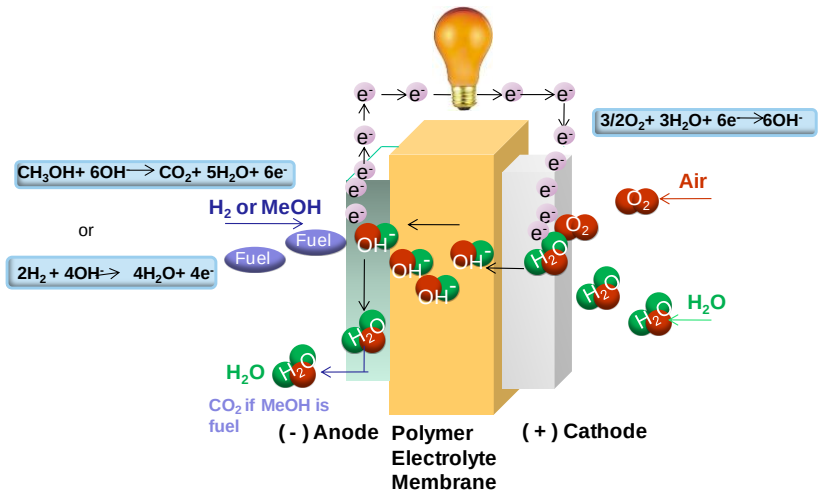

Figure 1.7. Schematic of AAEMFC.

Fuel cells operating under alkaline conditions (AFCs), have been used since the mid-1960s by NASA in the Apollo and Space Shuttle programs. These fuel cells generate electricity at nearly 70% efficiency.[1] In a traditional AFC, an aqueous solution of KOH is used as an electrolyte. CO_2 coming in through oxidant air stream and generated as by product from oxidation of methanol, if methanol is the fuel, reacts with electrolyte KOH forming CO_3^{2-}/HCO_3^-. Unfortunately as a consequence, K_2CO_3 or $KHCO_3^-$ precipitate on the electrodes and destroy the catalyst layer in AFCs. Replacing aqueous KOH with a solid polymer electrolyte membrane, that can conduct hydroxide ions could overcome the problems of electrolyte leakage and carbonate precipitation, though still taking advantage of the previously discussed benefits of operating a fuel cell in an alkaline environment.[48] In AAEMFCs, CO_2 reacts with water forming H_2CO_3, which further dissociate to HCO_3^- and CO_3^{2-}. The equilibrium concentration of CO_3^{2-}/HCO_3^- is less than 0.07% and there is no precipitation on the electrodes in the absence of cations (K^+, Na^+).[45, 48]

The biggest challenge in developing AAEMFCs is the anion exchange membrane. A typical AEM is composed of a polymer backbone with tethered cationic ion-exchange groups to facilitate the movement of free OH^- ions. This is the inverse of Nafion® used for PEMFCs, where an anion is covalently attached to the polymer and protons hop from one site to another. The

challenge is to fabricate AEM with high OH^- ion conductivity and mechanical stability without chemical deterioration at elevated pH and temperatures. The main mechanisms of degradation are Hoffmann elimination when β-hydrogens are present and direct nucleophilic attack by OH^- ion at the cationic site. The degradation pathways for membranes containing quaternary ammonium cations are shown in figure 1.8.[44, 49] One approach towards improving the chemical stability towards Hofmann elimination is to remove all β-hydrogens at the cationic site. All these degradation reactions limit the polymer backbone chemistries and the cations that can be incorporated for developing AEM. Another challenge is achieving OH^- ion conductivity comparable to H^+ conductivity observed in PEMFCs. Since the diffusion coefficient of OH^- ions is four times less than that of water,[50] four times higher concentration of OH^- ions is needed to achieve similar results, which in turn needs higher ion exchange capacity of the polymer. However, high ion exchange capacity leads to excessive swelling of polymer on hydration and concomitant loss of mechanical properties.[51] The need to develop AEMs immune to caustic degradation with high hydroxide ion conductivity is of paramount importance.

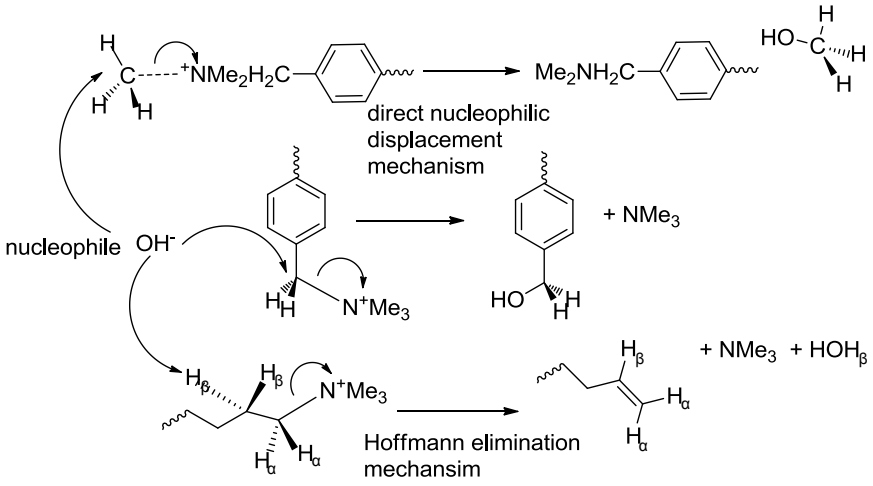

Figure 1.8. Degradation mechanisms of benzyltrimethylammonium group by OH^- ion in AEM.

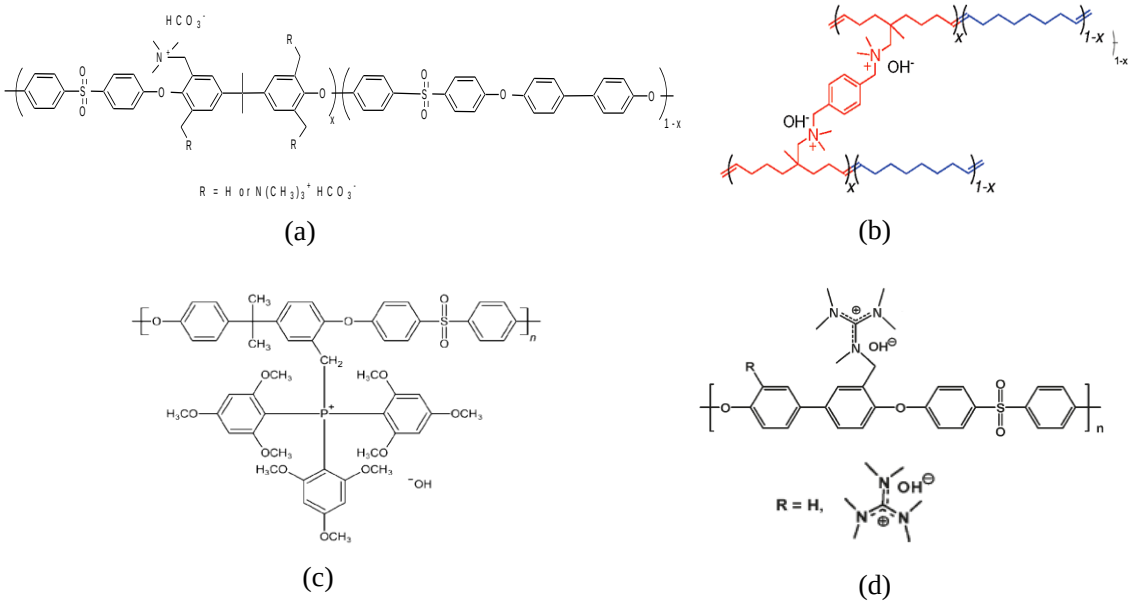

Figure 1.9. Structures of cation containing polymers for AEMs a) Benzylmethyl-containing poly(sulfone)s with pendant quaternary trimethylamine group[52] b) Cross-linked tetraalkylammonium-functionalized polyethylene[59] c) tris(2,4,6-trimethoxyphenyl) polysulfone-methylene quaternary phosphonium hydroxide[60] d) poly(arylene ether sulfone) containing guanidium hydroxide.[62]

Several research groups have demonstrated AEMs based on polymers containing quaternary ammonium groups such as quaternized poly(sulfone)s[52-53] (figure 1.9a),[52] quaternized and crosslinked polynorbornene,[54] quaternized polyphenylene,[55] radiation grafted vinylbenzylchloride on poly(tetrafluoroethylene-co-hexafluroropropylene) films[56-57] and quaternized polyethylene.[58] Of all the quaternary ammonium functionalized polymers, maximum room temperature conductivity of 69 mS/cm for crosslinked polyethylene (figure 1.9b) has been observed by Coates and coworkers.[59] Recently, Yan *et al*. developed quaternary phosphonium containing ionomer (figure 1.9c) having OH^- ion conductivity of 27 mS/cm at room temperature that are soluble in low boiling, water soluble solvents.[60] Beyer and coworkers synthesized trimethylphosphonium functionalized polystyrene ionomers and studied the relationship between ion content and T_g of ionomer.[61] Zhang *et al*. reported quaternary guanidinium functionalized poly(arylene ether sulfone) (figure 1.9d)[62] with conductivity up to 74 mS/cm at 60 °C. While all

these reports are promising for the feasibility of AAEMFC, successful production of AEMs requires improvement in conductivity, mechanical stability and chemical stability for long term operation under alkaline fuel cell environment. There needs to be further exploration of different classes of cations to develop chemically stable polymer electrolytes and a better understanding of degradation mechanisms and hydroxide ion migration.

1.2.3 Lithium ion batteries

Lithium ion polymer batteries are rechargeable batteries with energy density more than twice that of standard nickel cadmium and lead acid batteries. Lithium ion batteries have the added advantages of low maintenance, no memory or scheduled cycling necessary to increase the battery life, very low self-discharge and an output voltage of 3.6 volts from single cell. A schematic of a lithium ion cell during discharge is shown in figure 1.10. During discharge of the battery, oxidation takes place at the anode and reduction at the cathode. Lithium ions shuttle from lithium intercalated graphite anode through an electrolyte to the cathode where they are stored as transition metal oxide intercalation compound. The reverse reaction takes place during charging of the battery.[63]

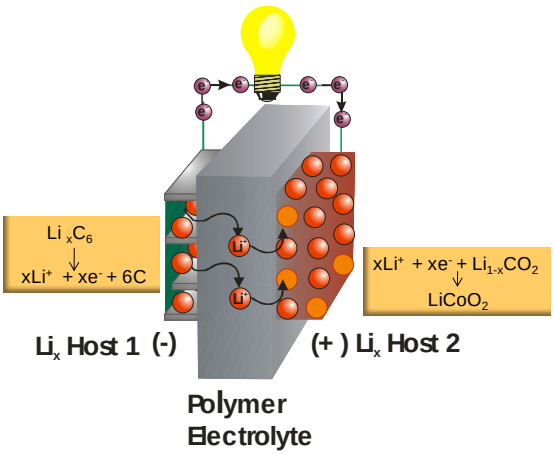

Figure 1.10. Schematic of a discharging lithium ion battery.

The traditional electrolyte in lithium ion batteries consist of lithium salts such as $LiPF_6$ or $LiBF_4$ dissolved in a mixture of organic solvents such as ethylene carbonate (EC), propylene carbonate (PC), diethyl carbonate (DEC) and dimethyl carbonate (DMC). There are safety issues with liquid electrolytes as they are prone to leakage. Use of polymer electrolyte membranes increases the safety, durability and flexibility of resulting lithium ion batteries.[64] Polymer electrolytes for use in Li^+ ion battery should have adequate conductivity ($\sigma > 10^{-5}$ S/cm in the temperature range from -20 °C to +60 °C), compatibility with electrodes and they should have electrochemical, chemical, thermal and mechanical stability over at least this temperature range, ifnot beyond for added safety considerations. Another requirement for the electrolytes is to have a high Li^+ transference number, i.e., a high ratio of the charge transported by Li^+ compared to the total charge transported.[65] This ambitious set of properties is difficult to obtain in a single material and a number of different classes of polymer electrolyte materials have been defined which possess most but not all of desired properties.[65-67]

The most widely studied polymers are based on aliphatic polyethers, mainly polyethylene oxide (PEO). PEO complexes Li^+ cation through coordination with ether oxygens and mobility of the Li^+ is related to the mobility of complexing segments of the PEO chain. This necessitates low T_g materials due to their high backbone mobility.[65] There are numerous reports focused on suppressing the crystallinity of PEO and achieving 'low T_g' polymers by incorporating short chains of PEO in the backbone or as a pendant group.[67-72] Polymer electrolytes are generally classified into solid polymer electrolytes (SPE) and gel polymer electrolytes. A large amount of literature exploits blending of polymers with lithium salts to make dry SPE.[71-73] These materials tend to suffer from low conductivity at room temperature restricting their use to large systems (electric traction or back-up power) and not to portable devices. Gel polymer electrolytes consist of moderately cross linked polymers swollen with plasticizers like EC, PC which are excellent

solvents for Li^+ salts.[74-75] Gel SPEs generally exhibit better conductivity than SPE but suffer from inferior mechanical properties.

There are few reports on polymers containing polar, five membered cyclic carbonate group for lithium ion battery applications.[76-80] These polymers have the structural element of the prototypical solvent such as EC or PC, which have proven to be excellent solvents for lithium salts. In these materials, Li^+ ions are solvated by carbonates forming a tetrahedral solvent shell. Li^+ ions migrate by a random hopping process activated by localized motions of the carbonate dipoles around the position of the ions (figure 1.11).[77] A better understanding of ion transport within these materials could lead to membranes with properties superior to those available today.

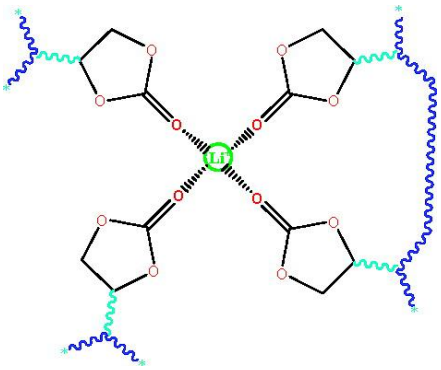

Figure 1.11. Model of lithium ion coordination to pendant cyclic carbonates of a polymer.[77]

1.3 Objectives

All the above energy devices need ion conducting polymer membrane as an integral part of their construction. It is the properties of the membrane that dictate the operating conditions, fuel requirements and packaging of the entire system to a significant extent. Ideally, all three energy devices require a membrane that is a true solid state material with no free solvents, high ionic conductivity in the desired temperature range and that can be tailored with respect to other auxiliary requirements. At the most fundamental level, the common feature of these membranes is the movement of ions through a robust, but locally dynamic polymeric media.

1.3.1 Proton and hydroxide ion mobility

The Grotthuss mechanism is one of the accepted mechanisms of proton transport in PEMFCs.[11] The mechanism of hydroxide ion transport has been little explored compared to extensive investigations done on proton transport mechanism. Tuckerman and coworkers have recognized similarities in structural complexes of H^+ hydration complexes and OH^- hydration complexes using *ab initio* molecular dynamic simulations. The simulations supported the structural diffusion mechanism for charge transport.[81] Molecular dynamic simulations on H^+ and OH^- ion migration within proteins spanning cell membranes have shown Grotthuss transport of both H^+ and OH^- ions. Protons hop from one water molecule to another while hydroxide ions migrate by sequentially accepting protons from the neighboring water molecules, along pre-organized "water wires", figure 1.12.[82] Thus, proton transport in one direction is equivalent to hydroxide ion transport in the other direction.

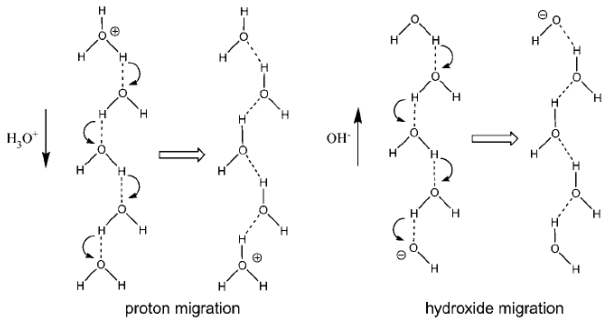

(a) (b)

Figure 1.12. Grotthuss transport of a) protons and b) hydroxide ions in monopolar water wires.[82]

Given the similarities in the conduction mechanism of H^+ and OH^- ions, one objective of this thesis is to explore the parallels between H^+ and OH^- ion transport, and in the process use these findings to develop robust polymer membranes with high ionic conductivity for proton exchange membrane fuel cells (PEMFCs) and alkaline anion exchange membrane fuel cells (AAEMFCs).

1.3.2 Proton and lithium ion mobility

In an anhydrous medium, protons move through the hydrogen bonded network formed by proton solvent, like 1*H*-1,2,3-triazole, figure 1.13a. The rate of proton transport depends upon local mobility of the protogenic groups and rate of hydrogen bond formation/breaking.[11] In case of lithium ion conduction through low T_g materials, for example polyethylene glycol, coordination bonding between ethereal oxygens and Li^+ ions are formed and broken. The net Li^+ ion transport is therefore dependent upon the rate of coordination and release as well as the mobility of the polymer segment, figure 1.13b.[65] Understanding more completely solvent free ion transport and thus achieving high ionic conductivity is the common intellectual challenge for understanding the relationship between anhydrous PEMFCs and lithium ion batteries.

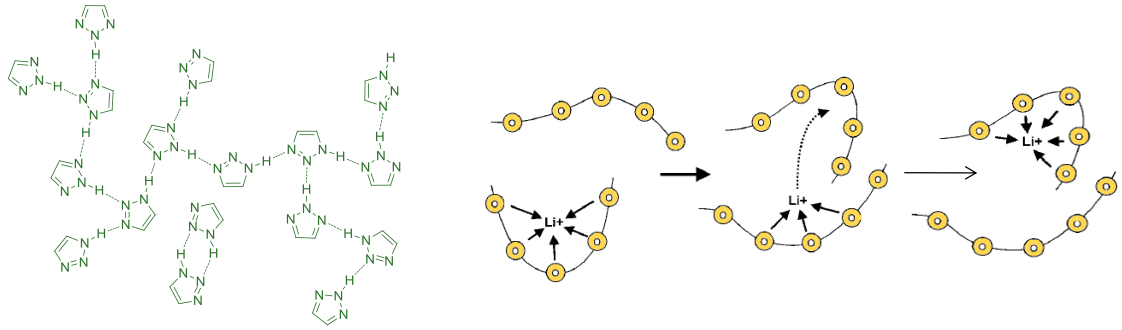

(a) (b)

Figure 1.13. a) Schematic of hydrogen bonding in 1*H*-1,2,3-triazole.[83] b) Representation of diffusion of Li^+ ion in PEO matrix. Circles represent ether oxygens of PEO.[65]

Considering the similarities in conduction mechanism and given the fact that Li^+ is the next stable cation to H^+, the other objective of this thesis is to attempt to answer the question whether the structure-property relationships developed between polymer membranes and H^+ mobility can be extended to that between polymer membranes and Li^+ ion mobility. This question is answered by exploring systems having carbonate attached as a pendant group to the polymer chain.

1.4 Outline of the dissertation

In this thesis, proton conductivity of poly(4-vinyl-1*H*-1,2,3-triazole), the simplest triazole containing polymer, is addressed on macroscopic and microscopic scale in chapter 2. In chapter 3, the effect of structural reinforcement on low T_g proton conducting polymers by crosslinking is studied, using 1*H*-1,2,3-triazole tethered poly(siloxane) as a model system. In chapter 4, a series of triazolium cations are synthesized and characterized. Their chemical stability under highly basic conditions is examined for incorporation in AEMs. Chapter 5 explores cationic metallocene analogues, cobaltocenium and cobaltocenium containing polymers for AEMs. In chapter 6, polymer membranes composed of carbonate functionalized polynorbornenes are studied for lithium ion battery. Based on the findings in this thesis, potential future directions are outlined in chapter 7.

1.5 References

1. Winter, M.; Brodd, R. J., *Chem. Rev.* **2004,** 104, 4245-4269.

2. Carrette, L.; Friedrich, K. A.; Stimming, U., *Fuel Cells* **2001,** 1, 5-39.

3. In http://howstuffworks.com (accessed March 14, 2011).

4. University of Cambridge, Teaching and Learning Packages - Fuel Cells. http://www.doitpoms.ac.uk/tlplib/fuel-cells/types.php (accessed March 14, 2011).

5. Hamrock, S. J.; Yandrasits, M. A., *J. Macromol. Sci., Part C: Polym. Rev.* **2006,** 46, 219-244.

6. Smitha, B.; Sridhar, S.; Khan, A. A., *J. Membr. Sci.* **2005,** 259, 10-26.

7. Knauth, P.; Schoonman, J., *Nanocomposites: Ionic Conducting Materials and Structural Spectroscopies*. 1st ed.; Springer: **2007**; pp 111.

8. Wu, Y.; Chen, H.; Wang, F.; Paesani, F.; Voth, G. A., *J. Phys. Chem. B* **2008,** 112, 467-482.

9. de Grotthuss, C. J. T., *Ann. Chim.* **1806,** LVIII, 54-74.

10. Kreuer, K.-D., *Chem. Mater.* **1996,** 8, 610-641.

11. Münch, W.; Kreuer, K. D.; Silvestri, W.; Maier, J.; Seifert, G., *Solid State Ionics* **2001,** 145, 437-443.

12. Voth, G. A., *Acc. Chem. Res.* **2006,** 39, 143-150.

13. Swanson, J. M. J.; Maupin, C. M.; Chen, H.; Petersen, M. K.; Xu, J.; Wu, Y.; Voth, G. A., *J. Phys. Chem. B* **2007,** 111, 4300-4314.

14. Gierke, T. D.; Munn, G. E.; Wilson, F. C., *J. Polym. Sci. Polym. Phys.* **1981,** 19, 1687-1704.

15. Schmidt-Rohr, K.; Chen, Q., *Nat. Mater.* **2008,** 7, 75-83.

16. Hickner, M.; Ghassemi, H.; Kim, Y.; Einsla, B.; McGrath, J., *Chem. Rev.* **2004,** 104, 4587-4612.

17. Rikukawa, M.; Sanui, K., *Prog. Polym. Sci.* **2000,** 25, 1463-1502.

18. Peckham, T. J.; Holdcroft, S., *Adv. Mater.* **2010,** 22, 4667-4690.

19. Elabd, Y. A.; Napadensky, E.; Sloan, J. M.; Crawford, D. M.; Walker, C. W., *J. Membr. Sci.* **2003,** 217, 227-242.

20. Elabd, Y. A.; Walker, C. W.; Beyer, F. L., *J. Membr. Sci.* **2004,** 231, 181-188.

21. Li, Q.; He, R.; Jensen, J. O.; Bjerrum, N. J., *Chem. Mater.* **2003,** 15, 4896-4915.

22. Deluca, N. W.; Elabd, Y. A., *J. Polym. Sci. Pol. Phys.* **2006,** 44, 2201-2225.

23. Elabd, Y. A.; Hickner, M. A., *Macromolecules* **2011,** 44, 1-11.

24. Hubner, G.; Roduner, E., *J. Mater. Chem.* **1999,** 9, 409.

25. Yu, J.; Yi, B.; Xing, D.; Liu, F.; Shao, Z.; Fu, Y.; Zhang, H., *Phys. Chem. Chem. Phys.* **2003,** 5, 611.

26. Liu, W.; Zuckerbrod, D., *J. Electrochem. Soc.* **2005,** 152, A1165-A1170.

27. Schuster, M. F. H.; Meyer, W. H., *Annu. Rev. Mater. Res.* **2003,** 33, 233-261.

28. Wainright, J. S.; Wang, J. T.; Weng, D.; Savinell, R. F.; Litt, M., *J. Electrochem. Soc.* **1995,** 142, L121-L123.

29. Xiao, L.; Zhang, H.; Jana, T.; Scanlon, E.; Chen, R.; Choe, E.-W.; Ramanathan, L. S.; Yu, S.; Benicewicz, B. C., *Fuel Cells* **2005,** 5, 287-295.

30. Sun, J.; Jordan, L. R.; Forsyth, M.; MacFarlane, D. R., *Electrochim. Acta* **2001,** 46, 1703-1708.

31. Kim, J.; Mori, T.; Hayashi, S.; Honma I., *J. Electrochem. Soc.* **2007,** 154, A290-A294.

32. Schuster, M. F. H.; Meyer, W. H.; Schuster, M.; Kreuer, K. D., *Chem. Mater.* **2004,** 16, 329-337.

33. Schuster, M.; Meyer, W. H.; Wegner, G.; Herz, H. G.; Ise, M.; Schuster, M.; Kreuer, K. D.; Maier, J., *Solid State Ionics* **2001,** 145, 85-92.

34. Herz, H. G.; Kreuer, K. D.; Maier, J.; Scharfenberger, G.; Schuster, M. F. H.; Meyer, W. H., *Electrochim. Acta* **2003,** 48, 2165-2171.

35. Scharfenberger, G.; Meyer, W. H.; Wegner, G.; Schuster, M.; Kreuer, K. D.; Maier, J., *Fuel Cells* **2006,** 6, 237-250.

36. Persson, J. C.; Jannasch, P., *Solid State Ionics* **2006,** 177, 653-658.

37. Woudenberg, R. C.; Yavuzcetin, O.; Tuominen, M. T.; Coughlin, E. B., *Solid State Ionics* **2007,** 178, 1135-1141.

38. Persson, J. C.; Jannasch, P., *Macromolecules* **2005,** 38, 3283-3289.

39. Persson, J. C.; Josefsson, K.; Jannasch, P., *Polymer* **2006,** 47, 991-998.

40. Zhou, Z.; Li, S.; Zhang, Y.; Liu, M.; Li, W., *J. Am. Chem. Soc.* **2005,** 127, 10824-10825.

41. Martwiset, S.; Woudenberg, R. C.; Granados-Focil, S.; Yavuzcetin, O.; Tuominen, M. T.; Coughlin, E. B., *Solid State Ionics* **2007,** 178, 1398-1403.

42. Granados-Focil, S.; Woudenberg, R. C.; Yavuzcetin, O.; Tuominen, M. T.; Coughlin, E. B., *Macromolecules* **2007,** 40, 8708-8713.

43. Subbaraman, R.; Ghassemi, H.; Zawodzinski Jr, T., *Solid State Ionics* **2009,** 180, 1143-1150.

44. Varcoe, J. R.; Slade, R. C. T., *Fuel Cells* **2005,** 5, 187-200.

45. Shen, P. K.; Xu, C.; Meng, H.; Zeng, R., *Adv. Fuel Cells* **2005**, 149-179.

46. Abdel Rahim, M. A.; Abdel Hameed, R. M.; Khalil, M. W., *J. Power Sources* **2004,** 134, 160-169.

47. Sleightholme, A. E. S.; Varcoe, J. R.; Kucernak, A. R., *Electrochem. Commun.* **2008,** 10, 151-155.

48. Adams, L. A.; Poynton, S. D.; Tamain, C.; Slade, R. C. T.; Varcoe, J. R., *ChemSusChem* **2008,** 1, 79-81.

49. Macomber, C. S.; Boncella, J. M.; Pivovar, B. S.; Rau, J. A., *J. Therm. Anal. Calorim.* **2008,** 93, 225-229.

50. Agel, E.; Bouet, J.; Fauvarque, J. F., *J. Power Sources* **2001,** 101, 267-274.

51. Arges, C. G.; Ramani, V.; Pintauro, P. N., *Electrochem. Soc. Interface* **2010,** 19, 31-35.

52. Yan, J.; Hickner, M. A., *Macromolecules* **2010,** 43, 2349-2356.

53. Tanaka, M.; Koike, M.; Miyatake, K.; Watanabe, M., *Macromolecules* **2010,** 43, 2657-2659.

54. Clark, T. J.; Robertson, N. J.; Kostalik Iv, H. A.; Lobkovsky, E. B.; Mutolo, P. F.; Abruña, H. c. D.; Coates, G. W., *J. Am. Chem. Soc.* **2009,** 131, 12888-12889.

55. Hibbs, M. R.; Fujimoto, C. H.; Cornelius, C. J., *Macromolecules* **2009,** 42, 8316-8321.

56. Slade, R. C. T.; Varcoe, J. R., *Solid State Ionics* **2005,** 176, 585-597.

57. Danks, T. N.; Slade, R. C. T.; Varcoe, J. R., *J. Mater. Chem.* **2003,** 13, 712.

58. Kostalik, H. A.; Clark, T. J.; Robertson, N. J.; Mutolo, P. F.; Longo, J. M.; Abruña, H. c. D.; Coates, G. W., *Macromolecules* **2010,** 43, 7147-7150.

59. Robertson, N. J.; Kostalik, H. A.; Clark, T. J.; Mutolo, P. F.; Abruña, H. c. D.; Coates, G. W., *J. Am. Chem. Soc.* **2010,** 132, 3400-3404.

60. Shuang, G.; Rui, C.; Ting, L.; Zhongwei, C.; Minwei, S.; Yan, L.; Gaohong, H.; Yushan, Y., *Angew. Chem. Int. Ed.* **2009,** 48, 6499-6502.

61. Stokes, K. K.; Orlicki, J. A.; Beyer, F. L., *Polym. Chem.* **2011,** 2, 80-82.

62. Wang, J. H.; Li, S. H.; Zhang, S. B., *Macromolecules* **2010,** 43, 3890-3896.

63. Tarascon, J. M.; Armand, M., *Nature* **2001,** 414, 359-367.

64. Wakihara, M., *Mater. Sci. Eng.* **2001,** R33, 109-134.

65. Meyer, W. H., *Adv. Mater.* **1998,** 10, 439-448.

66. Zhang, S. S., *J. Power Sources* **2007,** 164, 351-364.

67. Kerr, J. B.; Liu, G.; Curtiss, L. A.; Redfern, P. C., *Electrochim. Acta* **2003,** 48, 2305-2309.

68. Croce, F.; Appetecchi, G. B.; Persi, L.; Scrosati, B., *Nature* **1998,** 394, 456-458.

69. Allcock, H. R.; O'Connor, S. J. M.; Olmeijer, D. L.; Napierala, M. E.; Cameron, C. G., *Macromolecules* **1996,** 29, 7544-7552.

70. Takeoka, S.; Ohno, H.; Tsuchida, E., *Polym. Advan. Technol.* **1993,** 4, 53-73.

71. Buriez, O.; Han, Y. B.; Hou, J.; Kerr, J. B.; Qiao, J.; Sloop, S. E.; Tian, M.; Wang, S., *J. Power Sources* **2000,** 89, 149-155.

72. Hooper, R.; Lyons, L. J.; Moline, D. A.; West, R., *Organometallics* **1999,** 18, 3249-3251.

73. Fauteux, D.; McCabe, P., *Polym. Advan. Technol.* **1995,** 6, 83-90.

74. Song, J. Y.; Wang, Y. Y.; Wan, C. C., *J. Power Sources* **1999,** 77, 183-197.

75. Shukla, A. K.; Kumar, T. P., *Curr. Sci. India* **2008,** 94, 314-331.

76. Ochiai, B.; Ootani, Y.; Maruyama, T.; Endo, T., *J. Poly. Sci., Part A: Polym. Chem.* **2007,** 45, 5781-5789.

77. Britz, J.; Meyer, W. H.; Wegner, G., *Macromolecules* **2007,** 40, 7558-7565.

78. Zhu, Z.; Einset, A. G.; Yang, C.-Y.; Chen, W.-X.; Wnek, G. E., *Macromolecules* **1994,** 27, 4076-4079.

79. Wei, X.; Shriver, D. F., *Chem. Mater*. **1998,** 10, 2307-2308.

80. Golden, J. H.; Chew, B. G. M.; Zax, D. B.; DiSalvo, F. J.; Frechet, J. M. J.; Tarascon, J.-M., *Macromolecules* **1995,** 28, 3468-3470.

81. Tuckerman, M. E.; Laasonen, K.; Sprik, M.; Parrinello, M., *J. Chem. Phys.* **1995,** 103, 150-161.

82. Jensen, M. O.; Rothlisberger, U.; Rovira, C., *Biophys. J.* **2005,** 89, 1744-1759.

83. Woudenberg, R. C., Jr. Anhydrous proton conducting materials for use in high temperature polymer electrolyte membrane fuel cells. PhD Thesis, University of Massachusetts, Amherst, **2007**.

CHAPTER 2

PROTON CONDUCTIVITY OF POLY(4-VINYL-1*H*-1,2,3-TRIAZOLE)

2.1 Introduction

Proton transport across polymeric membranes under anhydrous conditions is a fundamental process for high temperature proton exchange membrane fuel cells (PEMFCs). Over two centuries ago, Grotthuss suggested a mechanism of proton transport as involving diffusion of an excess proton, or a protonic defect, through a hydrogen bonded network of water molecules through rapid formation/cleavage of covalent bonds.[1] Although extensive research involving computational simulations[2-5] and experimental results[6-7] have helped significantly advance our understanding of the fundamentals of proton transport, much more remains to be learned.

As described in chapter 1, extensive research efforts have been devoted towards achieving anhydrous proton transport using nitrogenous bases such as benzimidazole,[8-9] imidazole and imidazole derivatives,[10-11] and triazole and triazole derivatives.[12-17] These heterocycles are not only amphoteric, have high boiling point, and undergo autoprotolysis,[18] but also have an advantage of organic tunability and can be immobilized covalently to a polymer thereby avoiding leaching issues during fuel cell operation. Zawodzinski *et al*.[15] have shown that proton conductivity can be altered by tuning the proton affinity of the heterocycle. Zhou *et al*.[12] have reported that conductivity can be increased by five orders of magnitude, by substituting imidazole pendant groups in vinyl heterocycle polymers with 1*H*-1,2,3-triazole. In recent years, proton mobility of imidazole based materials,[19-21] acid-base polymer blends[22-23] and triazole containing polymers[24] have been probed by solid state magic angle spinning (MAS) NMR. These studies have reported huge discrepancies between macroscopic proton conductivity and local proton mobility due to the complex nature of the systems studied. In this chapter, we have investigated proton transport in poly(4-vinyl-1-*H*-1,2,3-triazole) (PVTz), a simple polymer spin

system, to help elucidate its reported significantly higher conductivity compared to structurally similar poly(4-vinylimidazole). We have studied the proton dynamics of poly(4-vinyl-1-*H*-1,2,3-triazole) on a local scale by solid state MAS NMR and proton conductivity by impedance spectroscopy.

2.2 Experimental

2.2.1 Materials

Chloromethyl pivalate, sodium azide, copper(II) sulfate ($CuSO_4 \cdot 5H_2O$), sodium ascorbate, t-butanol (t-BuOH), ammonium hydroxide (NH_4OH), magnesium sulfate ($MgSO_4$), dimethylformamide (DMF) and azobisisobutyronitrile (AIBN) were purchased from Sigma-Aldrich or VWR and used as received. 1-buten-3-yne was purchased from GFS chemicals. Regenerated Cellulose dialysis tubing with a molecular weight cut off of 500 Da was purchased from Fisher Scientific. Azidomethyl pivalate was prepared as reported in the literature.[25]

2.2.2 Instrumentation

Solution ^{1}H-NMR (300 MHz) and ^{13}C-NMR (75 MHz) spectra were obtained on a Bruker DPX-300 NMR spectrometer. Fourier transform infrared (FT-IR) spectra of the samples were obtained using a Perkin Elmer Spectrometer. Gel permeation chromatography (GPC) measurements were done in DMF at a flow rate of 1.0 mL/min using a refractive index detector and the molecular weights are reported relative to polystyrene standards. Thermogravimetric analysis (TGA) was performed using a TA instruments TGA 2950 thermogravimetric analyzer with a nitrogen flow of 20 mL/min and a heating rate of 10 °C/min. The glass transition temperatures (T_g) of the polymer samples were obtained by differential scanning calorimetry (DSC) using a TA instrument DSC 2910. 3-5 mg of sample was heated at a rate of 10 °C/min

from -50 °C to 150 °C under nitrogen flow, first heating cycle was used to erase the thermal history of the material, and T_g values are reported from the second heating cycle.

Proton conductivity was measured by AC impedance spectroscopy using a Solatron 1287 potentiostat/1252A frequency response analyzer. Measurements were done by pressing the material between two blocking electrodes followed by application of 100 mV voltage with a frequency sweep from 3×10^5 to 1×10^{-1} Hz under vacuum to ensure an anhydrous environment. The resulting Z" vs. Z' plot was used to determine the resistance value at the minimum imaginary response. Given the area and thickness of the membrane, conductivity can be calculated from the resistance measured.[26]

2.3 Poly(4-vinyl-1*H*-1,2,3-trizole)

2.3.1 Synthesis

2.3.1.1 Monomer synthesis

The pivaloyloxymethyl protected vinyl triazole was synthesized by Hüsgen 1,3-dipolar cycloaddition reaction between vinyl acetylene and azidomethyl pivalate followed by removal of protecting group using sodium hydroxide and ethylene diamine, scheme 2.1.[27] Our synthesis of 4-vinyl-1*H*-1,2,3-triazole was performed using a different acetylene derivative than what has been described previously.[16, 28-30] Notably, use of vinyl acetylene decreases the synthesis by one step and improves the overall yield of the monomer. The monomer **2.2** was polymerized immediately after the deprotection step, as it tends to undergo thermal autopolymerization during storage at room temperature.

Synthesis of 4-vinyl-1*H*-1,2,3-triazole (2.2). In a glass bottle equipped with a magnetic stir-bar, vinyl acetylene gas (3.2 mL, 61.5 mmol) was condensed using dry ice. Then azidomethyl pivalate (14.5 g, 92.3 mmol), $CuSO_4 \cdot 5H_2O$ (4.8 g, 19.2 mmol), sodium ascorbate (3.81 g, 19.2 mmol) and 80 mL of t-butanol/H_2O (2:1) were added to the glass bottle. The reaction mixture was

allowed to warm to room temperature and stirred for 2 days. The reaction was stopped by adding 500 mL of ethyl acetate followed by washing with 5% NH_4OH (5 × 100 mL) and then with brine. The organic fractions were combined and dried over $MgSO_4$ and then the solution was concentrated by rotary evaporation. The resulting mixture was purified by flash chromatography using ethyl acetate: hexane (1:2) to yield (11 g, 85.3%) of **2.1**. This was deprotected using a literature procedure to yield **2.2** in 75% yield.[16] ^{1}H NMR (CD_2Cl_2) δ 12.97 (bs, 1H), 7.83 (s, 1H), 6.82 (q, 1H), 5.92 (d, 1H), 5.47 (d, 1H). ^{13}C NMR (CD_2Cl_2) δ 144.6, 128.7, 124.7, 117.6. EI-HRMS (m/z): calculated: 95.10; found: 95.05.

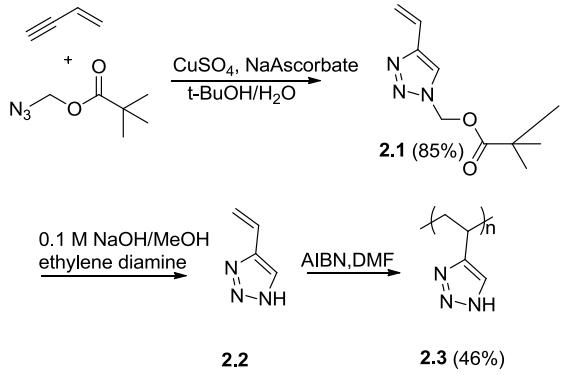

Scheme 2.1 Synthesis of poly(4-vinyl-1*H*-1,2,3-triazole)

2.3.1.2 Polymerization of 4-vinyl-1*H*-1,2,3-triazole

Free radical polymerization of **2.2** was performed in DMF (0.4 M) with AIBN (6% mole). The reaction mixture was subjected to 3 freeze-pump thaw cycles and then heated at 65 °C for 24 h. The resulting polymer (PVTz) (M_n = 14,000 g/mol, Đ = 1.6) was purified by membrane dialysis against water and methanol for 2 days each yielding 150 mg (46.8%) of **2.3**.

Pristine PVTz samples of two different molecular weights, 14,000 g/mol and 99,000 g/mol were purified by membrane dialysis. During the polymer isolation step, if membrane dialysis is not performed to purify the polymer, there is residual polymerization solvent, DMF in the polymer. Two non-purified samples contain 6 wt.% DMF (PVTz-6DMF) and 12 wt.% DMF

(PVTz-12DMF) as quantified by TGA. Polymers synthesized by free radical polymerization in DMF solvent were used for all the characterization and impedance spectroscopy measurements. Solid state NMR experiments were performed on a pristine PVTz sample, prepared by thermal autopolymerization of monomer **2.2**, thereby avoiding DMF contact with the sample prior to solid state NMR analysis.

2.3.1 FT-IR studies

Complete polymerization of monomer 4-vinyl-1*H*-1,2,3-triazole (VTz) was confirmed by FT-IR. The vinyl group C=C stretching absorption at 1640 cm^{-1} disappeared after polymerization, figure 2.1. N-H group in triazole ring showed a bending absorption near 1550 cm^{-1} and aromatic C=C group showed a stretching absorption near 1680 cm^{-1}. The presence of DMF in the wet polymer is indicated by a strong absorption of the carbonyl group at 1653 cm^{-1}.

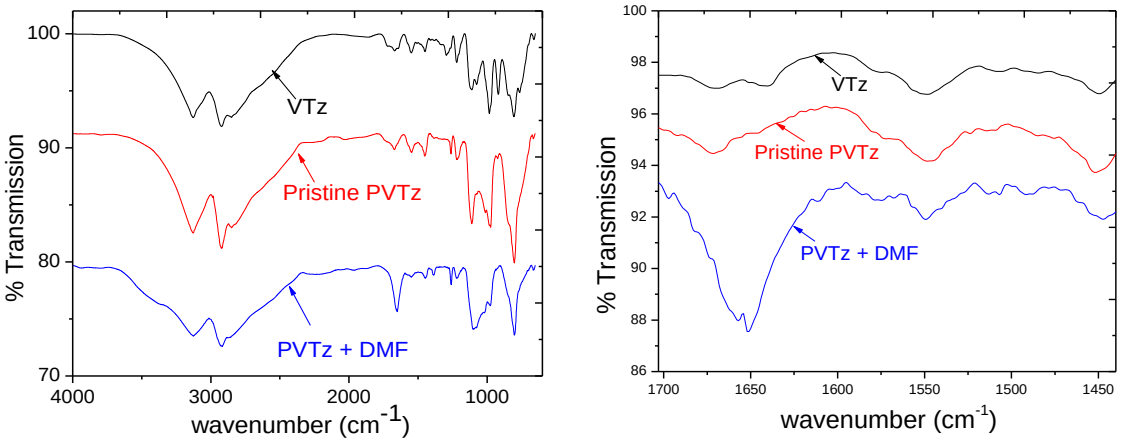

(a) (b)

Figure 2.1. FT-IR spectra of monomer VTz, pristine PVTz and wet PVTz. a) full spectra b) expanded view

2.3.3 Thermal properties

The onset of decomposition temperature corresponding to 2% weight loss, and glass transition temperature of all the samples are summarized in Table 2.1. Thermal analysis has shown that pristine PVTz is thermally stable up to 211 °C under nitrogen. The TGA traces of all the samples studied are shown in figure 2.2 and DSC traces are shown in figure 2.3. The glass transition temperature (T_g) of pristine PVTz is 38 °C, PVTz containing 6 wt. % DMF is 25 °C and that of containing 12 wt.% DMF is 18 °C. The glass transition temperature decreases as the DMF content increases due to the plasticization effect of the solvent.

Table 2.1. Thermal properties of the polymers studied.

Material	Wt. % DMF	T_{d2} (°C)	T_g (°C)
PVTz	0	211	38
PVTz-6DMF	6	175	25
PVTz-12DMF	12	53	18

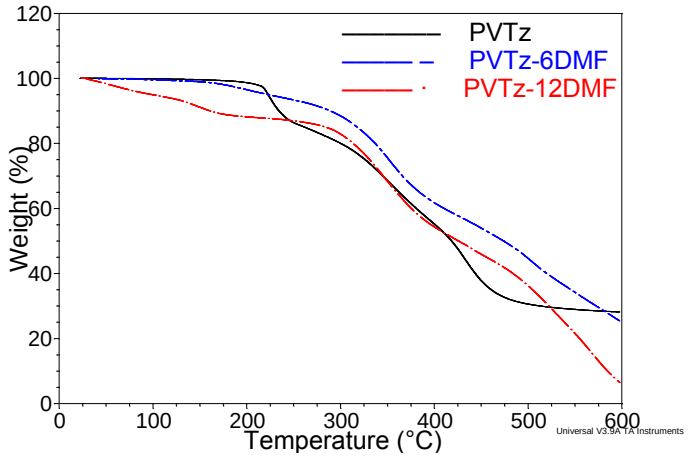

Figure 2.2. TGA traces of PVTz with varying residual DMF content.

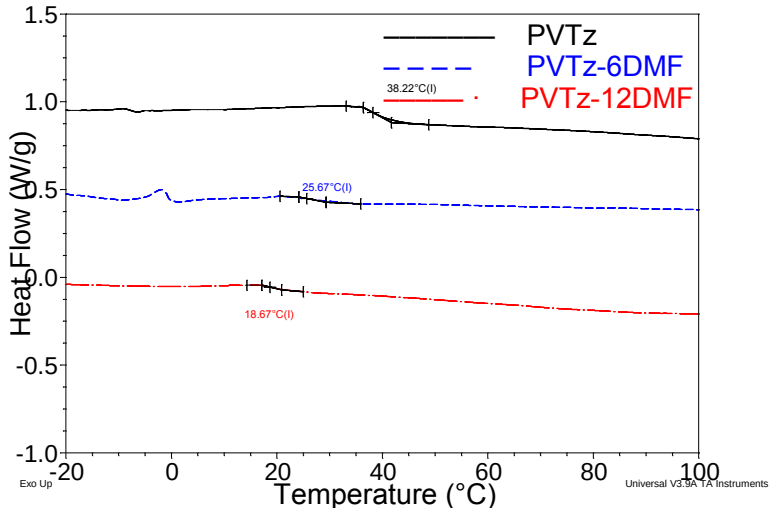

Figure 2.3. Heat flow vs. temperature curves for PVTz with varying residual DMF content. (The small spike in PVTz-6S at 0 °C is an instrument artifact.)

2.4 Proton transport

2.4.1 Impedance spectroscopy

The proton conductivity data of pristine PVTz of two different molecular weights and PVTz containing residual DMF are shown in figure 2.4 along with poly(4-vinylimidazole) conductivity data by Bozkurt *et al*.[31] and poly(4-vinyl-1*H*-1,2,3-triazole) conductivity data by Zhou *et al*.[12] for comparison.

The proton conductivity of pristine PVTz of two different molecular weights approaches 10^{-8} S/cm at 180 °C which is an order of magnitude greater than that reported for poly (4-vinylimidazole) by Bozkurt *et al*.[31] This can be explained by the difference in glass transition temperature of PVTz (T_g = 38 °C) compared to that of poly(4-vinylimidazole) (T_g = 160 °C[32]). It has been demonstrated that lower glass transition temperature facilitates proton conductivity due to improved segmental mobility.[16] The bulk proton conductivity of pristine PVTz of two different molecular weights (14,000 g/mol, 99,000 g/mol) is similar. This shows that proton conductivity is

almost independent of molecular weight. However, our data is four orders of magnitude lower that than reported by Zhou *et al*.[12] The proton conductivity of PVTz-6DMF containing 6 wt.% DMF is 2 orders of magnitude greater than that of pristine PVTz. For PVTz-12DMF, containing 12 wt.% DMF, the conductivity increases by four orders of magnitude compared to pristine PVTz. This conductivity data fortuitously is nearly identical to that reported by Zhou *et al*.[12] for poly(4-vinyl-1*H*-1,2,3-triazole). Overall, the presence of residual DMF in the polymer showed a dramatic ability to increase proton conductivity. Presumably, it is not a consequence of solvent plasticization effect as the presence of DMF resulted in only a moderate depression of glass transition temperature of the two polymers. However, DMF (being polarizable) may contribute to vehicular conduction of protons along with structure diffusion. Gas phase Gaussian calculations by Zawodzinski and coworkers have shown that presence of a solvent like water can dramatically reduce the activation barrier for proton transport between triazole molecules to the extent that process becomes almost barrierless.[33]

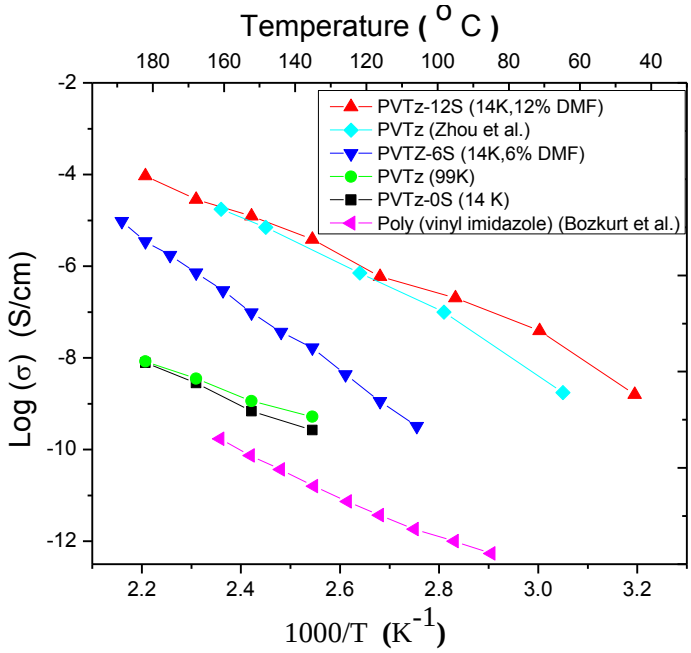

Figure 2.4. Proton conductivity of PVTz samples along with poly(4-vinylimidazole) and poly(4-vinyl-1*H*-1,2,3-triazole) from literature for comparison.[12, 31]

2.4.2 Solid state NMR

Local proton dynamics and hydrogen bond formation/breaking were studied by solid-state magic angle spinning (MAS) NMR. All the NMR studies are performed on pristine PVTz.

2.4.2.1 ^{1}H MAS NMR

The resonances of the aliphatic backbone CH_2 and CH protons appear at δ ~ 1-2 ppm, aromatic CH proton at δ ~ 8 ppm and hydrogen bonded acidic NH proton around δ 15.5 ppm, figure 2.5. The high chemical shift value of NH protons indicates their involvement in strong hydrogen bonds.[19] The stronger the hydrogen bond, the more is downfield shift. From quantum studies, it has been seen that the chemical shift of the hydrogen bonded protons can be correlated to the distance between hydrogen bonded atoms. The resonance with a chemical shift at 15 ppm indicates that the NH-NH contact is less than 3.5 Å.[34]

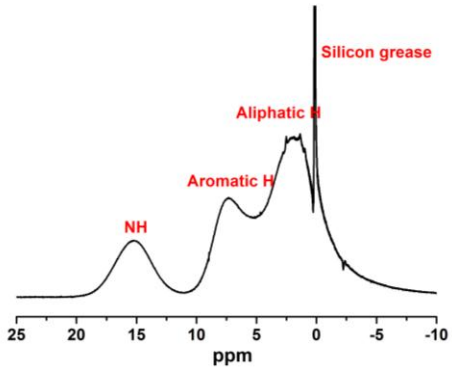

Figure 2.5. ^{1}H MAS NMR of PVTz at 260 K.

2.4.2.2 ^{13}C CP MAS NMR

In ^{13}C {1H} cross polarization (CP) MAS NMR, polarization is transferred from protons to a specific set of ^{13}C due to the ^{1}H-^{13}C dipolar interactions. The ^{13}C CP-MAS NMR spectrum of pristine PVTz, figure 2.6, exhibits three sets of signals of two aromatic carbons arising from an

inter conversion of the three possible tautomers on the NMR time scale. The percentages of three tautomers is approximately, a (15-17%), b (70-66%), c (15-17%).[35]

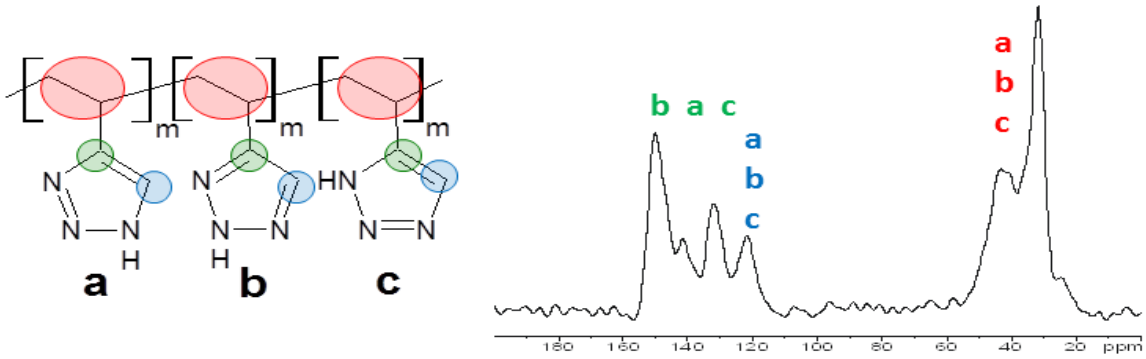

Figure 2.6. ^{13}C {1H} CP-MAS NMR @ 25 kHz (126 MHz) at 320 K.

2.4.2.3 Variable temperature ^{1}H MAS NMR

^{1}H variable-temperature (VT) MAS NMR were performed over a temperature range of 257- 419 K at 29762 Hz, figure 2.7, to help elucidate the effect of heating on local proton mobility. The molecular dynamics of the system were studied by analyzing the positions and intensities of the various resonances. With increase in temperature, the aromatic C-H proton signal at δ ~ 8 ppm becomes sharper indicating faster ring flipping. The NH protons show complex temperature dependence. As the temperature increases, the signal at δ 15 ppm first broadens, then shifts from δ 15 ppm to δ 9 ppm between 373 and 410 K, and then signal starts narrowing at δ 9 ppm indicating free NH sites at temperature above 410 K. The temperature range corresponding to the shift in the NH signal from δ 15 ppm to δ 9 ppm correlates to the temperature below which bulk H^{+} conductivity was too low to be measured by impedance spectroscopy.

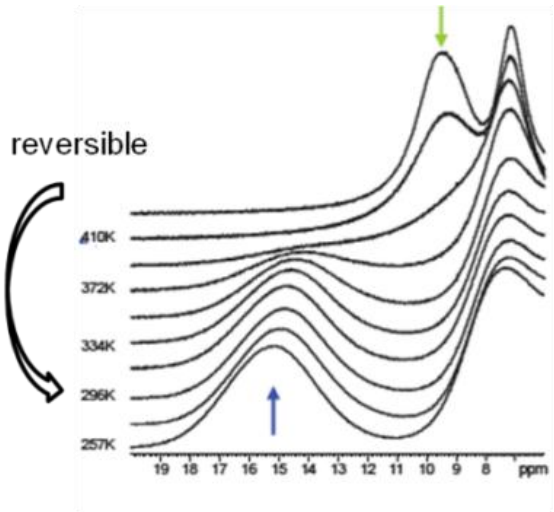

Figure 2.7. ^{1}H VT MAS NMR spectra of PVTz at 29762 Hz MAS (700.1 MHz)

2.4.2.4 ^{1}H-^{1}H SQ-DQ 2D MAS NMR

2.4.2.4.1 Description of 2D ^{1}H-^{1}H SQ-DQ NMR

High resolution two dimensional single-quantum double-quantum (2D SQ-DQ) ^{1}H-^{1}H MAS NMR spectroscopy provides semi-quantitative information about local structure and molecular dynamics. Graf *et al*. used this technique as a spectroscopic tool to study polymer chain dynamics in entangled polymer melts above their glass transition temperature,[36] and to monitor the crosslinking density in rubbery samples.[37] This technique when applied to study proton mobility helps identify the hydrogen bonded protons and thereby those H^{+} which contribute to charge transport.[19, 23-24]

In one-dimensional pulsed Fourier transform NMR, the spectrum is a function of one frequency variable, as it is obtained from the Fourier transformation of the free induction decay (FID) signal, which is a function of one time variable. In two-dimensional NMR, the FID signal is recorded as a function of two time variables, t_1 and t_2, and then Fourier transformation is applied twice to the resulting data to yield a spectrum which is a function of two frequency variables.

The ^{1}H-^{1}H double-quantum NMR experiment consists of four experimental periods, figure 2.8,[38] an initial double-quantum excitation t_{exc}, double-quantum evolution during t_1, followed by a double-quantum reconversion t_{rec}, and subsequent signal detection. In the first period, the sample is excited by one or two pulses, and the resulting magnetization is allowed to evolve over time t_1. In the reconversion period of the same duration as t_{exc}, also called the mixing time, the double-quantum coherences are transformed into longitudinal magnetization and after a 90° pulse, the FID signal is acquired, followed by recording of the signal as a function of time variable t_2. The signal is recorded only at the end of the sequence, during the time interval t_2.[36]

Figure 2.8. Experimental scheme for DQ NMR.[38]

The combination of double-quantum recoupling pulse sequences with fast MAS yields high resolution double-quantum NMR spectra of solid or partially mobile samples. In 2D DQ NMR, signals from dipolar coupled nuclear spin pairs are only seen. These dipolar interactions are strong in rigid molecules and are reduced with molecular motions occurring on the NMR time scale. As a result, strongly hydrogen bonded protons are clearly visible in the 2D ^{1}H DQ MAS NMR spectrum, while an isolated ^{1}H proton and a mobile ^{1}H proton do not contribute to the spectrum.[19]

To explain the general features of a 2D SQ-DQ NMR, a double-quantum spectrum of 1,4-polybutadiene as explained by Graf *et al*. is used as an example, figure 2.9.[37-38] In DQ NMR, each signal on single dimension gets split into multiple peaks depending upon its interaction with number of nuclei. On the DQ dimension, resonances are present at the sum of the ^{1}H-NMR frequencies of the two involved nuclei. The peaks arising from the interaction of protons with identical chemical shift are called auto peaks and are located on the diagonal, while the interactions between protons with different chemical shifts gives rise to cross peaks, located

symmetrically on either side of the diagonal. In the DQ spectrum of *cis*-polybutadiene, figure 2.9b, CH=CH and CH_2-CH_2 coherences are observed on the diagonal, and a cross peak for CH_2-CH coherence is observed on either side of the diagonal. As explained by Robert Graf, "the intensity of each peak is proportional to both the number of proton pairs giving rise to the double-quantum coherence and the efficiency of double-quantum excitation and reconversion, with the latter depending strongly on the strength of the dipolar coupling. The relative number of proton pairs in a polymer melt can be easily estimated by analyzing its monomeric unit, as indicated for *cis* poly-butadiene in the upper left corner of figure 2.9a by the dotted colored lines."[38]

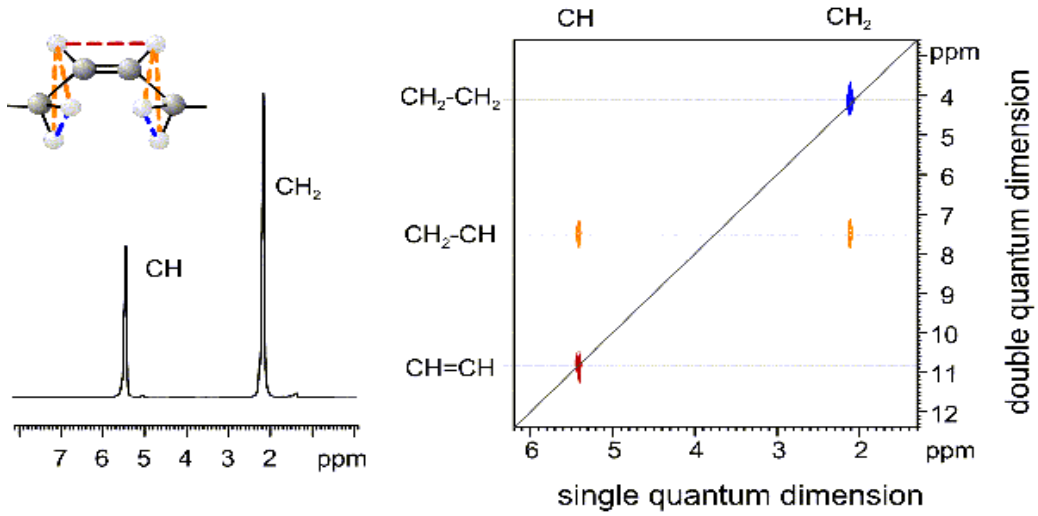

(a) (b)

Figure 2.9. a) ^{1}H MAS NMR of *cis*-polybutadiene. b) 2D ^{1}H-^{1}H SQ-DQ MAS NMR spectrum of *cis*-polybutadiene.[38]

2.4.2.4.2 ^{1}H-^{1}H SQ-DQ MAS NMR of pristine PVTz

Two-dimensional single-quantum double-quantum (2D SQ-DQ) ^{1}H-^{1}H MAS NMR spectroscopy was performed at two different temperatures; one close to T_g (determined by DSC), and the other ~ 100 °C above T_g, figure 2.10. It revealed not only spatial proximities among various proton sites but also identified hydrogen-bonded protons that are mobile on the time scale of this NMR experiment (33 µs) and thus potentially contribute to bulk proton conductivity.

The interaction between spins of aromatic protons gives an auto peak at δ 7.5/15 ppm (labeled as BB) at 324 K, indicating close spatial proximity of neighboring triazole rings as there is only one aromatic CH on each triazole ring. This auto peak is also visible in the spectrum at 410 K, though reduced in intensity. This indicates close packing between triazole rings which restricts ring mobility.[22] There is an auto-correlation peak for NH protons at δ 15/30 ppm (AA peak) at 324 K, but not seen at 410 K. At low temperatures, NH protons are involved in strong hydrogen bonding, connecting neighboring triazole rings forming dimer like structures. With increase in temperature, the hydrogen bond strength decreases and NH protons become mobile on the time scale of the NMR experiment.

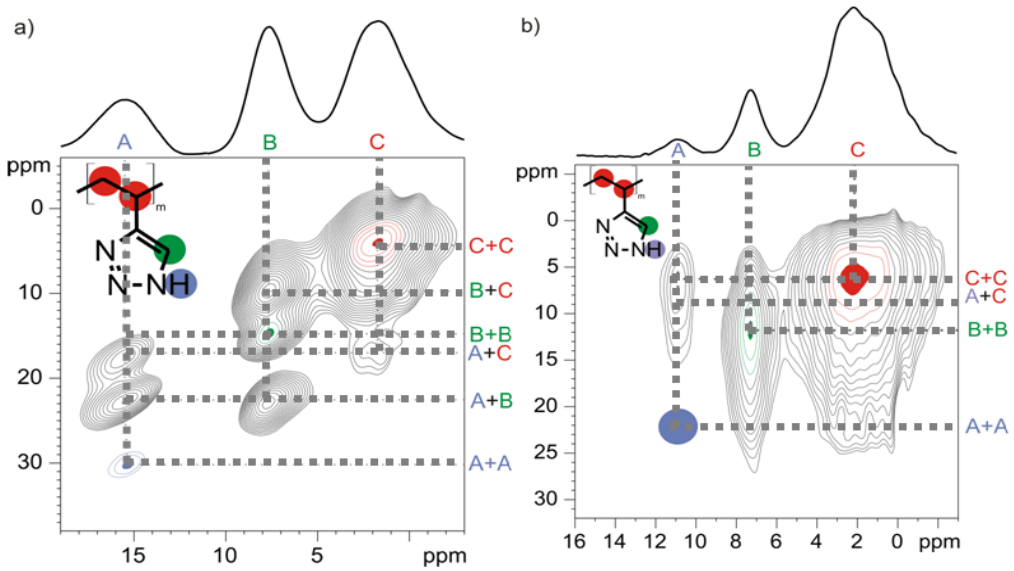

Figure 2.10. ^{1}H-^{1}H SQ-DQ MAS NMR spectra at 700.1 MHz and 29762 Hz MAS at a) 324 K and b) 410 K. Peak A can be assigned to the NH protons, B to the ring proton and C reflects the aliphatic backbone. Note the missing auto-peak AA at T > T_g, which indicates fast dynamics.

Thus the DQ NMR suggests that the triazole rings are in close spatial proximity of each other even at elevated temperature of 410 K which implies restricted ring mobility. The triazole rings are forming a dimeric structure limiting proton conductivity at low temperatures. Similar studies have been previously performed on poly(vinylphosphonic acid) derivatives[39] and triazole functionalized poly(siloxanes).[24]

2.4.3. Comparison of macroscopic and microscopic proton conductivity

The exchange between mobile and rigid N-H protons representing local proton mobility is probed by spin-spin relaxation and characterized by transverse relaxation time, T_2*. The temperature dependence of T_2* can be described by an Arrhenius relation, eq. 2-1, where Ω is the exchange rate and E_a is the activation energy.[19] From this correlation, figure 2.11a, an activation energy of 27 kJ/mol (0.28 eV) is obtained for the observed NH protons on the time scale of the NMR experiment (33 µs).

$$\Omega = \frac{1}{\pi T_2^*} = \Omega_o \, e^{-\frac{E_a}{RT}} \qquad 2\text{-}1$$

The proton conductivity data obtained from impedance spectroscopy represents macroscopic charge transport. The data can be fitted by the Arrhenius equation 2.2, indicating hopping like conduction mechanism.[40] In eq. 2.2, σ_o is the pre-exponential term, E_a is the activation energy and *k* is the Boltzmann constant. From figure 2.11b, an activation barrier of ~ 85 kJ/mol (0.88 eV) is obtained, almost thrice that is obtained from NMR measurements.

$$\sigma = \sigma_0 \cdot e^{-\frac{E_a}{kT}} \qquad 2\text{-}2$$

The NMR experiments were performed at a rotor speed of 29762 Hz, corresponding to the time scale of 33 µs. The impedance spectroscopy measurements were performed over a frequency range of 0.1 Hz – 300 kHz (10 sec to 3.3 µs), however an intermediate frequency range was chosen for data analysis. The DC limit resistance, derived from impedance spectroscopy is dependent upon the sample geometry and not specifically on the frequency range. However, for approximate comparison purposes, the time scales probed by impedance to obtain the resistance were in the range of 1 ms – 300 ms. Comparison between local processes probed by NMR techniques and bulk measurements is not straightforward. Nevertheless, evaluation of macroscopic proton conductivity obtained from impedance spectroscopy and local proton mobility from NMR studies show that they both exhibit Arrhenius type temperature dependence. Significantly larger activation energy for macroscopic proton transport indicates that in addition

to local hydrogen bond dynamics observed by NMR, there are other processes affecting the macroscopic proton transport. There could be several reasons for this discrepancy. The Grotthuss mechanism involves solvent reorientation and bond formation/ cleavage whereas only bond formation and breaking were taken into account in calculating the microscopic scale activation energy. SQ-DQ MAS NMR results indicate limited reorientation of triazolium rings due to steric confinement. Secondly, it has been reported that proton transport in triazole takes place along a zig-zag like pathway which leads to parasitic proton transfer and does not contribute to bulk proton conductivity.[41] Goward *et al*. reported similar differences in micro- and macroscopic activation energy for imidazole based proton conductors.[19] From NMR studies on imidazole rings, it was seen that the different activation energies arise from relative strength of electrostatic interactions and from packing geometries.[42] Also, similar discrepancies in the bulk and the local activation energy were observed in triazole functionalized poly(siloxanes).[24]

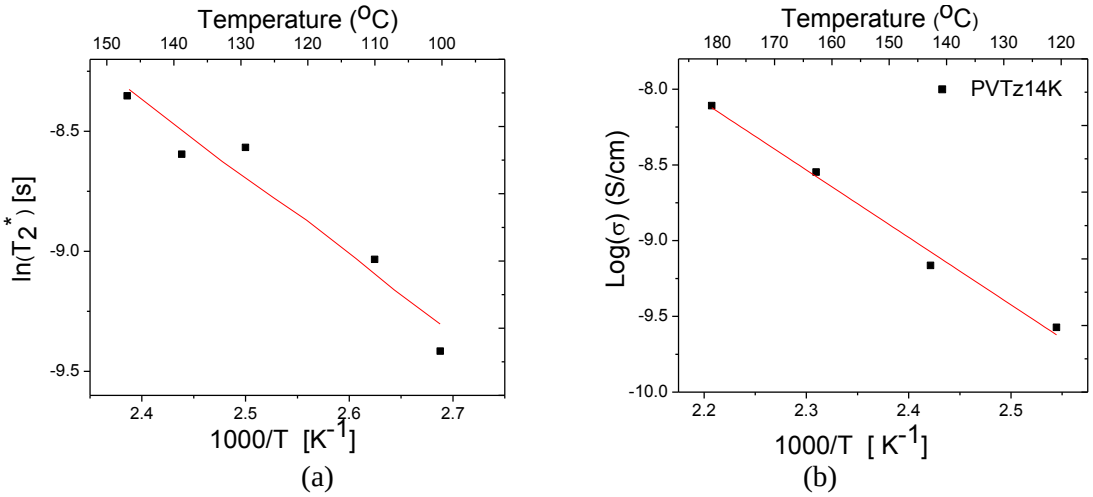

Figure 2.11. a) Arrhenius plot of temperature dependent relaxation behavior of mobile protons, obtained from the ^{1}H-NMR resonance linewidth b) Arrhenius plot of macroscopic conductivity from impedance spectroscopy.

2.5 Conclusions

In summary, poly(4-vinyl-1*H*-1,2,3-triazole) constitutes a rather simple polymeric system to study the Grotthuss-type mechanism of proton transport on both the macroscopic and the

microscopic scale. While the proton conductivity of poly(4-vinyl-1*H*-1,2,3-triazole) does not depend significantly on the molecular weight of the respective polymer, presence of residual solvent (i.e. DMF) showed a remarkable increase in proton conductivity. Local dynamic processes on the molecular level that contribute to bulk proton transport in poly(4-vinyl-1*H*-1,2,3-triazole) were studied by ^{1}H MAS NMR. These NMR studies help to relate local structure and mobility of protons to macroscopic proton conductivity measured by impedance spectroscopy, which will allow for a more rationalized tailoring of proton-conducting polymers.

2.6 References

1. de Grotthuss, C. J. T., *Ann. Chim.* **1806,** LVIII, 54-74.

2. Roscioli, J. R.; McCunn, L. R.; Johnson, M. A., *Science* **2007,** 316, 249-254.

3. Münch, W.; Kreuer, K. D.; Silvestri, W.; Maier, J.; Seifert, G., *Solid State Ionics* **2001,** 145, 437-443.

4. Lobaugh, J.; Voth, G. A., *J. Chem. Phys.* **1996,** 104, 2056-2069.

5. Schmitt, U. W.; Voth, G. A., *J. Chem. Phys.* **1999,** 111, 9361-9381.

6. Kreuer, K.-D., *Chem. Mater.* **1996,** 8, 610-641.

7. Hickner, M.; Ghassemi, H.; Kim, Y.; Einsla, B.; McGrath, J., *Chem. Rev.* **2004,** 104, 4587-4612.

8. Xiao, L.; Zhang, H.; Scanlon, E.; Ramanathan, L. S.; Choe, E.-W.; Rogers, D.; Apple, T.; Benicewicz, B. C., *Chem. Mater.* **2005,** 17, 5328-5333.

9. Woudenberg, R. C.; Yavuzcetin, O.; Tuominen, M. T.; Coughlin, E. B., *Solid State Ionics* **2007,** 178, 1135-1141.

10. Schuster, M. F. H.; Meyer, W. H.; Schuster, M.; Kreuer, K. D., *Chem. Mater.* **2004,** 16, 329-337.

11. Schuster, M. F. H.; Meyer, W. H., *Annu. Rev. Mater. Res.* **2003,** 33, 233-261.

12. Zhou, Z.; Li, S.; Zhang, Y.; Liu, M.; Li, W., *J. Am. Chem. Soc.* **2005,** 127, 10824-10825.

13. Li, S.; Zhou, Z.; Zhang, Y.; Liu, M.; Li, W., *Chem. Mater.* **2005,** 17, 5884-5886.

14. Celik, S. U.; Aslan, A.; Bozkurt, A., *Solid State Ionics* **2008,** 179, 683-688.

15. Subbaraman, R.; Ghassemi, H.; Zawodzinski, T. A. J., *J. Am. Chem. Soc.* **2007,** 129, 2238-2239.

16. Granados-Focil, S.; Woudenberg, R. C.; Yavuzcetin, O.; Tuominen, M. T.; Coughlin, E. B., *Macromolecules* **2007,** 40, 8708-8713.

17. Martwiset, S.; Yavuzcetin, O.; Thorn, M.; Versek, C.; Tuominen, M.; Coughlin, E. B., *J. Polym. Sci.,Part A: Polym. Chem.* **2009,** 47, 188-196.

18. Scharfenberger, G.; Meyer, W. H.; Wegner, G.; Schuster, M.; Kreuer, K. D.; Maier, J., *Fuel Cells* **2006,** 6, 237-250.

19. Goward, G. R.; Schuster, M. F. H.; Sebastiani, D.; Schnell, I.; Spiess, H. W., *J. Phys. Chem. B* **2002,** 106, 9322-9334.

20. Hickman, B. S.; Mascal, M.; Titman, J. J.; Wood, I. G., *J. Am. Chem. Soc.* **1999,** 121, 11486-11490.

21. Bureekaew, S.; Horike, S.; Higuchi, M.; Mizuno, M.; Kawamura, T.; Tanaka, D.; Yanai, N.; Kitagawa, S., *Nat. Mater.* **2009,** 8, 831-836.

22. Celik, S. U.; Akbey, U.; Graf, R.; Bozkurt, A.; Spiess, H. W., *Phys. Chem. Chem. Phys.* **2008,** 10, 6058-6066.

23. Ümit, A.; Robert, G.; Peng, Y. G.; Chu, P. P.; Spiess, H. W., *J. Polym. Sci., Polym. Phys.* **2009,** 47, 138-155.

24. Akbey, Ü.; Granados-Focil, S.; Coughlin, E. B.; Graf, R.; Spiess, H. W., *J. Phys. Chem. B* **2009,** 113, 9151-9160.

25. Loren, J. C.; Krasinski, A.; Fokin, V. V.; Sharpless, K. B., *Synlett* **2005**, 2847-2850.

26. Bruce, P. G., *Polymer Electrolyte Reviews*. 1 ed.; Elsevier Applied Science: New York, **1987**; Vol. 1, pp 237-274.

27. Rostovtsev, V. V.; Green, L. G.; Fokin, V. V.; Sharpless, K. B., *Angew. Chem., Int. Ed.* **2002,** 41, 2596-2599.

28. Thibault, R. J.; Takizawa, K.; Lowenheilm, P.; Helms, B.; Mynar, J. L.; Frechet, J.; Hawker, C. J., *J. Am. Chem. Soc.* **2006,** 128, 12084-12085.

29. Wouters, G.; Smets, G., *Makromol. Chem.* **1982,** 183, 1861-1868.

30. Takizawa, K.; Nulwala, H.; Thibault, R. J.; Lowenhielm, P.; Yoshinaga, K.; Wooley, K. L.; Hawker, C. J., *J. Polym. Sci.,Part A: Polym. Chem.* **2008,** 46, 2897-2912.

31. Bozkurt, A.; Meyer, W. H., *Solid State Ionics* **2001,** 138, 259-265.

32. Li, X.; Goh, S. H.; Lai, Y. H.; Wee, A. T. S., *Polymer* **2001,** 42, 5463-5469.

33. Subbaraman, R.; Ghassemi, H.; Zawodzinski Jr, T., *Solid State Ionics* **2009,** 180, 1143-1150.

34. Schnell, I.; Spiess, H. W., *J. Magn. Reson.* **2001,** 151, 153.

35. Toppet, S.; Wouters, G.; Smets, G., *J. Polym. Sci. Pol. Lett.* **1976,** 14, 389-394.

36. Graf, R.; Heuer, A.; Spiess, H. W., *Phys. Rev. Lett.* **1998,** 80, 5738-5741.

37. Graf, R.; Demco, D. E.; Hafner, S.; Spiess, H. W., *Solid State Nucl. Magn. Reson.* **1998,** 12, 139-152.

38. Graf, R. http://www.mpip-mainz.mpg.de/~graf/documents/research.html (accessed April 30, 2011).

39. Brunklaus, G.; Schauff, S.; Markova, D.; Klapper, M.; Mullen, K.; Spiess, H.-W., *J. Phys. Chem. B.* **2009,** 113, 6674-6681.

40. Ünügür-Celik, S.; Akbey, Ü.; Bozkurt, A.; Graf, R.; Spiess, H. W., *Macromol. Chem. Phys.* **2008,** 209, 593-603.

41. Woudenberg, R. C., Jr. Anhydrous proton conducting materials for use in high temperature polymer electrolyte membrane fuel cells. PhD Thesis, University of Massachusetts, Amherst, **2007**.

42. Fischbach, I.; Spiess, H. W.; Saalwachter, K.; Goward, G. R., *J. Phys. Chem. B* **2004,** 108, 18500-18508.

CHAPTER 3

HYBRID INORGANIC-ORGANIC PROTON EXCHANGE MEMBRANES CONTAINING 1*H*-1,2,3-TRIAZOLE MOIETIES

3.1 Introduction

Intensive research efforts have been made to achieve anhydrous proton conduction by replacing water with heterocycles, e.g., imidazole, benzimidazole.[1-4] In these amphoteric nitrogen containing heterocycles, proton transport takes place through a hydrogen bonded network of heterocycles by a process of hydrogen bond formation and breaking.[5-6] Previously, the proton conducting properties of poly(acrylates), poly(siloxanes) and poly(phosphazenes) with pendant 1*H*-1,2,3-triazole as a protogenic group have been studied in our group.[7-10] The amorphous nature of these low T_g polymers allows for high local mobility of triazoles, thereby giving proton conductivity in the range of 0.01 – 1 μS/cm at 180 °C; however, they do not form self-supporting membranes. For efficient fuel cell operation, membranes must also be mechanically robust. Developing a membrane with good mechanical properties along with high conductivity is a challenge.

Proton exchange membranes can be mechanically reinforced by crosslinking or nano-confinement in a porous medium.[11-14] Li *et al*. reported mechanically robust hybrid inorganic-organic membranes containing condensed organosilicon precursors with grafted imidazole and benzimidazole. These membranes were shown to have conductivity of the order of 10^{-3} S/cm at 120 °C after doping with H_3PO_4.[15] Similarly, membranes composed of benzimidazole covalently bonded to an inorganic SiO_2 network by a flexible spacer were investigated by Herz *et al*.[16] Furthermore, Li and coworkers reported that the grafting of 1*H*-1,2,4-triazole onto a hybrid inorganic-organic polymer network enhances the proton conductivity of the hybrid membranes doped with H_3PO_4.[17]

In the present work, we have focused on structural reinforcement of 1*H*-1,2,3-triazole functionalized poly(siloxane), a low T_g polymer, by crosslinking using sol-gel chemistry.[18] The macroscopic and microscopic proton conduction behavior of 1*H*-1,2,3-triazole functionalized poly(siloxane) (Tz5Si) was reported recently.[19] In this work, we have studied the effect of crosslinking on proton conductivity and mechanical properties of triazole functionalized poly(siloxane) which has the same spacer length between the 1*H*-1,2,3-triazole and polymer backbone as that of the previously reported Tz5Si.

3.2 Experimental

3.2.1 Materials

Allyl bromide, propargyl alcohol, sodium hydride, chloromethyl pivalate, sodium azide, tetraethoxy silane (TEOS), triethoxy silane, copper(II) sulfate ($CuSO_4 \cdot 5H_2O$), sodium ascorbate, t-butanol (t-BuOH), ammonium hydroxide (NH_4OH), Karstedt's catalyst, trifluoroacetic acid (TFA), phosphoric acid (H_3PO_4) and hydroxyl terminated polyethylene glycol (PEG) ($M_n \sim 300$ g/mol) were purchased from Sigma-Aldrich or VWR and used as received. Azidomethyl pivalate was prepared as reported in the literature.[20] 3-allyloxyprop-1-yne was synthesized as previously reported.[19]

3.2.2 Instrumentation

^{1}H-NMR and ^{13}C-NMR spectra were obtained on a Bruker DPX-300 NMR spectrometer. Fourier-transform infrared (FT-IR) spectra were obtained using a Perkin Elmer Spectrometer. Thermogravimetric analysis (TGA) was performed using a TA instruments TGA 2950 thermogravimetric analyzer at a heating rate of 10 °C/min under nitrogen flow of 20 mL/min. Glass transition temperatures were obtained using TA instrument DSC 2910 differential scanning calorimeter (DSC) by heating the samples at a rate of 10 °C/min under nitrogen flow (50

mL/min). Electrochemical impedance data was obtained using a Solatron 1287 potentiostat/1252A frequency response analyzer. Measurements were done by pressing the polymer samples between two gold coated blocking electrodes followed by an application of 100 mV excitation voltage with a logarithmic frequency sweep from 3×10^5 to 1×10^{-1} Hz under vacuum to ensure an anhydrous environment. Z" vs. Z' plot was used to determine the resistance values at the minimum imaginary response.[21] A Hysitron Triboindenter was used for nanoindentation studies.

3.3 1*H*-1,2,3-triazole functionalized polysiloxane crosslinked membranes

3.3.1 Synthesis

Azide-alkyne Hüsgen 1,3-dipolar cycloaddition reaction, "click" chemistry, was used to synthesize 4-(allyloxymethyl)-[1,2,3]triazol-1-ylmethyl pivalate **3.3**, scheme 3.1. The Pt^0 catalyzed hydrosilylation[22-23] reaction between vinyl group of **3.3** and Si-H bond of triethoxy silane gave the sol-gel monomer **3.4** (Tz5TrS). The triazole terminated sol-gel monomer **3.4** was deprotected and then crosslinked with tetraethoxy silane (TEOS) and polyethylene glycol (PEG) by hydrolysis and condensation in the presence of acidified water, scheme 3.2. Polyethylene glycol being a flexible spacer, reduces shrinkage during drying and brittleness of the membrane.[14] In order to confirm that PEG is covalently bonded in the crosslinked network, a 1PEG-1TEOS-1Tz5TrS film was submerged in D_2O at room temperature for 2 d. ^{1}H-NMR analysis of that D_2O showed no presence of PEG indicating that PEG is covalently bonded to the network and not just trapped within the network as a dopant. All the membranes studied have residual ethylene diamine and NaCl from the deprotection step to remove the pivalate group. These byproducts were not removed by washing of membranes with water as that will lead to leaching of doped acid as well, making it difficult to quantify the amount of acid present in the material. At the same

time, acid doping cannot be done after crosslinking and washing steps, due to the insolubility of the crosslinked membranes.

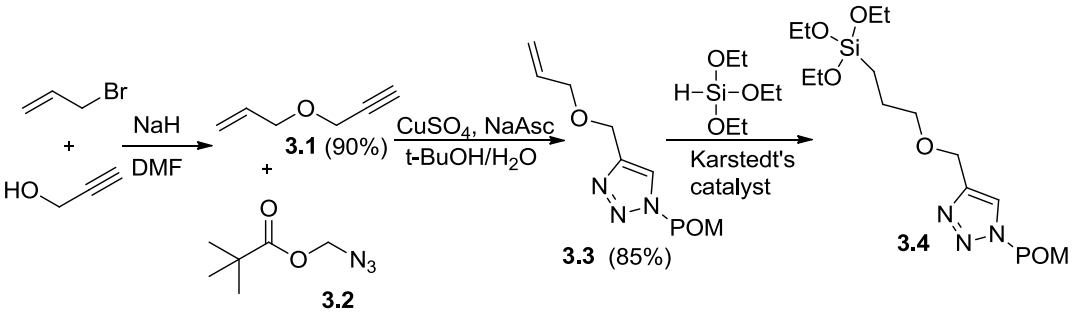

Scheme 3.1. Synthetic route to 2,2-dimethyl-propionic acid-4-(3-triethoxysilylpropyloxymethyl)-[1,2,3]triazol-1-ylmethyl ester (Tz5TrS). [Pivaloxymethyl group is abbreviated as POM]

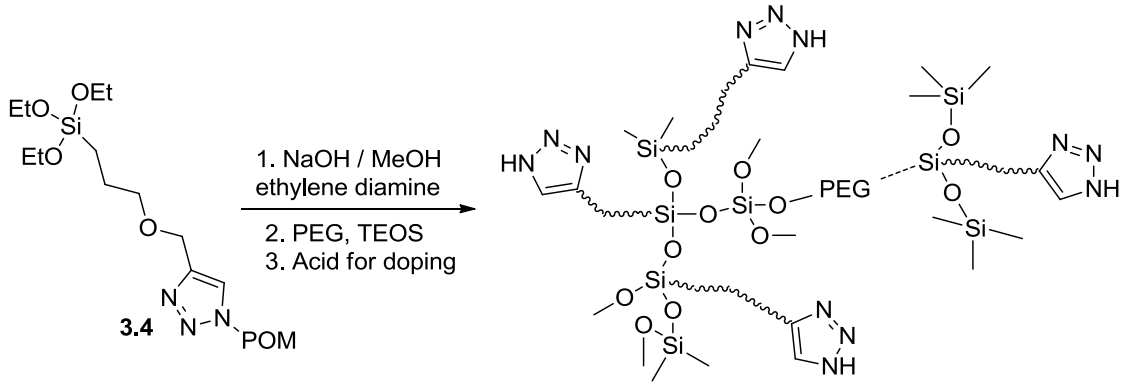

Scheme 3.2. Preparation of hybrid inorganic-organic copolymer

Synthesis of 4-(allyloxymethyl)-[1,2,3]triazol-1-ylmethyl pivalate (3.3). To a 250 mL nitrogen purged round bottom flask, **3.1** (2 g, 0.02 mol) was added to 40 mL of *t*-butanol/water (2/1) mixture, followed by the addition of $CuSO_4 \cdot 5H_2O$ (0.79 g, 3.15 mmol), sodium ascorbate (0.83 g, 4.2 mmol) and azidomethyl pivalate **3.2** (3.63 g, 90 mol). The reaction mixture was allowed to stir for 2 days at room temperature. The reaction was terminated by adding water (50 mL), followed by extraction with ethyl acetate (5 × 100 mL) and then washing with 5% NH_4OH solution. The organic layers were combined and washed with brine, dried over $MgSO_4$ and the solvent was removed under reduced pressure. The crude product obtained was purified by flash

chromatography using ethyl acetate: hexane (1:4) and then (1:3) to yield **3.3** as an oily-yellow liquid. Yield = 4.5 g, 84.7%. ^{1}H-NMR ($CDCl_3$, 300 MHz) δ 1.13 (s, 9H), 4.07 (t, 2H), 4.63 (s, 2H), 5.15 (d, 1H), 5.24 (d, 1H), 5.9 (m, 1H), 6.2 (s, 2H), 7.78 (s, 1H). ^{13}C-NMR ($CDCl_3$, 75 MHz) δ 26.72, 38.68, 63.21, 69.62, 71.45, 117.58, 123.94, 134.11, 145.63, 177.61.

Synthesis of 2,2-dimethyl-propionic acid-4-(3-triethoxysilylpropyloxymethyl)-[1,2,3]triazol-1-ylmethyl ester (3.4) (Tz5TrS). In a dry box, **3.3** (159 mg, 0.63 mmol), triethoxysilane (154 mg, 0.94 mmol) and toluene (0.38 mL, 4 M) were combined in a small reaction vial equipped with a magnetic stirrer. The mixture was allowed to stir for 5 min followed by an addition of 5 drops of Karstedt's catalyst. The vial was then removed from the dry box and the solution was allowed to stir at 70 °C for 2 days. The solvent was removed under vacuum and the resulting product was an oily yellow liquid. It was used without further purification as exposure to moisture leads to hydrolysis of alkoxysilyl groups. ^{1}H-NMR ($CDCl_3$, 300 MHz) δ 0.7 (m, 2H), 1.2 (s, 9H), 1.28-1.42 (m, 9H), 1.85 (m, 2H), 3.56 (t, 2H), 3.9-4.05 (m, 6H), 4.68 (s, 2H), 6.25 (s, 2H), 7.83 (s, 1H). ^{13}C-NMR ($CDCl_3$, 75 MHz) δ 6.53, 18.35, 26.85, 38.82, 64.14, 69.16, 73.18, 123.84, 146.16, 177.80.

3.3.2 Preparation of membranes

The first step involved removal of the pivaloxymethyl (POM) protecting group from the precursor by using sodium methoxide. Precursor Tz5TrS-POM (0.3 g, 0.7 mmol), ethylene diamine (75 μL, 1.12 mmol) and 0.1 M NaOH/MeOH (10.5 mL, 1.05 mmol) were combined in a vial and allowed to stir for 2 h. The reaction mixture was then concentrated to half of its original volume by rotary evaporation. The pH of the solution was adjusted to 4 using a 1 M solution of HCl followed by addition of TEOS and PEG. The mixture was allowed to stir at room temperature for at least 12 h. Then TFA or H_3PO_4 was added and the solution was allowed to stir for 2 h to form uniform sols. Films were then cast and dried in a stepwise manner; 24 h at room

temperature and atmospheric pressure followed by drying under vacuum at room temperature for 24 h, then 55 °C - 60 °C for 2 days, 80 °C for 3 h and then finally at 100 °C for 2 h to evaporate organic solvents and water. These membranes were stored under vacuum at 30 °C as they are hygroscopic in nature. The samples are labeled by their mole composition as *x*PEG-*y*TEOS-*z*Tz5TrS-*a*TFA-*b*P where *x*, *y*, *z*, *a*, *b* refer to moles of PEG, TEOS, precursor Tz5TrS, TFA and H_3PO_4 respectively.

3.3.3 FT-IR study

The removal of the POM-protecting group from the 1,2,3-triazole tethered to siloxane was confirmed by FT-IR spectrum of the condensed Tz5TrS membrane. The C=O group absorption at 1740 cm^{-1} in protected Tz5TrS disappeared after deprotection indicating complete removal of POM group. The deprotection was also confirmed by the presence of N-H group absorption at 3424 cm^{-1}. Figure 3.1 shows the IR spectra of condensed Tz5TrS, before and after deprotection.

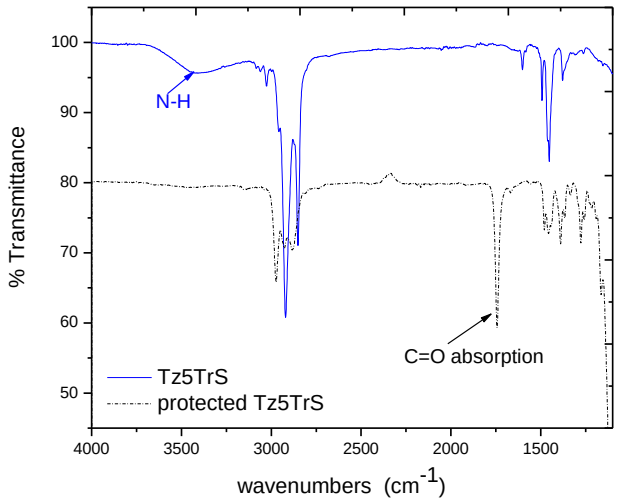

Figure 3.1. FT-IR spectra of condensed Tz5TrS

3.3.4 Appearance of hybrid inorganic-organic membranes

Free-standing membranes with thicknesses of 100 µm – 150 µm were obtained. Membranes without PEG were stiff and brittle. Addition of PEG imparts flexibility to these membranes, as highly flexible ethylene oxide chains connect the three dimensional Si-O-Si network. The membranes shown in figure 3.2 are self-supporting.

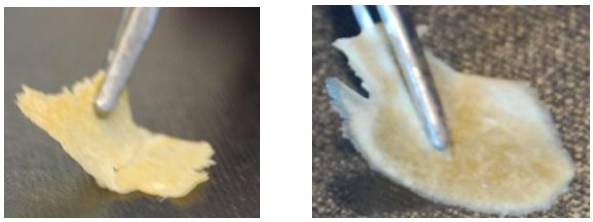

(a) (b)

Figure 3.2. Appearance of membranes a) 1PEG-1TEOS -1Tz5TrS-1TFA b) 1PEG-1TEOS -1Tz5TrS-2.5P

3.3.5 Thermal properties

The decomposition temperatures of all the samples studied were determined by TGA. Thermogravimetric analysis has shown that all the materials are thermally stable up to 180 °C under nitrogen. The small weight loss below the decomposition temperature is due to the loss of water and solvents which tend to remain in the membrane, figure 3.3. The onset of decomposition, temperature corresponding to 5% weight loss (T_{d5}), and glass transition temperatures of all the samples are summarized in Table 3.1. The decomposition temperatures for crosslinked membranes are in the temperature range similar to that reported for Tz5Si and other triazole functionalized siloxane polymers.[7, 19]

The shape of the decomposition curve of materials doped with TFA is similar to that of condensed Tz5TrS. Similarly, no change in decomposition behavior of triazole functionalized polysiloxane homopolymers after doping with TFA has been reported.[7] However, degradation of phosphoric acid doped samples is lower over the measured temperature range. This is due to the

complexation of phosphoric acid with the polymer, similar to that observed for phosphoric acid doped polybenzimidazole (PBI).[24]

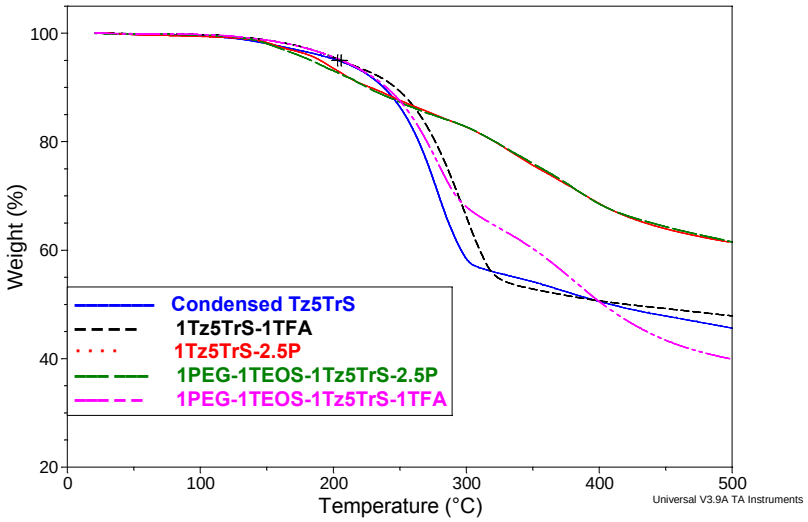

Figure 3.3. TGA traces of the membranes studied

All the polymers show a single glass transition temperature (T_g). The relevant traces obtained from DSC on the second heating cycle are shown in figure 3.4. The glass transition temperature of condensed Tz5TrS is higher than that of other materials due to the restricted segmental relaxation in the crosslinked network. As expected, the glass transition temperature of PEG containing hybrid membranes is lower. Also, addition of acid leads to lowering of glass transition temperature due to a plasticization effect.

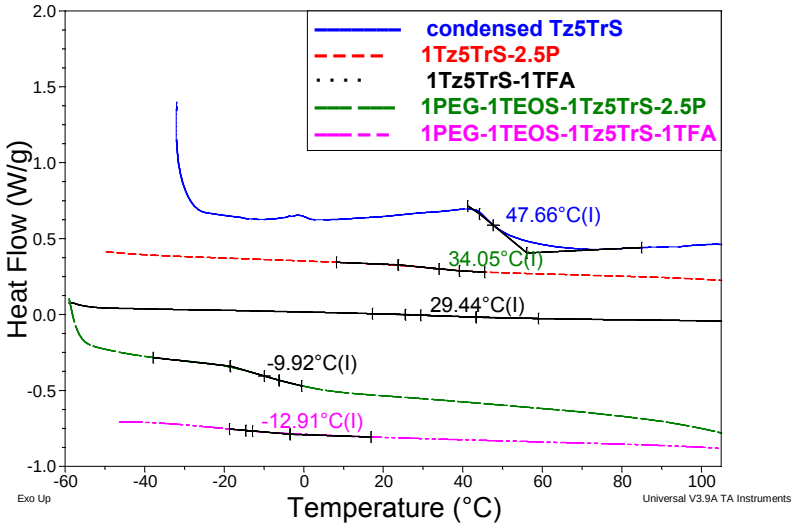

Figure 3.4. DSC traces of the membranes studied

Table 3.1. Thermal properties of the materials studied

Material	T_g (°C)	Triazole mass fraction (wt %)[a]	T_{d5} (°C)
Condensed Tz5TrS	47	33	204
1TzTrS-TFA	29	21	205
1TzTrS-2.5P	23	15	189
1PEG-1TEOS-1Tz5TrS-2.5P	-12	8	182
1PEG-1TEOS-1Tz5TrS-1TFA	-19	10	206
Tz5Si[b]	5	34	

[a] Mass fraction of triazole in the heterocycle matrix is calculated after accounting for the weight of the doped acid.

[b] Thermal properties of Tz5Si from the literature.[19]

3.4 Proton conductivity

3.4.1 Proton conductivity of 1*H*-1, 2, 3-triazole grafted condensed organosilicon precursor

The temperature dependent proton conductivity of condensed sol-gel monomer Tz5TrS, before, and after, doping with TFA or H_3PO_4 was measured and compared with the previously reported linear homopolymer Tz5Si which has the same tether length as Tz5TrS, figure 3.5.[19] The

conductivity of the condensed Tz5TrS is three orders of magnitude lower than that of homopolymer Tz5Si. This is presumably because the dominant conduction process in triazole functionalized membranes is structural diffusion, which involves intermolecular proton transfer and reorganization by a hydrogen bond breaking and forming process, and as a result proton conductivity depends on the local mobility of the matrix.[25-27] In condensed Tz5TrS, the tight Si-O-Si crosslinked network reduces chain mobility as reflected by the higher glass transition temperature of condensed Tz5TrS (T_g = 47 °C) compared to that of homopolymer Tz5Si (T_g = 5 °C). The proton conductivity of the condensed Tz5TrS after doping with TFA or H_3PO_4 is comparable to the homopolymer Tz5Si, since conductivity depends upon both the local mobility and the charge carrier density. Addition of acid introduces extrinsic charge carriers leading to an increase in conductivity. An increase in conductivity of up to 2 orders of magnitude after doping with TFA has been reported previously.[7-8] At the highest temperature measured, the improvement in conductivity with H_3PO_4 doping is even greater that that observed for TFA doping. However, membranes comprising condensed Tz5TrS, both doped and undoped, are rigid and fragile, and lack the flexibility needed to be used as proton exchange membranes in fuel cells.

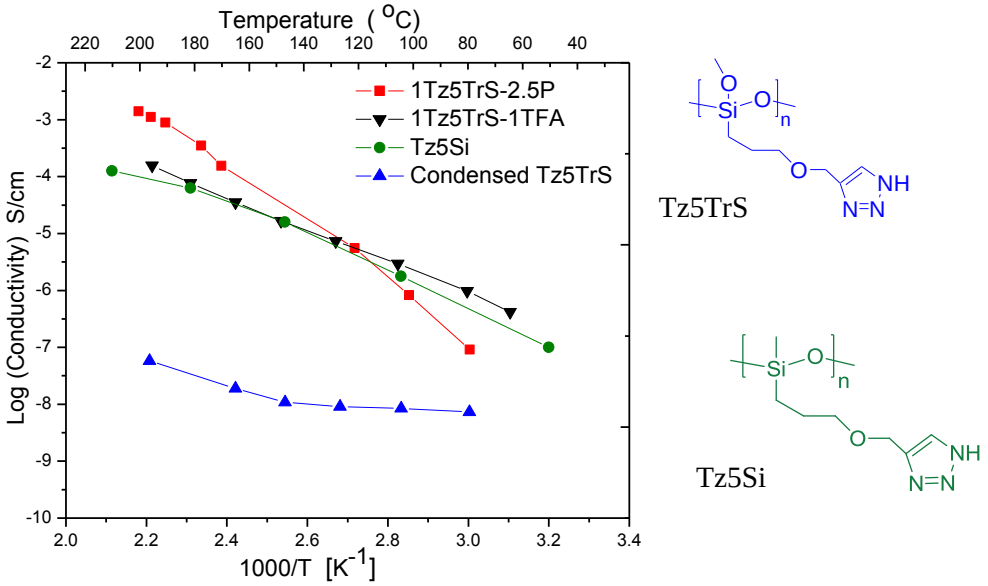

Figure 3.5. Proton conductivity of condensed Tz5TrS, Tz5TrS-1TFA and Tz5TrS-2.5P along with Tz5Si for comparison

3.4.2 Proton conductivity of hybrid inorganic-organic membranes

The proton conductivity of the hybrid inorganic-organic membranes, 1PEG-1TEOS-1Tz5TrS-1TFA and 1PEG-1TEOS-1Tz5TrS-2.5P, increases with increasing temperature reaching 1.6 mS/cm at 180 °C for 1PEG-1TEOS-1Tz5TrS-2.5P, figure 3.6. These conductivities are slightly higher than that of the homopolymer Tz5Si.[19] Although the high temperature proton conductivity of the two membranes doped with TFA or H_3PO_4 at 180 °C are similar, the shape of the Log (σ) versus 1000/T curves are different suggesting a difference in proton transport mechanism. This could be explained by the fact that H_3PO_4 molecules interact quantitatively with the protogenic group and so an excess of H_3PO_4 to triazole group is necessary to give sufficient proton conductivity.[24] When H_3PO_4 is used as a dopant, another conduction mechanism is also possible; proton transport taking place along a $H_2PO_4^-/HPO_4^{2-}$ anionic chain by consecutive proton transfer between phosphate species and anion reorientation steps.[15, 28-29] In TFA doped materials, maximum ion conductivity is attributed to the proton exchange between protonated and non-protonated heterocycle sites.[29]

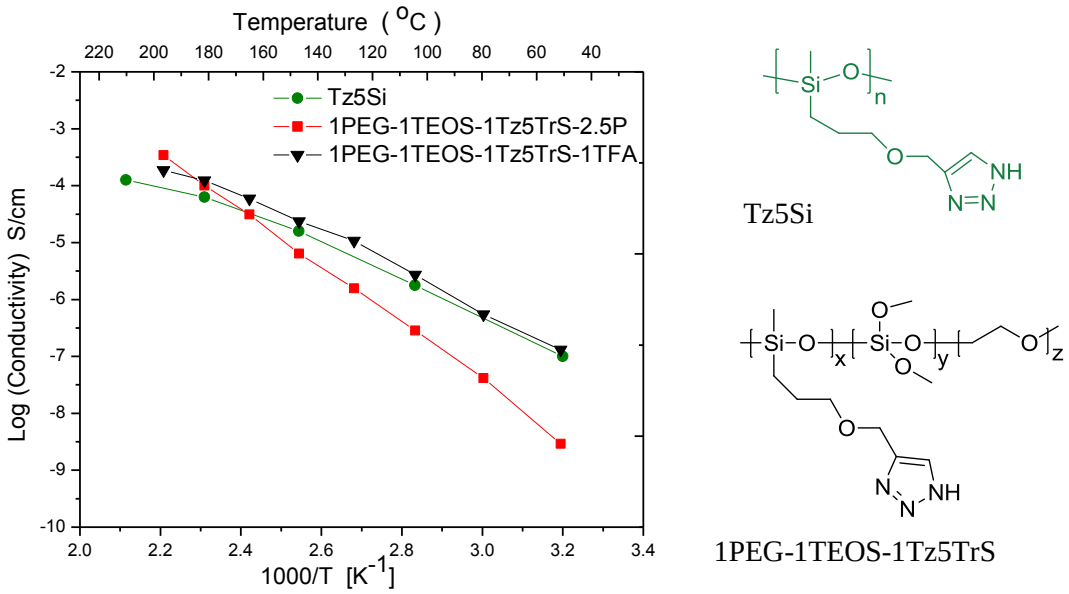

Figure 3.6. Proton conductivity of 1PEG-1TEOS-1Tz5TrS-1TFA and 1PEG-1TEOS-1Tz5TrS-2.5P along with Tz5Si for comparison.

3.5 Mechanical properties

The mechanical properties of the membranes were studied using nanoindentation.[30] Condensed Tz5TrS, 1Tz5TrS-1TFA and 1Tz5TrS-2.5P were too fragile for mechanical testing. Only the mechanical properties of PEG containing membranes were studied, and were compared to that of hydrated Nafion-112.

A peak load of 20 μN was applied at the rate of 4 μN/s and then the sample was held under maximum load for 5 sec, followed by unloading at the same rate of 4 μN/s. During the indentation process, the penetration depth (*h*) was measured and the area of the indent (*A*) was determined using the known geometry of the indentation tip. The indenter was a diamond Berkovich (or triagonal pyramid) geometry with a geometric constant (ε) of 0.75, center to face angle of 65.35 degrees and tip radius ~ 150 nm as quoted by the manufacturer. The modulus and the hardness of the samples were obtained from the unloading portion of the curve by plotting load versus displacement and then using Oliver and Pharr analysis.[30] The load versus displacement curves of the samples studied are shown in figure 3.7. The slope of the unloading

curve at the maximum loading point (h_{max}) gave the contact stiffness of the material, eq. 3-1. Knowing the projected area of the tip-sample contact A_c, at the peak load P_{max}, and the stiffness S at the onset of loading, the reduced modulus, E_r was calculated by using eq. 3-2. Since an elastic displacement occurs both in the specimen and the indenter; reduced modulus accounts for deformation of both the indenter and the sample and is related to the Young's modulus of the specimen E_s, by eq. 3-3; where E_s and v_s are Young's modulus and Poisson's ratio for the specimen and E_i and v_i are the same parameters for the indenter (diamond in this case).[30-31] Hardness is the ratio of the peak load to the corresponding contact area, eq. 3-4.[30-31]

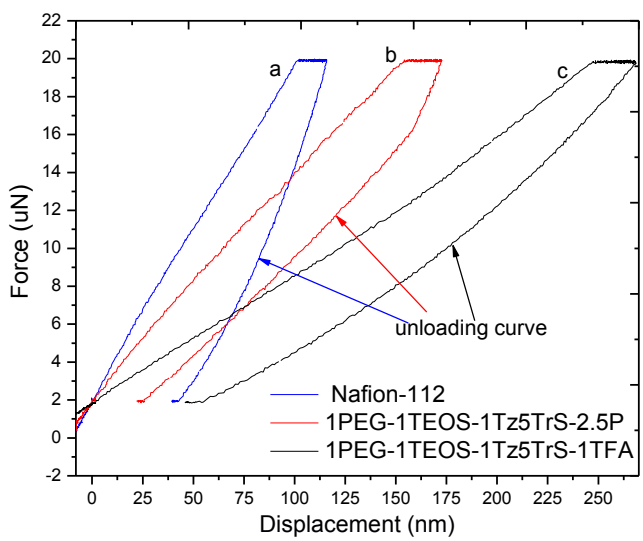

Figure 3.7. Load vs. displacement curves a) Nafion-112 b) 1PEG-1TEOS-1Tz5TrS-2.5P c) 1PEG-1TEOS-1Tz5TrS-1TFA

Contact Stiffness $$S = \frac{dP}{dh}\Big|h_{max} \quad (3\text{-}1)$$

Reduced Modulus $$E_r = \frac{\sqrt{\pi}}{2}\frac{1}{\sqrt{A_c}}S \quad (3\text{-}2)$$

Sample's Elastic (Young's) Modulus, E_s $$E_{sample} = (1 - v_s^2)/(\frac{1}{E_r} - \frac{1-v_i^2}{E_i}) \quad (3\text{-}3)$$

(E_i = 1141 GPa, v_i = 0.07 for diamond)

Hardness $$H = \frac{P_{max}}{A_c}$$ 3-4

Table 3.2. Reduced modulus and hardness from nanoindentation

	1PEG-1TEOS-1Tz5TrS-2.5P	1PEG-1TEOS-1Tz5TrS-1TFA	Nafion-112
Reduced Modulus (MPa)	315	139	765
Hardness (MPa)	92	40	113

The reduced modulus and hardness of the hybrid inorganic –organic samples and Nafion 112 are summarized in Table 3.2. The modulus of TFA doped membrane is approximately one fifth that of Nafion, while modulus of H_3PO_4 doped membrane is approximately half that of Nafion. The membrane doped with H_3PO_4 was stronger than that doped with TFA. This could be due to the complexation of phosphoric acid molecules to the hybrid inorganic-organic polymer network.

For polymers, the Oliver and Pharr analysis over estimates the modulus compared to the macroscopic Young's elastic modulus, as polymers creep, being viscoelastic in nature, while the Oliver and Pharr model analyzes the load-displacement curve with elastic contact mechanics models.[32-33] The modulus obtained by this analysis may be greater than the actual values, the relative comparison with Nafion, however, would be similar. From the reduced modulus of Nafion (765 MPa), its Young's modulus was calculated as 643 MPa using eq. 3.3 (ν = 0.4 for Nafion).[34] The Young's modulus of Nafion obtained by DMA (dynamic mechanical analyzer) for similar hydration levels was reported as 437 MPa.[35]

3.6 Conclusions

The anhydrous proton conducting, low T_g triazole functionalized poly(siloxane) was mechanically reinforced by crosslinking using sol-gel condensation. The resulting hybrid

inorganic-organic membranes are self-supporting and thermally stable up to 180 °C. The incorporation of PEG imparts flexibility to the crosslinked membrane. Crosslinking leads to a decrease in conductivity due to the restricted local mobility of the triazole group. However, addition of acid helps restore the conductivity of crosslinked membranes up to $10^{-2.5}$ S/cm at 180 °C which is slightly greater than that of the uncrosslinked, low T_g homopolymer and the same as that of acid doped homopolymer. Compared to organic polymers containing acid doping, hybrid inorganic-organic copolymer membranes containing acid doping can achieve high proton conductivity along with good mechanical properties.

3.7 References

1. Schuster, M. F. H.; Meyer, W. H.; Schuster, M.; Kreuer, K. D., *Chem. Mater.* **2004,** 16, 329-337.

2. Persson, J. C.; Jannasch, P., *Macromolecules* **2005,** 38, 3283-3289.

3. Schuster, M.; Meyer, W. H.; Wegner, G.; Herz, H. G.; Ise, M.; Schuster, M.; Kreuer, K. D.; Maier, J., *Solid State Ionics* **2001,** 145, 85-92.

4. Woudenberg, R. C.; Yavuzcetin, O.; Tuominen, M. T.; Coughlin, E. B., *Solid State Ionics* **2007,** 178, 1135-1141.

5. Münch, W.; Kreuer, K. D.; Silvestri, W.; Maier, J.; Seifert, G., *Solid State Ionics* **2001,** 145, 437-443.

6. Kreuer, K.-D., *Chem. Mater.* **1996,** 8, 610-641.

7. Granados-Focil, S.; Woudenberg, R. C.; Yavuzcetin, O.; Tuominen, M. T.; Coughlin, E. B., *Macromolecules* **2007,** 40, 8708-8713.

8. Martwiset, S.; Woudenberg, R. C.; Granados-Focil, S.; Yavuzcetin, O.; Tuominen, M. T.; Coughlin, E. B., *Solid State Ionics* **2007,** 178, 1398-1403.

9. Martwiset, S.; Yavuzcetin, O.; Thorn, M.; Versek, C.; Tuominen, M.; Coughlin, E. B., *J. Polym. Sci.,Part A: Polym. Chem.* **2009,** 47, 188-196.

10. Higami, M.; Woudenberg, R. C.; Granados-Focil, S.; Yavuzcetin, O.; Tuominen, M. T.; Coughlin, E. B. PMSE Preprints, **2007**; 97 pp 551-552.

11. Chen, H.; Palmese, G. R.; Elabd, Y. A., *Chem. Mater.* **2006,** 18, 4875-4881.

12. Tezuka, T.; Tadanaga, K.; Hayashi, A.; Tatsumisago, M., *J. Am. Chem. Soc.* **2006,** 128, 16470-16471.

13. Tezuka, T.; Tadanaga, K.; Hayashi, A.; Tatsumisago, M., *Solid State Ionics* **2008,** 179, 1151-1154.

14. Li, S.; Zhou, Z.; Abernathy, H.; Liu, M.; Li, W.; Ukai, J.; Hase, K.; Nakanishi, M., *J. Mater. Chem.* **2006,** 16, 858.

15. Li, S.; Zhou, Z.; Liu, M.; Li, W.; Ukai, J.; Hase, K.; Nakanishi, M., *Electrochim. Acta* **2006,** 51, 1351-1358.

16. Herz, H. G.; Kreuer, K. D.; Maier, J.; Scharfenberger, G.; Schuster, M. F. H.; Meyer, W. H., *Electrochim. Acta* **2003,** 48, 2165-2171.

17. Li, S.; Zhou, Z.; Zhang, Y.; Liu, M.; Li, W., *Chem. Mater.* **2005,** 17, 5884-5886.

18. Wright, J. D.; Sommerdijk, N. A. J. M., *Sol-Gel Materials: Chemistry and Applications*. CRC Press: London, **2001**; pp 15.

19. Akbey, Ü.; Granados-Focil, S.; Coughlin, E. B.; Graf, R.; Spiess, H. W., *J. Phys. Chem. B* **2009,** 113, 9151-9160.

20. Loren, J. C.; Krasinski, A.; Fokin, V. V.; Sharpless, K. B., *Synlett* **2005**, 2847-2850.

21. Bruce, P. G., *Polymer Electrolyte Reviews*. 1 ed.; Elsevier Applied Science: New York, **1987**; Vol. 1, pp 237-274.

22. Chalk, A. J.; Harrod, J. F., *J. Am. Chem. Soc.* **1965,** 87, 16-21.

23. Marko, I. E.; Sterin, S.; Buisine, O.; Mignani, G.; Branlard, P.; Tinant, B.; Declercq, J.-P., *Science* **2002,** 298, 204-206.

24. Rikukawa, M.; Sanui, K., *Prog. Polym. Sci.* **2000,** 25, 1463-1502.

25. Subbaraman, R.; Ghassemi, H.; Zawodzinski, T. A. J., *J. Am. Chem. Soc.* **2007,** 129, 2238-2239.

26. Zhou, Z.; Liu, R.; Wang, J.; Li, S.; Liu, M.; Bredas, J.-L., *J. Phys. Chem. A* **2006,** 110, 2322-2324.

27. Scharfenberger, G.; Meyer, W. H.; Wegner, G.; Schuster, M.; Kreuer, K. D.; Maier, J., *Fuel Cells* **2006,** 6, 237-250.

28. Kreuer, K. D., *J. Membr. Sci.* **2001,** 185, 29-39.

29. Colomban, P., *Proton Conductors: Solids, Membranes and Gels--Materials and Devices*. Cambridge University Press: Cambridge, **1992**; Vol. 2, pp 311.

30. Oliver, W. C.; Pharr, G. M., *J. Mater. Res.* **1992,** 7, 1564-1583.

31. VanLandingham, M. R.; Villarrubia, J. S.; Guthrie, W. F.; Meyers, G. F., *Macromol. Symp.* **2001,** 167, 15-43.

32. Davide, T.; Stefano, P.; Joachim, L.; Alexander, A., *Macromolecules* **2007,** 40, 1259-1267.

33. Kranenburg, J. M.; Tweedie, C. A.; Vliet, K. J. v.; Schubert, U. S., *Adv. Mater.* **2009,** 21, 3551-3561.

34. Solasi, R.; Zou, Y.; Huang, X.; Reifsnider, K.; Condit, D., *J. Power Sources* **2007,** 167, 366-377.

35. Kundu, S.; Simon, L. C.; Fowler, M.; Grot, S., *Polymer* **2005,** 46, 11707-11715.

CHAPTER 4

SYNTHESIS AND CHARACTERIZATION OF 1,2,3-TRIAZOLIUM IONIC LIQUIDS

4.1 Introduction

In chapters 2 and 3, 1*H*-1,2,3 triazole was used as a protogenic group to facilitate H^+ transport, where H^+ migration through the hydrogen bonded network formed by 1*H*-1,2,3-triazole occurs by a continuous process of hydrogen bond formation and breaking. As discussed in chapter 1, the transport of H^+ in one direction is conceptually equivalent to transport of OH^- ions in the opposite direction in extended chains of water molecules, when one considers a proton defect. A surplus proton defect is responsible for proton transport, while a proton defect deficiency is responsible for hydroxide transport. This chapter is focused on extending the work on 1,2,3-triazole functionalized polymers for proton exchange membranes (PEMs) to anion exchange membranes (AEMs) by converting the 1,2,3-triazoles into triazolium cations with hydroxides as the counter ion. Our approach is to first study small molecule triazolium salts i.e. triazolium ionic liquids and their stability for AAEMFC applications and then covalently attach them to a polymer to develop AEMs.

Triazolium cations are analogous to imidazolium cations, which are well established in the ionic liquid literature. Ionic liquids have a unique set of properties that include negligible vapor pressure, wide usable temperature range, nonflammability, excellent thermal stability and solvating properties, high ionic conductivity and wide electrochemical stability window.[1-2] These properties of ionic liquids have made them useful in a broad range of chemical reactions and separation processes,[3] as additives[1] and electrolytes in electronic devices.[4-5] Ionic liquids are composed of a bulky, organic cation such as quaternary ammonium,[6-7] 1,3-dialkylimidazolium,[8-10] sulfonium,[11] phosphonium ion[12] and an inorganic or organic counter anion. A wide range of anions are employed in ionic liquids, ranging from simple halides, to main group anions such as

tetrafluoroborate or hexafluorophosphate, and organic anions such as triflate or tosylate. The advantage of having such a wide selection of cations and anions is that it is possible to tailor the properties of ionic liquids for a specific application by suitable choice of component ions.

Ionic liquids composed of 1-methyl-3-alkylimidazolium cation have dominated the field due to their wide liquidus range, high conductivities and low viscosities, necessary for a multitude of applications, especially electrochemistry. Moreover, properties of these ionic liquids can be tuned by varying the alkyl group of imidazolium cation. Although progress has been made in the field of ionic liquids, to date, there are essentially no caustic ionic liquids. Reported ionic liquids have been made by combining various cations and anions. However, hydroxide ion, one of the most commonly encountered anions in organic chemistry, has not been used as a counterion in ionic liquids. This is because hydroxide ion is both a strong base and a nucleophile capable of degrading ammonium, phosphonium and imidazolium cations.

The synthesis of 1,2,3-triazole is quite facile by the Huisgen 1,3-dipolar cycloaddition reaction.[13] This heterocycle can be modified at nitrogens 1 and 3 to form substituted 1,2,3-triazolium cation. Although, the 1,2,3-triazolium cation has a structure analogous to imidazolium cation, research on triazolium based ionic salts[14-20] is quite limited compared to imidazolium salts. This is partially due to the paucity of methyl triazole unlike 1-methyl imidazole and the explosive nature of organic azides involved in the synthesis of 1,2,3-triazole. Recent reports have described the two-step one pot synthesis of 1,2,3-triazolium salts using Cu catalyzed Huisgen 1,3-dipolar cycloaddition reaction,[20] their thermal properties[17, 19] and used them as a reaction media.[14-16] Ryu and coworkers have recognized that 1,2,3-triazolium salts have higher chemical stability in basic medium compared to the imidazolium salts, due to the facile deprotonation of C-2 hydrogen of imidazolium salts.[21] However, information about the physiochemical properties of 1,2,3-triazolium salts is relatively limited in the literature. In our search for stable solvents to be used as an electrolyte in alkaline fuel cells, we have synthesized substituted 1,2,3-triazolium salts and

studied their ion cluster behavior, thermal properties, chemical stability towards hydroxide ion and electrochemical properties, and compared them with properties of analogous imidazolium salts. We report the properties of 1,2,3-triazolium salts with two representative anions, tosylate (Tos) and triflate (OTf). Herein, we report the synthesis and characterization of ten different ionic liquids comprising five cations and two anions. Out of the five cations, three are derivatives of 1-alkyl/aryl-3-methyl-4-butyl triazolium ion, a fourth cation is 1,3-dimethyl triazolium which provides an insight on the effect of butyl group at the 4 position of triazolium, and dimethyl imidazolium was studied for comparison.

4.2 Experimental

4.2.1 Materials

1-hexyne, benzyl azide, phenyl bromide, N,N'-dimethylethylenediamine, copper (II) sulfate ($CuSO_4 \cdot 5H_2O$), sodium ascorbate, t-butanol (t-BuOH), methyl tosylate, methyl triflate, 1-methyl imidazole, sodium hydroxide (NaOH), methyl iodide, sodium azide, acetonitrile and 1*H*-1,2,3-triazole were purchased from Alfa - Aesar or Sigma Aldrich and were used as received. Phenyl azide was synthesized as reported in the literature.[22]

4.2.2 Instrumentation

^{1}H-NMR and ^{13}C-NMR spectra were obtained on a Bruker DPX-300 or Bruker Avance-400 NMR spectrometer. Electrospray ionization mass spectra were acquired using an Esquire-LC ion trap instrument (Bruker Daltonics, Billerica MA) equipped with a standard ESI source. Spectra were obtained in positive ion modes from samples dissolved in methanol (10^{-5} M), infused into the spectrometer using a syringe pump at a constant flow rate of 2 uL/min. Typical operating conditions employed were: needle voltage 3.5 kV, N_2 nebulizer gas, desolvation temperature 150 °C, capillary exit voltage 110 V, scan range 50 - 1200 m/z. Thermogravimetric

analysis (TGA) was performed using a TA instruments TGA 2950 thermogravimetric analyzer at a heating rate of 10 °C/min under nitrogen flow of 20 mL/min. Glass transition temperatures, crystallization temperatures and melting points were obtained using TA instrument DSC Q200 differential scanning calorimeter (DSC) by heating and cooling the samples at a rate of 10 °C/min under helium flow (25 mL/min). All the transitions are reported from the second heating and cooling cycles.

Conductivity versus temperature data were obtained via impedance spectroscopy measurements using a Solartron 1260 Impedance/Gain Phase Analyzer by applying an excitation voltage of 30 mV with a logarithmic frequency sweep from 1 MHz to 0.1 Hz under vacuum to ensure an anhydrous environment. Samples were placed in home-built cells composed of ~4 mm section of polytetrafluoroethylene tubing sealed between two tight-fitting brass electrodes and clamped into custom holders of identical construction. Using customized in house developed software and hardware, the samples were kept at 180 °C under vacuum for ~10 hours and then the system was allowed to cool slowly under vacuum to near ambient temperature, while impedance spectra were continually sampled; this method ensures that samples are brought to a thermally stable condition before temperature dependence data is recorded on the cooling phase, mitigating artifacts due to thermal history and solvent or humidity effects. For each spectrum, the plateau of the impedance magnitude Bode plot occurring in the intermediate frequency range was fit to a constant value function; this plateau also corresponds to a region of minimal phase angle and likewise minimal imaginary component magnitude (reactance) response. Thus, the value of impedance magnitude in this regime was taken to be the resistance of ionic transport in the bulk of the sample. Conductivity σ was computed from the fitted resistance R and the known sample geometry as $\sigma = t/(R*A)$, where t and A are the thickness and area of the sample geometry respectively.

Cyclic Voltammetry was conducted on a Basi Epsilon MF 9092. The salts were dried under vacuum overnight and 0.1 M solution in anhydrous acetonitrile was prepared, and then the solution was purged with nitrogen for at least 10 minutes to minimize the effect of water and oxygen on cyclic voltammograms. Measurements were carried out over a voltage range of ± 3.2 V by sweeping the potential at a rate of 50 mV/sec, using a platinum working electrode, silver wire immersed in 0.01 M $AgNO_3$ in acetonitrile reference electrode, and platinum counter electrode. The ferrocene/ferrocenium couple had a measured potential of 0.124 V versus Ag/Ag^+ in acetonitrile. In order to avoid the effect of degradation products deposited on the electrode from scanning to one potential limit on reversing the potential, potential was swept either between 0 to +3.2 V or 0 to -3.2 V with clean electrodes and fresh electrolyte. The positive and the negative scans were then combined and plotted for each of the salts. The values for the cathodic and anodic limit are reported from the second scan which was reproducible upon further scans.

4.3 Synthesis

The 1,2,3-triazolium salts were synthesized by the Huisgen 1,3-dipolar cycloaddition reaction between the corresponding azide and 1-hexyne, followed by alkylation with either methyl tosylate or methyl triflate, scheme 4.1. The structures and abbreviations of the five cations and two anions comprising the ten different ionic liquids studied are shown in figure 4.1. For Tz1 salts, benzyl azide was purchased. For Tz2 salts, phenyl azide was synthesized as per a literature procedure,[22] and for Tz3 salts, methyl azide was generated in situ by reacting sodium azide and methyl iodide. 1-methyl-4-butyl-1,2,3-triazole for Tz3 salts was synthesized under microwave conditions as described previously.[23] Alkylation was done using methyl tosylate or methyl triflate in almost 100% yields according to the procedure described by Begtrup *et al*.[24] Tz4 salts were synthesized by deprotonation of 1,2,3-triazole by sodium hydroxide, followed by alkylation.[25]

Due to synthetic limitations, there is a trace of residual sodium tosylate and sodium triflate in Tz4Tos and Tz4OTf respectively. The synthesized salts were characterized by ^{1}H-NMR, ^{13}C-NMR and FAB-HRMS or ESI-MS. All the characterization data are consistent with the expected structures and compositions.

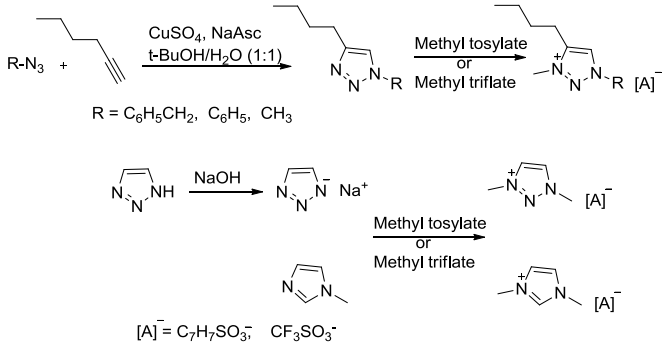

Scheme 4.1. Synthesis of ionic liquids studied.

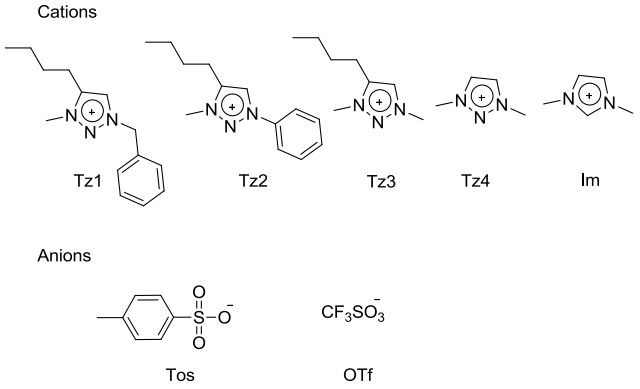

Figure 4.1. Structures and abbreviations of cations and anions studied.

General procedure for Tz1 and Tz2 salts. In a 100 mL round bottom flask equipped with a magnetic stir-bar, 1-hexyne (0.68 g, 8.3 mmol), $CuSO_4$ $5H_2O$ (0.19 g, 0.75 mmol), sodium ascorbate (0.3 g, 1.5 mmol) and 30 mL of t-butanol/H_2O (2:1) were combined. Then the corresponding azide (7.52 mmol) was added to the reaction mixture and the solution was allowed to stir at room temperature for 2 days. The reaction was terminated by adding H_2O (50 mL) and the product was extracted using ethyl acetate (4 × 50 mL). The organic fractions were washed

with 5% NH_4OH (4 × 50 mL) and then with brine. Further, the organic fractions were combined and dried over $MgSO_4$ and then the solution was concentrated by rotary evaporation. The crude product was purified by flash chromatography using ethyl acetate : hexane (1:1) to yield (80 - 90%) of triazole as a white solid which was used for further alkylation with methyl tosylate or methyl triflate to yield 1,2,3-triazolium salts.

General Procedure for Tz3 salts Synthesis modified from a literature procedure.[23] 1-hexyne (86 mg, 1.05 mmol), sodium azide (68 mg, 1.05 mmol), methyl iodide (0.06 mL, 1 mmol), $CuSO_4 \cdot 5H_2O$ (49 mg, 0.2 mmol), sodium ascorbate (49 mg, 0.25 mmol) and 3 mL of t-butanol/H_2O (1:1) were combined in a microwave vial equipped with a stir bar and then the vial was sealed with an aluminium crimp top. The mixture was irradiated at 100 °C for 15 minutes. The microwave power fluctuated between 20 W - 25 W to maintain a constant temperature of 100 °C. The mixture was then diluted with water and the product was extracted with dichloromethane (3 × 10 mL). The product was purified by passing through neutral alumina giving 1-methyl-4-butyl-1,2,3-triazole as a white solid (27 mg, 18%) and was used for further alkylation.

General procedure for Tz4 salts Synthesis modified from a literature procedure.[25] 1*H*-1,2,3-triazole (0.39 g, 5.6 mmol, 1eq.), sodium hydroxide (0.23 g, 1.05 eq.) and water (0.5 mL) were combined in a round bottom flask and heated at 100 °C for 15 minutes. The solution was further dried under vacuum overnight to remove water and then the resulting sodium salt of 1,2,3-triazole was used for further alkylation.

1-benzyl-3-methyl-4-butyltriazolium tosylate (Tz1Tos): Yield = 87%, yellow viscous liquid. ^{1}H-NMR (300 MHz, D_2O) δ 0.76 (t, 3H), 1.22 (m, 2H), 1.49 (m, 2H), 2.21 (s, 3H), 2.64 (t, 2H), 3.99 (s, 3H), 5.56 (s, 2H), 7.19 (m, 2H), 7.34(m, 5H), 7.52 (m, 2H), 8.14 (s, 1H). ^{13}C-NMR (75 MHz, D_2O) δ 12.67, 20.38, 21.22, 22.2, 28.04, 36.79, 56.69, 125.24, 127.27, 129.00, 129.35, 129.64, 131.93, 139.35, 142.38, 145.07. FAB-HRMS calcd: m/z: 230.16 $[C_{14}H_{20}N_3]^+$; found: m/z: 230.2.

1-benzyl-3-methyl-4-butyltriazolium triflate (Tz1OTf): Yield = 87%, brown viscous liquid. ^{1}H-NMR (400 MHz, CD_3OD) δ 0.96 (t, 3H), 1.45 (m, 2H), 1.71 (m, 2H), 2.81 (t, 2H), 4.21 (s, 3H), 5.72 (s, 2H), 7.45 (m, 5H), 8.44 (s,1H). ^{13}C-NMR (100 MHz, CD_3OD) δ 13.48, 22.33, 23.15, 28.94, 37.54, 57.64, 120.64 ($^{1}J_{CF}$ = 317 Hz), 128.09, 129.61, 130.03, 131.36, 145.11. EI-HRMS calcd: m/z: 230.16 $[C_{14}H_{20}N_3]^+$; found: m/z: 230.12.

1-phenyl-3-methyl-4-butyltriazolium tosylate (Tz2Tos): Yield = 82%, white powder. ^{1}H-NMR (300 MHz, D_2O) δ 0.85 (t, 3H), 1.35 (m, 2H), 1.65 (m, 2H), 2.24 (s, 3H), 2.81 (t, 2H), 4.18 (s, 3H), 7.19 (d, 2H), 7.5 (m, 5H), 7.74 (m, 2H), 8.72 (s, 1H). ^{13}C-NMR (75 MHz, D_2O) δ 13.55, 21.23, 22.19, 23.18, 29.10, 38.05, 121.27, 125.83, 127.23, 128.46, 130.24, 131.41, 134.91, 138.96, 143.99, 146.11. FAB-HRMS calcd: m/z : 216.15 $[C_{13}H_{18}N_3]^+$; found: m/z: 216.2.

1-phenyl-3-methyl-4-butyltriazolium triflate (Tz2OTf): Yield = 82%, white powder. ^{1}H-NMR (400 MHz, CD_3OD) δ 0.98 (t, 3H), 1.49 (m, 2H), 1.82 (m, 2H), 2.98 (t, 2H), 4.3 (s, 3H), 7.63 (m, 3H), 7.93 (m, 2H), 8.94 (s, 1H). ^{13}C-NMR (100 MHz, CD_3OD) δ 13.49, 22.31, 23.35, 29.06, 38.05, 120.82 ($^{1}J_{CF}$ = 329 Hz), 121.59, 126.61, 130.59, 131.97, 134.91, 146.15. EI-MS calcd: m/z: 216.15 $[C_{13}H_{18}N_3]^+$; found: m/z: 216.08.

1,3-dimethyl-4-butyltriazolium tosylate (Tz3Tos): Yield = 18%, yellow solid. ^{1}H-NMR (300 MHz, CD_3OD) δ 1.03 (t, 3H), 1.52 (m, 2H), 1.75 (m, 2H), 2.4 (s, 3H), 2.87 (t, 2H), 4.26 (s, 3H), 4.3 (s, 3H), 7.26 (d, 2H), 7.73 (d, 2H), 8.51 (s, 1H). ^{13}C-NMR (75 MHz, CD_3OD) δ 12.64, 20.35, 21.25, 22.15, 28.11, 36.66, 39.25, 125.35, 128.33, 129.42, 139.45, 142.43, 144.78. ESI-MS calcd: m/z: 154.23 $[C_8H_{16}N_3]^+$; found: m/z: 154.6.

1,3-dimethyl-4-butyl triazolium triflate (Tz3OTf): Yield = 18%, brown liquid. ^{1}H-NMR (300 MHz, CD_3OD) δ 0.99 (t, 3H), 1.46 (m, 2H), 1.73 (m, 2H), 2.85 (t, 2H), 4.19 (s, 3H), 4.26 (s, 3H), 8.45 (s, 1H). ^{13}C-NMR (75 MHz, CD_3OD) δ 13.84, 22.98, 23.09, 29.88, 37.67, 40.23, 121.76 ($^{1}J_{CF}$ = 324 Hz), 130, 146.20. ESI-MS calcd: m/z: 154.23 $[C_8H_{16}N_3]^+$; found: m/z: 154.6.

1,3-dimethyl triazolium tosylate (Tz4Tos): Yield = 25%, white powder. ^{1}H-NMR (300 MHz, D_2O) δ 2.26 (s, 3H), 4.16 (s, 6H), 7.24 (d, 2H), 7.54 (d, 2H), 8.33 (s, 1H). ^{13}C-NMR (75 MHz, D_2O) δ 20.37, 39.39, 125.33, 129.6, 131.15, 139.3, 142.6. ESI-MS calcd: m/z: 98.13 $[C_4H_8N_3]^+$; found: m/z: 98.8.

1,3-dimethyl triazolium triflate (Tz4OTf): Yield = 25%, brown viscous liquid. ^{1}H-NMR (400 MHz, D_2O) δ 4.17 (s, 6H), 8.33 (s, 2H). ^{13}C-NMR (100 MHz, D_2O) δ 39.64, 119.67 ($^{1}J_{CF}$ = 315 Hz), 131.17. ESI-MS calcd: m/z: 98.13 $[C_4H_8N_3]^+$; found: m/z: 98.8.

1,3-dimethylimidazolium tosylate (ImTos): Yield = 99%, white solid. ^{1}H-NMR (300 MHz, D_2O) δ 2.23 (s, 3H), 3.68 (s, 6H), 7.2 (m, 4H), 7.52 (d, 2H), 8.41 (s, 1H). ^{13}C-NMR (75 MHz, D_2O) δ 0.38, 35.44, 123.23, 125.21, 129.31, 136.25, 139.42, 142.29. ESI-MS calcd: m/z: 97.14 $[C_5H_9N_2]^+$; found: m/z: 97.8.

1,3-dimethylimidazolium triflate (ImOTf): Yield = 99%, light yellow solid. ^{1}H-NMR (300 MHz, D_2O) δ 3.79 (s, 6H), 7.31(s, 2H), 8.53 (s, 1H). ^{13}C-NMR (75 MHz, D_2O) δ 35.51, 119.63 ($^{1}J_{CF}$ = 315 Hz), 123.33, 136.44. ESI-MS calcd: m/z: 97.14 $[C_5H_9N_2]^+$; found: m/z: 97.8.

All these ionic liquids are hydrophilic in nature. To determine their moisture sensitivity, salts were dried under vacuum at 90 °C overnight and then exposed to 80 % RH at 21 °C for 1 h. It was found that Tz1 and Im salts with both Tos and OTf anion absorb moisture faster (~ 800 ppm in 1 h) than the other salts studied. Tz2 salts are the least hydrophilic with their water content being less than 400 ppm after 1 h of exposure. The qualitative order of hygroscopic nature for the studied salts with a given anion was found to be: Tz1 > Im > Tz3 ≈ Tz4 > Tz2. Since the properties of ionic liquids change drastically by small amounts of water, all the salts were dried overnight at 80 °C under vacuum, prior to use. All the investigated ionic liquids are miscible with solvents of high polarity: water, methanol and acetonitrile. They are immiscible with diethyl ether, chloroform and ethyl acetate. The characterization data has been classified in

two series. The first contains five salts with tosylate anion and varying cations; while the second includes five salts with triflate anion and varying cations.

4.4 Characterization

4.4.1 ESI-MS

Electrospray ionization mass spectrometry (ESI-MS) has been used to measure the intrinsic solvent-free strength of cation-anion interactions in ionic liquids.[11, 26] These interactions influence their physical and chemical properties.[27] Positive ion mode ESI-MS experiments were performed using dilute methanol solution of the ionic salts. The positive ion mode mass spectrum consisted of naked cation $[C]^+$, dimeric clusters $[C_2A_1]^+$ with a single anion $[A^-]$ and trimeric clusters $[C_3A_2]^+$. Compositions higher than $[C_3A_2]^+$ were not observed for any of these salts.

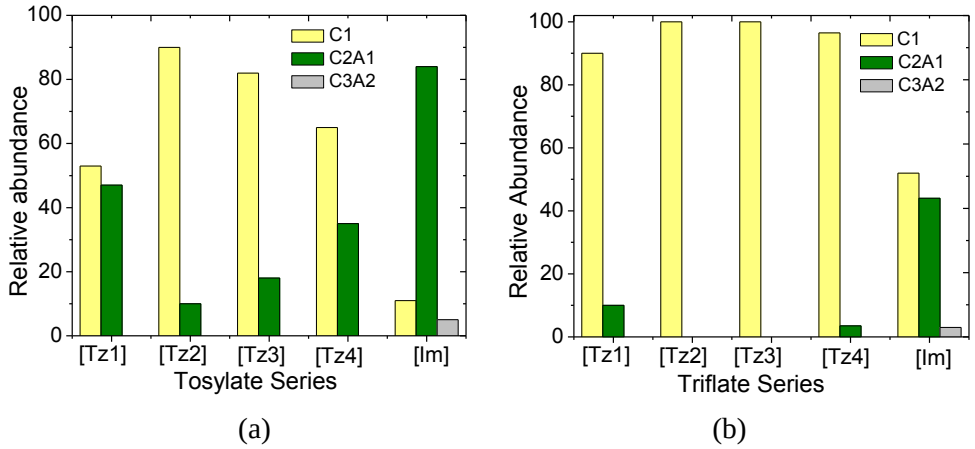

Figure 4.2. Relative abundance in ESI mass spectra a) tosylate series b) triflate series

The graphical representations of relative abundance of charged clusters of ionic liquids with tosylate anion and triflate anion are shown in figure 4.2a and 4.2b respectively. No trimeric clusters were observed for any of the 1,2,3-triazolium salts. Trimeric clusters were observed for the imidazolium salts. Bini *et al*.[27] reported the existence of multiple higher order clusters for imidazolium salts. As observed from the above comparison between triazolium salts and dimethyl

imidazolium salt, the triazolium cations have lower binding strength to tosylate and triflate counter ions compared to the imidazolium cations.

From the relative abundance data, for the 1,2,3-triazolium cations studied in this paper, the qualitative order of interaction with a given anion was found to be: $[Tz1]^{+} > [Tz4]^{+} > [Tz3]^{+} > [Tz2]^{+}$. This trend shows that the solvent-free binding strength of triazolium cations depends on the substitution at the 1 and 3 position of triazolium ring. Alkyl substitution influences the intrinsic binding strength of imidazolium cations as well.[27] The distribution of ESI mass spectra peaks show that the tosylate anion is much more strongly bound to the cations compared to the triflate anion. This is in agreement with the report of Bini *et al*.[27] where tosylates show stronger bonding ability than triflates with substituted imidazolium cations. These ESI-MS results explain the higher melting point and glass transition temperature observed for tosylate salts compared to triflate salts (*vide supra*).

4.4.2 Thermal stability

The thermal stability of the salts were studied by thermogravimetric analysis (TGA) and the temperatures corresponding to 5% weight loss for all the samples are reported in table 4.1. The TGA traces are shown in figure 4.3. Thermal stability of 1,2,3-triazolium salts are in the range of 200 – 300 °C, which is lower than that of 1,3-dialkyl imidazolium based ionic liquids (generally, T_d > 300 °C). It was observed that the thermal stability of these salts is significantly influenced by the identity of the anion, similar to that reported previously.[11, 21]. Except for 1,3-dimethyl triazolium salts, the triflate salts have greater thermal stability than tosylate salts. It is generally observed that the weaker the coordinating anion, the higher the thermal stability of ionic liquids.[1]

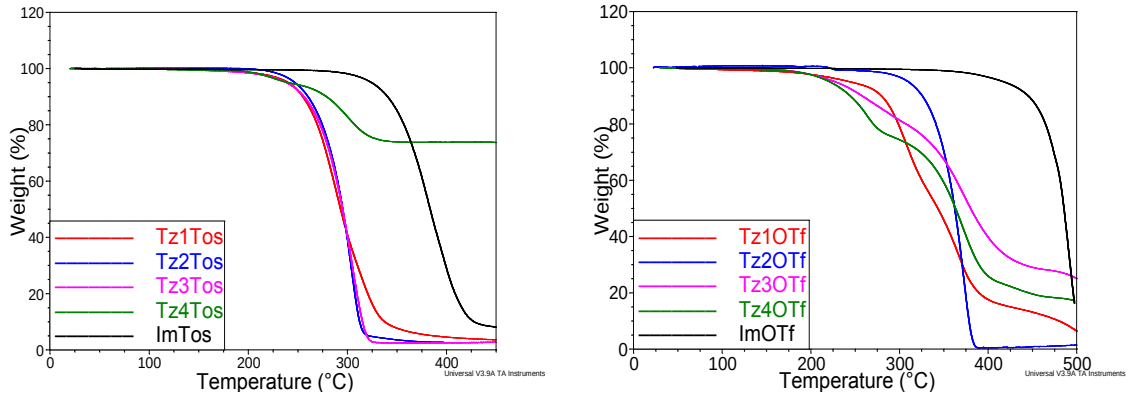

(a) (b)

Figure 4.3. TGA traces a) tosylate series b) triflate series

4.4.3 Phase behavior, melting point and glass transition temperatures

The phase behaviors of these salts were studied by DSC and the data for glass transition temperatures (T_g), crystallization temperatures (T_c) and melting points (T_m) are summarized in table 4.1. Tz1 salts are amorphous while Tz2 salts are crystalline in nature. The glass transition temperature of all the salts studied is below 0 °C. Tz3Tos, Tz4Tos, ImTos are liquids at high temperature and become glassy upon cooling. One of the reasons for high T_m of Tz3, Tz4 and Im salts is symmetrical substitution at the 1 and 3 position of these cations. Salts with symmetrical cations exhibit high melting point compared to salts with asymmetrical cations due to their higher lattice energy.[10] For e.g., if the structure of symmetrical dimethyl imidazolium triflate is changed to asymmetrical ethyl methyl imidazolium triflate, the melting point decreases from 37 °C to -9 °C.[10] The phase behavior of Tz3 and Tz4 salts are very similar indicating that the thermal properties are influenced only by the substitution at the 1 and 3 position of triazolium ring and not by the butyl group at the 4 position.

Table 4.1. Thermal properties of the salts investigated.

Entry	Salts	T_g	T_c	T_m	T_d
1	Tz1Tos	-22	NA	NA	240
2	Tz1OTf	-45	NA	NA	245
3	Tz2Tos	NA	96	146	247
4	Tz2OTf	NA	62	102	310
5	Tz3Tos	-33	73	106	238
6	Tz3OTf	-67	NA	NA	228
7	Tz4Tos	-25	29	99	240
8	Tz4OTf	-77	NA	NA	221
9	ImTos	-29	28	95	324
10	ImOTf	NA	-37	37	417

NA = not applicable

All the tosylate salts exhibit T_m around 100 °C, at much higher temperature compared to the triflate salts. This could be explained by the higher binding strength of cations with tosylates compared to triflates as seen by ESI-MS. The ionic salts reported with tosylate anion, such as 1-alkyl-3-methylbenzotriazolium tosylate, 1,2,3-triazolium tosylate, 1,3-dialkyl imidazolium tosyalte exhibited melting points at higher temperatures compared to salts with halides, triflate or tetrafluoroborate anions.[17, 28-29] Although the triazolium salts reported here are not room temperature ionic liquids, they could be useful for solid electrolyte applications.

4.4.4 Chemical stability towards hydroxide ion

The stability of ionic liquids in alkaline environment is an important property towards making caustic ionic liquids. The alkaline stability of quaternary ammonium cations has been studied quite extensively by Pivovar and coworkers for fuel cell applications.[30-31] We investigated the chemical stability of 1,2,3-triazolium and imidazolium salts under alkaline conditions. We prepared 0.05 M solutions of Tz1Tos, Tz2Tos, Tz3Tos and ImTos in 0.05 M NaOH/D_2O and heated these at 80 °C in NMR tubes. The stability of each of these cations was evaluated by recording ^{1}H-NMR spectra at regular intervals. In ^{1}H NMR, the integration of the area under the butyl group resonances at 4 position of triazolium cation, versus that of the substituents at 1 and 3 position yielded a quantitative measure of the cation remaining. The counterion, p-toluene sulfonate acts as an internal standard (singlet at δ 2.2 ppm and doublets at δ 7.4 and δ 7.2 ppm).

Tz2 and Tz3 cations were stable for up to 10 days while Tz1 cation degraded in 1 day forming 1-methyl-5-butyl triazole and the Im cation degraded within 2 h upon heating, figure 4.4. Dimethyl imidazolium cation degrades rapidly due to the deprotonation at C(2) forming a stable carbene.[32]

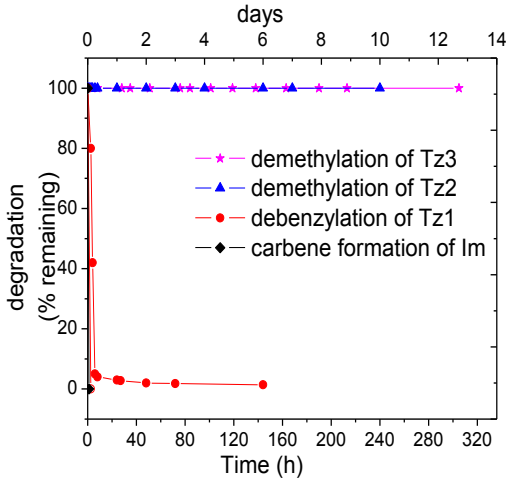

Figure 4.4. Degradation of cations in 0.05 M NaOH/D_2O at 80 °C.

The ^{1}H-NMR of Tz2 and Tz3 cations, showed a gradual decrease in the intensity of resonances corresponding to protons at the 5 position of triazole, while in ^{13}C-NMR, the singlet corresponding to the carbon at the 5 position changed to a 1:1:1 triplet. This indicates the ^{1}H for ^{2}H exchange at the 5 position of Tz2 and Tz3 cations. The rate of hydrogen for deuterium exchange was higher in Tz2 salt compared to Tz3 salt as seen in figure 4.5. Similar observations related to hydrogen for deuterium exchange rates have been reported previously.[24, 33]

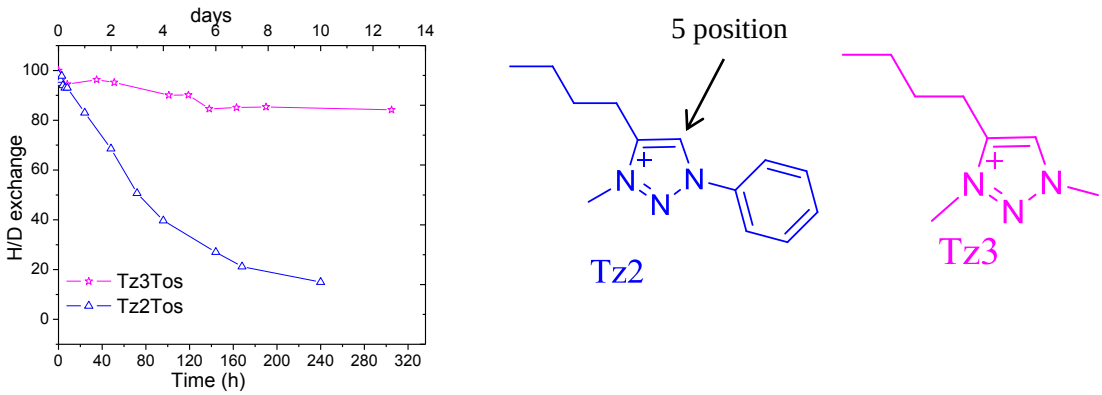

Figure 4.5. Hydrogen for deuterium exchange in solutions of Tz2Tos and Tz3Tos in 0.05 M NaOH/D_2O at 80 °C.

The most caustic test conditions reported to validate the stability of cations for alkaline anion exchange membrane fuel cells are 2 M NaOH at a temperature of 80 °C.[30] When the concentration of NaOH was increased to 2 M in the above NMR experiments, Tz2 and Tz3 cations degraded within a day. This indicates that 1,2,3-triaolium salts have chemical stability in basic medium suitable for base catalyzed reactions, but not enough for their applicability in alkaline fuel cell membranes.

4.4.5 Conductivity

The conductivity of ionic liquid is an important property for use as an electrolyte in batteries, fuel cells, solar cells and double layer capacitors. We measured the conductivity of

eight neat ionic liquids based on Tz1, Tz2, Tz3 and Im cations with tosylate or triflate anions, over a temperature range of 25 °C to 180 °C under anhydrous conditions.

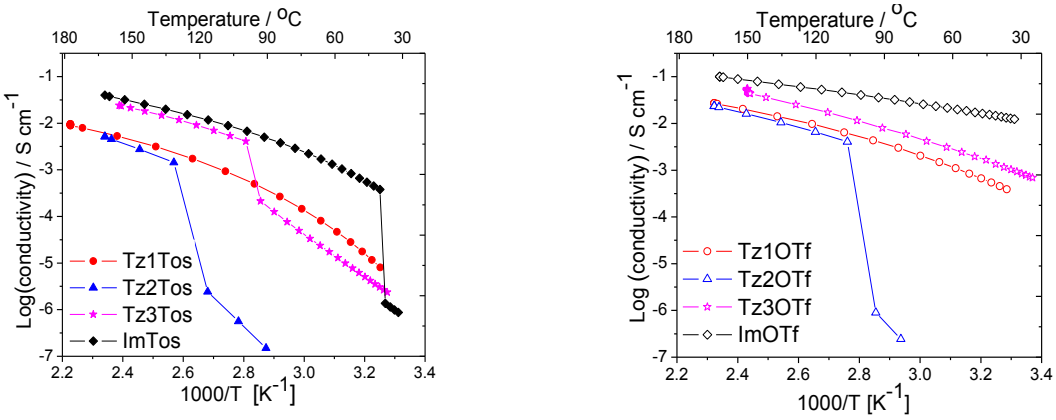

(a) (b)

Figure 4.6. Ionic conductivity a) tosylate series b) triflate series

The measured conductivity of imidazolium salts, figure 4.6, is in good agreement with the published data on similar imidazolium salts, thereby confirming the accuracy of our conductivity measurements.[34-35] Tz2Tos, Tz2OTf and Tz3Tos show a sudden drop in conductivity due to crystallization in the conductivity cell during cooling.

From both the tosylate salt and triflate salt series, it can be seen that conductivity decreases in the order: Im ≈ Tz3 > Tz1 ≈ Tz2. This trend is consistent with the size of cation.[34] The conductivity of Tz2 and Tz1 salts are almost identical, while that of Tz3 and Im salts are similar. Given that the substituents at N-atom of imidazolium and triazolium cations are same, their ionic conductivity is of the same order of magnitude. This conductivity is more than that reported for quaternary ammonium and sulfonium salts.[1] From the Walden's rule, the conductivity of ionic liquids is mainly governed by their viscosity, with conductivity being inversely proportional to the viscosity.[1] Since the conductivity of 1,2,3-triazolium and imidazolium salts with analogous structures are similar, the viscosity of 1,2,3-triazolium salts would be as low as that of imidazolium salts.

Pairwise comparisons between any two ionic salts studied here with the same cation and different anion, figure 4.7, shows that triflates have higher ionic conductivity than tosylates. This could be explained by two reasons: a) smaller size of triflate ion than tosylate ion, which imparts higher mobility to triflate ion b) less ionic association between triflate anion and cations compared to that between tosylate anion and cations, as observed by ESI-MS, generates more diffusive species that can contribute to ionic conductivity.

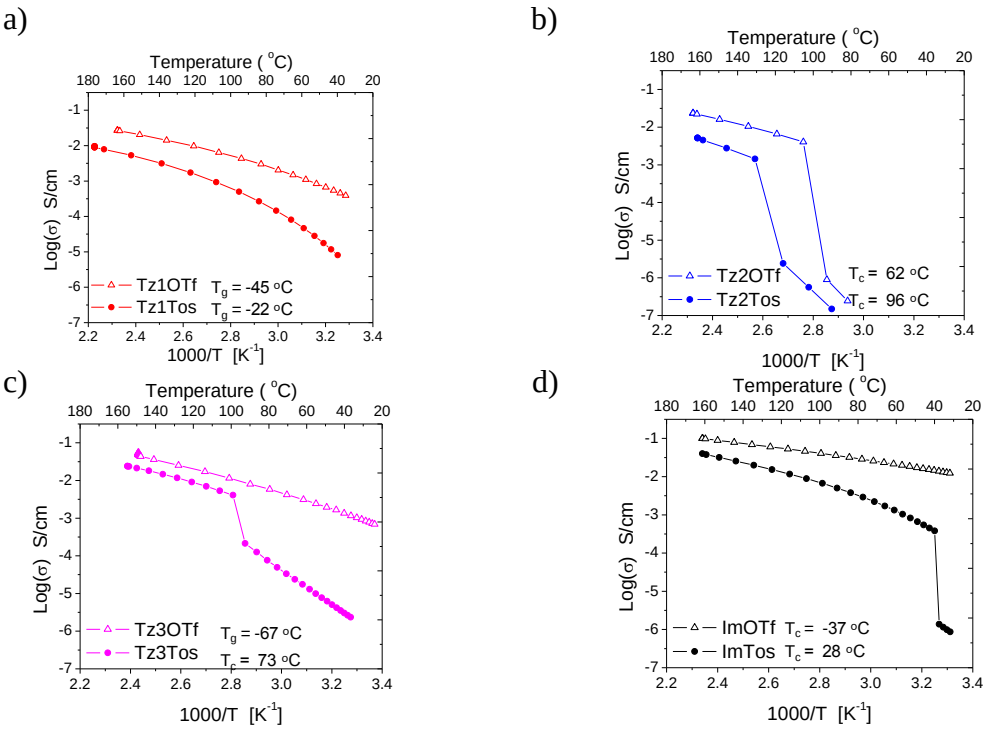

Figure 4.7. Comparison of ionic conductivity between two salts with same cation and different anion a) Tz1Tos vs. Tz1OTf b) Tz2Tos vs. Tz2OTf c) Tz3Tos vs. Tz3OTf d) ImTos vs. ImOTf

4.4.6 Electrochemical stability

The electrochemical stability of ionic liquids is an important parameter for their application in electrochemical devices (batteries, supercapacitors), electrochemical synthesis, metal deposition etc. The electrochemical stability of the salts was evaluated by cyclic voltammetry. The electrochemical window of ImOTf was measured as 4.31 V which is similar to

that reported for ethylmethylimidazolium triflate (EMIM-OTf) by Grätzel *et al*. on a platinum electrode.[1, 10]

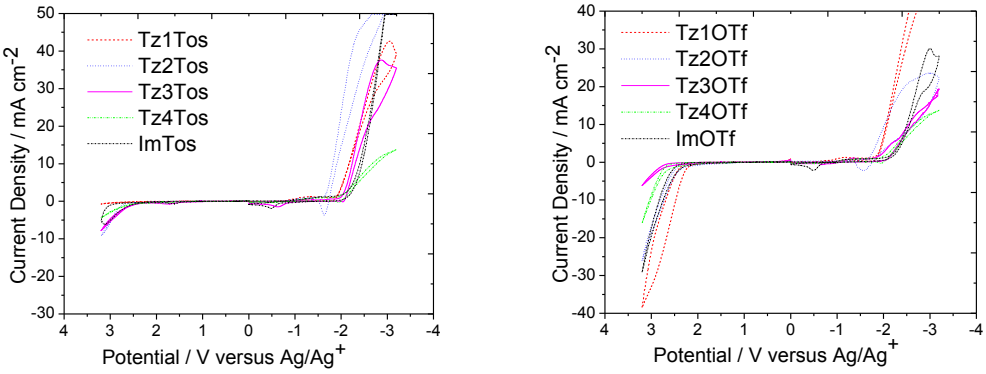

(a) (b)

Figure 4.8. Cyclic voltammograms a) toslyate series b) triflate series.

The cyclic voltammograms of both; tosylate series and triflate series are shown in figure 4.8 and the data for cathodic ($E_{cathodic}$) and anodic (E_{anodic}) limits and electrochemical windows (EW) are summarized in table 4.2. All the triazolium salts prepared, except Tz2OTf, have an electrochemical stability window of more than 4 V. For each pair of salts with the same cation, but different anion, $E_{cathodic}$ values are similar indicating that the cathodic stability of these salts with electrochemically stable anions is limited by the decomposition of the cation. The cations studied here, exhibit reductive stability in the following order: Tz3 ≈ Tz4 ≈ Im > Tz1 > Tz2. The reduction potential of salts containing Tz3, Tz4 and Im cation are similar. This indicates that electrochemical stabilities of 1,2,3-triazolium cations are influenced by the substitution pattern at the 1 and 3 positions and not the 4 position of the triazole ring. Also, these results clearly indicate that depending upon the substituents at the nitrogen atom, the triazolium salts may have cathodic stability comparable to imidazolium salts.

Table 4.2. Cathodic and anodic limits ($E_{cathodic}$ and E_{anodic} vs. Ag/Ag^+ are set at a threshold of 1.0 mA/cm^2) and electrochemical window (EW) for the ionic salts at room temperature.

Entry	Salts	$E_{cathodic}$ (V)	E_{anodic} (V)	EW (V)
1	Tz1Tos	-1.79	2.56	4.35
2	Tz1OTf	-1.86	2.17	4.03
3	Tz2Tos	-1.6	2.53	4.13
4	Tz2OTf	-1.67	2.12	3.79
5	Tz3Tos	-2.1	2.52	4.62
6	Tz3OTf	-2.1	2.4	4.5
7	Tz4Tos	-2.08	2.58	4.66
8	Tz4OTf	-2.08	2.39	4.47
9	ImTos	-2.12	2.55	4.67
10	ImOTf	-2.13	2.18	4.31

The oxidative stability of all tosylates is in the range of 2.5 V -2.6 V while for triflate containing salts is in the range of 2.15 - 2.4 V. The tosylate salt series exhibit higher stability towards oxidation than triflates. Different E_{anodic} values for the salts with the same triflate anion show that the anodic decomposition of the salts is influenced by the cations as well. The anions might be more stable towards reduction and oxidation than the cations. Thus, both the cathodic and anodic decomposition potentials are influenced by the cations in case of 1,2,3-triazolium

salts, which is similar to that observed for 1,3-dialkyl imidazolium salts and unlike quaternary ammonium salts, where cathodic limit is governed by reduction of cation and anodic limit by oxidation of anions.[6, 9] Overall, 1,2,3-triazolium cations have better cathodic stability than pyridinium cations, similar to imidazolium cations and inferior to quaternary ammonium cations.[1, 9, 36-37]

The oxidation current observed around -0.5 V for Tz3 salts and around -1.6 V for Tz2 salts in figure 4.8, results from the formation of a surface film due to the reduction of some species at potentials more negative than their respective $E_{cathodic}$ limit. If the potential is scanned between 0 to -1.6 V for Tz2Tos and from 0 to -2.1 V for Tz3Tos, no oxidation current is observed at -0.5V and at -1.6 V respectively, figure 4.9. Tz2 cation is stable up to -1.6 V (bold line) and shows an oxidation current around -1.6 V (dotted line) only when scanned to a potential more negative than its $E_{cathodic}$ limit. Similarly Tz3 cation is stable up to -2.1 V and shows an oxidation current around -0.5 V (dotted line), when scanned above its $E_{cathodic}$ limit.

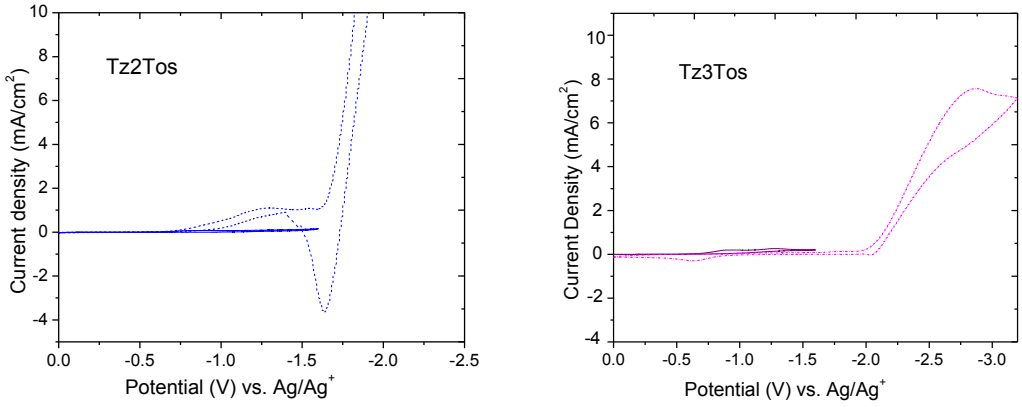

Figure 4.9. Discharge effect

4.5 Conclusions

A series of 1,2,3-triazolium salts comprising two different anions (toslyate and triflate) were synthesized and characterized. Their key properties; thermal stability, ion aggregation behavior, alkaline stability, conductivity and electrochemical stability were evaluated and

compared to those of imidazolium salts. It was found that all the above properties were influenced by the substituents at the 1 and 3 positions of triazolium cation and by the nature of the anion. All the 1,2,3-triazolium salts have thermal stability in the range of 200 – 250 °C. Although triazolium salts studied here have melting points greater than 95 °C, room temperature 1,2,3-triazolium based ionic liquids could be synthesized by appropriate choice of anion and tuning the substituents at the 1 and 3 positions. 1,2,3-triazolium salts exhibit ionic conductivity up to 0.1 S/cm at 150 °C, comparable to imidazolium salts. Their high ionic conductivity is an indicator of low viscosity similar to imidazolium salts, according to Walden's rule. The 1,2,3-triazolium based ionic salts exhibit a large stable electrochemical window (> 4 V). They have excellent chemical stability towards alkaline conditions compared to imidazolium salts, though not stable enough to survive the high pH environment of alkaline fuel cells.

4.6 References

1. Wasserscheid, P.; Welton, T., *Ionic Liquids in Synthesis*. Wiley-VCH: Weinheim, **2002**; pp 41-118.

2. Zhang, S. J.; Sun, N.; He, X. Z.; Lu, X. M.; Zhang, X. P., *J. Phys. Chem. Ref. Data* **2006,** 35, 1475-1517.

3. Domanska, U., *Ionic Liq. Chem. Anal.* **2009,** 1, 1-72.

4. Egashira, M.; Todo, H.; Yoshimoto, N.; Morita, M., *J. Power Sources* **2008,** 178, 729-735.

5. Sirisopanaporn, C.; Fernicola, A.; Scrosati, B., *J. Power Sources* **2009,** 186, 490-495.

6. Zhou, Z.-B.; Matsumoto, H.; Tatsumi, K., *Chem. Eur. J.* **2005,** 11, 752-766.

7. Sun, J.; Forsyth, M.; MacFarlane, D. R., *J. Phys. Chem. B* **1998,** 102, 8858-8864.

8. Tokuda, H.; Hayamizu, K.; Ishii, K.; Susan, M.; Watanabe, M., *J. Phys. Chem. B* **2005,** 109, 6103-6110.

9. Zhou, Z.-B.; Matsumoto, H.; Tatsumi, K., *Chem. Eur. J.* **2004,** 10, 6581-6591.

10. Bonhote, P.; Dias, A.-P.; Papageorgiou, N.; Kalyanasundaram, K.; Gratzel, M., *Inorg. Chem.* **1996,** 35, 1168-1178.

11. Zhang, Q.; Liu, S.; Li, Z.; Li, J.; Chen, Z.; Wang, R.; Lu, L.; Deng, Y., *Chem. Eur. J.* **2009,** 15, 765-778.

12. Fraser, K. J.; MacFarlane, D. R., *Aust. J. Chem.* **2009,** 62, 309-321.

13. Rostovtsev, V. V.; Green, L. G.; Fokin, V. V.; Sharpless, K. B., *Angew. Chem., Int. Ed.* **2002,** 41, 2596-2599.

14. Liebscher, J.; Shah, J.; Yacob, Z.; Sadiq, S.; Hanelt, S.; Blumenthal, H., *J. Phys. Conf. Ser.* **2009,** 182.

15. Jeong, Y.-K.; Kim, D.-Y.; Choi, Y.-S.; Ryu, J.-S., *Org. Biomol. Chem.* **2011,** 9, 374-378.

16. Shah, J.; Khan, S. S.; Blumenthal, H.; Liebscher, J., *Synthesis* **2009**, 3975-3982.

17. Khan, S. S.; Hanelt, S.; Liebscher, J., *ARKIVOC (Gainesville, FL, U. S.)* **2009**, 193-208.

18. Ivashkevich, O. A.; Matulis, V. E.; Lyakhov, A. S.; Grigorieva, I. N.; Gaponik, P. N.; Sukhanov, G. T.; Filippova, Y. V.; Sukhanova, A. G., *Chem. Heterocycl. Compd.* **2009,** 45, 1218-1225.

19. Zhao, F. Q.; Xue, L.; Xing, X. L.; Hu, R. Z.; Zhou, Z. M.; Gao, H. X.; Yi, J. H.; Xu, S. Y.; Pei, Q., *Sci. China Chem.* **2011,** 54, 461-474.

20. Fletcher, J. T.; Keeney, M. E.; Walz, S. E., *Synthesis* **2010**, 3339-3345.

21. Jeong, Y.; Ryu, J.-S., *J. Org. Chem.* **2010,** 75, 4183-4191.

22. Anderson, J.; Madsen, U.; Bjorkling, F.; Liang, X., *Synlett* **2005**, 2209-2213.

23. Appukkuttan, P.; Dehaen, W.; Fokin, V. V.; Van der Eycken, E., *Org. Lett.* **2004,** 6, 4223-4225.

24. Begtrup, M., *Acta Chem. Scand.* **1971,** 25, 249-259.

25. Begtrup, M.; Larsen, P., *Acta Chem. Scand.* **1990,** 44, 1050-1057.

26. Gozzo, F. C.; Santos, L. S.; Augusti, R.; Consorti, C. S.; Dupont, J.; Eberlin, M. N., *Chem. Eur. J.* **2004,** 10, 6187-6193.

27. Bini, R.; Bortolini, O.; Chiappe, C.; Pieraccini, D.; Siciliano, T., *J. Phys. Chem. B* **2007,** 111, 598-604.

28. Forsyth, S. A.; MacFarlane, D. R., *J. Mater. Chem.* **2003,** 13, 2451-2456.

29. Strehmel, V.; Reynaud, E.; Wetzel, H.; Görnitz, E.; Laschewsky, A., *Macromol. Symp.* **2009,** 275-276, 242-249.

30. Einsla, B. R.; Chempath, S.; Pratt, L. R.; Boncella, J. M.; Rau, J.; Macomber, C.; Pivovar, B. S., *ECS Trans.* **2007,** 11, 1173-1180.

31. Macomber, C. S.; Boncella, J. M.; Pivovar, B. S.; Rau, J. A., *J. Therm. Anal. Calorim.* **2008,** 93, 225-229.

32. Arduengo, A. J.; Harlow, R. L.; Kline, M., *J. Am. Chem. Soc.* **1991,** 113, 361-363.

33. Begtrup, M., *Bull. Soc. Chim. Belg.* **1988,** 97, 573-597.

34. Vila, J.; Varela, L. M.; Cabeza, O., *Electrochim. Acta* **2007,** 52, 7413-7417.

35. Zech, O.; Stoppa, A.; Buchner, R.; Kunz, W., *J. Chem. Eng. Data* **2010,** 55, 1774-1778.

36. Zhou, Z.-B.; Matsumoto, H.; Tatsumi, K., *Chem. Eur. J.* **2006,** 12, 2196-2212.

37. Noda, A.; Watanabe, M., *Electrochim. Acta* **2000,** 45, 1265-1270.

CHAPTER 5

HYDROXIDE CONDUCTING POLYELECTROLYTES COMPOSED OF COBALTOCENIUM DERIVATIVES

5.1 Introduction

The exploration of stable cations to develop AEMs to date, has mostly involved tailoring of electronic and steric components of ammonium or phosphonium cations. In our quest to identify the most stable cation at elevated pH and temperatures, we have decided to study cobaltocenium derivatives $[Cp_2Co]^+$, cationic analogues of neutral metallocenes.

Traditional AFCs employ aqueous KOH as an electrolyte and have excellent chemical stability. This is due to the closed shell noble gas configuration of K^+ cation, which makes it stable. However, K^+ is difficult to immobilize. On the other hand, ammonium and phosphonium cations are formed by oxidation at N and P centers respectively, which makes them susceptible to reduction by nucleophilic attack leading to the loss of cationic charge. This motivated us to explore cations that have noble gas configuration similar to alkali metal cations and those that can be immobilized. Cobaltocenium cation, isoelectronic with ferrocene, has an 18 electron closed valence-shell configuration. It can also potentially be attached to polymers through functionalization of the cyclopentadienyl ring.

The cobaltocenium cation is formed by oxidation of cobaltocene which has 19 electrons in valence shell, one electron over a closed shell configuration and an ionization potential of 6.2 V, slightly more than that of alkali metals.[1-3] Cobaltocenium ion behaves like a large alkali metal ion in aqueous solution.[4] Cobaltocenium salts are extremely stable with decomposition in the range of 250 °C - 350 °C and resistant to attack by strong acids and bases.[1] They are stable at 175 °C in the presence of NaOH over 4 days.[5-6] They are also reported to be stable in the presence of hydrogen peroxide.[4] Cobaltocenium ions tend to reduce to cobaltocene solely by complex

hydrides such as aluminium hydride and borohydride.[7] Both theory and experimental results of cobaltocene have shown a redox potential due to the Co(III)/Co(II) couple at about -0.9 - -1.1 V relative to a saturated calomel electrode and there is a negative shift in redox potential when metallocenes are tethered to a polymer.[8-10] This makes cobaltocenium salts electrochemically stable for fuel cell applications as typical fuel cell generates 0.6 - 0.8 Volt at full rated load.

Polymers containing cobaltocenium ion have been investigated for potential use as anion exchange resins at temperatures up to 220 °C. Ito *et al*. reported loss of 30% ion exchange capacity at 150 °C for polymeric pentamethylene cobaltocenium hydroxide compared to 100% loss for quaternary ammonium cation based ion exchange resins when heated in air. Polymeric pentamethylene cobaltocenium hydroxide is reported to be stable up to 140 °C when heated in water.[11]

This chapter will explore synthetic pathways to prepare cobaltocenium monomers followed by polymerization strategies. As a first step, the chemical stability of the unfunctionalized cobaltocenium cation was studied (section 5.3), for evaluation of its applicability in fuel cell environment. With the goal of making side chain cobaltocenium containing polymers, attempts were made to synthesize monosubstituted cobaltocenium functionalized styrene monomers as described in section 5.4.1. Two different types of disubstituted cobaltocenium monomers were synthesized to make main chain cobaltocenium containing polymers as detailed in section 5.4.2. In section 5.5, all polymerization strategies tried for polymerization of these monomers are discussed.

5.2 Experimental

5.2.1 Materials

Bis(cyclopentadienyl) cobalt (III) hexafluorophosphate, allylmagnesium bromide as a 1 M solution in diethyl ether, anhydrous DMSO, lithium chloride, acetonitrile, 6,6-dimethylfulvene,

6,6-diphenylfulvene, ammonium hexafluorophosphate, trityl hexafluorophosphate, 4-bromostyrene and 2.5 M solution of n-butyllithium in hexane were purchased from Sigma Aldrich. Cobalt(II) chloride, ultra dry was purchased from Alfa Aesar and the sealed bottle was cracked open in the dry box to avoid contamination by exposure to moisture.

5.2.2 Instrumentation

^{1}H-NMR, ^{13}C-NMR and ^{19}F-NMR spectra were obtained on a Bruker DPX-300 or Bruker Avance-400 NMR spectrometer. Infrared Spectroscopy (IR) was performed on Perkin Elmer Spectrum 100 FT-IR spectrometer using attenuated total reflection (ATR) crystal. Electrospray ionization mass spectra were acquired using an Esquire-LC ion trap instrument (Bruker Daltonics, Billerica MA) equipped with a standard ESI source. Spectra were obtained in positive ion modes from samples dissolved in acetonitrile (10^{-5} M). UV-Vis spectra were obtained with a Shimadzu UV-3600 UV-Vis-NIR spectrophotometer. Thermogravimetric analysis (TGA) was performed using a TA instruments TGA 2950 thermogravimetric analyzer at a heating rate of 10 °C/min under nitrogen flow of 20 mL/min. Glass transition temperature was obtained using TA instrument DSC Q200 differential scanning calorimeter by heating and cooling the samples at a rate of 10 °C/min under helium flow (25 mL/min).

5.3 Chemical stability of cobaltocenium salts

Pivovar and coworkers reported the chemical stability of benzyltrimethylammonium hydroxide $[BnMe_3N]^+[OH]^-$ in 2M NaOH at 80 °C over 30 days.[12] To date, these are the most caustic test conditions studied and $[BnMe_3N]^+[OH]^-$ has been the only cation with reported stability under these conditions. The stability of cobaltocenium hexafluorophosphate $(C_5H_5)_2Co^+PF_6^-$ in 2 M NaOH at 80 °C was studied using ^{1}H NMR, ^{13}C NMR, mass spectroscopy and UV-Vis spectroscopy.

A solution (0.01 M) of $(C_5H_5)_2Co^+$ PF_6^- in 2.0 M NaOH/D_2O was prepared and sodium tosylate (0.025 M) was used as an internal standard. It was not possible to increase the concentration of $(C_5H_5)_2Co^+$ PF_6^- due to its poor solubility in water. The solution was heated at 80 °C in a NMR tube and the chemical stability was studied by monitoring ^{1}H-NMR, ^{13}C-NMR and UV-Vis spectra at regular intervals.

The ^{1}H-NMR spectra of $(C_5H_5)_2Co^+$ PF_6^- in 2M NaOH, before and after heating, at 80 °C are shown in figure 5.1. The singlet at δ 2.2 ppm (CH_3) and doublets at δ 7.2 and δ 7.5 ppm (aromatic CH) correspond to the internal standard, sodium tosylate. The intensity of the peak at δ 5.6 ppm corresponding to Cp-H, decreases substantially after heating with no other change in the ^{1}H-NMR spectrum. In the ^{13}C-NMR spectra shown in figure 5.2, peaks at δ 20.5, 125.4, 129.5, 139.3 and 142.5 ppm correspond to the internal standard, sodium tosylate. The singlet at δ 84.5 ppm corresponding to the Cp carbons, changed from a singlet to a 1:1:1 triplet during the experiment. This is due to ^{1}H for ^{2}H exchange in NaOH/D_2O, quantitatively converting $(C_5H_5)_2Co^+$ PF_6^- to $(C_5D_5)_2Co^+$ PF_6^-. In ^{1}H-NMR, from the integration of area under the peak for Cp-H protons compared to that of sodium tosylate, the rate of H-D exchange was studied and it was found that more than 80% of the protons were replaced by deuterium within the first day of heating, figure 5.3. For comparison, we reproduced the reported alkaline stability of $[BnMe_3N]^+[OH]^-$ to benchmark it with that of $(C_5H_5)_2Co^+$ PF_6^-.

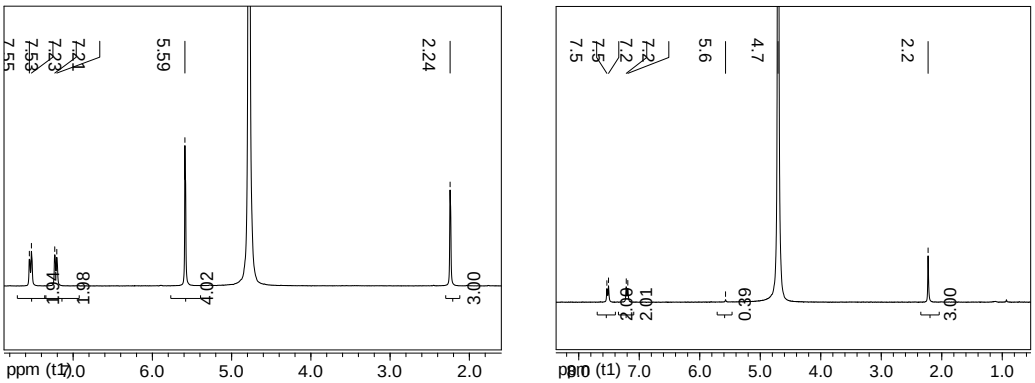

Figure 5.1. ^{1}H-NMR of 0.01 M $[Cp_2Co]^+$ PF_6^- in 2 M NaOH/D_2O with sodium tosylate (0.025 M) as an internal standard a) initial NMR b) after heating at 80 °C for 40 days

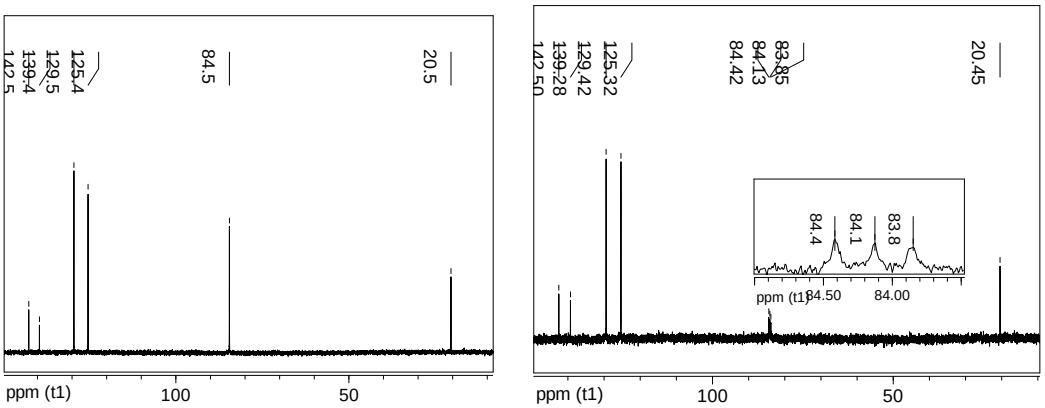

Figure 5.2. ^{13}C-NMR of 0.01 M $[Cp_2Co]^+$ PF_6^- in 2M NaOH/D_2O with sodium tosylate (0.025 M) as an internal standard a) initial NMR b) after heating at 80 °C for 40 days

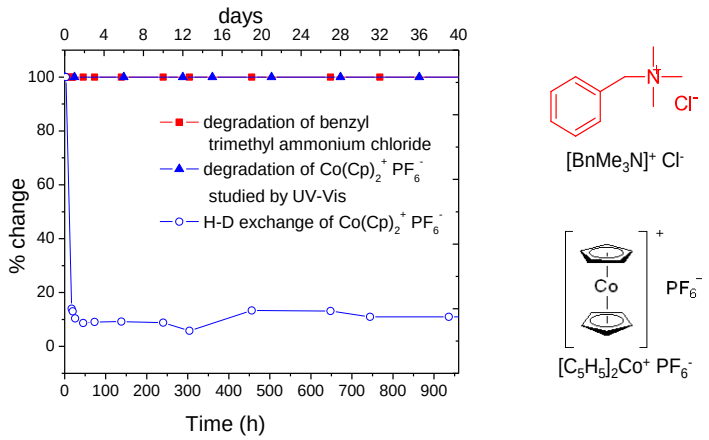

Figure 5.3. Stability of $[C_5H_5]_2Co^+$ PF_6^- compared to the stability of $[BnMe_3N]^+$ $[OH]^-$

The stability of $(C_5H_5)_2Co^+$ was also monitored by taking absorption spectra in the wavelength range of 200 to 600 nm using a UV-Vis spectrophotometer. As expected from the literature values,[2] the $(C_5H_5)_2Co^+PF_6^-$ salt showed three absorption peaks, 261 nm ($\varepsilon = 10^4$), 300 nm ($\varepsilon = 10^3$) and 403 nm ($\varepsilon = 10^2$), figure 5.4. Since the extinction coefficient of the three peaks differ by orders of magnitude, three different concentrations were used to observe all the peaks. Only at higher dilutions, peak at 261 nm was clearly visible, though peak at 403 nm becomes unnoticeable at that concentration. All the three peaks remained unchanged over 30 days. The electrospray ionization mass spectrometry (ESI-MS) was used to confirm the H for D exchange process in $(C_5H_5)_2Co^+$ PF_6^-. Mass spectra of $(C_5H_5)_2Co^+$ PF_6^- in 2 M $NaOH/D_2O$ before and after heating for 40 days is shown in figure 5.5. Mass of cobaltocenium increased from 189.4 g/mol to 199.5 g/mol due to the replacement of 10 hydrogens by 10 deuteriums. These results confirm the stability of $(C_5H_5)_2Co^+$ PF_6^- under test conditions, with the unexpected finding of ^1H for ^2H exchange.

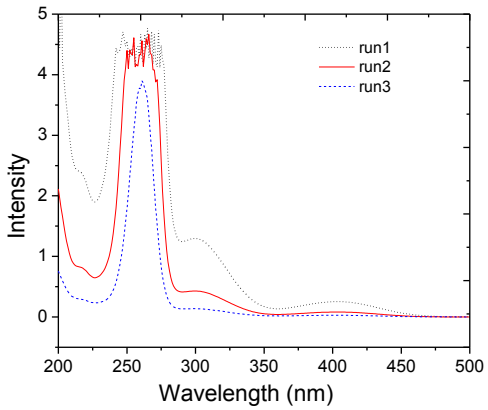

Figure 5.4. UV-Vis spectra of $[C_5H_5]_2Co^+$ PF_6^-

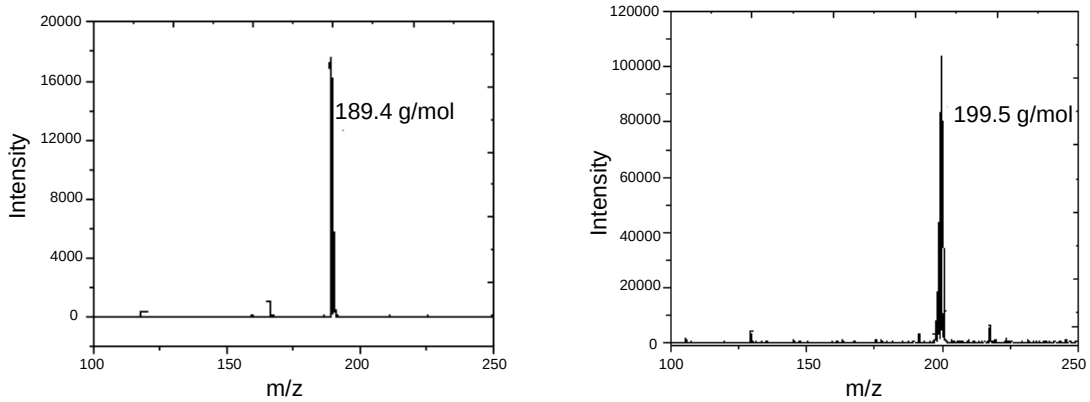

Figure 5.5. ESI-MS plots of 0.01 M $[Cp_2Co]^+$ PF_6^- in 2 M $NaOH/D_2O$ a) before and b) after heating at 80 °C for 40 days.

5.4 Monomer synthesis

Sheats *et al.* have done pioneering work in the synthesis of derivatives of cobaltocenium salts.[1, 13-14] Methylcyclopentadiene dimer being commercially available, a majority of the published literature reports use of 1-1'dimethyl cobaltocenium salts as the starting material followed by conversion to carboxylic acids, esters, amides, acid chlorides and amines.[1, 13-15] Among the very few reports of monosubstituted cobaltocenium derivatives, most involve ester or amide linkages that are unsuitable for AAEMFC applications.[16-18]

While designing the monomer synthesis for AEM, it is necessary to avoid CH_2 or CH group at the α position of cobaltocenium moiety. This is because hydroxide ion can abstract a proton at the α position and the resulting negative charge interacts strongly with the Co(III) center, figure 5.6. Structure **5.2** is very stable as it retains 18 electrons, closed valence shell configuration about cobaltocene. The oxidation state of cobalt changes from +3 to +1.[19]

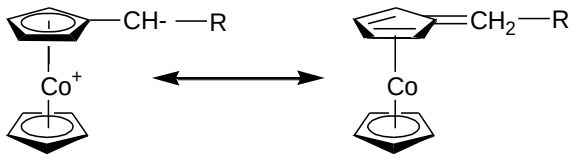

5.1 **5.2**

Figure 5.6. Stabilization of negative charge at α position of cobaltocenium nucleus.

5.4.1 Monosubstituted cobaltocenium salt

Depending upon the nature of functional group present on monosubstituted cobaltocenium salt, it could either be directly polymerized[17, 20] or attached to a preformed polymer.[16, 18] Attempts have been made to synthesize cobaltocenium functionalized styrene that could be polymerized to yield polystyrene containing cobaltocenium moiety as a pendant group. The benefit of exploring styrenic monomers is the versatility of polymerizations which can be utilized to produce well-defined styrene based polymers, copolymers, and block copolymers.

The synthetic route used to prepare cobaltocenium immobilized styrene monomer is shown in scheme 5.1. The reaction involves nucleophilic attack of a styrene para carbanion on the cobaltocenium cation, followed by hydride abstraction. In the first step of monomer synthesis, **5.3** was synthesized by the reaction of 4-lithiostyrene with $Co(Cp_2)^+PF_6^-$, however purification of the intermediate product **5.3** proved difficult. ^{1}H-NMR of the crude product (figure 5.7), showed byproducts including unreacted bromostyrene, 1-bromobutane, and perhaps the product obtained by direct nucleophilic attack of n-butyllithium on $Co(Cp_2)^+ PF_6^-$. Purification of **5.3** was attempted

using column chromatography on either silica gel or basic alumina. Inspite of using various solvent combinations and solvent gradients, ranging from hexane, to methanol, only unreacted bromostyrene was eluted and no product eluted from the column. Due to these difficulties, purification of **5.3** was not pursued further. Instead, the reaction mixture containing intermediate **5.3** was used directly for the next step to synthesize monomer **5.4**, by oxidation with trityl hexafluorophosphate ($Ph_3C^+ PF_6^-$) in dichloromethane at room temperature. To purify **5.4** several work-up conditions were evaluated; washing with water, ether, filtration and rotary evaporation. ^{1}H-NMR of the residue left behind showed removal of aliphatic impurities present in intermediate **5.3**, the presence of Cp ring and aromatic ring, however vinyl groups were absent. It could be due to the strong oxidizing nature of $Ph_3C^+ PF_6^-$ or polymerization occurred during rotary evaporation. Use of a milder oxidizing agent is suggested as an alternative. Synthesis of monomer **5.4** was not pursued further.

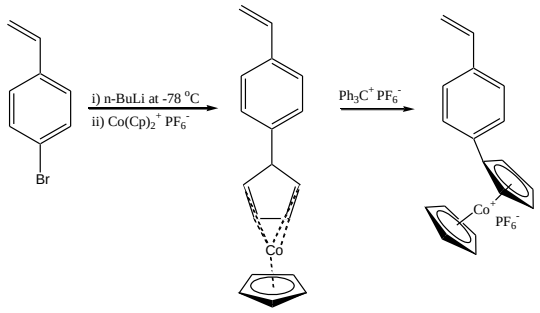

5.3 **5.4**

Scheme 5.1. Synthetic route to monosubstituted cobaltocenium functionalized styrene

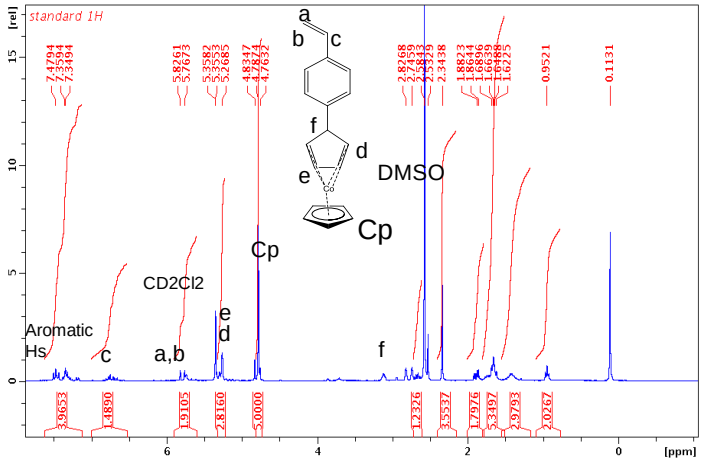

Figure 5.7. ^{1}H-NMR of crude intermediate **5.3**

Synthesis of intermediate 5.3. 4-bromo styrene was purified by passing through basic alumina prior to the reaction. A solution of 4-bromostyrene (0.17 mL, 1.32 mmol) in 10 mL of THF was subjected to one freeze pump thaw cycle and then cooled to -78 °C using dry ice-acetone bath, followed by dropwise addition of 0.48 mL of 2.5 M n-butyllithium in hexane to the stirred solution. After stirring the solution at -78 °C for 1 h, the mixture was cannulated to a solution of $Co(Cp_2)^+ PF_6^-$ (0.4g, 1.2 mmol) in 1.5 mL dry DMSO under dry nitrogen atmosphere. The mixture was allowed to warm to room temperature and allowed to stir overnight. The reaction was quenched by adding water followed by removal of THF by rotary evaporation. The product was extracted using CH_2Cl_2 and then washed with brine. The organic fractions were dried over $MgSO_4$ and then the solution was concentrated by rotary evaporation.

5.4.2 Disubstituted cobaltocenium salt

Two different disubstituted cobaltocenium monomers, **5.6a** and **5.6b** as shown in scheme 5.2 were synthesized. The synthesis involves reaction of allylmagnesium bromide with 6,6-dimethylfulvene or 6,6-diphenylfulvene forming the corresponding cyclopentadienyl anion, which was allowed to react with cobalt(II) chloride forming **5.5**. We expect formation of **5.5** from the rapid oxidation of initially formed cobaltocene derivative, presumably due to trace amounts of

H_2O or O_2 present. Use of lithium chloride enhances the reactivity of Grignard reagent by cleaving polymeric aggregates formed in solution.[21] Ion exchange reaction to convert **5.5** to monomer **5.6** was performed using $Ph_3C^+PF_6^-$ or ammonium hexafluorophosphate ($NH_4^+PF_6^-$) Superior yields were obtained with $NH_4^+PF_6^-$ due to facile removal of excess $NH_4^+PF_6^-$ by washing with water, as monomer is water insoluble. The overall yields ranged from 25 to 55 %. The monomers were characterized by ^{1}H-NMR, ^{13}C-NMR, ^{19}F-NMR, IR and mass spectroscopy and the data obtained are consistent with the structures. The monomer **5.5a** shows three absorption peaks at 276 nm, 324 nm and 415 nm in UV vis spectroscopy. Several attempts were made to grow crystals of monomer **5.6a** and **5.6b** for X-ray crystallography by slow evaporation of saturated acetonitrile solution, slow evaporation of saturated dichlorobenzene solution, slow diffusion of hexane into saturated acetonitrile solution and slow diffusion of ether into acetonitrile solution, all attempts were in vain. For fuel cell applications, chemical stability of monomer **5.6a** was studied in 0.36 M NaOH solution in 5:2 v:v mixture of DMSO-d_6/D_2O at 80 °C by ^{1}H-NMR and ^{13}C-NMR, similar to the procedure used for $Co(Cp_2)^+$ PF_6^-. The monomer was found to be stable over 27 days.

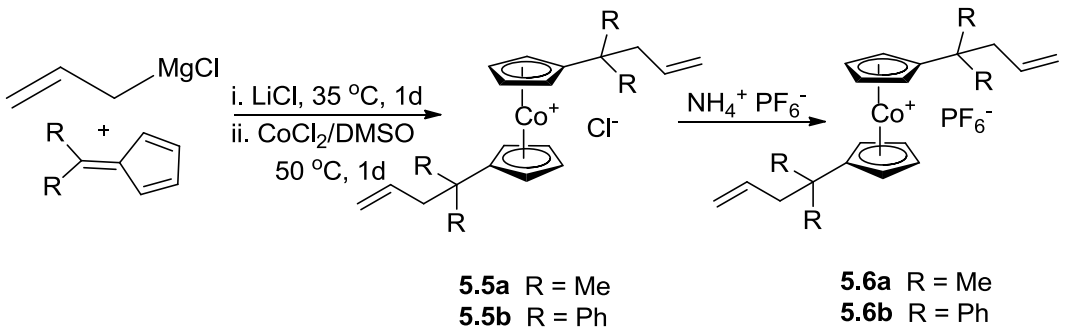

Scheme 5.2. Synthesis of disubstituted cobaltocenium monomers

Synthesis of monomer 5.6a. In a 200 mL Schlenk flask equipped with a stir bar, dry LiCl (1.7 g, 40 mmol) was added and the flask was flushed with nitrogen. Under nitrogen, allylmagnesium bromide (1 M solution in ether, 40 mL) was added and the solution was subjected to one freeze pump thaw cycle followed by addition of 6,6-dimethyl fulvene (2 mL,

16.6 mmol). The resulting solution was allowed to stir at 35 °C for 1 d. Then cobalt(II) chloride (1.1 g, 8.32 mmol) dissolved in anhydrous DMSO (10 mL) was added to the reaction mixture and the solution was allowed to stir at 50 °C for 18 h. The resultant solid product obtained was removed from the Schlenk flask by dissolving in acetonitrile. Solvent was removed under reduced pressure and the resultant green solid was washed with diethyl ether (50 mL) and dried at 30 °C under vacuum for 4 h giving **5.5a**, a green product. To a stirred suspension of **5.5a** in water (150 mL), excess $NH_4^+PF_6^-$ (4.1 g, 25 mmol) was added and the solution was allowed to stir at room temperature for 4 h. Then the solution was centrifuged to remove water followed by washing with water and ether (1 × 100 mL). The product was dissolved in acetonitrile and passed through a column of basic alumina followed by removal of solvent by rotary evaporation and drying under vacuum overnight at 40 °C giving a brown product. Overall yield = 52%. ^{1}H-NMR (CD_3CN, 300 MHz) δ 5.67 (m, =CH), 5.58 (t, C_5H_4), 5.51 (t, C_5H_4), 4.96 (dd, CH_2=), 2.18 (d, CH_2), 1.27 (s, CH_3). ^{13}C-NMR (CD_3CN, 75 MHz) δ 134.61, 120.6, 119.37, 83.84, 82.21, 48.92, 35.08, 27.90. ^{19}F-NMR (CD_3CN, 282 MHz) δ -72.8 ($^1J_{PF}$ = 705.9 Hz). FT-IR: 3075, 2969, 2924, 1697, 1639, 1475, 1397,827, 555 cm^{-1}. ESI-MS: (m/z) found: 353.3; calculated: 353.41

Synthesis of 5.6b. Monomer **5.6b** was prepared as described for 5.6a.^{1}H-NMR (CD_3CN, 300 MHz) δ 7.5 (m, Ph), 5.47 (m, =CH), 5.26, 5.15 (2 × t, C_5H_4), 5.02 (q, CH_2=), 3.17 (d, CH_2). ^{13}C-NMR (CD_3CN, 75 MHz) δ 146.76, 129.8, 129.15, 128.7, 128.28, 120.6, 119.3, 85.28, 84.87, 51.64, 44.58. ^{19}F-NMR (CD_3CN, 282 MHz) δ -72.87 ($^1J_{PF}$ = 705.9 Hz). ESI-MS: (m/z) found: 601.3; calculated: 601.7

5.5 Polymerization

As discussed in section 5.4.1, synthesis of mono substituted cobaltocenium rings proved difficult. Polymerization of disubstituted cobaltocenium monomers was attempted using acyclic diene metathesis polymerization (ADMET), step growth polymerization using thiol-ene

chemistry and hydrosilylation chemistry. Polymerization of these monomers should yield polymers containing cobaltocenium moiety in the backbone. Also disubstituted monomers could be used to make crosslinked membranes.

5.5.1 ADMET

Acyclic diene metathesis polymerization is a step growth condensation polymerization, carried out using Schrock catalyst or Grubbs catalyst.[22] ADMET of monomer **5.6a** was attempted using Grubbs third generation catalyst[23] under dry nitrogen atmosphere, scheme 5.3. ADMET was performed in different solvents, CH_2Cl_2, dichlorobenzene and 1:1 mixture of CH_3OH:CH_2Cl_2, several other reaction parameters were also varied, reaction times of 1, 2 or 3 days, reaction temperatures of 30 °C, 40 °C and 50 °C. Concentration of the solutions were varied from 0.2 M for 1,2-dichlorobenzene to 2 M for CH_2Cl_2 solution. However, in most of the attempts, ring closing metathesis (RCM) was the dominant reaction, giving product **5.7**. This was confirmed by ^{1}H-NMR and mass spectroscopy. In the mass spectrum of the product, shown in figure 5.8, peak at m/z = 325 corresponds to RCM product **5.7** and peak at m/z = 353 corresponds to unreacted monomer **5.6a**. No peaks of dimers (m/z = 339) or trimers (m/z = 334) were observed. The relatively low concentration of monomer, due to solubility limitation facilitates intramolecular cyclization over intermolecular condensation reaction. Given these findings, ADMET polymerization was not pursued further.

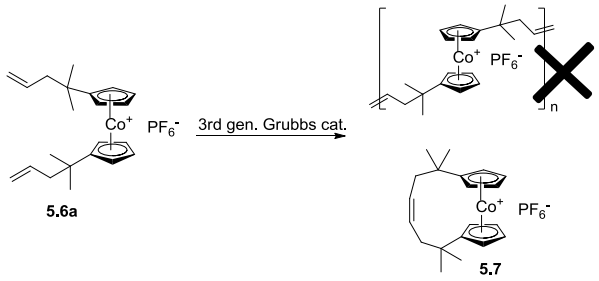

Scheme 5.3. ADMET polymerization of monomer **5.6a**

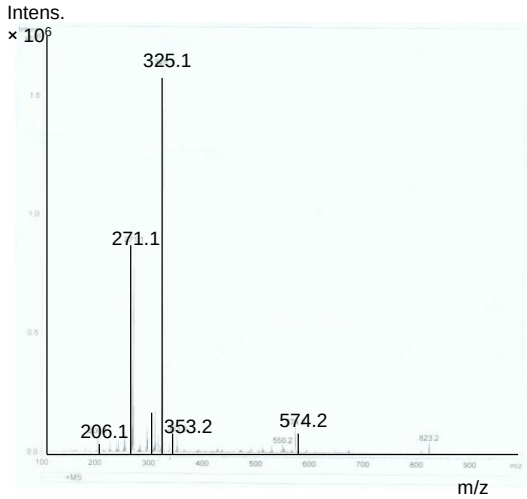

Figure 5.8. Mass spectrum of product obtained by ADMET polymerization of monomer **5.6a**

5.5.2 Thiol-ene coupling

Polymerization of monomer **5.6a** was attempted by step-growth photopolymerization with a dithiol using thiol-ene coupling.[24-25] Polymerization attempts were made with 1:1 molar ratio of monomer **5.6a** and 1,10-decanedithiol using 0.2 - 5 wt% dimethoxyphenyl acetophenone (DMPA) as the initiator, as shown in scheme 5.4. 1,10-decanedithiol, a longer alkyl chain dithiol was used to reduce formation of cyclic products. Reaction was performed on 0.1 - 0.3 g scale in a sealed quartz glass crucible with a minimum amount of solvent and the reaction mixture was deoxygenated by bubbling with nitrogen for 5 min. The reaction was followed by FT-IR for conversion of both the S-H (2559 cm^{-1}) and C=C (1639 cm^{-1}) functional groups independently. Although thiol-ene coupling is generally completed with irradiation time of few seconds to minutes,[25-27] no polymerization was observed even after 1 day. To check the validity of thiol-ene coupling with cobaltocenium salt, thiol-ene reaction of monomer **5.6a** was performed with excess of propanethiol as shown in scheme 5.5. In spite of using excess DMPA initiator, nitrogen atmosphere and longer reaction times, no product was obtained. All the resonances of monomer were intact in the ^{1}H-NMR spectrum with some formation of disulfide linkages. This lead us to

the conclusion that the vinyl groups of cobaltocenium monomer are not amenable to thiol ene radical reactions.

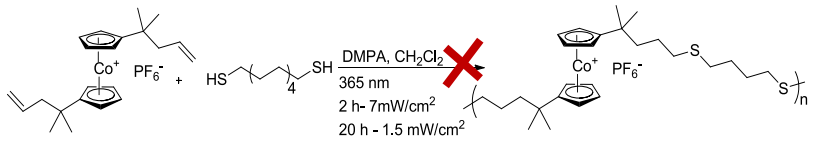

Scheme 5.4. Step-growth photopolymerization using thiol-ene coupling

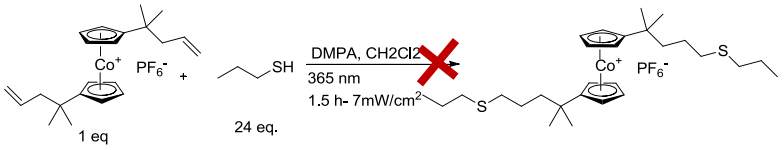

Scheme 5.5. Thiol-ene reaction of monomer **5.6a** with propanethiol

5.5.3 Hydrosilylation

Step-growth polymerization using Pt^{o} catalyzed hydrosilylation chemistry[28-29] was attempted as an alternative polymerization technique. Hydrosilylation reaction of divinyl monomer **5.6a** with diethyl silane in 1:1 molar ratio, using Karstedt's catalyst under dry nitrogen atmosphere was performed as shown in scheme 5.6. The reaction was performed at 30 °C with CH_2Cl_2 solvent and at 70 °C with 1,2-dichlorobenzene solvent for 1 day. However, all the attempts gave unreacted monomer and diethylsilane, confirmed by ^{1}H-NMR (figure 5.9a). In ^{1}H-NMR of crude reaction mixture, the integration of peak at δ 4.96 ppm corresponding to the vinyl group of monomer indicates completely unreacted monomer. To check the validity of hydrosilylation chemistry with cobaltocenium monomer, hydrosilylation of monomer **5.6a** with 4 equivalents of triethylsilane was performed as shown in scheme 5.7. After 1 day of reaction, all the monomer was consumed giving product **5.8** as expected. This is confirmed from ^{1}H-NMR (figure 5.9b) where peaks corresponding to vinyl group at δ 4.96 ppm vanished. It is likely that mismatch of stoichiometries due to unavoidable weighing error while working with small

amounts of reactants (~ 30 uL), lead to the failed step-growth polymerization reaction with diethyl silane.

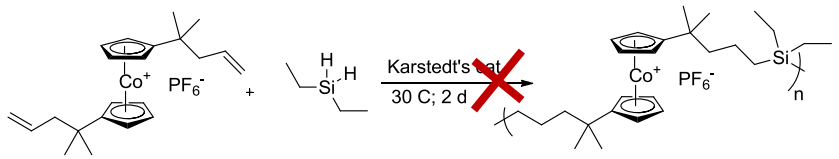

Scheme 5.6. Step-growth polymerization using hydrosilylation

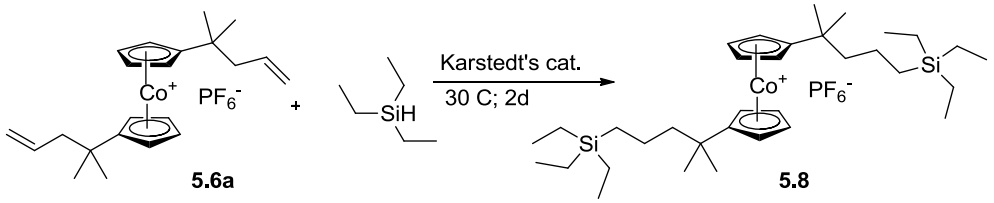

Scheme 5.7. Hydrosilylation reaction of monomer **5.6a** with triethylsilane

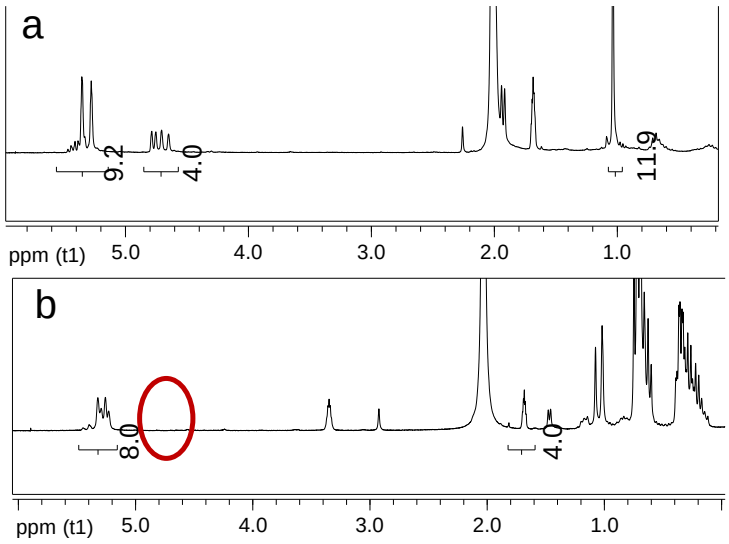

Figure 5.9. ^{1}H-NMR of a) reaction mixture after proposed polymerization of monomer **5.6a** with diethylsilane b) product from hydrosilylation reaction of monomer **5.6a** with triethylsilane.

It was decided to make crosslinked films of monomer **5.6a** using Pt^{0} catalyzed hydrosilylation with tetramethylcyclotetrasiloxane, scheme 5.8. Preparation of the crosslinked

network was performed according to the following protocol. In a 20 mL reaction vial, monomer **5.6a** (105 mg, 0.21 mmol) and tetramethylcyclotetrasiloxane (51 mg, 0.21 mmol) were dissolved in 0.3 mL of CH_2Cl_2 and purged with nitrogen. The vial was taken inside the glove box for addition of 4-5 drops of Karstedt's catalyst followed by stirring at 30 °C for 2 days. The solid product obtained was washed with CH_2Cl_2 to remove unreacted starting material. Polymerization was confirmed by FT-IR. The vinyl group, C=C stretching absorption at 1640 cm^{-1} disappeared after polymerization, figure 5.10. The crosslinked films are thermally stable up to 260 °C as determined by TGA, figure 5.11. Glass transition temperature of this crosslinked film was found to be -47 °C, indicating soft nature of the film.

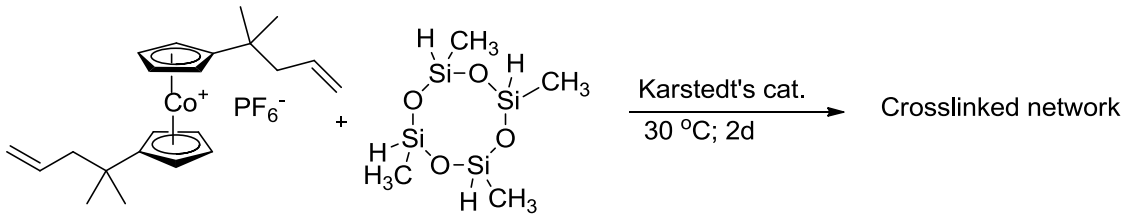

Scheme 5.8. Hydrosilylation of monomer **5.6a** with tetramethylcyclotetrasiloxane.

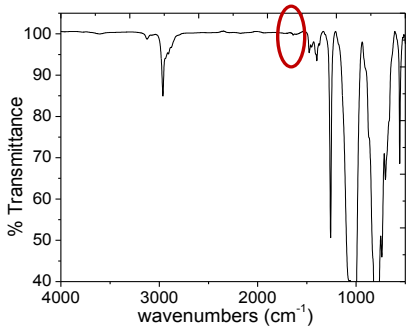

Figure 5.10. FT-IR spectrum of crosslinked network obtained by hydrosilylation reaction between monomer **5.6a** and tetramethylcyclotetrasiloxane.

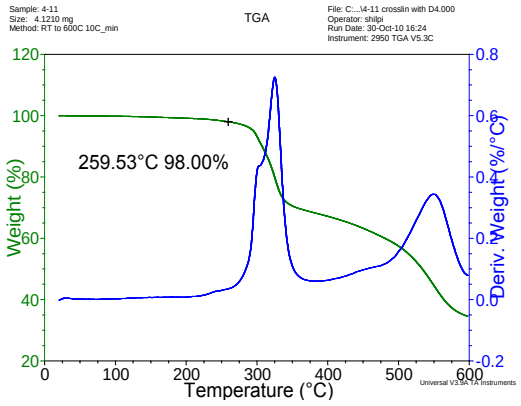

Figure 5.11. TGA plot of crosslinked network obtained by hydrosilylation reaction between monomer **5.6a** and tetramethylcyclotetrasiloxane.

5.6 Conclusions

It was theorized that the cobaltocenium $[Cp_2Co]^+$ cation will be stable under caustic conditions at elevated temperature due to its closed valence shell configuration, making it an an adequate cation for incorporation in AEMs. Preliminary investigations on the stability of $[Cp_2Co]^+$ framework were performed under the most caustic test conditions reported to date for the benchmark $[BnMe_3N]^+$ Cl^-,[12] and it was found that $[Cp_2Co]^+$ cation is as robust as the benchmark cation, with an interesting finding of ^1H for ^2H exchange.

The challenge remaining is to find a robust method to attach cobaltocenium cations to polymer scaffolds. Synthesis of cobaltocenium attached styrene monomer was pursued to achieve side chain cobaltocenium containing polymers. However, synthetic difficulties were encountered during this synthesis of mixed ring cobaltocenium salts that have polymerizable functionality attached to one of the cyclopentadienyl rings. The synthesis of disubstituted monomer with polymerizable vinyl groups attached to both the cyclopentadienyl rings of $[Cp_2Co]^+$, to achieve main chain cobaltocenium containing polymers was accomplished. Two different cobaltocenium monomers, one in which α hydrogens were replaced by methyl groups **5.6a** and other by phenyl groups **5.6b** were synthesized in good yields. The step-growth polymerizations of divinyl

monomers **5.6a** and **5.6b** were attempted using acyclic diene metathesis polymerization (ADMET), thiol-ene coupling and hydrosilylation chemistry. In all the attempts to polymerize the divinyl monomer using ADMET, ring closing metathesis (RCM) dominated the reaction giving a cyclic product. Preliminary investigations of thiol-ene coupling between divinyl monomer and dithiol or excess mono thiol were unsuccessful, under the conditions attempted. Although step-growth polymerization of divinyl monomer with diethyl silane was unsuccessful, hydrosilylation chemistry is feasible with the divinyl monomers as observed from the positive outcome of the reaction between divinyl monomer and triethyl silane. The reason for failure of step-growth polymerization could be imprecise stoichiometry of the reactants, or the presence of impurities. Crosslinking of monomer **5.6a** with tetramethylcyclotetrasiloxane using hydrosilylation resulted in films with adequate thermal stability.

The results of this chapter indicate the promising use of cobaltocenium cations to facilitate hydroxide ion conduction in AEMs. However, up to this point, synthetic challenges have hampered the efforts to develop polymers containing cobaltocenium cations. Several possible synthetic pathways to overcome the challenges mentioned in this work are discussed in chapter 7.

5.7 References

1. Sheats, J. E.; Hlatky, G., *J. Chem. Edu.* **1983,** 60, 1015.

2. Sheats, J. E., *J. Organomet. Chem. Libr*. **1979,** 7, 461-521.

3. Wilkinson, G.; Cotton, F. A., *Prog. Inorg. Chem.* Interscience Publishers, Inc: New York, **1959**; Vol. 1.

4. Wilkinson, G., *J. Am. Chem. Soc.* **1952,** 74, 6148-6149.

5. Balkus, K. J., Jr.; Shepelev, S., *Microporous Mater.* **1993,** 1, 393-391.

6. Balkus, K. J., Jr.; Gabrielov, A. G.; Shepelev, S., *Microporous Mater.* **1995,** 3, 489-495.

7. Green, M.; Pratt, L.; Wilkinson, G., *J. Chem. Soc*. **1959**, 3753.

8. Page, J. A.; Wilkinson, G., *J. Am. Chem. Soc.* **1952,** 74, 6149-6150.

9. Baik, M.-H.; Friesner, R. A., *J. Phys. Chem. A* **2002,** 106, 7407-7412.

10. Kondo, M.; Hayakawa, Y.; Miyazawa, M.; Oyama, A.; Unoura, K.; Kawaguchi, H.; Naito, T.; Maeda, K.; Uchida, F., *Inorg. Chem.* **2004,** 43, 5801-5803.

11. Ito, T.; Kenjo, T., *Bull. Chem. Soc. Japan* **1968,** 41, 614-619.

12. Einsla, B. R.; Chempath, S.; Pratt, L. R.; Boncella, J. M.; Rau, J.; Macomber, C.; Pivovar, B. S., *ECS Trans.* **2007,** 11, 1173-1180.

13. Sheats, J. E.; Rausch, M. D., *J. Org. Chem.* **1970,** 35, 3245-3249.

14. Sheats, J. E.; Kirsch, T., *Syn. Inorg. Metal-Org. Chem.* **1973,** 3, 59.

15. Takada, K.; Díaz, D. J.; Abruña, H. D.; Cuadrado, I.; González, B.; Casado, C. M.; Alonso, B.; Morán, M.; Losada, J., *Chem. Eur. J.* **2001,** 7, 1109-1117.

16. Ren, L.; Hardy, C. G.; Tang, C., *J. Am. Chem. Soc.* **2010,** 132, 8874-8875.

17. Ren, L.; Hardy, C. G.; Tang, S.; Doxie, D. B.; Hamidi, N.; Tang, C., *Macromolecules* **2010,** 43, 9304-9310.

18. Cuadrado, I.; Casado, C. M.; Lobete, F.; Alonso, B.; Gonzalez, B.; Losada, J.; Amador, U., *Organometallics* **1999,** 18, 4960-4969.

19. Sheats, J. E.; Miller, W.; Kirsch, T., *J. Organomet. Chem.* **1975,** 91, 97-104.

20. Mayer, U. F. J.; Gilroy, J. B.; O'Hare, D.; Manners, I., *J. Am. Chem. Soc.* **2009,** 131, 10382-10383.

21. Stefan, M. C.; Javier, A. E.; Osaka, I.; McCullough, R. D., *Macromolecules* **2008,** 42, 30-32.

22. Baughman, T. W.; Wagener, K. B., *Adv. Polym. Sci.* **2005,** 176, 1-42.

23. Love, J. A.; Morgan, J. P.; Trnka, T. M.; Grubbs, R. H., *Angew. Chem., Int. Ed.* **2002,** 41, 4035-4037.

24. Hoyle, C. E.; Lee, T. Y.; Roper, T., *J. Polym. Sci., Part A Polym. Chem.* **2004,** 42, 5301-5338.

25. Hoyle, C. E.; Bowman, C. N., *Angew. Chem., Int. Ed.* **2010,** 49, 1540-1573.

26. Wilderbeek, H. T. A.; van der Meer, M. G. M.; Bastiaansen, C. W. M.; Broer, D. J., *J. Phys. Chem. B* **2002,** 106, 12874-12883.

27. Cramer, N. B.; Scott, J. P.; Bowman, C. N., *Macromolecules* **2002,** 35, 5361-5365.

28. Chalk, A. J.; Harrod, J. F., *J. Am. Chem. Soc.* **1965,** 87, 16-21.

29. Marko, I. E.; Sterin, S.; Buisine, O.; Mignani, G.; Branlard, P.; Tinant, B.; Declercq, J.-P., *Science* **2002,** 298, 204-206.

CHAPTER 6

POLYMERS BEARING CYCLIC CARBONATES FOR LITHIUM ION BATTERIES

6.1 Introduction

The similarities between the transport mechanism of protons and lithium ions in an anhydrous medium were discussed in chapter 1. In chapters 2 and 3, proton mobility in 1*H*-1,2,3-triazole functionalized polymers was studied and it was observed that the local mobility of the protogenic group, and the rate of hydrogen bond making/breaking are critical to achieving high proton conductivity. Previous work on polymers functionalized with benzimidazole,[1] imidazole[2] and triazole[3-4] as proton conducting moieties has revealed that anhydrous proton conductivity depends on the local mobility of the protogenic group in the polymer film, and on the effective concentration of the heterocycle. Given that Li^+ is the next stable cation after H^+, the objective of this chapter is to understand if local mobility and concentration of Li^+ ion conducting moieties have similar influence on Li^+ ion transport as observed in the case of H^+ mobility.

Cyclic carbonates, especially ethylene carbonate (EC), are found in most of the liquid electrolyte formulations that are essential to form a good solid electrolyte interphase (SEI) on the anode and they serve as excellent solvents for lithium salts.[5] Commonly used electrolytes used in Li^+ ion batteries are composed of lithium salts dissolved in a mixture of cyclic carbonates and gelled in a suitable porous polymer matrix.[6] These gel polymer electrolytes typically exhibit conductivity of the order of 10^{-3} S/cm at room temperature,[6] higher than that of solid polymer electrolytes (SPE) and overcome safety concerns related to the use of liquid electrolytes. However, gel polymer electrolytes have disadvantages such as loss of liquid solvent and deterioration of mechanical properties.[7] There remains a need to develop all solid polymer electrolytes with improved conductivity. Immobilization of cyclic carbonates as a pendant group to the polymer backbone results in polymers containing structural element of the prototypical

solvent. Shriver and coworkers[8] reported promising results related to their initial work on poly(vinylene carbonate) (PVIC) and poly(1,3-dioxolan-2-one-4,5-diyloxalate), both rigid polymers containing covalently attached carbonate moieties. There are a few other reports of carbonates in the main chain[9] and tethered to low T_g polymers such as polyacrylates[10-11] and polysiloxanes[12] with conductivity reported up to 10^{-4} S/cm at 150 °C.[11]

To expand the understanding of structure-property relationships involved in carbonate tethered polymers, and to obtain a membrane with good mechanical properties, polynorbornenes containing carbonate moieties were studied. The polynorbornene backbone was chosen to achieve a balance between low T_g polymer backbones such as polysiloxanes and polyacrylates, and high T_g polymers such as polystyrene that are too rigid for ionic conductivity. The low T_g polymers have high segmental mobility and therefore higher ionic conductivity, but they lack mechanical strength.[13-14] On the other hand, though high T_g polymers can provide freestanding membranes, they exhibit poor ionic conductivity, and hence the polynorbornene backbone was selected. The four carbonate functionalized polymers targeted in this study are polyvinylene carbonate (PVIC), poly(5-norbornene-2,3-ylene ester) (PNbC), polynorbornene with one pendant carbonate per repeat unit (PNb3C) and polynorbornene with two pendant carbonate groups per repeat unit (PNbdi3C). The norbornene polymers are represented in figure 6.1 as the all *cis* configuration relative to the double bond and *cis* configuration relative to the cyclopentylene ring. PVIC is the simplest polymer containing the carbonate group in the main chain and has the highest density of carbonate groups for coordination to Li^+ ions. PNbC also contains carbonate group in the main chain, but has more free volume than PVIC and lower density of coordinating sites compared to PVIC. In PNbC and PNbdi3C, the concentration of coordinating sites is diluted, but carbonate groups are immobilized through a flexible spacer which allows for higher local mobility of the coordinating moieties. Studies on these materials will help understand how local mobility of

carbonates immobilized to a polymer and concentration of coordinating sites influence Li^+ ion conductivity.

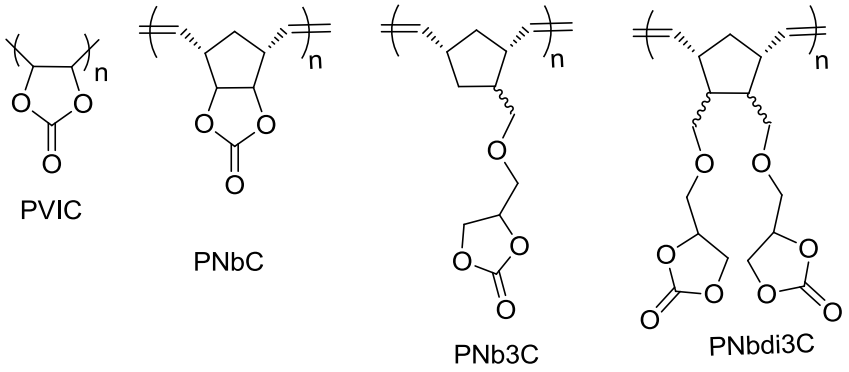

Figure 6.1. Structures of carbonate functionalized polymers studied.

6.2 Experimental

6.2.1 Materials

Vinylene carbonate, dicyclopentadiene, second generation Grubbs catalyst, cesium carbonate ($CsCO_3$), epichlorohydrin, 3-bromopyridine, benzene, dichloromethane (CH_2Cl_2), 5-norbornene-2-methanol, (chloromethyl)ethylene carbonate, 5-norbornen-2,3-dimethanol, aluminium chloride, zinc bromide, hydroquinone, sodium hydride, sodium bromide, N-methylpyrrolidone (NMP), dimethylformamide (DMF) and lithium triflate ($LiCF_3SO_3$) were purchased from Sigma Aldrich or VWR and used as received. CO_2 gas cylinder was purchased from Airgas. Azobisisobutyronitrile (AIBN) was purchased from Sigma Aldrich and recrystallized from methanol prior to use. Cyclopentadiene was obtained from cracking of dicyclopentadiene at 170 °C. Third generation Grubbs catalyst was synthesized as reported in the literature.[15]

6.2.2 Instrumentation

^{1}H-NMR and ^{13}C-NMR spectra were obtained on a Bruker DPX-300 NMR spectrometer. Solid state ^{13}C cross polarization magic angle spinning (CP MAS) NMR experiments were performed on a DSX 300 spectrometer. Molecular weight and dispersity (Đ) were determined by gel permeation chromatography (GPC) in THF or DMF with a flow rate of 1.0 mL/min using a refractive index detector and the molecular weights are reported relative to polystyrene standards. Fourier transform Infrared (FT-IR) spectra were obtained on a Perkin Elmer Spectrometer. Thermogravimetric analysis (TGA) were performed using a TA instruments TGA 2950 thermo gravimetric analyzer at a heating rate of 10 °C/min under nitrogen flow of 20 mL/min. Glass transition temperatures (T_g) and melting points (T_m) were obtained using TA instrument DSC Q200 differential scanning calorimeter by heating and cooling the samples at a rate of 10 °C/min under helium flow (25 mL/min). Wide angle X-ray scattering (WAXS) experiments were performed using Ni filtered Cu-Kα radiation (λ = 1.54 Å) from a Rigaku rotating anode (operated at 60 kV, 45 mA) and the photographic plate was kept at a distance of 139 nm. Conductivity versus temperature data were obtained via impedance spectroscopy measurements using Solartron 1260 Impedance/Gain Phase Analyzer by applying an excitation voltage of 100 mV with a logarithmic frequency sweep from 1 MHz to 0.1 Hz. A detailed description of the method and the hardware used is described in Appendix A

6.3 Carbonate functionalized norbornene polymers

In this section, synthesis and characterization of carbonate functionalized polymers and preparation of polymer electrolytes are detailed. Polyvinylene carbonate (PVIC) was synthesized by free radical polymerization of vinylene carbonate at 65 °C for 24 h using AIBN as an initiator. Molecular weight determination by DMF GPC indicated M_n = 530 K g/mol and Đ = 1.12. The synthesis and characterization of the other polymers used in this study are described below.

6.3.1 Synthesis of PNbC

5-norbornene-2,3-ylene ester **6.1** was synthesized by Diels-Alder reaction, [4+ 2] cyclo addition between cyclopentadiene and vinylene carbonate, scheme 6.1, using a modification of literature procedures.[16-18] The Diels-Alder reaction gives endo 5-norbornene-2,3-ylene ester as the dominant product.[19] The reaction was performed with use of excess vinylene carbonate, over a period of 3 days, and the resultant maximal yield was 46%. The monomer **6.1** is crystalline in nature with a T_m at 115 °C and is thermally stable up to 170 °C, the temperature corresponding to 2 % wt. loss as determined by TGA. Attempts were made to improve the yield of the reaction, to reduce the reaction time and to use cyclopentadiene in excess instead of vinylene carbonate, by using Lewis acid $AlCl_3$ or $ZnCl_2$ as a catalyst. Lewis acids catalyze the Diels-Alder reaction by complexing with carbonyl groups of dienophile.[20] Lewis acid catalyzed Diels-Alder reaction was attempted by varying several reaction parameters, complexation time between catalyst and vinylene carbonate from 10 minutes to 1 h, complexation temperature from 0 °C to room temperature and overall reaction times and temperatures. However, all the attempts resulted in degradation of the vinylene carbonate as observed from the absence of absorption peak of carbonyl group (C=O) in the FT-IR spectrum. Vinylene carbonate undergoes reductive degradation forming a radical anion when used as a solvent additive in lithium ion batteries.[21] Similarly, vinylene carbonate could degrade in the presence of Lewis acids, figure 6.2.

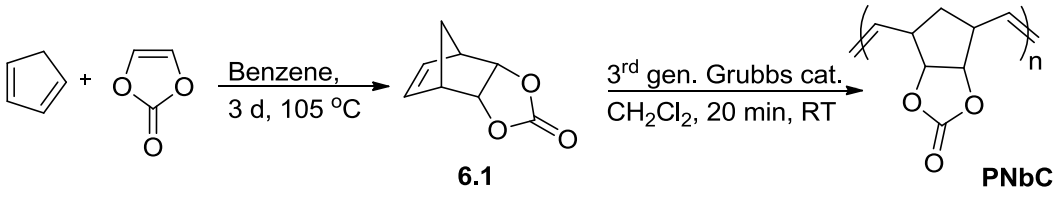

Scheme 6.1. Synthesis of polymer PNbC

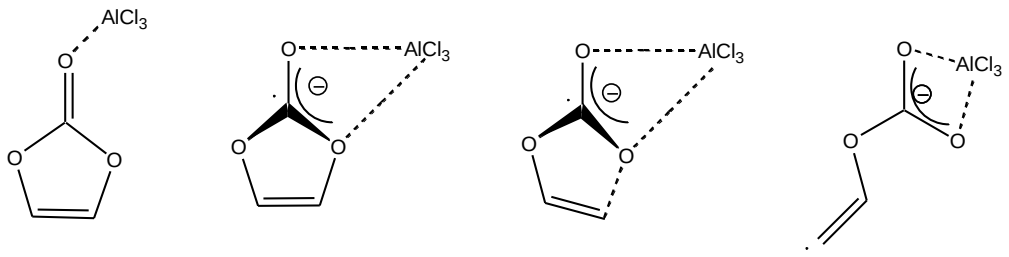

Figure 6.2. Degradation mechanism of vinylene carbonate in the presence of Lewis acids

Synthesis of 5-norbornene-2,3-ylene ester (6.1). In a 100 mL round bottom flask, freshly distilled cyclopentadiene (0.21 mL, 1eq.), vinylene carbonate (0.68 g, 2.5 eq.), benzene (0.4 mL) and a trace quantity of hydroquinone were combined and the mixture was allowed to stir at 105 °C for 3 days. The excess vinylene carbonate was recovered from the reaction mixture using vacuum distillation. The residue was purified by recrystallization from CCl_4/hexane (1:1) solution giving white crystalline monomer. Yield = 0.175 g (46%). ^{1}H-NMR ($CDCl_3$, 300 MHz) δ 6.25 (s, 2H), 5.02 (s, 2H), 3.31 (s, 2H), 1.81 (d, 1H), 1.32 (d, 1H).^{13}C-NMR ($CDCl_3$, 75 MHz) δ 155.52, 134.34, 78.91, 45.54, 42.51. FT-IR: 2994, 2940, 1775, 1511, 1455, 1369, 1246, 1159, 1048, 947, 756 cm^{-1}. EI-HRMS (m/z) found 153.10; calculated:153.16 [M + 1].

Monomer was polymerized by ring-opening metathesis polymerization (ROMP) using third generation Grubbs catalyst.[22-23] The polymerization was performed accroding to the following protocol. In a reaction vial, monomer **6.1** (75 mg, 0.49 mmol) was dissolved in CH_2Cl_2 (0.8 mL) and the resulting solution (0.6 M) was purged with nitrogen followed by addition of third generation Grubbs catalyst (2 mg). The reaction mixture was allowed to stir at room temperature for 30 minutes and then the reaction was quenched with (0.3 mL) ethyl vinyl ether. The solution was concentrated and precipitated in excess cold methanol giving a white colored polymer (M_n = 170 K g/mol, Đ = 1.07). The polymerization was confirmed by ^{1}H-NMR, figure 6.3, by the disappearance of C=C resonance at δ 6.25 ppm corresponding to the monomer and emergence of peaks at δ 5.6 ppm corresponding to the backbone unsaturation. Polymer PNbC is soluble in DMF, DMSO and nitromethane, and insoluble in THF.

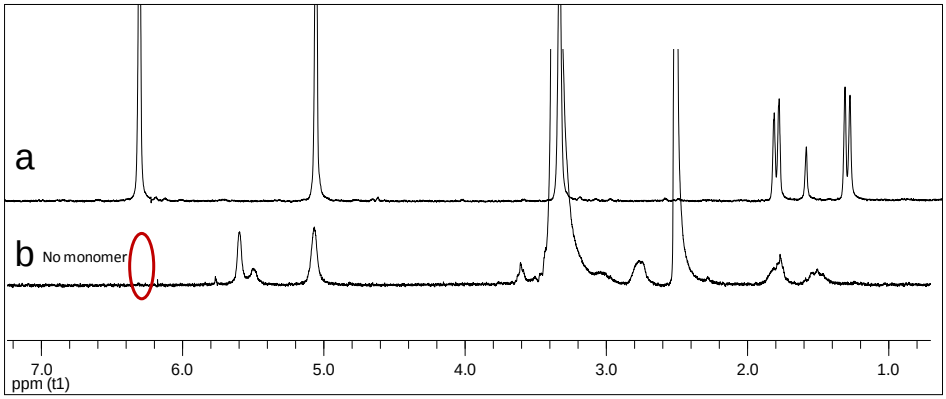

Figure 6.3. ^{1}H-NMR spectra of a) monomer b) PNbC

6.3.2 Synthesis of PNb3C

Attempts to synthesize monomer 5-norbornene-2-methoxy-(2-Oxo-[1,3]dioxolan-4ylmethyl) ether **6.2** were made by deprotonation of 5-norbornene-2-methanol with sodium hydride followed by nucleophilic substitution reaction with (chloromethyl)ethylene carbonate, scheme 6.2. All attempts resulted in degradation of carbonates. Rokicki *et al*.[24] reported the reaction between phenoxide ion and (chloromethyl)ethylene carbonate with resultant formation of phenoxy methyl carbonate **6.4** and 3-phenoxypropan-1,2-diol **6.6**, scheme 6.3. The mechanism involves attack of alkoxide on the methylene carbon atom of (chloromethyl)ethylene carbonate forming **6.3**. This intermediate can then undergo intramolecular cyclization forming the desired product **6.4**, or react with alcohol present in the reaction mixture forming **6.5** by decarboxylation. Although the reaction of **6.4** with a base to form **6.6** should take place only in the presence of strong base, absence of carbonate groups observed in attempted synthesis suggests this side reaction. We hypothesized that use of a milder base, $CsCO_3$[25] and a better leaving group will help to circumvent these side reactions. (Chloromethyl)ethylene carbonate was converted to (iodomethyl)ethylene carbonate by the Finkelstein reaction,[26] iodine being a better leaving group compared to chloride. However, use of milder base and a better leaving group did not help to prevent degradation of carbonates.

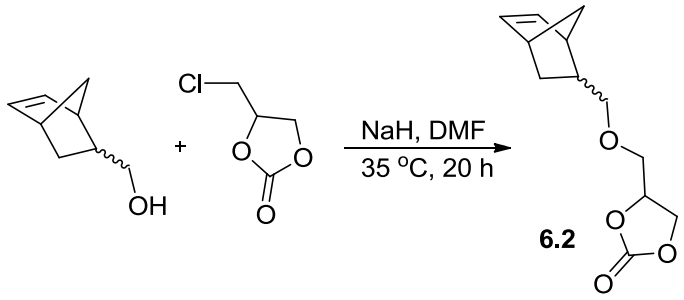

Scheme 6.2. Synthetic route to norbornene monomer containing pendant carbonate

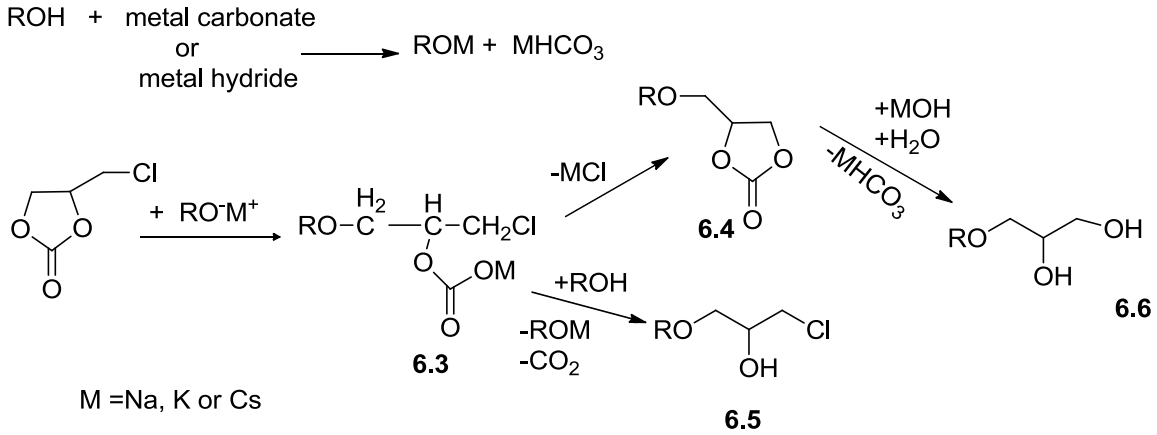

Scheme 6.3. Proposed mechanism for degradation of carbonates during synthesis of norbornene containing pendant carbonate.

An alternate synthetic route was adopted for the synthesis of monomer **6.2** as shown in scheme 6.4. The first step in the synthesis is epoxidation of 5-norbornene-2-methanol to form 5-norbornene glycidyl methyl ether **6.7**, followed by a ring expansion reaction of the oxirane ring with CO_2 to form a cyclic carbonate. The carbonation reaction was performed at atmospheric pressure, as per the reaction conditions reported by Endo and coworkers.[27] Formation of **6.2** was confirmed by ^{13}C-NMR and FT-IR. In the FT-IR spectrum of **6.2**, a distinct carbonyl absorption is observed at 1794 cm^{-1}, figure 6.4. Monomer synthesis was performed in NMP solvent and it was difficult to remove the solvent completely due to its high boiling point and so the monomer was used for polymerization without further purification. ROMP of monomer **6.2** was performed

and monitored by ^{1}H-NMR using similar procedure, as reported for PNbC. The resultant polymer PNb3C (M_n = 11.5 K g/mol and Đ= 1.65) is soluble in THF, DMF and DMSO.

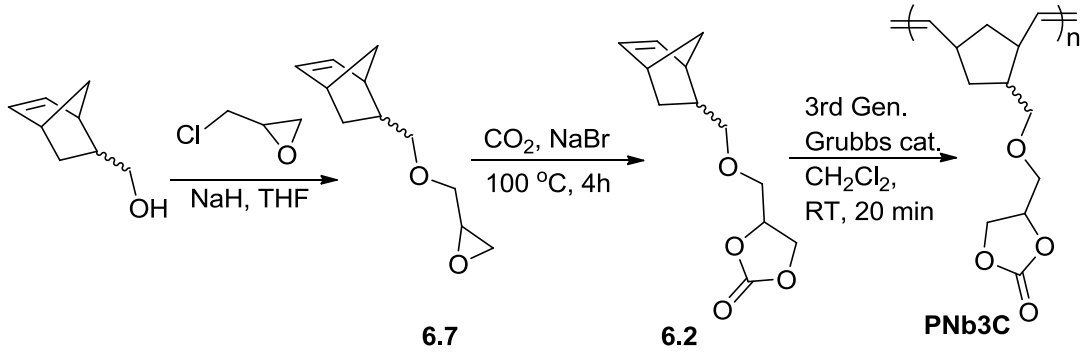

Scheme 6.4. Synthesis of PNb3C

Synthesis of 5-norbornene glycidyl methyl ether (6.7). In a 100 mL round bottom flask equipped with a reflux condenser, sodium hydride (0.42 g, 3 eq.) and dry THF (20 mL) were combined and the flask was purged with N_2 for 5-10 minutes. The solution was then cooled in an ice bath and 5-norbornene-2-methanol (0.7 mL, 1 eq.) was added slowly. The reaction mixture was allowed to stir at 80 °C for 1h. The solution was then cooled to 0 °C using an ice bath, followed by drop wise addition of epichlorohydrin (0.9 ml, 2 eq.). The reaction mixture was left for 22 h with continuous stirring at 70 °C. The reaction was terminated by adding ice cold water followed by extraction of the product with ether (4 × 50 mL). The organic layers were combined and washed with brine, dried over $MgSO_4$ and the solvent was removed under reduced pressure. The crude product obtained was purified by flash chromatography using ethyl acetate: hexane (1:3) to give **6.7** as a yellow colored liquid. Yield = 0.5 g, 50%. ^{1}H-NMR ($CDCl_3$, 300 MHz) δ 6.05 (m, 1H), 5.95 (m, 1H), 4.1 (q, 2H), 3.7 (m, 1H), 3.55 (m, 1H), 3.35 (m, 1H), 3.1-3.3 (m, 2H), 2.9 (m, 1H), 2.75 (m, 1H), 2.3 (m, 1H), 1.8 (m, 2H),1.4 (m, 1H), 0.47 (d, 1H). ^{13}C-NMR ($CDCl_3$, 75 MHz) δ 137.2, 136.66, 132.39, 75.32, 71.69, 50.95, 49.39, 44.99, 44.27, 38.77, 29.64. EI-HRMS (m/z) found 180.2; calculated: 180.25.

Synthesis of 5-norbornene-2-methoxy-(2-Oxo-[1,3]dioxolan-4ylmethyl) ether (6.2). In a round bottom flask, **6.7** (6.43 mmol) and sodium bromide (0.643 mmol) were dissolved in NMP (6.85 mL) and the resultant mixture was allowed to stir at 100 °C for 6 hours under an atmosphere of CO_2. The product was diluted with CH_2Cl_2 and washed with water (3 × 50 mL), brine and dried over $MgSO_4$. The solvent was removed under reduced pressure to give 5-norbornene-2-methoxy-(2-Oxo-[1,3]dioxolan-4ylmethyl) ether **6.2**. Yield = 87 %. ^{1}H-NMR ($CDCl_3$, 300 MHz) δ 5.95 (m, 1H), 5.75 (m, 1H), 4.7 (m, 1H), 4.4 (m, 2H), 4.25 (m, 1H), 3.5 (m, 2H), 3.1 (m, 2H), 2.95 (m, 2H), 1.65 (d, 1H), 1.25 (d, 1H), 1.1 (m, 2H). ^{13}C-NMR ($CDCl_3$, 75 MHz) δ 137.45, 132.35, 75.45, 75.14, 69.81, 66.35, 44.5, 43.37, 41.38, 24.49. FT-IR: 2966, 2255, 1794, 1478, 1393, 1260, 1171, 1104, 904, 835, 725 cm^{-1}. FAB-HRMS (m/z) found 225.17; calculated: 225.26

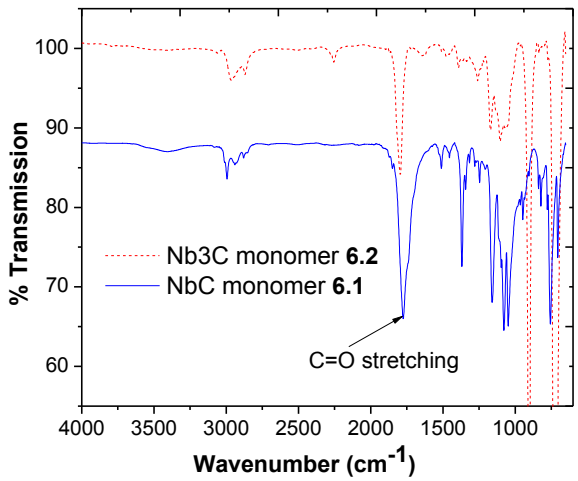

Figure 6.4. FT-IR spectra of monomer **6.1** and **6.2**

6.3.3 Synthesis of PNbdi3C

The synthesis of disubstituted norbornene monomer **6.9** was attempted by the procedure similar to that used for PNb3C. Synthesis involved reaction of epichlorohydrin with 5-norbornene-2,3-dimethanol forming 5-norbornene-2-3-dimethoxy-gylcidyl-ether **6.8** and then

carbonation of **6.8** to produce **6.9**, scheme 6.5. However, the reaction between 5-norbornene-2,3-dimethanol with epichlorohydrin using reaction conditions similar to that used for **6.7**, resulted in the formation of a solid product, insoluble in $CHCl_3$, benzene, toluene, CH_3OH, NMP and DMSO. Due to these solubility issues, further synthesis of PNb3diC was not pursued.

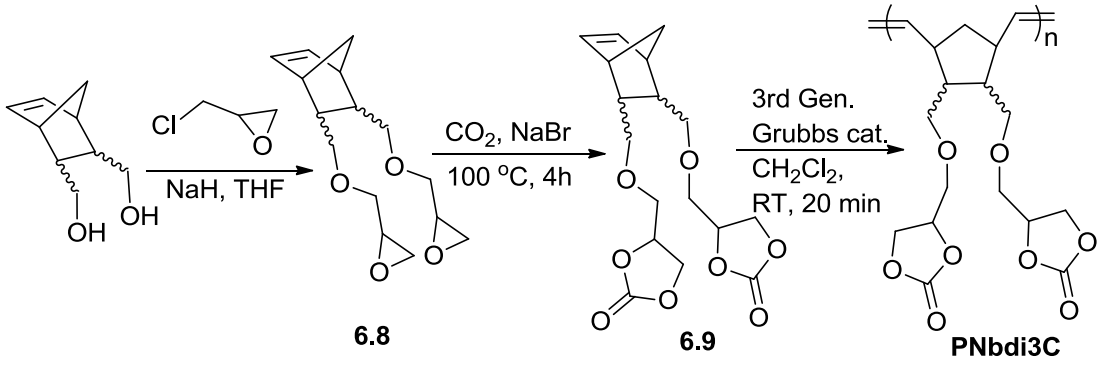

Scheme 6.5. Synthetic route to PNbdi3C

6.3.4 Preparation of polymer electrolytes

Polymer electrolytes were prepared in dry box to avoid contamination by moisture. Measured quantities of polymers and lithium triflate (LiOTf) in 1:1 molar ratio were dissolved in a minimum amount of suitable solvent (DMF for PVIC and PNbC, THF for PNb3C). Polymer electrolyte membranes were prepared by casting films from these solutions. The films were dried in a stepwise manner; 24 h at room temperature and atmospheric pressure followed by drying under vacuum at room temperature for 1 day, 70 °C for 2 days and then 110 °C for at least 2 days.

6.4 Thermal analysis

The decomposition temperatures (T_d) of all the polymers studied were determined by TGA. The onset of decomposition is reported as the temperature corresponding to 2% weight loss, Table 6.1. All the polymers are thermally stable up to 250 °C. The decomposition of PNbC and PNb3C proceeds in two steps as displayed in figure 6.5. The first weight loss step corresponds to the loss of carbon dioxide as calculated from the weight percentage.

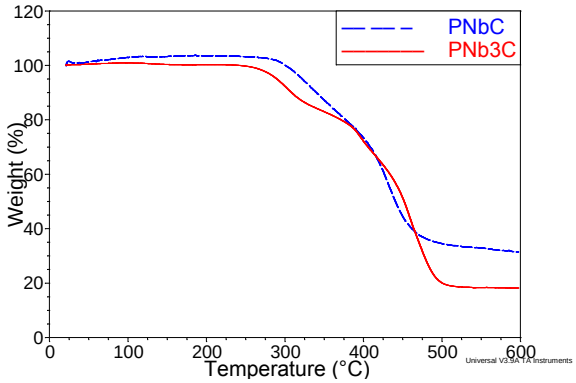

Figure 6.5. TGA traces of carbonate functionalized polymers

The thermal transitions for the polymers and polymer electrolytes were obtained by differential scanning calorimetry. The first heating cycle was used to erase the thermal history and the transitions from second heating cycle are reported in Table 6.1, and the relevant DSC traces are shown in figure 6.6. No T_g or T_m was observed for PVIC up to 200 °C, PNbC and PNb3C are amorphous in nature. On blending with LiOTf, PVIC-LiOTf exhibited a melting point at 102 °C, no melting points were observed for PNbC-LiOTf and PNb3C-LiOTf in the temperature range of -20 °C to 160 °C.

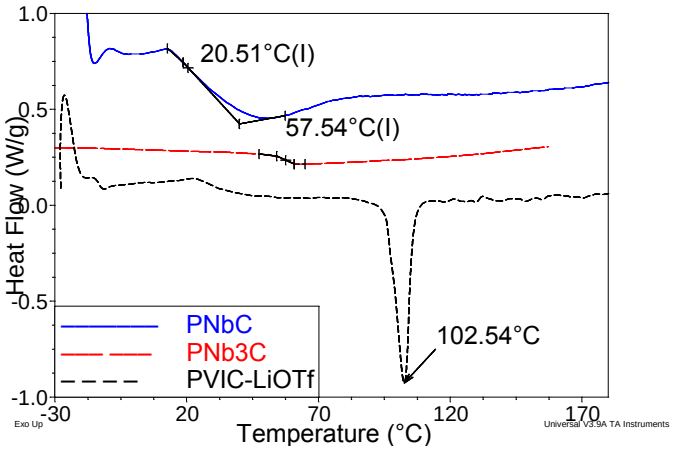

Figure 6.6. DSC traces of carbonate functionalized polymers

PVIC does not exhibit a T_m, but PVIC-LiOTf is crystalline in nature. Shriver *et al.*[8] reported similar results and presumed that T_m in PVIC-LiOTf is observed due to the formation of an eutectic mixture. This hypothesis is supported by our observation of no T_m up to 220 °C in the same PVIC-LiOTf sample after two years of storage at temperatures below 0 °C. It is likely that LiOTf crystals grew over time to the point that there is a phase separation and so no T_m was observed as polymer does not have its own T_m. All conductivity measurements and NMR studies for PVIC-LiOTf reported are for freshly prepared, i.e. phase mixed samples.

Table 6.1. Thermal properties of the carbonate functionalized materials

	T_g of pristine polymer (°C)	T_m of polymer electrolyte Polymer:LiOTf (1:1)	Wt.% carbonate	T_{d2} (°C)
PVIC	NA	102	100	250
PNbC	20	NA	56	277
PNb3C	57	NA	38	272

6.5 Conductivity

The lithium ion conductivities of the polymer electrolytes were measured by impedance spectroscopy. Polymer electrolyte films were sandwiched between two gold coated electrodes and the assembly was placed in a vacuum oven to ensure an anhydrous environment. The membrane thickness was measured using digital calipers prior to the conductivity measurements. The samples were heated to 160 °C, held at that temperature under vacuum for 40 h until conductivity stabilized, to ensure removal of moisture and solvent from the sample and then the conductivity data was obtained as a function of temperature upon cooling.

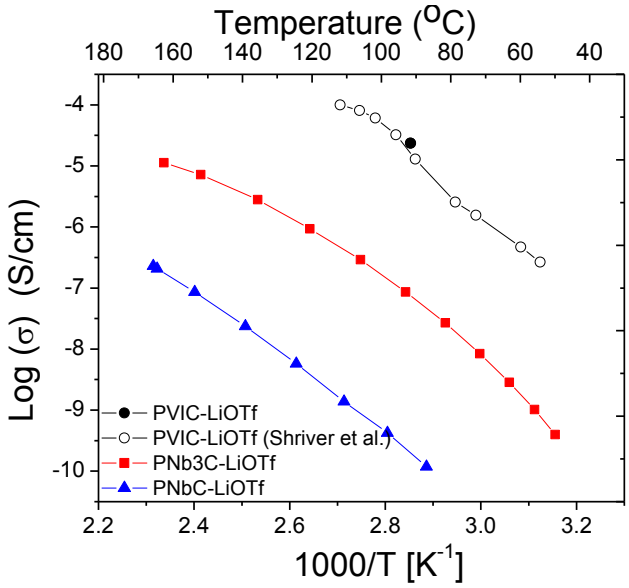

Figure 6.7. Conductivity of carbonate functionalized polymer electrolytes

The conductivity data of PVIC-LiOTf, PNb3C-LiOTf and PNbC-LiOTf are shown in figure 6.7, with the corresponding wt.% carbonate content listed in Table 6.1. The measured conductivity of PVIC-LiOTf at 90 °C is in good agreement with that reported by Shriver and coworkers.[8] Conductivity of PVIC-LiOTf is two orders of magnitude higher than that of PNb3C-LiOTf which is two orders of magnitude higher than that of PNbC-LiOTf over the entire temperature range. Li^+ ion conductivity depends upon the concentration of carbonate groups, crystalline/amorphous nature of the polymer electrolytes, coordination of the carbonate moieties with Li^+ cation and the mobility of the system, such that changes in either variable influences the conductivity. All these variables are discussed in the following sections to rationalize the observed trends.

6.5.1 Effect of weight fraction

In all the studied polymer electrolytes, carbonates with high dielectric constant are the coordinating sites which facilitate lithium salt dissociation. High density of carbonate groups is expected to reduce the activation energy of ion hoping from one site to other.[8] Although the

molar ratio of carbonates to LiOTf is the same in all the polymer electrolytes studied, wt.% of carbonate per repeat unit is different as listed in Table 6.1. PVIC with 100 % carbonate content exhibits the highest conductivity. The wt.% of carbonate per repeat unit in PNbC and PNb3C is 56% and 38% respectively. No linear trend is observed between wt.% of carbonates and Li^+ ion conductivity.

6.5.2 Coordination with lithium salts by solid state NMR

Extent of coordination between carbonates and Li^+ ion in a tetrahedral shell influences the dissociation of lithium salts and the diffusion of Li^+ ions which in turn influences conductivity.[28] Solvation of cations causes a shift of ^{13}C NMR signals of carbon atoms next to oxygen atoms, coordinated to the cation. When carbonates coordinate with Li^+ ion, a shift in the resonance peak of C=O carbon is observed in ^{13}C-NMR and this shift is a measure of coordinating ability of carbonates.[29] From the ratio of the signals for coordinated and uncoordinated carbonyl groups observed on the NMR time scale, the quantity of carbonyl groups involved in coordination can be estimated.[10]

In solid state ^{13}C CP MAS NMR spectrum of PNbC-LiOTf, figure 6.8a, the complexed carbonyl resonance was difficult to distinguish as it was beneath the peak corresponding to double bond carbons. In order to understand the interaction of cyclic carbonate with Li^+ cation, a dipolar dephasing experiment was performed, in which the signal from the protonated carbons are removed due to strong C-H dipolar coupling, figure 6.8b. The uncomplexed carbonyl resonance is observed at δ 156.9 ppm and complexed carbonyl resonance at δ 121.3 ppm with a relative ratio of 2:1 for the two carbonyl peaks. Tarascon and coworkers have reported a 3:1 ratio of uncomplexed to complexed carbonyl resonance in PVIC blended with LiOTf in the molar ratio of 1:0.85.[10]

Assuming that Li^+ ion is coordinated to four carbonate groups, there is four fold excess of LiOTf in PNbC-LiOTf. Presence of contact ion pairs is likely and it will influence the solvation number. We believe that there is a saturation limit for the solubility of LiOTf in these carbonate systems and excess LiOTf could be present as higher order ionic aggregates or ion pairs, which are less mobile.

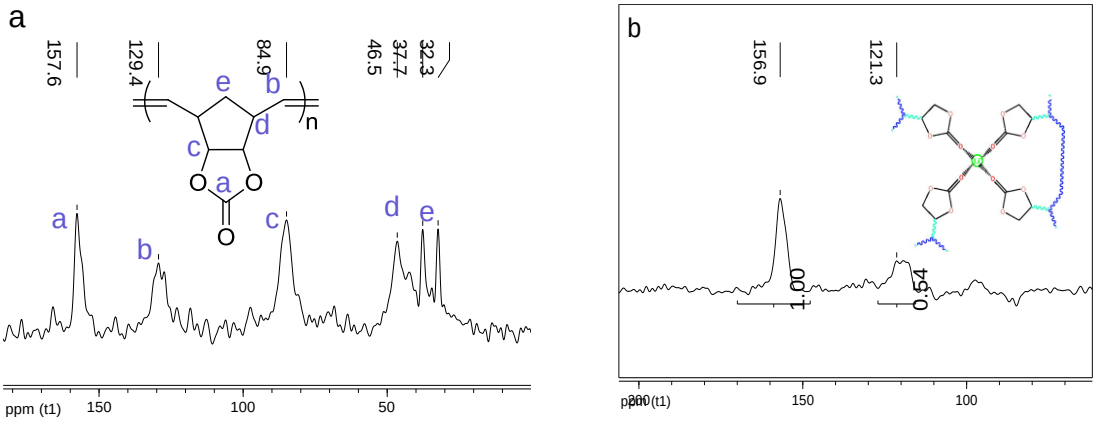

Figure 6.8. ^{13}C CP MAS NMR spectra a) PNbC-LiOTf b) PNbC-LiOTf spectrum obtained by dipolar dephasing experiment

6.5.3 Crystallinity

In conventional polymer electrolytes, it is generally agreed that amorphous domains contribute to ion transport and intensive efforts have been made to develop low T_g amorphous polymers.[13] In the polymer electrolytes studied in this chapter, the crystalline phase is facilitating ion transport as inferred from the highest conductivity being observed for PVIC-LiOTf. The WAXS data will be useful in understanding the dissolution of LiOTf in PVIC and the associated structural changes in polymer electrolytes. The WAXS spectra of pure LiOTf, pristine PVIC and PVIC-LiOTf are presented in figure 6.9. LiOTf salt exhibits several sharp crystalline peaks at scattering wave vector q of 10.41, 12.6, 14.4, 15.9 nm^{-1} similar to the peak positions reported in the literature.[30] Pristine PVIC shows an amorphous halo and PVIC-LiOTf has both amorphous halo and crystalline peaks present.

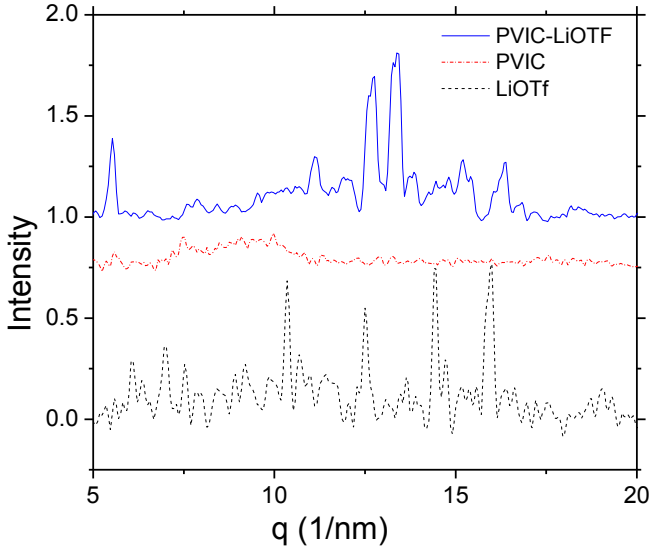

Figure 6.9. WAXS data for pure LiOTf, pristine PVIC and PVIC-LiOTf

6.5.4 Mobility

Intuitively, the conductivity of PNb3C-LiOTf was expected to be the highest among the polymer electrolytes studied, because carbonate groups in PNb3C are attached by a flexible spacer allowing for higher translational and rotational mobility around the spacer. This factor does explain the higher conductivity of PNb3C-LiOTf observed compared to PNbC-LiOTf, inspite of lower carbonate wt.% in PNb3C-LiOTf. However, the observed trends do not appear to be explained completely by the above hypothesis. Another factor that may influence the conductivity which we have not considered yet is mobility around the backbone. There is unsaturation in the backbone of both PNbC and PNb3C polymers restricting the rotation of carbonate groups around the polymer backbone unlike PVIC, figure 6.10. The investigation into the effect of backbone mobility can be accomplished by hydrogenating the backbone of PNbC and PNb3C polymers, resulting in saturated polymers with free mobility of pendant carbonate groups around the backbone, similar to PVIC system. Overall, the observed trends underscore the importance of backbone mobility in achieving high ionic conductivity.

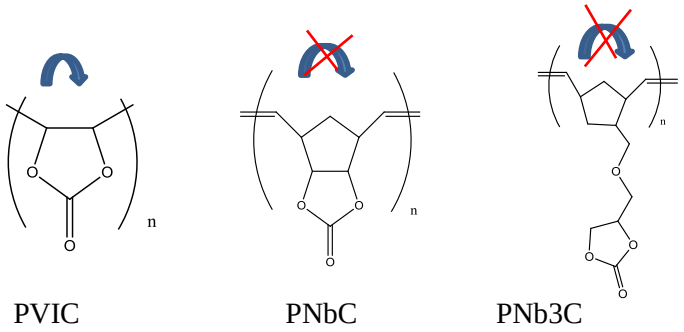

Figure 6.10. Restricted mobility around backbone in PNbC and PNb3C compared to PVIC.

6.6 Conclusions

Polynorbonenes containing covalently attached carbonate groups were studied to understand the structure-property relationships involved in carbonate immobilized polymers and Li^+ ion conductivity. Polymers containing covalently attached carbonate groups were synthesized using ROMP and fully characterized. All the studied polymers are thermally stable up to 250 °C. The polymers were blended with LiOTf in 1:1 molar ratio and the ionic conductivities were measured by impedance spectroscopy as a function of temperature. The conductivities of the studied polymer electrolytes increase with increase in temperature with maximal conductivities for PVIC system. High concentration of carbonates, the coordinating moieties, seemed to influence the conductivity, but no linear trend was observed. ^{13}C CP MAS NMR was used to understand the interactions between carbonates and Li^+ cation and it was found that less than half of carbonates are coordinated to Li^+ cation on the NMR time scale. Use of WAXS data to probe the solvation of lithium salts indicated the presence of crystals in PVIC-LiOTf. Mobility of the polymer backbone and pendant carbonate groups was observed as one of the most important factors influencing Li^+ ion conductivity. This observation is similar to the correlation between high anhydrous proton conductivity and segmental mobility in proton exchange membrane fuel cells.[1-4]

6.7 References

1. Persson, J. C.; Jannasch, P., *Macromolecules* **2005,** 38, 3283-3289.

2. Scharfenberger, G.; Meyer, W. H.; Wegner, G.; Schuster, M.; Kreuer, K. D.; Maier, J., *Fuel Cells* **2006,** 6, 237-250.

3. Granados-Focil, S.; Woudenberg, R. C.; Yavuzcetin, O.; Tuominen, M. T.; Coughlin, E. B., *Macromolecules* **2007,** 40, 8708-8713.

4. Martwiset, S.; Woudenberg, R. C.; Granados-Focil, S.; Yavuzcetin, O.; Tuominen, M. T.; Coughlin, E. B., *Solid State Ionics* **2007,** 178, 1398-1403.

5. Nazri, G.-A.; Pistoia, G., *Lithium Batteries:Science and Technology*. 1 ed.; Springer: **2004**.

6. Celik, S. U.; Aslan, A.; Bozkurt, A., *Solid State Ionics* **2008,** 179, 683-688.

7. Song, J. Y.; Wang, Y. Y.; Wan, C. C., *J. Power Sources* **1999,** 77, 183-197.

8. Wei, X.; Shriver, D. F., *Chem. Mater.* **1998,** 10, 2307-2308.

9. Kaplan, M. L.; Rietman, E. A.; Cava, R. J.; Holt, L. K.; Chandross, E. A., *Solid State Ionics* **1987,** 25, 37-40.

10. Golden, J. H.; Chew, B. G. M.; Zax, D. B.; DiSalvo, F. J.; Frechet, J. M. J.; Tarascon, J.-M., *Macromolecules* **1995,** 28, 3468-3470.

11. Britz, J.; Meyer, W. H.; Wegner, G., *Macromolecules* **2007,** 40, 7558-7565.

12. Zhu, Z.; Einset, A. G.; Yang, C.-Y.; Chen, W.-X.; Wnek, G. E., *Macromolecules* **1994,** 27, 4076-4079.

13. Meyer, W. H., *Adv. Mater.* **1998,** 10, 439-448.

14. Kerr, J. B.; Liu, G.; Curtiss, L. A.; Redfern, P. C., *Electrochim. Acta* **2003,** 48, 2305-2309.

15. Love, J. A.; Morgan, J. P.; Trnka, T. M.; Grubbs, R. H., *Angew. Chem., Int. Ed.* **2002,** 41, 4035-4037.

16. Hino, T.; Inoue, N.; Endo, T., *Macromolecules* **2004,** 37, 9660-9663.

17. Borsato, G.; De Lucchi, O.; Fabris, F.; Groppo, L.; Lucchini, V.; Zambon, A., *J. Org. Chem.* **2002,** 67, 7894-7897.

18. Russell, G. A.; Schmitt, K. D.; Mattox, J., *J. Am. Chem. Soc.* **1975,** 97, 1882-1891.

19. Kwart, H.; Vosburgh, W. G., *J. Am. Chem. Soc.* **1954,** 76, 5400-5403.

20. Fringuelli, F.; Pizzo, F.; Taticchi, A.; Wenkert, E., *J. Org. Chem.* **1983,** 48, 2802-2808.

21. Wang, Y.; Nakamura, S.; Tasaki, K.; Balbuena, P. B., *J. Am. Chem. Soc.* **2002,** 124, 4408-4421.

22. Grubbs, R. H., *Handbook of Metathesis*. Wiley-VCH: Weinheim, **2003**; Vol. 2.

23. Grubbs, R. H., *Handbook of Metathesis*. Wiley-VCH Weinheim, **2003**; Vol. 3.

24. Rokicki, G.; Pawlicki, J.; Kuran, W., *J. Prakt. Chem.* **1985,** 327, 718-722.

25. Dueno, E. E.; Chu, F.; Kim, S.-I.; Jung, K. W., *Tetrahedron Lett.* **1999,** 40, 1843-1846.

26. Finkelstein, H., *Chem. Ber.* **1910,** 43, 1528-1532.

27. Kihara, N.; Hara, N.; Endo, T., *J. Org. Chem.* **1993,** 58, 6198-6202.

28. Kang, K.; Meng, Y. S.; Breger, J.; Grey, C. P.; Ceder, G., *Science* **2006,** 311, 977-980.

29. Matsubara, K.; Kaneuchi, R.; Maekita, N., *J. Chem. Soc., Faraday Trans.* **1998,** 94, 3601-3605.

30. Koh, J. H.; Lee, K. J.; Seo, J. A.; Kim, J. H., *J. Polym. Sci., Part B: Polym. Phys.* **2009,** 47, 1443-1451.

CHAPTER 7

SUMMARY AND FUTURE WORK

There are two sections in this chapter. In the first section, the results and conclusions from chapters 2-6 are summarized. The second section outlines the future directions and the possible extensions of this body of work.

7.1 Dissertation summary

There were two main goals at the beginning of this dissertation, the first was to understand the similarities and/or differences in the structure-property relationship of polymer membranes and the conductivity of H^+ and OH^- ions. The second goal was to address the idea of extending the structure property relationship between polymer membranes and anhydrous H^+ mobility to that between polymers and Li^+ ion mobility. Within each research topic, the challenges addressed, had a goal to gain knowledge that would be useful to develop durable polymer membranes with high H^+, OH^- and Li^+ ion conductivity for PEMFCs, AAEMFCs and lithium ion batteries respectively.

For PEMFCs, previous work in our group has systematically studied the effect of charge carrier density and flexibility of polymers containing 1*H*-1,2,3-triazole as a protogenic group for proton conductivity.[1-4] In an extension of that work, proton conduction in poly(4-vinyl-1*H*-1,2,3-triazole), the simplest 1*H*-1,2,3-triazole containing polymer, was studied and described in chapter 2. Proton conducting properties of poly(4-vinyl-1*H*-1,2,3-triazole) were investigated and compared; on a macroscopic scale by impedance spectroscopy and microscopic scale by solid state MAS NMR. It was found that proton conductivity of pristine, anhydrous poly(4-vinyl-1*H*-1,2,3-triazole) approaches 10^{-8} S/cm at 180 °C; independent of molecular weight of the polymer. Proton conductivity was found to be significantly influenced by presence of residual dimethyl

formamide. Insights into local proton dynamics were derived from ^{1}H variable temperature MAS NMR and two dimensional single-quantum double-quantum NMR spectroscopy.

The literature reports on proton conducting properties of poly(acrylates), poly(siloxanes) and poly(phosphazenes) with pendant 1*H*-1,2,3-triazole as a protogenic group, have shown that the use of low T_g polymers allow for high local mobility of triazoles, thereby giving proton conductivity in the range of 0.01 – 1 μS/cm at 180 °C, but they are liquid-like materials.[1-4] To develop self-supporting membranes, hybrid inorganic-organic polymer electrolyte membranes (PEMs) were synthesized from a combination of 1*H*-1,2,3-triazole grafted alkoxy silanes, tetraethoxy silane (TEOS), polyethylene glycol (PEG) and trifluoroacetic acid (TFA) or phosphoric acid as described in chapter 3. The resulting hybrid inorganic-organic proton exchange membranes were self-supporting and thermally stable up to 180 °C. Evaluation of proton conductivity as a function of temperature indicates that by using sol-gel chemistry, it is possible to achieve mechanically robust membranes having proton conductivity comparable to uncrosslinked, liquid-like 1*H*-1,2,3-triazole functionalized polysiloxane homopolymers. Mechanical properties of these hybrid inorganic-organic membranes were investigated using nanoindentation.

Compared to the extensive literature on PEMFCs, AAEMFCs are in their infancy. There are no commercial state of the art membranes for AAEMFCs unlike Nafion® for PEMFCs. A goal of this thesis was to identify robust building blocks, cations and polymers, to make stable AEMs, and then understand the effect of charge carrier density and flexibility of polymers containing cationic sites on hydroxide ion conductivity, and to further compare it with proton conductivity. Two different families of cations were investigated, 1,2,3-triazolium cations in chapter 4 and cobaltocenium cations in chapter 5.

To determine the applicability of 1,2,3-triazolium cations in AEMs, a range of 1,2,3-triazolium salts were synthesized and their ion-cluster behavior, thermal properties,

electrochemical stability, ionic conductivity and chemical stability under alkaline environment were investigated. It was found that 1,2,3-triazolium salts have excellent electrochemical stability, ionic conductivity, and chemical stability under alkaline conditions compared to imidazolium salts. However, the chemical stability of 1,2,3-triazolium salts is not sufficient to survive the high pH environment of alkaline fuel cells.

The chemical stability of cobaltocenium cation $[Cp_2Co]^+$ having an eighteen electron closed shell valence configuration, similar to alkali metal cations, was studied using ^1H NMR, ^{13}C NMR, mass spectroscopy and UV-Vis spectroscopy. It was found that the $[Cp_2Co]^+$ framework is stable at 80 °C in 2 M NaOH over 40 days, making it suitable for AEMs. Attempts were made to synthesize side chain cobaltocenium containing polymers and main chain cobaltocenium containing polymers. The synthesis of monomer with polymerizable vinyl groups attached to both the cyclopentadienyl rings of $[Cp_2Co]^+$, to achieve main chain cobaltocenium containing polymers was accomplished. This work will be further continued to make cobaltocenium containing polymers and measure their OH^- ion conductivity. Several possible synthetic routes are outlined in section 7.2.2.

In chapter 6, the objective was to make polymeric membranes containing carbonates as the coordinating sites to facilitate Li^+ ion transport, and compare the structure property relationships involved in carbonate tethered polymers for Li^+ ion conductivity to that for anhydrous H^+ transport. Three polymers containing covalently attached carbonates were synthesized and blended with lithium triflate in 1:1 molar ratio. The Li^+ ion conductivity was measured as a function of temperature by impedance spectroscopy. The polymer blend, PVIC-LiOTf, with the highest weight percentage of carbonates and maximal backbone mobility had the highest Li^+ ion conductivity over the measured temperature range. These results underscore the importance of charge carrier density and flexibility of the polymer matrix in achieving high Li^+ ion conductivity, a finding that is directly similar to the key features for high H^+ conductivity.

This project can be expanded to gain further insight into the effect of mobility on Li^+ ion conductivity as detailed in section 7.2.3.

7.2 Future directions

7.2.1 PS-PVTz block copolymer

A report by Zhou *et al*. claiming that the proton conductivity of poly(4-vinyl-1*H*-1,2,3-triazole) is 10^5 times higher than that of poly(4-vinylimidazole) guided our initial approach to develop anhydrous/hydrated dual function PEMs.[5] The objective was to synthesize a block copolymer combining sulfonated material for hydrous proton transport below 100 °C, and nitrogenous heterocycle containing polymer for anhydrous proton transport, to make dual mechanism membranes that can transport H^+ over broad range of temperatures (room temperature to 200 °C) and humidity levels. In particular, the goal was to synthesize sulfonated polystyrene-*b*-poly(4-vinyl-1*H*-1,2,3-triazole) (sPS-*b*-PVTz), where sulfonated PS would conduct H^+ in a hydrated environment and presumably PVTz would conduct H^+ in anhydrous environment, thereby giving a flat conductivity curve over broad range of temperatures and humidities. The synthetic route adopted is shown in scheme 7.1.

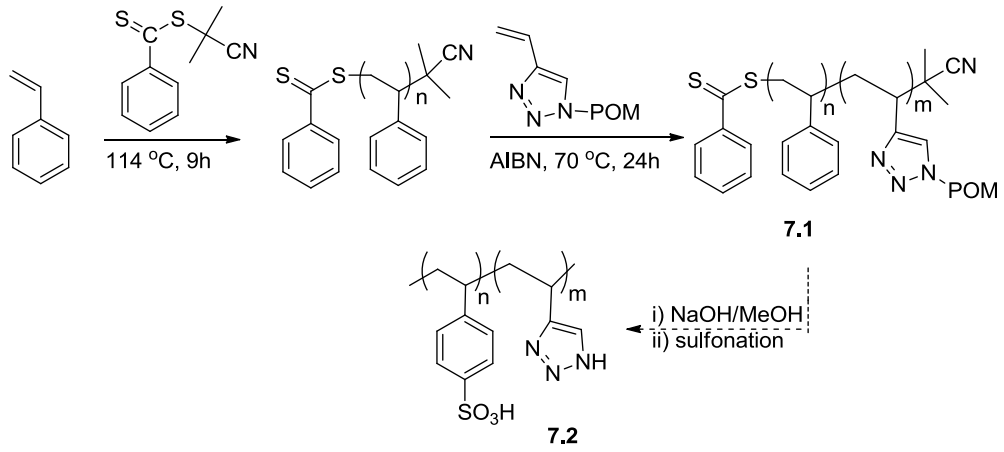

Scheme 7.1. Synthesis of sPS-*b*-PVTz copolymer (Pivaloxymethyl group is abbreviated as POM)

Synthesis of PS-PVTz (7.1) The chain transfer agent 2-cyanoprop-2-yl dithiobenzoate was synthesized as reported in the literature.[6] The polystyrene block was synthesized by thermal reversible addition-fragmentation chain transfer (RAFT) polymerization. Freshly distilled styrene (4.54 g, 0.04 mol) and chain transfer agent (0.035 g, 0.158 mmol) were combined in a Schlenk flask and subjected to three freeze-pump-thaw cycles followed by heating at 115 °C for 9 h. The resulting polymer (PS) was dissolved in THF (20 mL) and precipitated in ice-cold methanol yielding 2.23 g (49.1%) of pink colored product. M_n = 8.9 K g/mol, Đ = 1.17. The PS was washed with ether to remove the unreacted chain transfer agent as the chain transfer agent is soluble in ether while PS is insoluble. 4-vinyl-1-pivaloxymethyl-1,2,3-triazole was synthesized as reported in chapter 2. Polystyrene end-capped with the chain transfer agent (0.18 g, 0.02 mmol), 4-vinyl-1-pivaloxymethyl-1,2,3-triazole (0.2 g, 0.96 mmol) and AIBN (0.65 mg, 0.004 mmol) were dissolved in 0.5 mL of DMF (2 M) in a round bottom flask and degassed by three successive freeze-pump-thaw cycles. Polymerization was carried out at 70 °C for 24 h. The product was precipitated in hexane and dried under vacuum at 40 °C for 3 h. The product was washed with water to remove DMF and then dried again under vacuum at 70 °C for 10 h. M_n = 16.9 K g/mol, Đ = 1.28.

The GPC traces of the homopolymer PS and block copolymer **7.1** are shown in figure 7.1. From GPC results, the PS and protected PVTz are present in equal wt.% in the block copolymer **7.1**, which implies 2:1 molar ratio of PS : protected PVTz as the molecular weight of styrene and 4-vinyl-1-pivaloxymethyl-1,2,3-triazole are 104 g/mol and 209 g/mol respectively. The molar ratio was confirmed by ^{1}H-NMR of **7.1**, figure 7.2. Using resonances corresponding to aromatic ring protons, labeled as *a*, and pivaloxymethyl group protons, labeled as *b*, the molar ratio of PS:PVTz was calculated as ~ 2:1. In figure 7.2, the absence of resonances at δ 2.96 ppm and δ 2.88 ppm indicate removal of residual DMF from the polymer. The thermal transitions of the block copolymer **7.1** were obtained by differential scanning calorimetry (DSC) by heating the

sample at 10 °C/min under a flow of nitrogen. From the second heating cycle, figure 7.3, two glass transition temperatures were observed at 69 °C and 91 °C corresponding to protected PVTz and PS respectively.

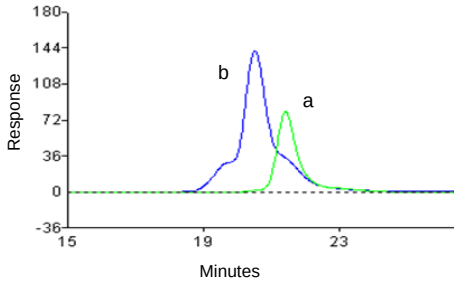

Figure 7.1. GPC traces a) homopolymer PS b) PS-PVTz (**7.1**)

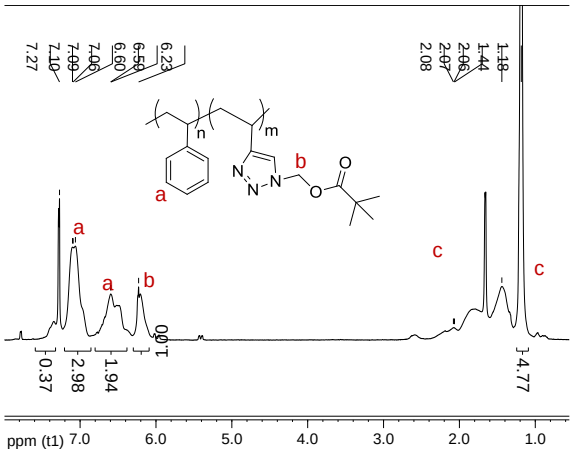

Figure 7.2. ^{1}H-NMR of block copolymer **7.1**

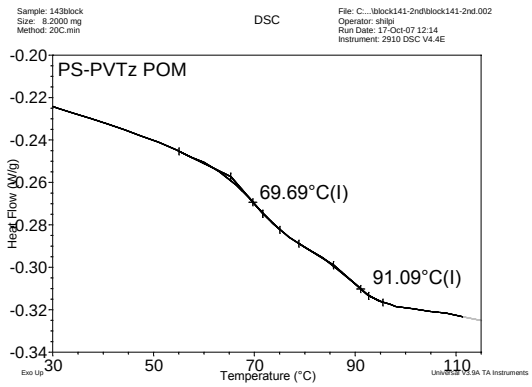

Figure 7 3. DSC trace of block copolymer **7.1**

The solution cast films of the block copolymer **7.1** were prepared by dissolving in minimum amount of toluene and then evaporating the solvent in a partially covered glass dish under vacuum at 35 °C for 18 h. The sample was annealed at 120 °C for 48 h under vacuum. Small angle X-ray scattering (SAXS) experiments were performed on this annealed sample, figure 7.4. The block copolymer **7.1** displays distinct reflections in the intensity maxima at scattering vector positions q and $3q$, with the suppression of second and fourth order maxima. This scattering pattern suggests lamellar morphology with volume fraction of each domain close to 0.5.[7] The density of amorphous PS is 1.04 mg/m^3 and assuming that the density of protected PVTz is equal to that of polyvinyl pyridine (1.14 mg/m^3),[8] the volume fraction of PS was calculated as ϕ_{PS} = 0.55 and that of protected PVTz as ϕ_{PVTz} = 0.45. The Bragg spacing, d, calculated from the first order reflection q from the SAXS intensity profile using the equation, $d = 2\pi/q$,[9-10] was found to be 24 nm.

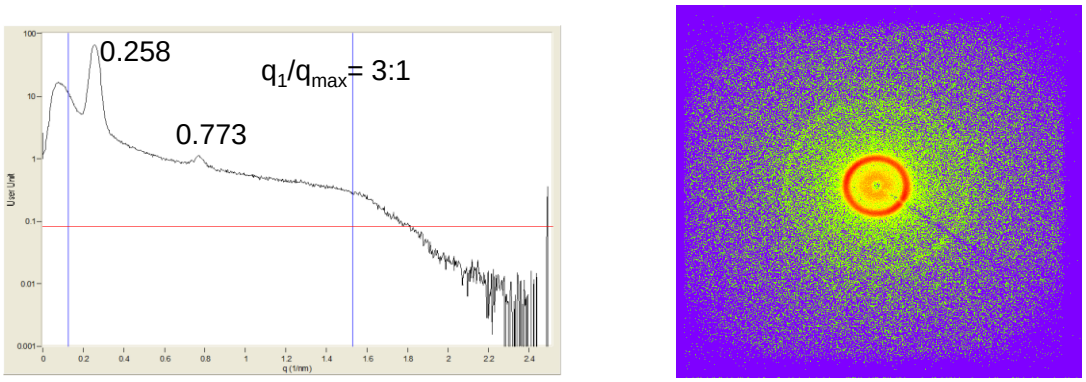

Figure 7.4. SAXS data for block copolymer **7.1**

During the course of synthesis of sPS-*b*-PVTz copolymer, our parallel investigations on macroscopic and microscopic proton conductivity of poly(4-vinyl-1*H*-1,2,3-triazole) revealed that the maximum conductivity of pristine PVTz approaches 10^{-8} S/cm at 180 °C, 4 orders of magnitude lower than that previously reported. Hence, no further work was performed with PS-*b*-PVTz scaffold to facilitate H^+ transport. However, synthesis of PS-*b*-PVTz using living radical polymerization is a novel finding and this synthetic route can be used to make phase separated, ordered PS-*b*-PVTz block copolymers. Polystyrene (PS)-polyvinyl pyridine (PVP) block copolymers have been studied extensively as templates for nanoscale patterning,[11] templates for creating ordered arrays of catalysts[12-13] and for surface modifications.[14] In PS-PVTz block copolymer, PVTz has a 5 membered ring with three ring nitrogens and presumably differences in polarity compared to pyridine. PS-*b*-PVTz copolymer could be further studied for interesting applications in nanotechnology and surface modifications.

7.2.2 Cobaltocenium containing polymers

There are challenges involved in making cobaltocenium containing polymers as described in chapter 6. Synthetic pathways that could yield novel cobaltocenium containing polymers are detailed in this section. One possible route is to synthesize dialkyne functionalized

cobaltocenium monomer **7.3** and then react it with a diazide using Huisgen 1,3-dipolar cycloaddition reaction to develop a step-growth polymer **7.4**, scheme 7.2.

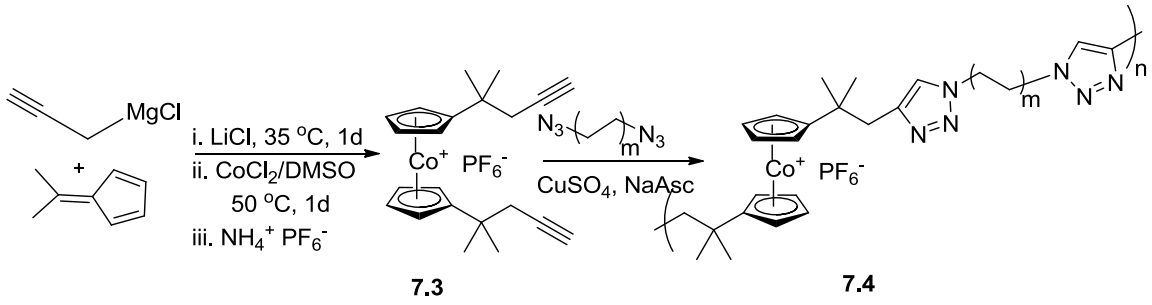

Scheme 7.2. Step-growth polymerization using Huisgen 1,3-dipolar cycloaddition reaction

Another possible synthetic route is shown in scheme 7.3, modified from a literature report.[15] It involves reaction of two moles of sodium cyclopentadienide with a dihalide compound to form a dicyclopentadienyl intermediate **7.5**, followed by reaction with n-butyllithium to abstract a proton from the cyclopentadiene ring and then reaction with cobalt (II) chloride to give polymer **7.6**. Suitable choice of the dihalide compound (Br-X-Br) is important, such that there are no CH_2 or CH groups at the α position of cobaltocenium moiety, in order to achieve sufficient stability in highly alkaline conditions to find utility as AEM.

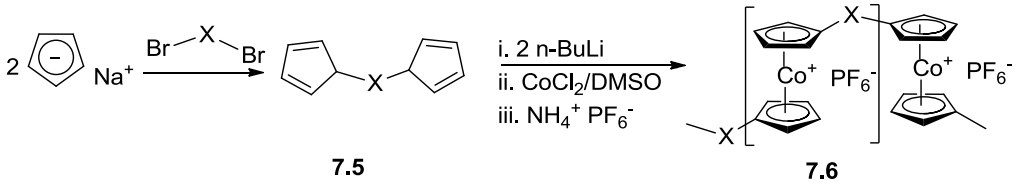

Scheme 7.3. Proposed synthetic route for cobaltocenium containing polymers

7.2.3 Hydrogenation of carbonate functionalized polynorbornenes

As mentioned in chapter 6, the observed conductivity trends indicate the importance of backbone mobility in achieving high Li^+ ion conductivity. The effect of backbone mobility can be studied by hydrogenating the polynorbornene backbone using p-toluenesulfonyl hydrazide using

a literature procedure, scheme 7.4.[16-17] The resulting hydrogenated PNbC and PNb3C will have backbone mobilities equivalent to that observed in PVIC. The comparison of Li^+ ion conductivity of hydrogenated PNbC-LiOTf and hydrogenated PNb3C-LiOTf with the unsaturated polynorbornene-carbonate systems and PVIC would help to elucidate the contribution of backbone mobility and side chain mobility, independently, to their respective impacts on measured conductivity values.

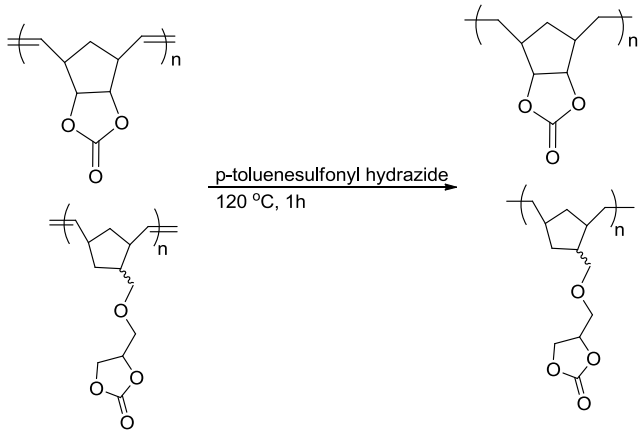

Scheme 7.4. Hydrogenation of carbonate functionalized polynorbornenes

7.3 References

1. Martwiset, S.; Yavuzcetin, O.; Thorn, M.; Versek, C.; Tuominen, M.; Coughlin, E. B., *J. Polym. Sci.,Part A: Polym. Chem.* **2009,** 47, 188-196.

2. Martwiset, S.; Woudenberg, R. C.; Granados-Focil, S.; Yavuzcetin, O.; Tuominen, M. T.; Coughlin, E. B., *Solid State Ionics* **2007,** 178, 1398-1403.

3. Granados-Focil, S.; Woudenberg, R. C.; Yavuzcetin, O.; Tuominen, M. T.; Coughlin, E. B., *Macromolecules* **2007,** 40, 8708-8713.

4. Higami, M.; Woudenberg, R. C.; Granados-Focil, S.; Yavuzcetin, O.; Tuominen, M. T.; Coughlin, E. B. PMSE Preprints, **2007**; 97 pp 551-552.

5. Zhou, Z.; Li, S.; Zhang, Y.; Liu, M.; Li, W., *J. Am. Chem. Soc.* **2005,** 127, 10824-10825.

6. Moad, G.; Chiefari, J.; Chong, Y. K.; Krstina, J.; Mayadunne, T. A.; Postma, A.; Rizzardo, E.; Thang, S. H., *Polym. Int.* **2000,** 49, 993-1001.

7. Yamaguchi, D.; Hasegawa, H.; Hashimoto, T., *Macromolecules* **2001,** 34, 6506-6518.

8. Bloch, D., *Polymer Handbook*. 4 ed.; Wiley-Interscience: **1999**.

9. Hickner, M.; Ghassemi, H.; Kim, Y.; Einsla, B.; McGrath, J., *Chem. Rev.* **2004,** 104, 4587-4612.

10. Chu, B.; Hsiao, B. S., *Chem. Rev.* **2001,** 101, 1727-1762.

11. Jeong, J.-R.; Choi, M. C.; Im, M.-Y.; Kim, M. W.; Shin, S.-C. Magnetics Conference, INTERMAG, IEEE International, 28 March-3 April **2003**; pp GC-10.

12. Lu, J. Q., *J. Phys. Chem. C* **2008,** 112, 10344-10351.

13. Hwang, Y. K.; Lee, J.-M.; Sathaye, S. D.; Cho, G.; Hwang, J.-S.; Chang, J.-S., *J. Nanosci. Nanotechnol.* **2006,** 6, 1850-1853.

14. Wang, W.; Liang, H.; Favis, B. D.; Schreiber, H. P., *J. Appl. Polym. Sci.* **2001,** 81, 1891-1901.

15. Ito, T.; Kenjo, T., *Bull. Chem. Soc. Japan* **1968,** 41, 614-619.

16. Hahn, S. F., *J. Polym. Sci., Part A Polym. Chem.* **1992,** 30, 397-408.

17. Yang, Z.; Han, C. D., *Polymer* **2008,** 49, 5128-5136.

APPENDIX A

ELECTROCHEMICAL IMPEDANCE SPECTROSCOPY

All the conductivity data reported in this thesis were obtained using alternating current (AC) electrochemical impedance spectroscopy (EIS).

A.1 Theory

Impedance spectroscopy is a commonly used technique to determine electrical properties of polymer electrolytes. The use of alternating current (AC) techniques are preferred over direct current (DC) measurements because the data obtained by AC measurements contains information about long range migration of ionic species and polarization phenomena.

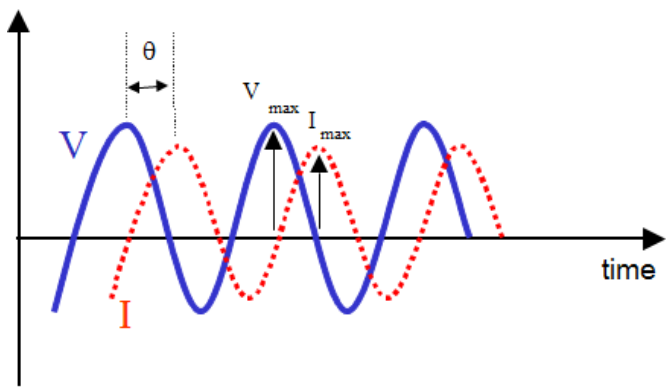

Figure A.1. Representation of applied sinusoidal voltage, resulting current and phase angle.

In an AC experiment, a sinusoidal potential is applied to a cell and the resulting sinusoidal current passing through the cell is measured. The measured AC current *I* has a phase lag with the applied potential *V*, figure A.1, and the phase difference between *V* and *I* is given by the phase angle θ. In AC techniques, *I* is related to *V* by two parameters, resistance *R* representing the opposition to the flow of charge and phase angle θ; unlike in DC techniques where *I* is related to *V* by one parameter, the resistance *R*, obeying Ohm's law, eq. A-1. In AC measurements, *R* and θ together define the impedance *Z* of the cell. Both the magnitude of impedance and phase angle

θ are frequency, ω, dependent, eq. A-2. Thus AC measurements involve measuring impedance Z over a wide frequency range as a function of frequency of the applied signal. The relationship between radial frequency ω (radians/second) and frequency f (Hertz (1/sec)) is given in eq. A-3.

$$V = I\,R \qquad \text{A-1}$$

$$|Z(\omega)| = \frac{V_{max}}{I_{max}} \qquad \text{A-2}$$

$$\omega = 2\pi f \qquad \text{A-3}$$

The impedance at any ω is a vector quantity because it contains both phase information and magnitude and can be represented as a complex number Z^*, eq. A-4. To avoid confusion with the symbol for current, j is used to represent the complex number operator instead of i.

$$Z^* = Z' - jZ'' \qquad \text{A-4}$$

$$j = \sqrt{-1}$$

Z' is the real component of complex number Z*, $Z' = |Z| \cos\theta$

Z'' is the imaginary component of complex number Z*, $Z'' = |Z| \sin\theta$

As the interpretation of measured complex impedance is difficult, AC experiment results are interpreted by constructing different models of AC response and determining which model fits the data well. The model is an electrical circuit consisting of resistors and transistors. For a purely resistive system, the applied voltage is in phase with current, $\theta = 0$ and $|Z| = R$, and impedance is frequency independent. In a complex impedance plot, it is represented by a single point on the real axis Z', at a distance R, figure A.2. For a purely capacitive system, voltage lags behind the current by 90°, $\theta = -\pi/2$ and $|Z| = 1/\omega C$, where C is the capacitance. Here $|Z|$ is frequency dependent. In a complex impedance plot, this result is represented by series of points on the imaginary axis Z'', figure A.2.

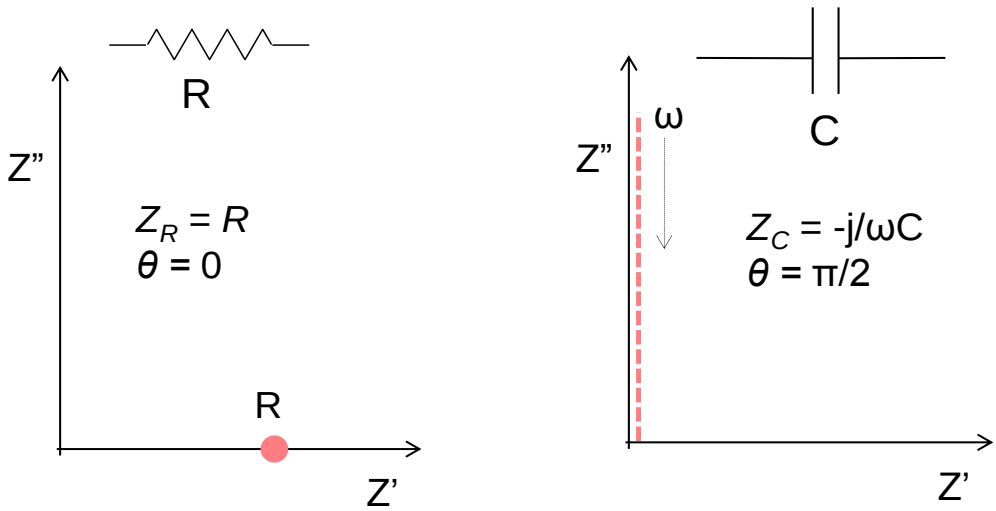

Figure A.2. Graphical representation of a resistor *R* and capacitor *C* in complex impedance plane.

The circuit model generally used to describe the AC response of polymer electrolytes is shown in figure A.3. The electrical circuit consists of a parallel combination of a resistor R_b and a capacitor C_b, and they are together connected in series with capacitor C_e. The migration of ions in polymer electrolyte accounts for resistance R_b and dielectric polarization of the polymer is represented by capacitance C_b. The dielectric constant ε of the polymer is related to C_b by eq. A.5. where ε_o is the vacuum permittivity, *A* is the electrode area and *d* is the separation between two electrodes. When AC current is applied, ions migrate back and forth in the polymer matrix and at the same time, polymer chains become polarized. Thus, ion migration and polarization are two parallel processes and therefore C_b and R_b are connected in parallel. The capacitance C_e represents the interface between electrode and electrolyte, as each electrode is similar to a parallel plate capacitor.

$$C_b = \frac{\varepsilon\varepsilon_o A}{d} \qquad \text{A-5}$$

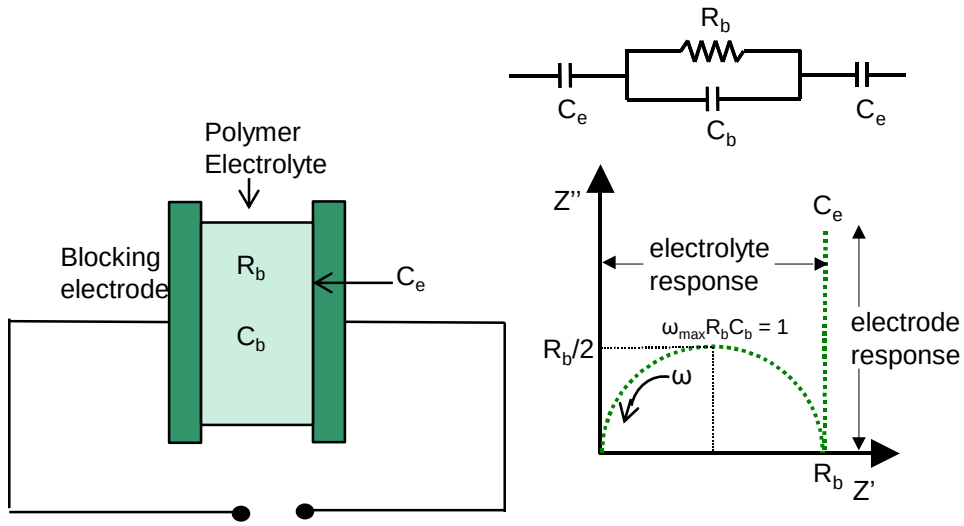

Figure A.3. Cell for polymer electrolyte sandwiched between two blocking electrodes and its equivalent circuit.

The complex impedance response Z* for the circuit shown in figure A.3 is calculated below.

$$Z^* = \left[\frac{1}{\left(\frac{1}{R_b} - \frac{\omega C_b}{j}\right)}\right] + \frac{-j}{\omega C_e}$$

$$= \left[\left(\frac{R_b}{1 + j\omega C_b R_b}\right) \times \left(\frac{1 - j\omega C_b R_b}{1 - j\omega C_b R_b}\right)\right] - \frac{j}{\omega C_e}$$

$$= \frac{R_b}{1 + \omega^2 C_b^2 R_b^2} - \frac{j\omega C_b R_b^2}{1 + \omega^2 C_b^2 R_b^2} - \frac{j}{\omega C_e}$$

$$Z^* = R_b\left[\frac{1}{1 + (\omega R_b C_b)^2}\right] - j\left(R_b\left[\frac{\omega R_b C_b}{1 + (\omega R_b C_b)^2}\right] + \frac{1}{\omega C_e}\right) \qquad \text{A-6}$$

In figure A.3, the high frequency semicircle gives information about the properties of the polymer electrolyte. At minimum imaginary response, the capacitive contribution becomes negligible and eq. A-6 reduces to $Z^*=R_b$, giving the bulk resistance of polymer electrolyte. In high frequency regime, at the highest point on semicircle, ω_{max}, bulk resistance and capacitance contribute equally to the impedance, $R_b=1/\omega_{max}C_b$. Capacitance of the electrolyte can be

calculated from this relation, knowing R_b and ω_{max}. The conductivity, σ , of the polymer electrolyte is determined from the eq. A-7., where *A* is the area of the sample in contact with the electrodes and *t* is the sample thickness.

$$\sigma = \frac{t}{R_b A} \qquad \text{A-7}$$

A.2 Hardware

All the impedance spectroscopy experiments reported in this thesis were performed using a customized in-house developed hardware and software. Samples were placed in the sample holder with adequate electrodes and placed inside a temperature controlled vacuum oven. Impedance spectra were sampled using a Solartron 1260 Impedance/Gain Phase Analyzer over the frequency range from 32×10^6 to 10^{-1} Hz, although an intermediate frequency range was chosen for data analysis. Excitation voltage of 100 mV was used for most of the samples except for the ionic liquids reported in chapter 4. Due to the high conductivity of ionic liquids, excitation voltage of 30 mV was used for conductivity measurements of ionic liquids. The impedance analyzer was multiplexed to gather spectra for multiple samples (up to eight at a time) at a regular time interval of ~30 min, while the oven was heated to the highest temperature value. The samples were held at this temperature under vacuum for 10 – 40 h and impedance data was continuously collected until conductivity stabilized. The system was then allowed to cool slowly while still under vacuum, to near ambient temperature while impedance spectra were continually sampled; this method ensures that samples are brought to a thermally stable condition before temperature dependence data was recorded upon cooling. This procedure mitigates artifacts due to thermal history and residual solvent or humidity effects. Because of known thermal gradients in the vacuum oven chamber, the temperature of each sample at each measurement time was deduced from a position based calibration relative to a custom thermistor probe that closely

matches the sample holding fixtures. The image of the entire impedance measurement configuration is shown in figure A.4.

Figure A.4. Image of the hardware used for AC impedance measurements.

A picture of sample holder is shown in figure A.5a. It consists of polyether ether ketone (PEEK) fittings to provide electrical insulation and blocking electrodes are press fit into these fittings. The top fixture is adjustable and its vertical motion is governed by screw mechanism. The aluminium or stainless steel electrodes (stubs) were purchased and sputter coated with gold to avoid interactions with the polymer electrolytes, i.e. to make non-blocking electrodes. For self-standing films, the thickness of the films were measured using Vernier Calipers and the films were then pressed between two gold coated electrodes, figure A.5b. For liquid like viscous polymers, a Kapton film with a punched hole in it was used as a spacer between the electrodes and thickness of the Kapton film was used as sample thickness. For liquid samples such as ionic liquids, samples were placed in cells composed of ~4 mm section of polytetrafluoroethylene (PTFE) tubing that was sealed on each side with tight-fitting brass electrodes and clamped into custom holders of identical construction, figure A.5c. The geometry of the cell was taken to have the cross-sectional area of the 1/8" diameter tube and the inter-electrode spacing was measured for each assembly. For measurements under humidified conditions, porous electrodes, shown in figure A.5d allow quick equilibration of the samples to target relative humidity.

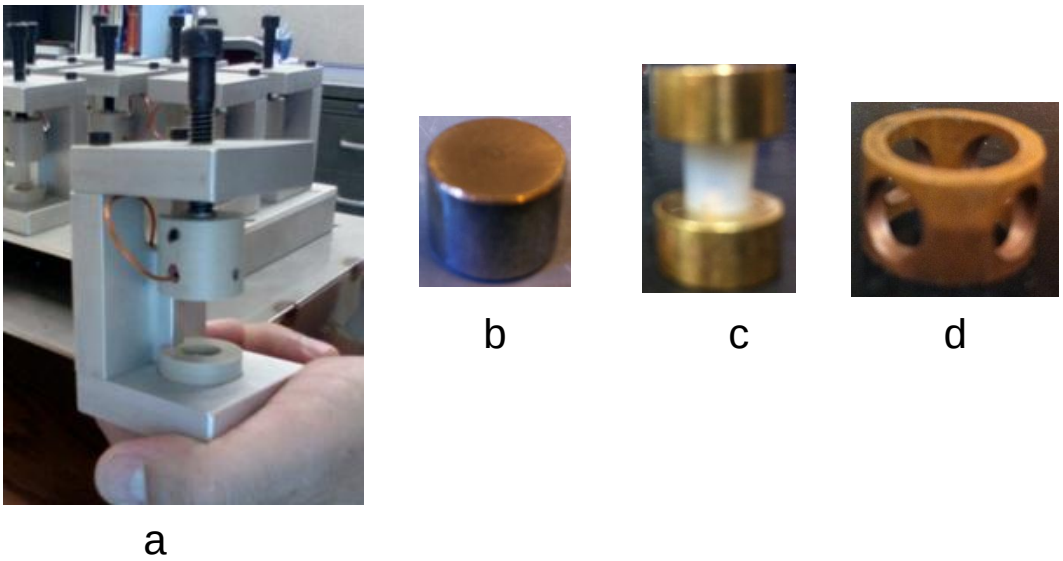

Figure A.5. a) Sample holder used for AC impedance measurements. b) electrode used for measuring conductivity of films under anhydrous conditions c) electrode assembly for liquids under anhydrous conditions d) electrode for measuring conductivity of films under humidified environment.

A.3 Representative data

Typical complex impedance plots obtained consisted of Nyquist plot (Z" vs. Z') and Bode plots (|Z| vs. frequency and θ vs. frequency) as shown in figure A.6. For each spectrum, the plateau of the |Z| Bode plot occurring in the intermediate frequency range was fit to a constant value function; this plateau also corresponds to a region of minimal phase angle and likewise minimal imaginary component magnitude (reactance) response. Thus, the value of impedance magnitude in this regime was taken to be the resistance of ionic transport in the bulk of the sample; whereas, the increase in both the real and imaginary components of impedance at frequencies lower than this plateau is likely due to complicated interfacial processes such as electrode polarization. Effects in the spectra at frequencies higher than the plateau regime are interpreted to be due to both the dielectric response of the cell and artifacts created by stray inductances. Conductivity was computed from the fitted resistance and the known sample geometry.

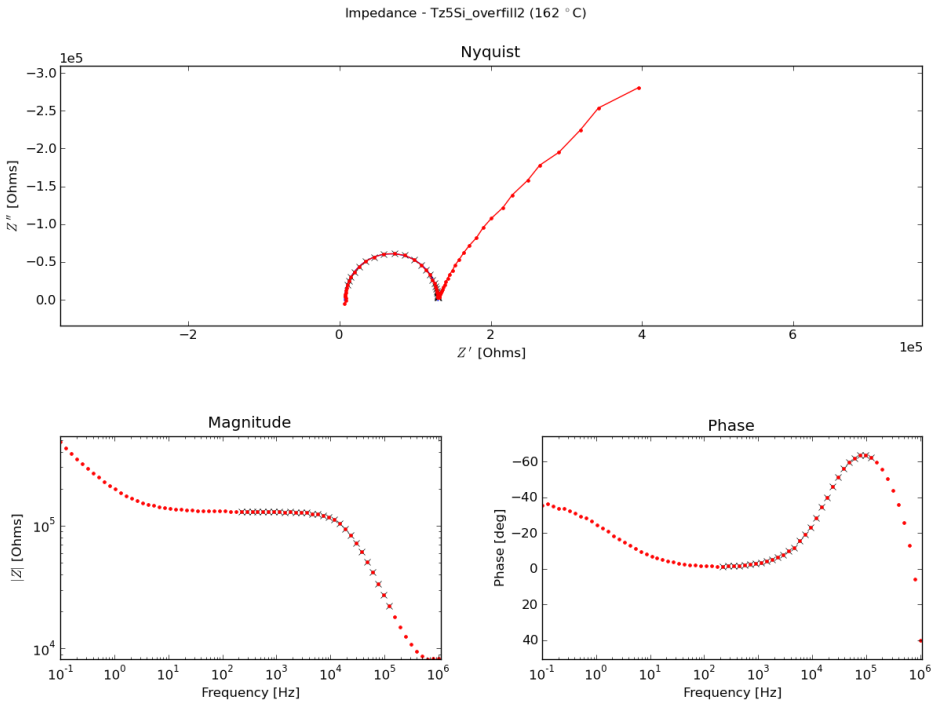

Figure A.6. Representative data obtained from AC impedance measurements.

Attribution: The theory described in section A.1 was summarized from a chapter written by Peter Bruce on impedance measurements in polymer electrolytes, the PhD thesis of Rich Woudenberg and other sources.[1-4] Michael Thorn and Craig Versek contributed to the writing of sections A.2 and A.3.

A.4 References

1. Bruce, P. G., *Polymer Electrolyte Reviews*. 1 ed.; Elsevier Applied Science: New York, **1987**; Vol. 1, pp 237-274.

2. Woudenberg, R. C., Jr. Anhydrous proton conducting materials for use in high temperature polymer electrolyte membrane fuel cells. PhD Thesis, University of Massachusetts, Amherst, **2007**.

3. Instruments, G. Electrochemical Impedance Spectroscopy Primer. http://gamry.com/App_Notes/EIS_Primer/Basics_Of_EIS.pdf (accessed May 5, 2011).

4. Macdonald, B., *Impedance Spectroscopy: Theory, Experiment, and Applications*. 2 ed.; Wiley-Interscience: **2005**.

APPENDIX B

SUPPORTING NMR SPECTRA AND CONDUCTIVITY PLOTS FOR CHAPTER 2

NMR

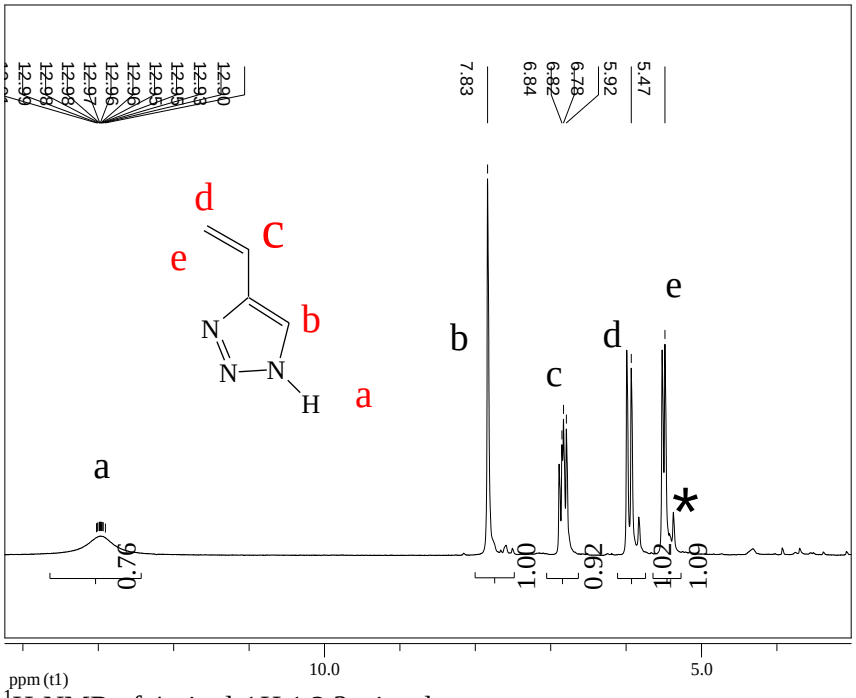

^{1}H-NMR of 4-vinyl-1*H*-1,2,3-triazole

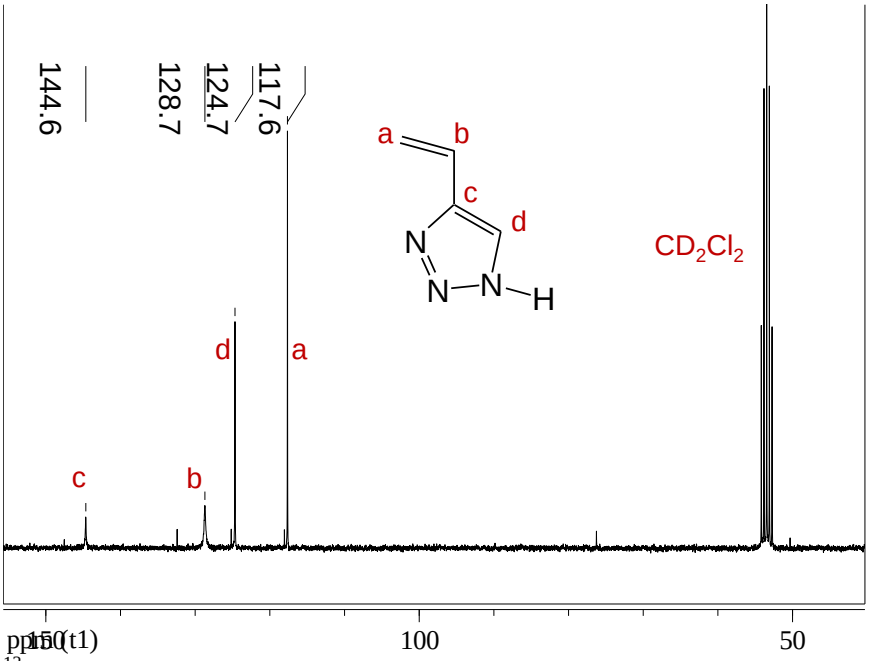

^{13}C-NMR of 4-vinyl-1*H*-1,2,3-triazole

Impedance spectroscopy data for poly(4-vinyl-1*H*-1,2,3-triazole)

A sample impedance spectroscopy plot for poly(4-vinyl-1*H*-1,2,3-triazole) obtained at 120 °C is shown below for estimation of time scale probed by impedance spectroscopy.

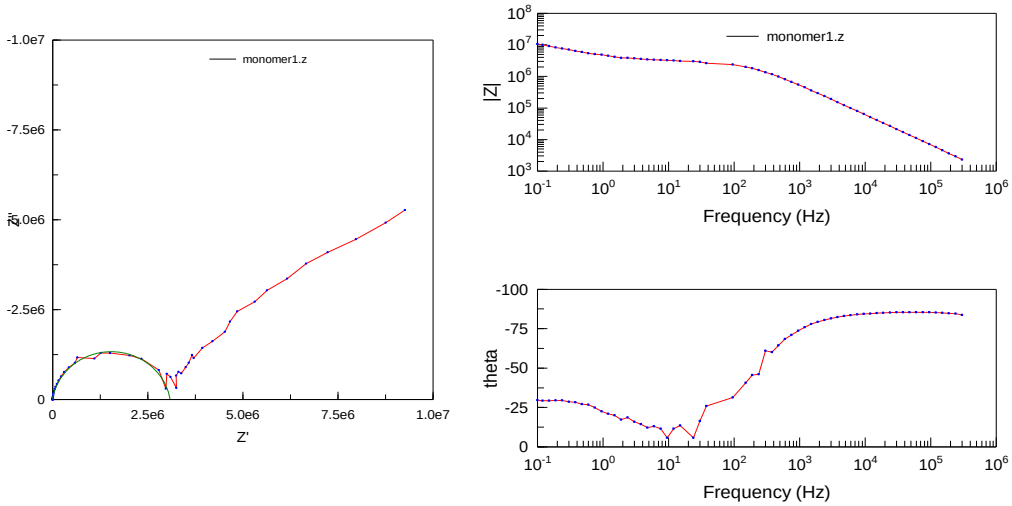

Circle fit

ω_{max} = 969.26 rad/sec = 154.34 Hz

This ω_{max} corresponds to time scale of 6.48 ms.

Resistance = $3.09 \times 10^{6}\ \Omega$

Capacitance = 3.3×10^{-10} Farad

APPENDIX C

SUPPORTING NMR SPECTRA FOR CHAPTER 3

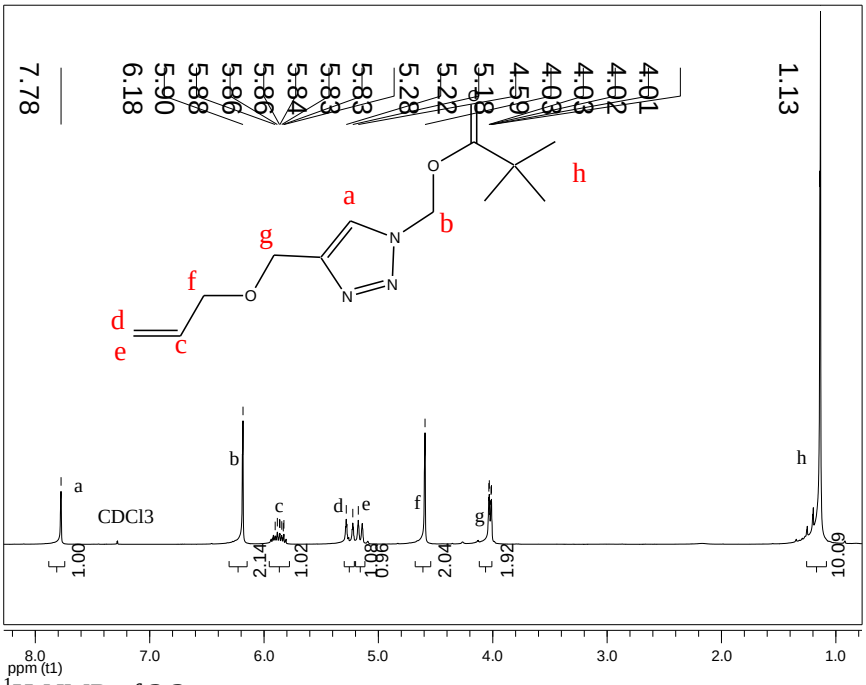

^{1}H-NMR of **3.3**

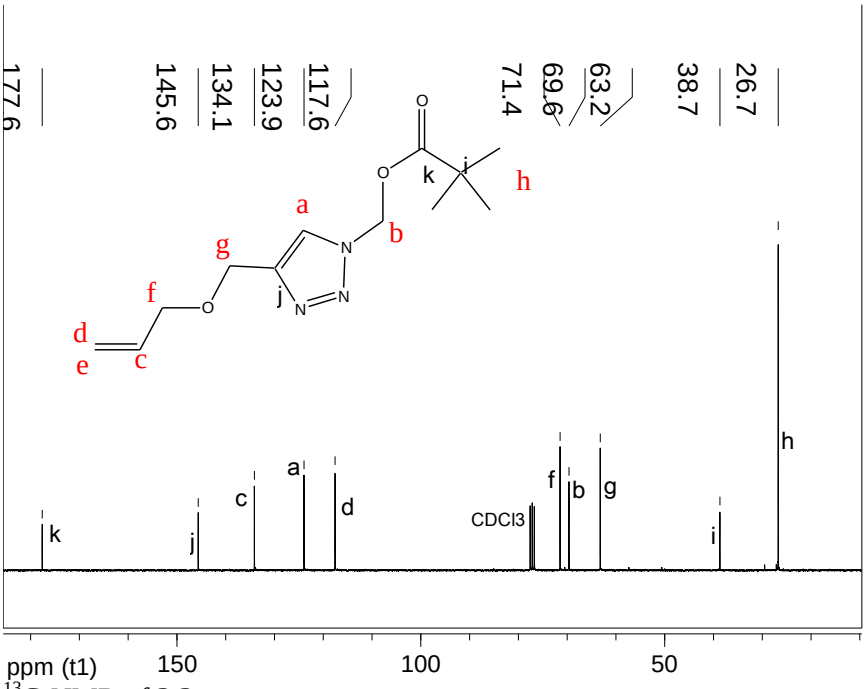

^{13}C-NMR of **3.3**

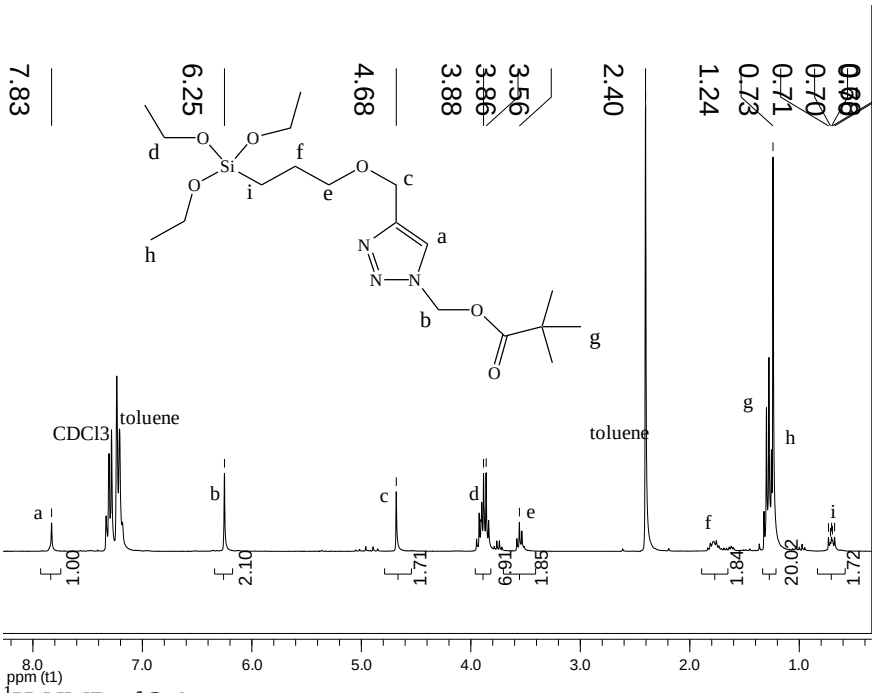

^{1}H-NMR of **3.4**

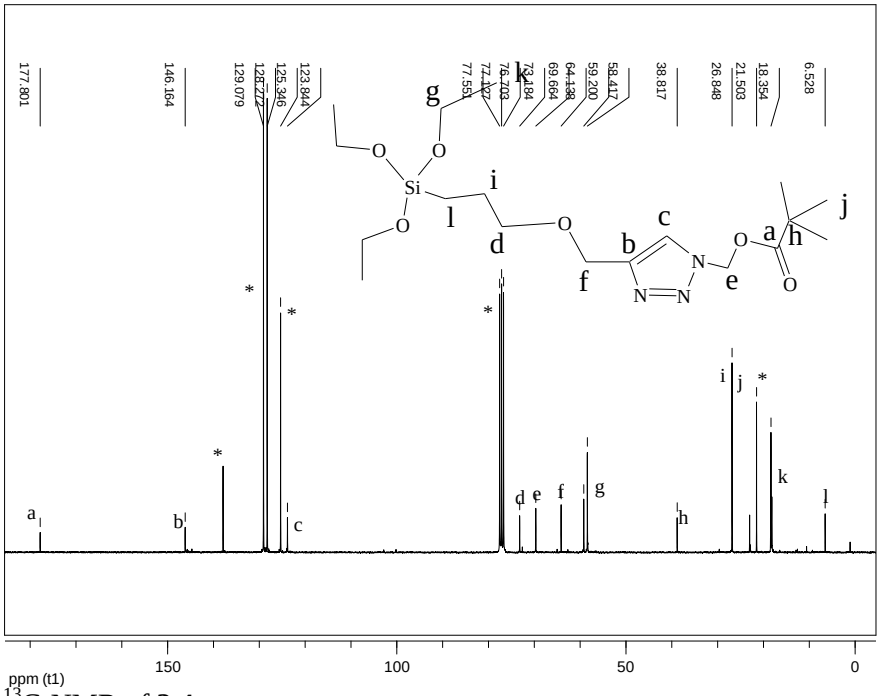

^{13}C-NMR of **3.4**

APPENDIX D

SUPPORTING NMR SPECTRA FOR CHAPTER 4

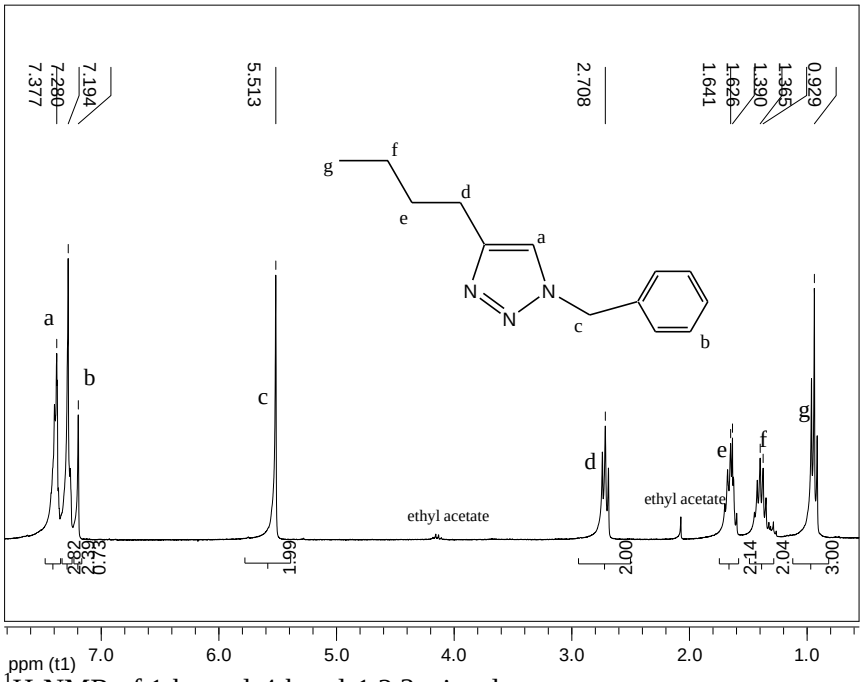

^{1}H-NMR of 1-benzyl-4-butyl-1,2,3-triazole

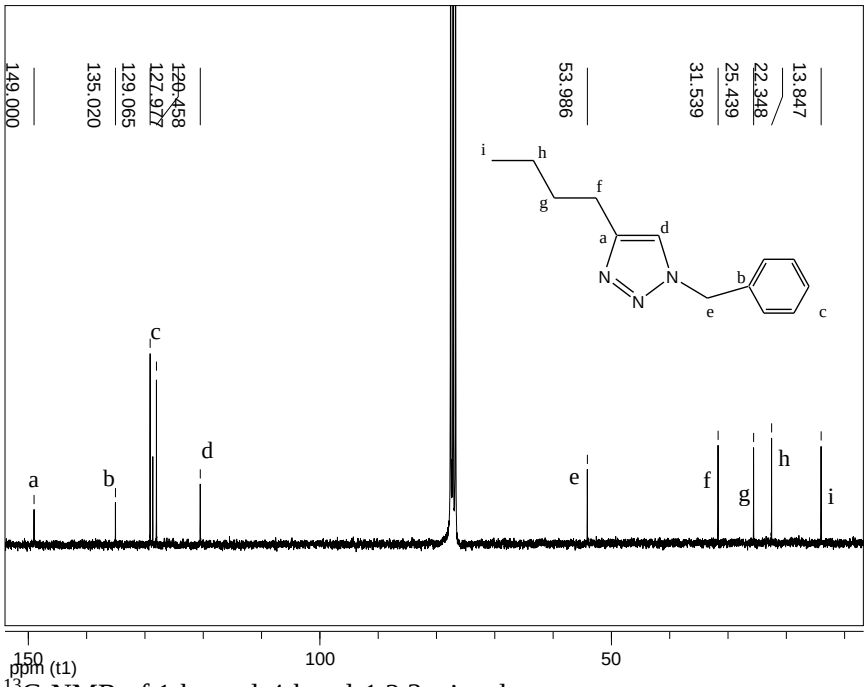

^{13}C-NMR of 1-benzyl-4-butyl-1,2,3-triazole

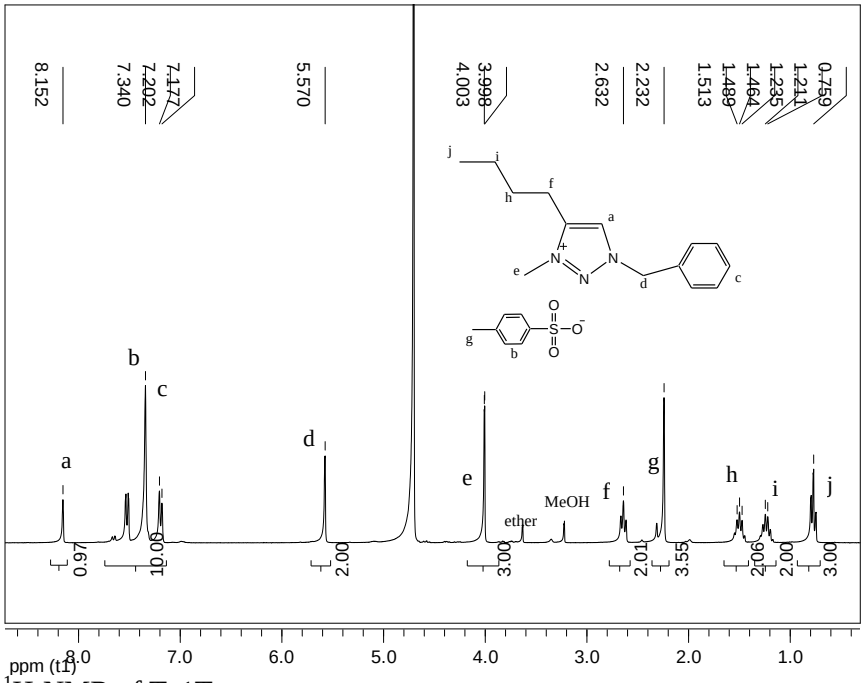

^{1}H-NMR of Tz1Tos

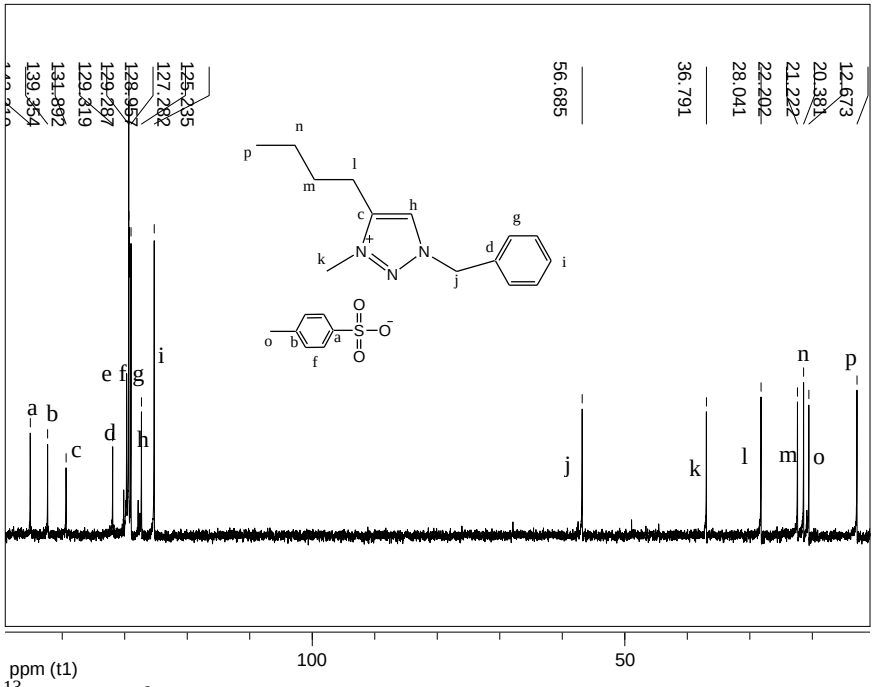

^{13}C-NMR of Tz1Tos

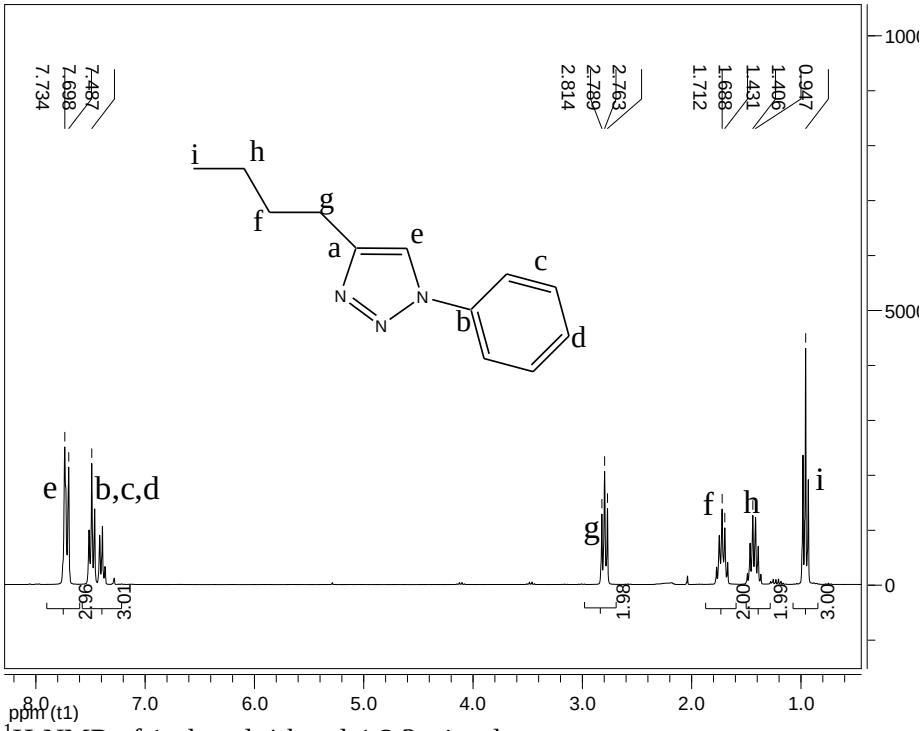

^{1}H-NMR of 1-phenyl-4-butyl-1,2,3-triazole

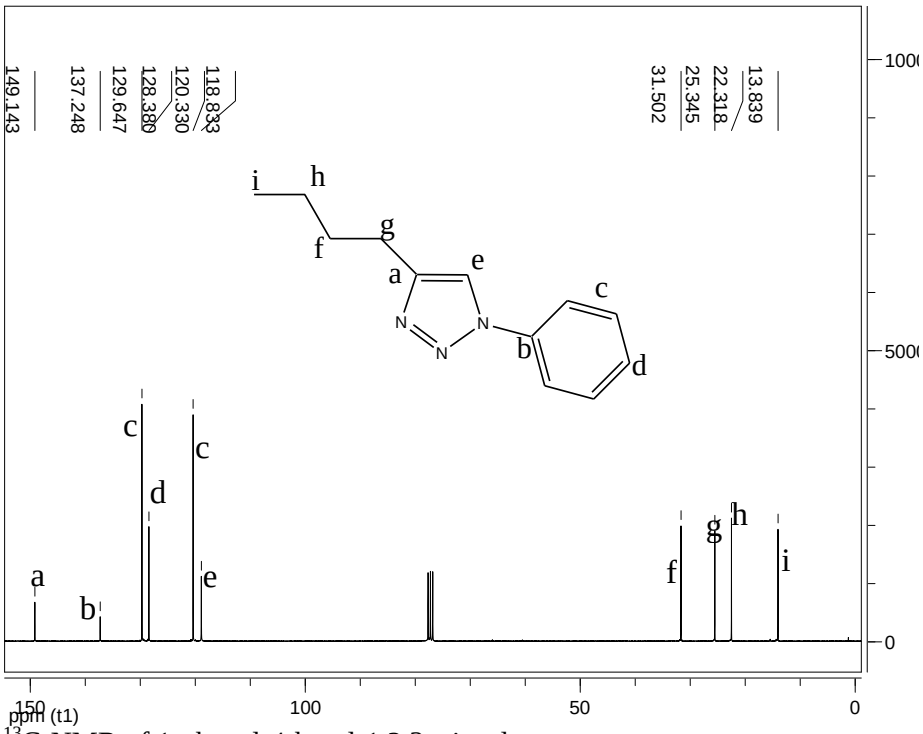

^{13}C-NMR of 1-phenyl-4-butyl-1,2,3-triazole

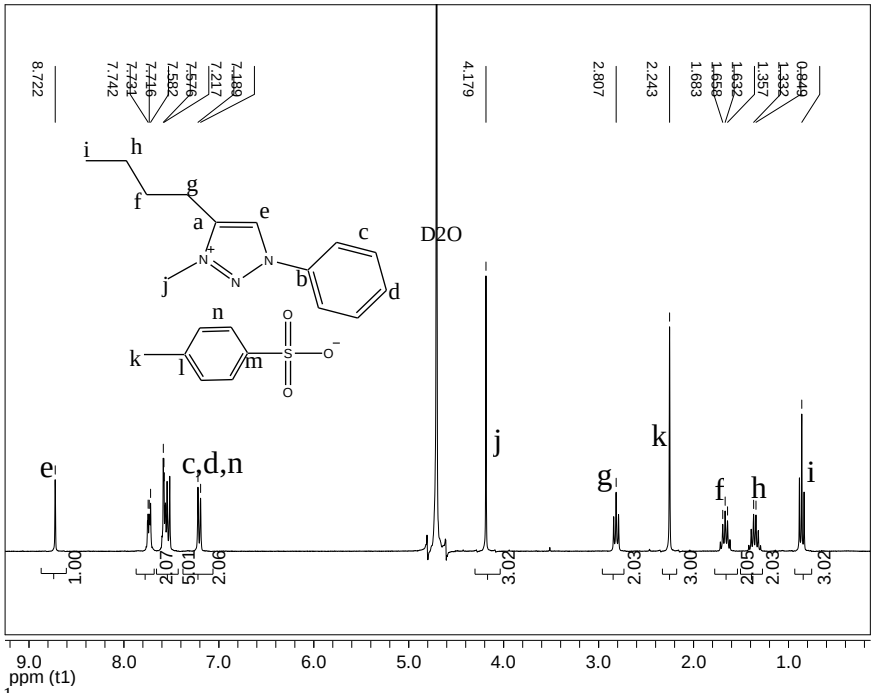

^{1}H-NMR of Tz2Tos

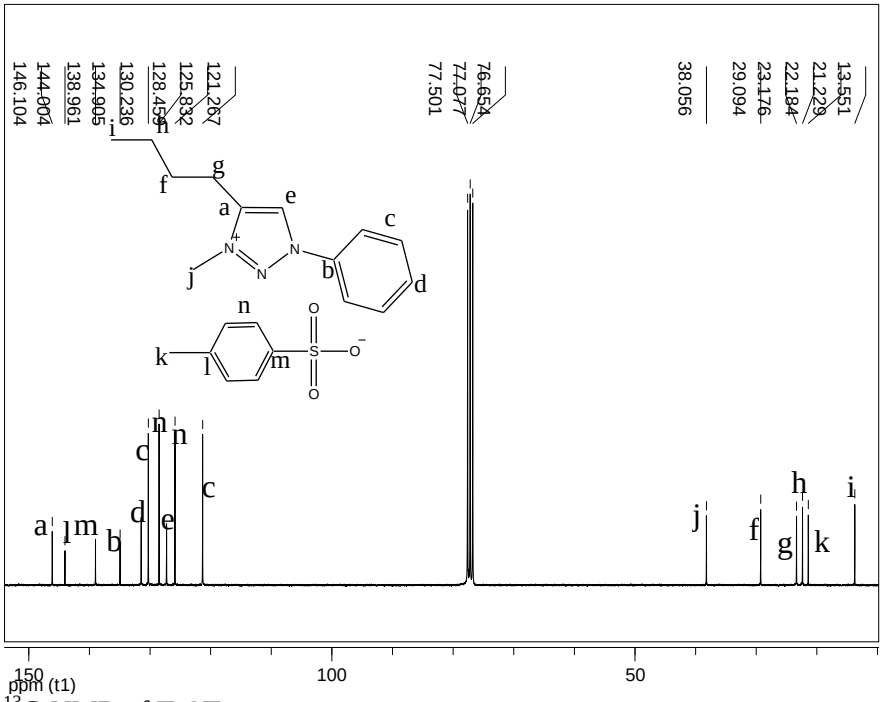

^{13}C-NMR of Tz2Tos

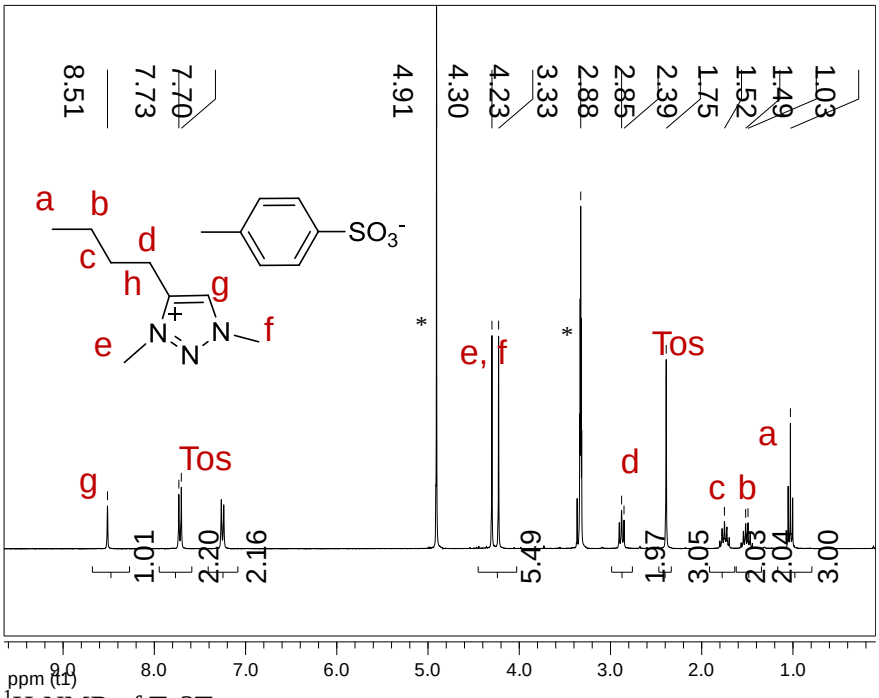

^{1}H-NMR of Tz3Tos

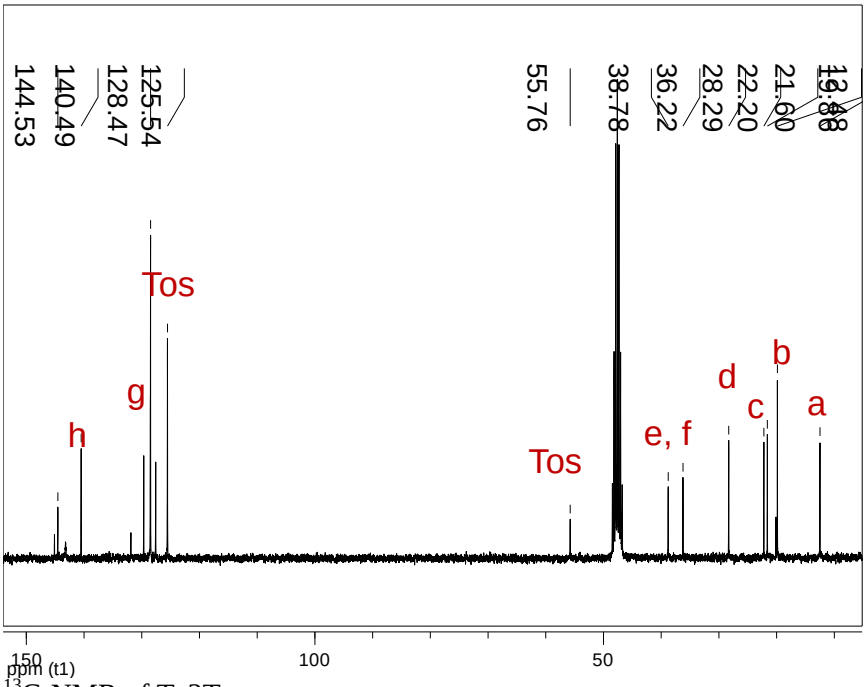

^{13}C-NMR of Tz3Tos

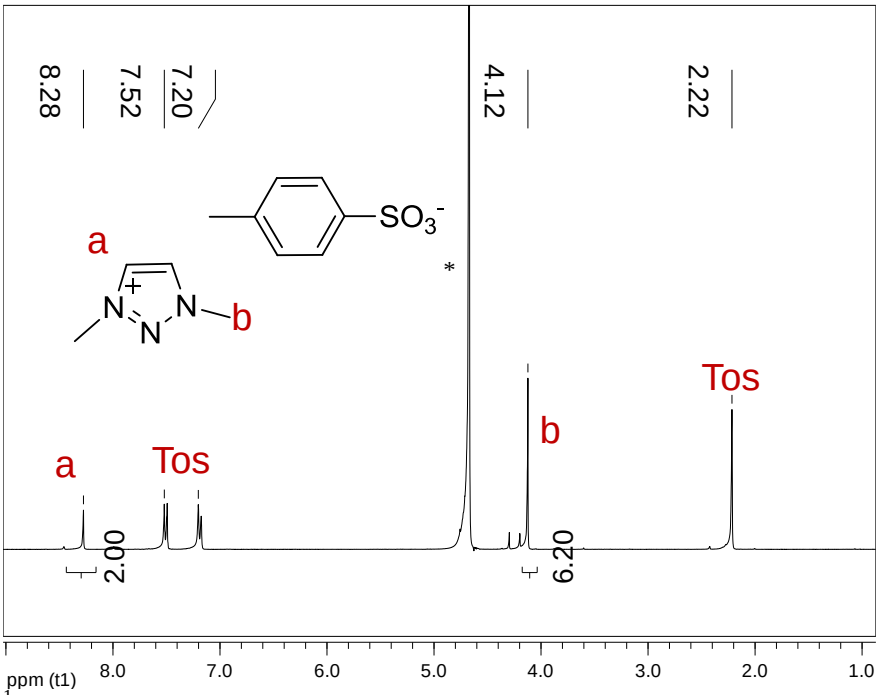

^{1}H-NMR of Tz4Tos

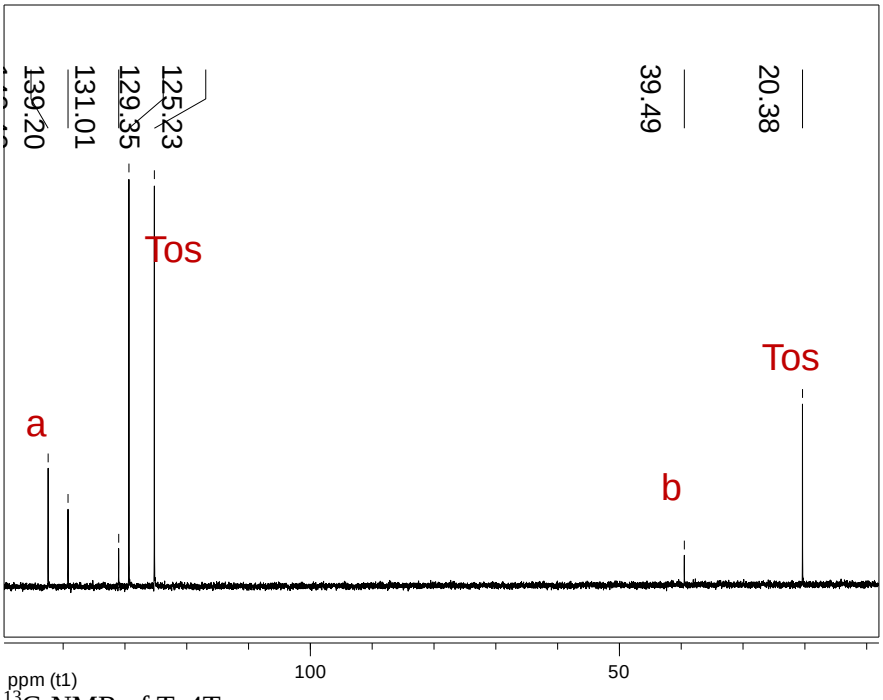

^{13}C-NMR of Tz4Tos

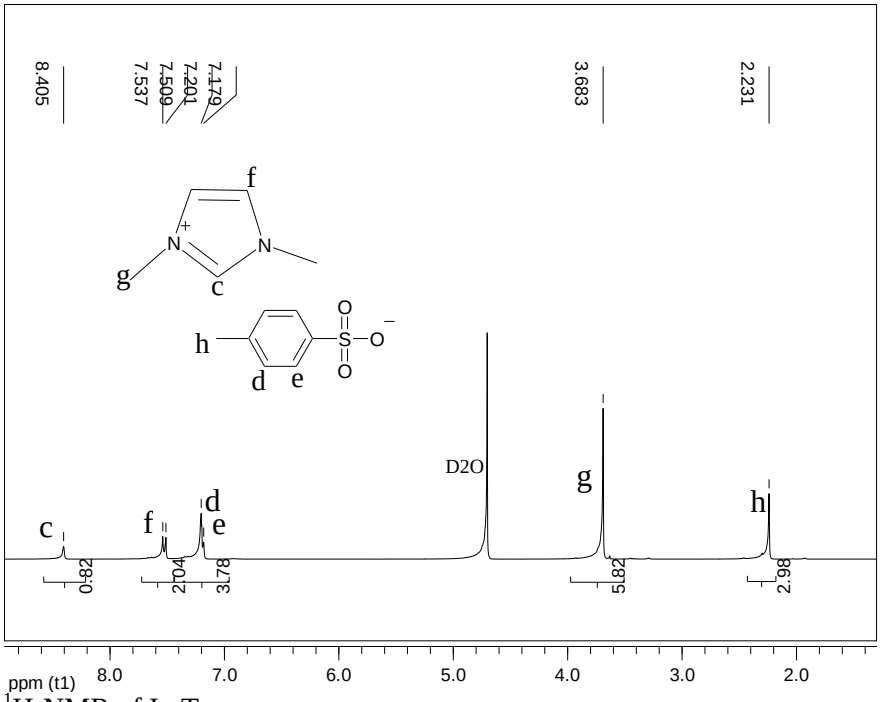

^{1}H-NMR of ImTos

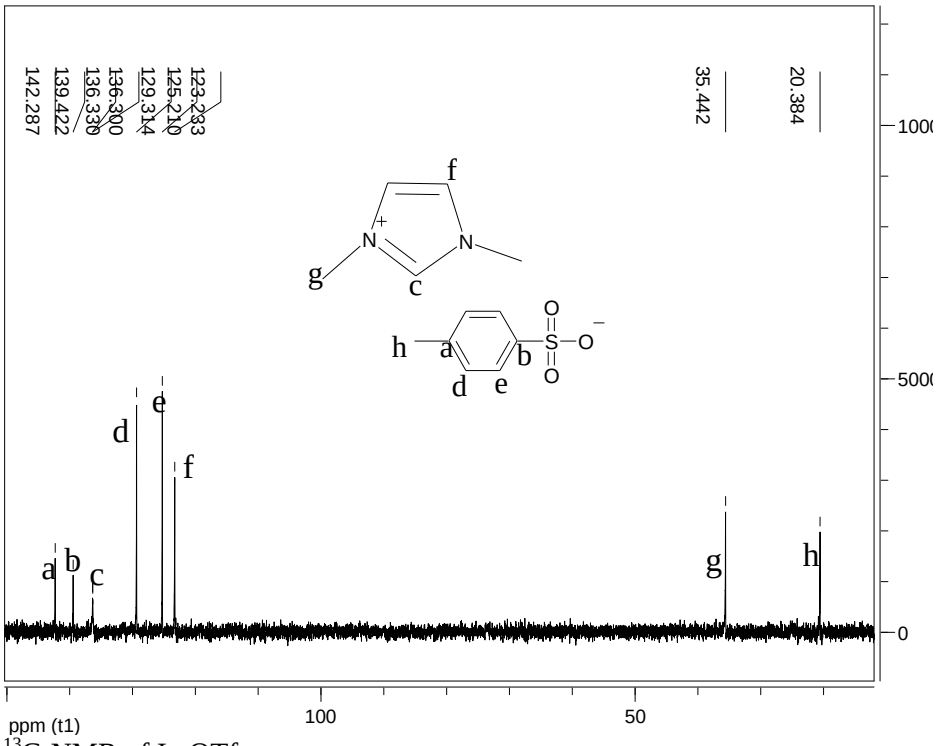

^{13}C-NMR of ImOTf

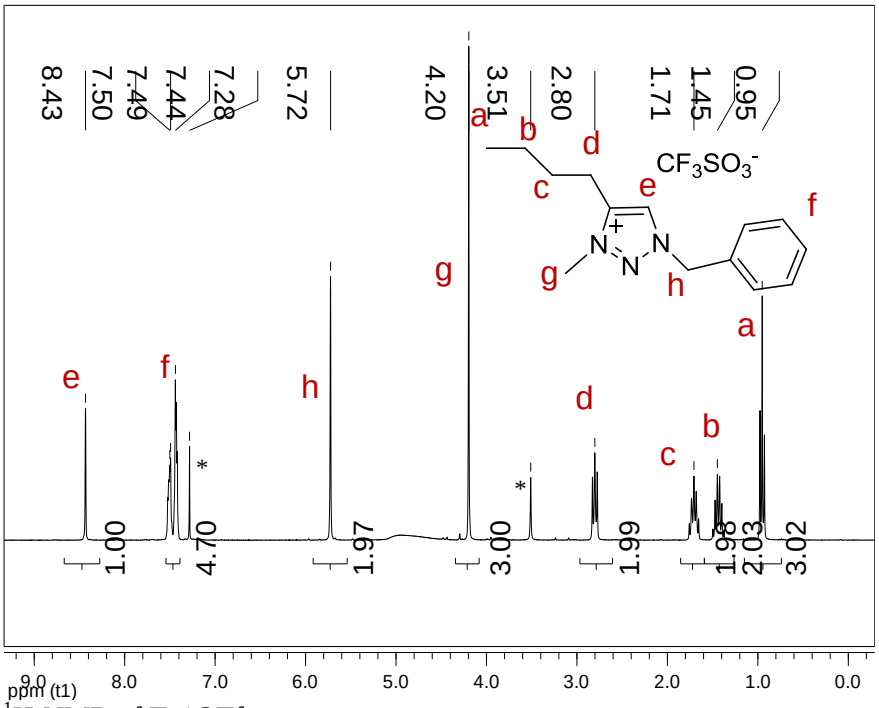

^{1}H-NMR of Tz1OTf

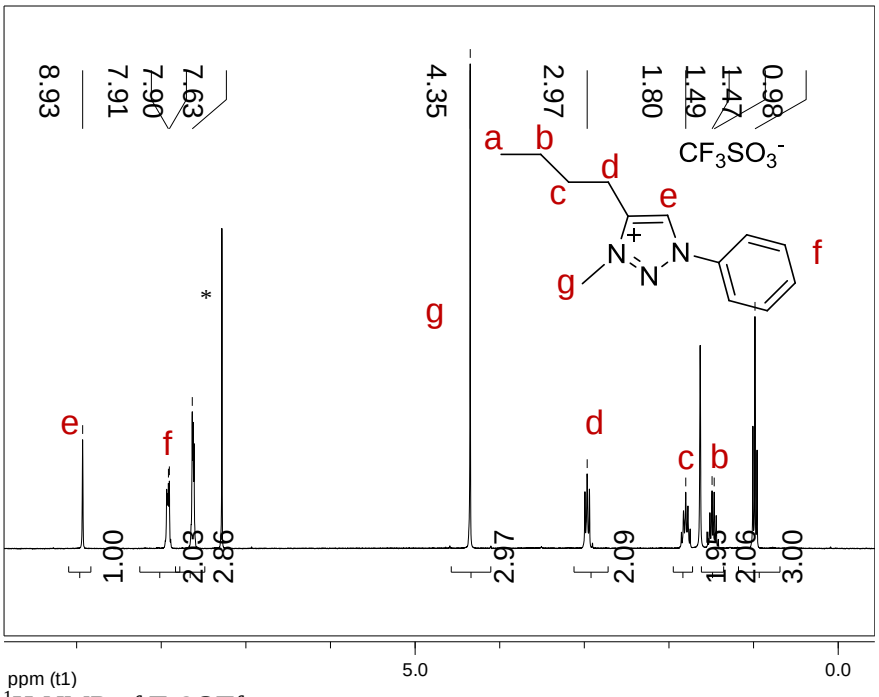

^{1}H-NMR of Tz2OTf

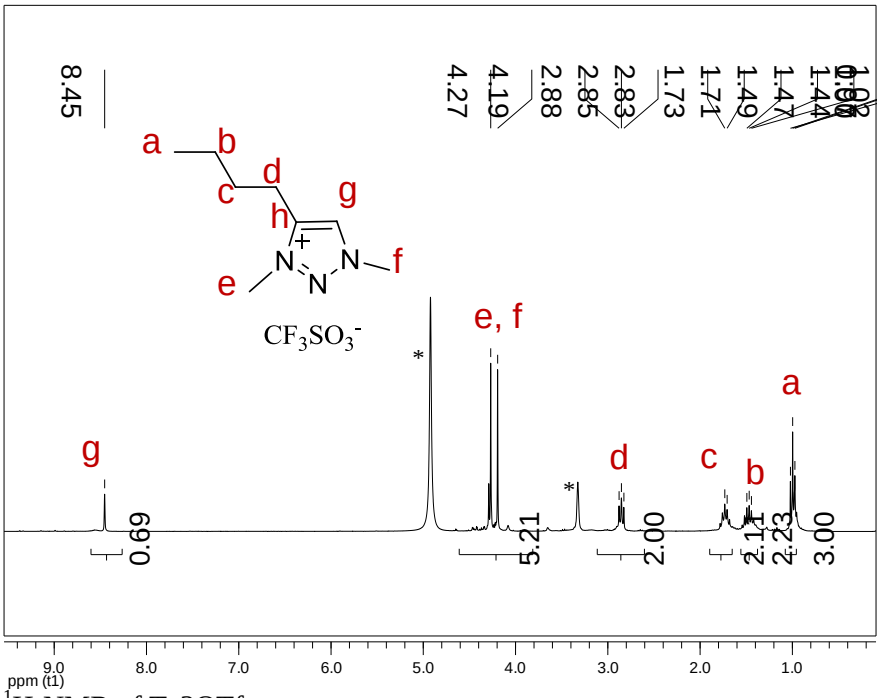

^{1}H-NMR of Tz3OTf

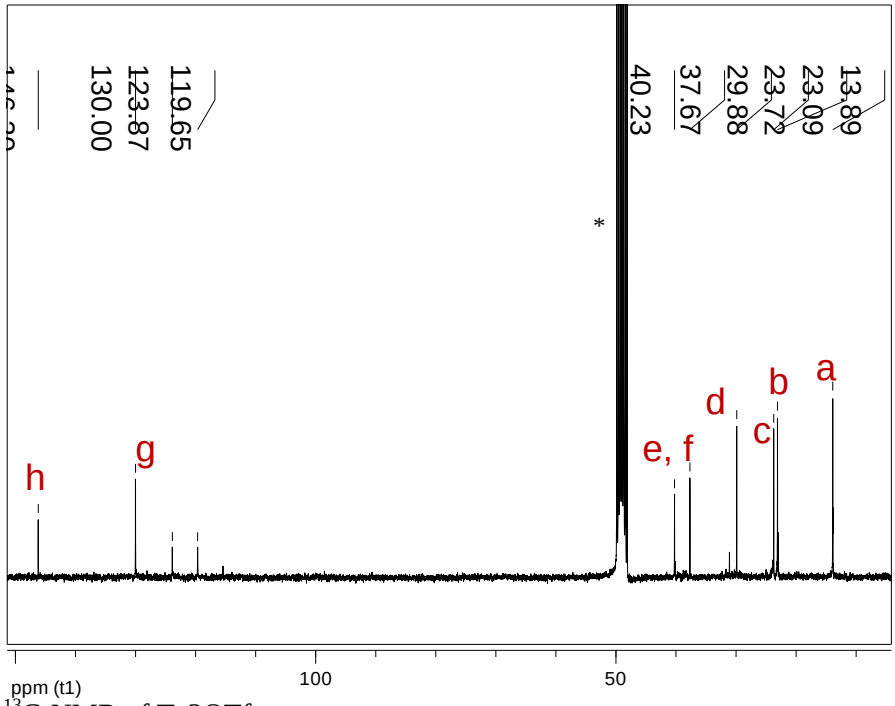

^{13}C-NMR of Tz3OTf

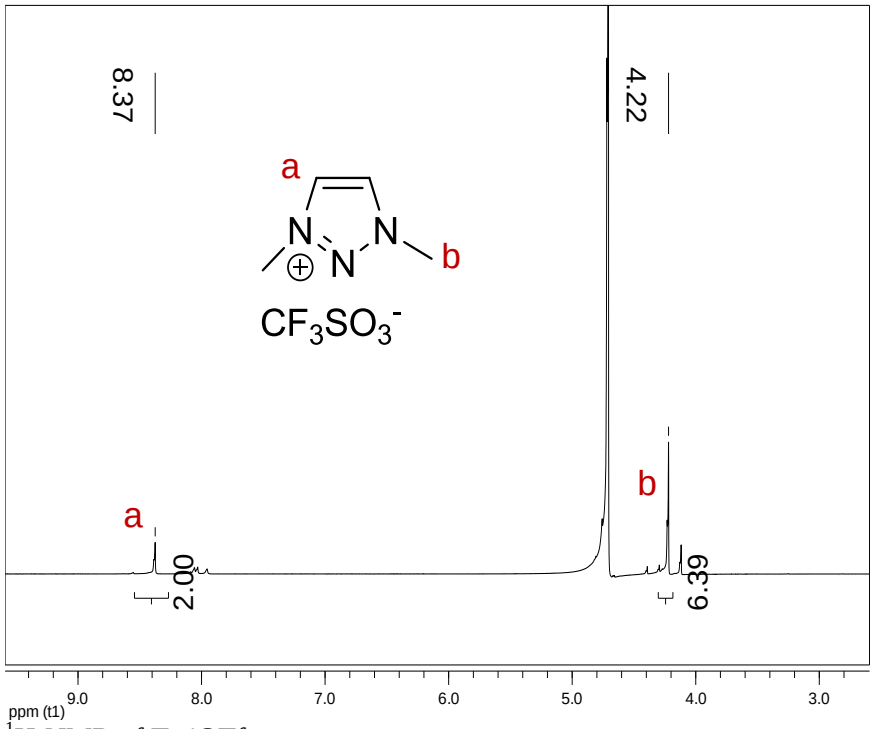

^{1}H-NMR of Tz4OTf

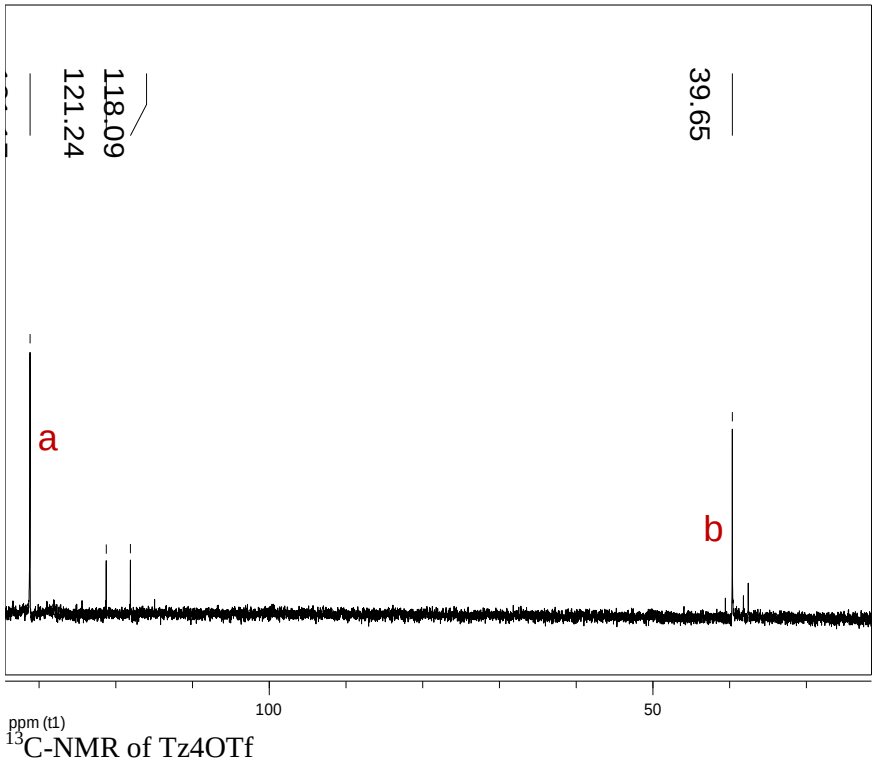

^{13}C-NMR of Tz4OTf

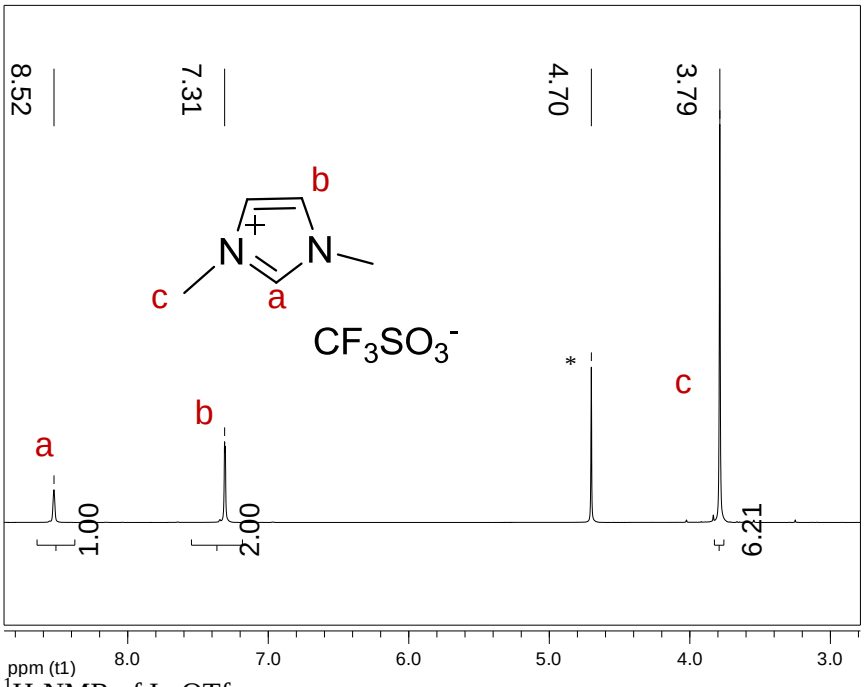

^{1}H-NMR of ImOTf

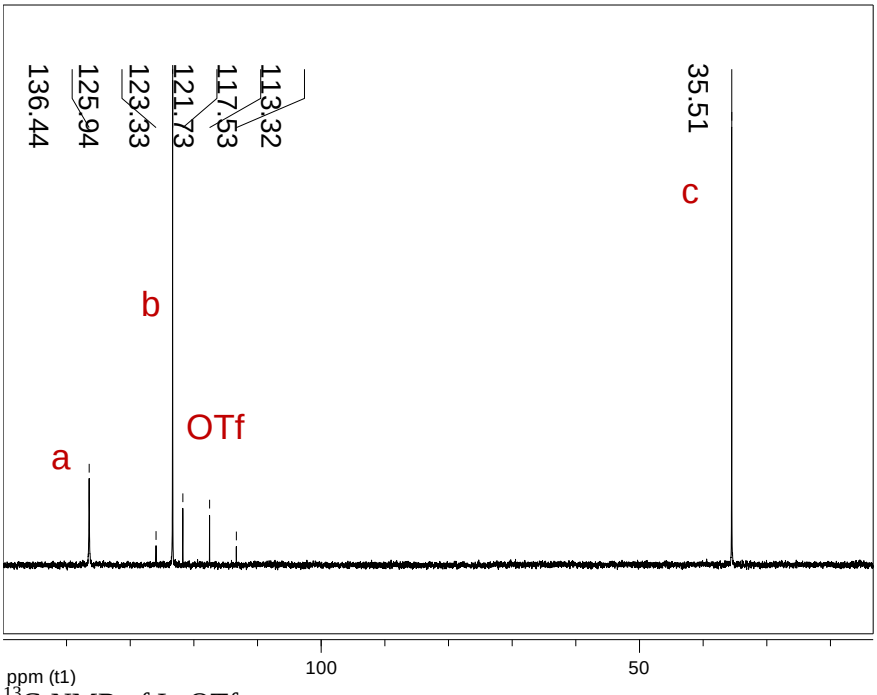

^{13}C-NMR of ImOTf

APPENDIX E

SUPPORTING NMR SPECTRA FOR CHAPTER 5

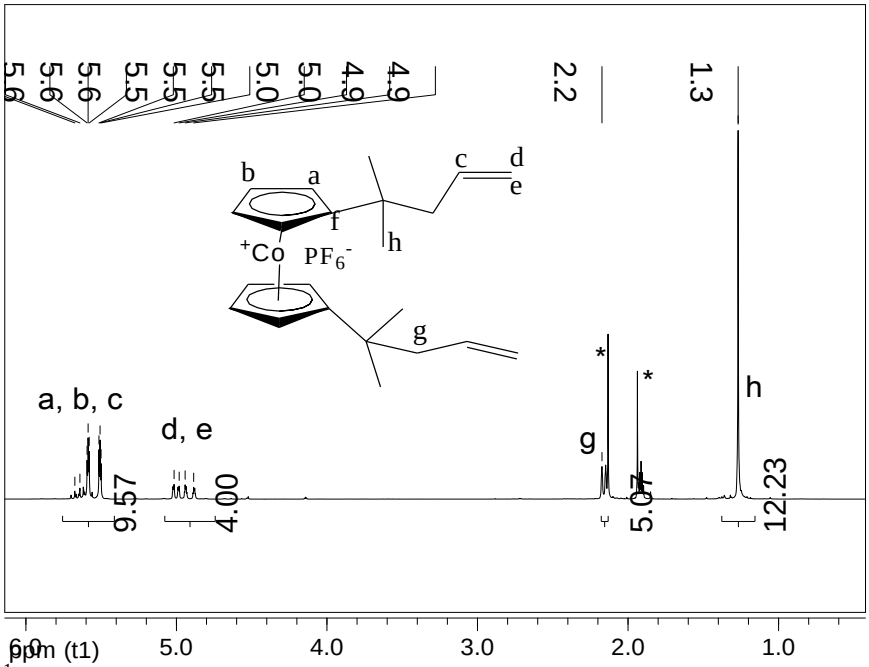

^{1}H-NMR of **5.6a**

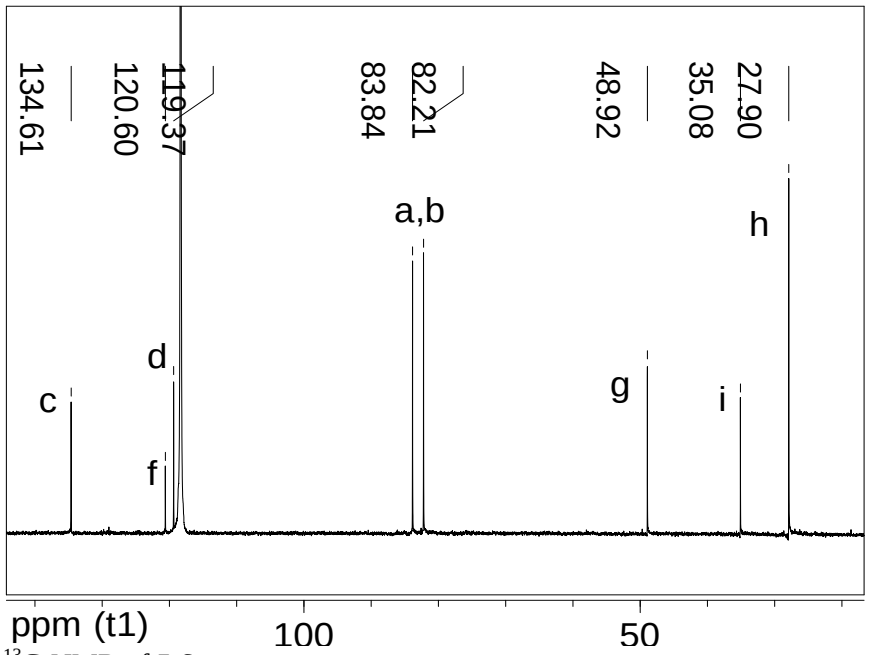

^{13}C-NMR of **5.6a**

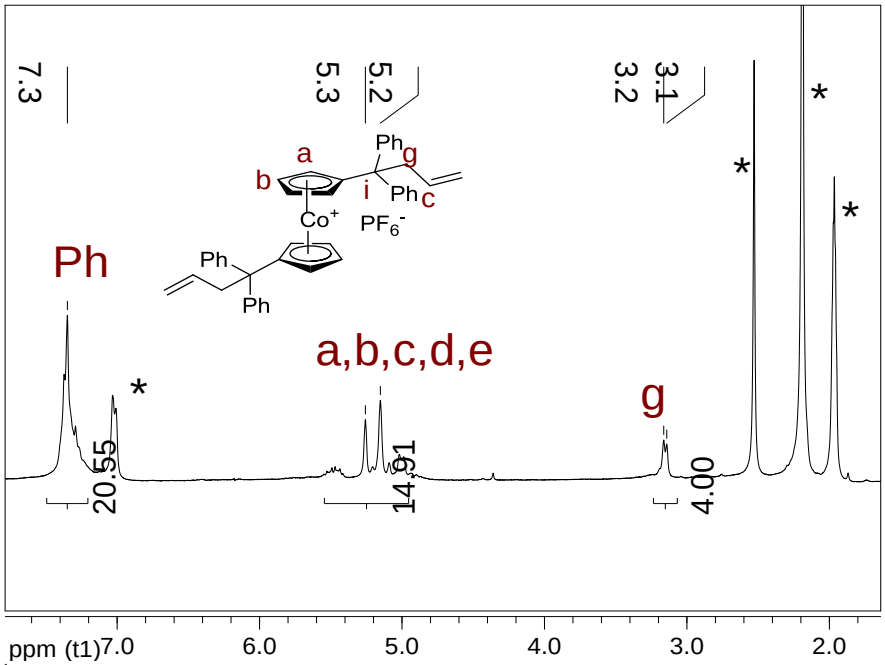

^{1}H-NMR of **5.6b**

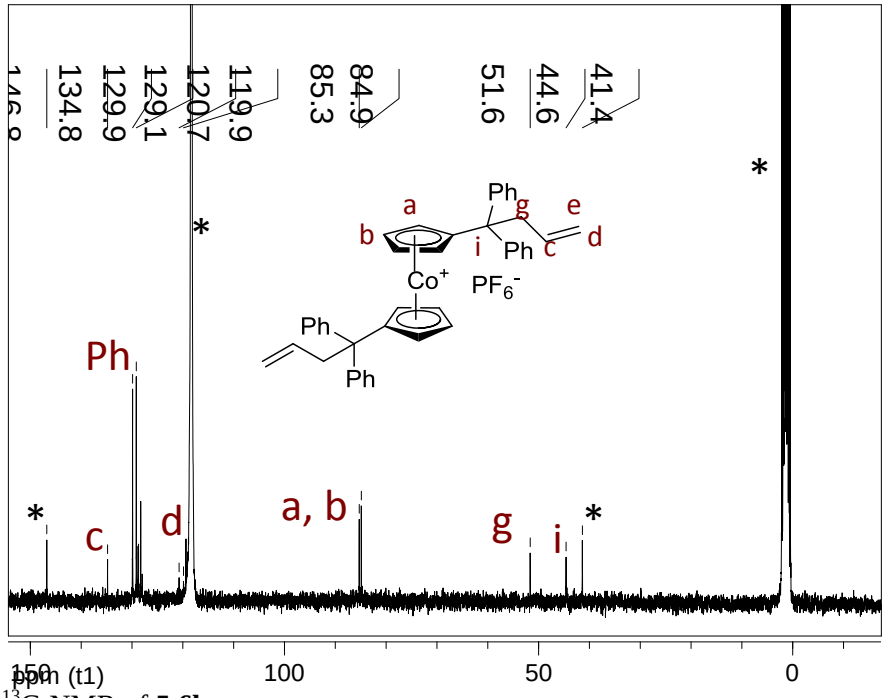

^{13}C-NMR of **5.6b**

APPENDIX F

SUPPORTING NMR SPECTRA FOR CHAPTER 6

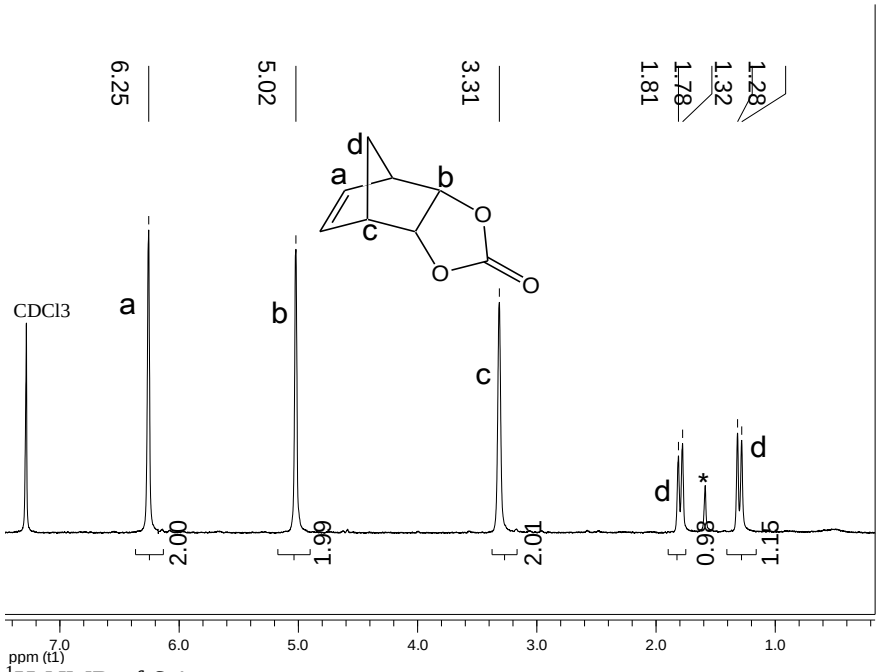

^{1}H-NMR of **6.1**

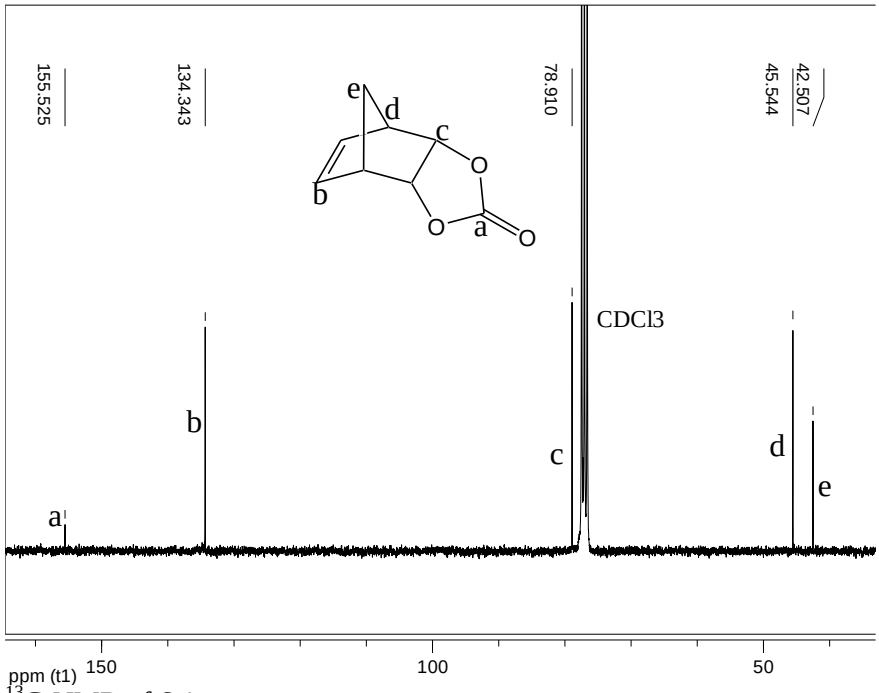

^{13}C-NMR of **6.1**

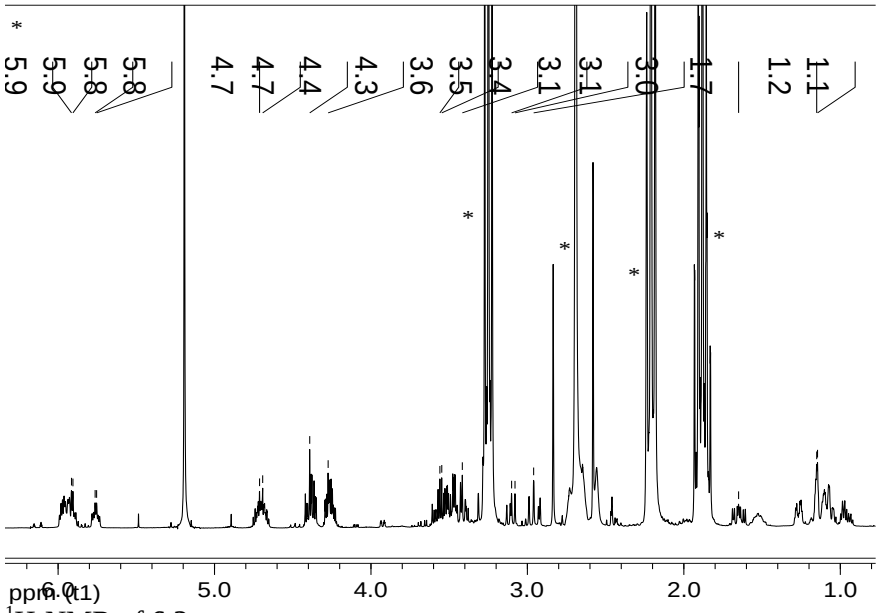

^{1}H-NMR of **6.2**

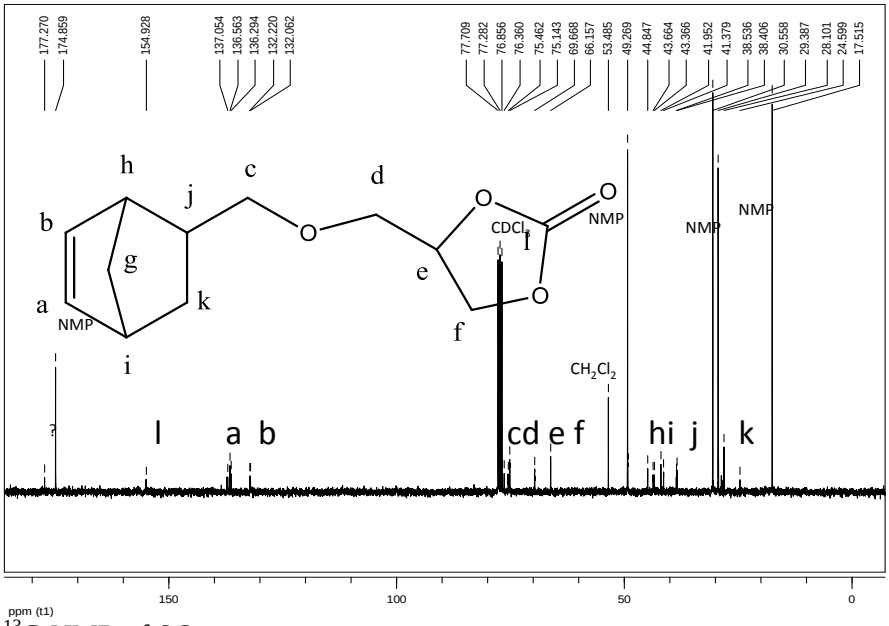

^{13}C-NMR of **6.2**

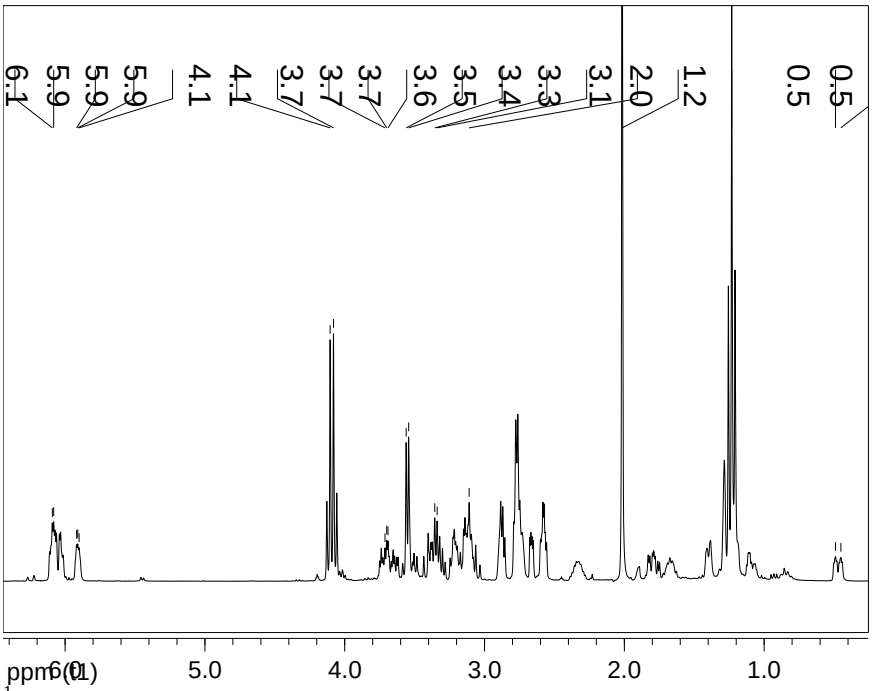

^{1}H-NMR of **6.7**

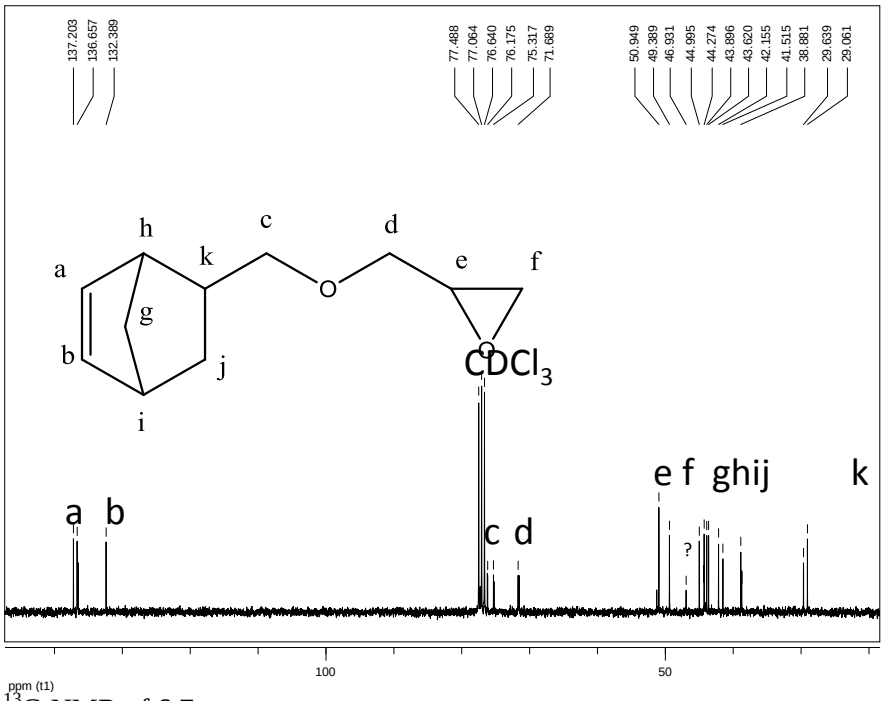

^{13}C-NMR of **6.7**

BIBLIOGRAPHY

Abdel Rahim, M. A.; Abdel Hameed, R. M.; Khalil, M. W., *J. Power Sources* **2004,** 134, 160-169

Adams, L. A.; Poynton, S. D.; Tamain, C.; Slade, R. C. T.; Varcoe, J. R., *ChemSusChem* **2008,** 1, 79-81

Agel, E.; Bouet, J.; Fauvarque, J. F., *J. Power Sources* **2001,** 101, 267-274

Akbey, Ü.; Granados-Focil, S.; Coughlin, E. B.; Graf, R.; Spiess, H. W., *J. Phys. Chem. B* **2009,** 113, 9151-9160

Allcock, H. R.; O'Connor, S. J. M.; Olmeijer, D. L.; Napierala, M. E.; Cameron, C. G., *Macromolecules* **1996,** 29, 7544-7552.

Anderson, J.; Madsen, U.; Bjorkling, F.; Liang, X., *Synlett* **2005**, 2209-2213

Appukkuttan, P.; Dehaen, W.; Fokin, V. V.; Van der Eycken, E., *Org. Lett.* **2004,** 6, 4223-4225.

Arduengo, A. J.; Harlow, R. L.; Kline, M., *J. Am. Chem. Soc.* **1991,** 113, 361-363.

Arges, C. G.; Ramani, V.; Pintauro, P. N., *Electrochem. Soc. Interface* **2010,** 19, 31-35.

Baik, M.-H.; Friesner, R. A., *J. Phys. Chem. A* **2002,** 106, 7407-7412.

Balkus, K. J., Jr.; Gabrielov, A. G.; Shepelev, S., *Microporous Mater.* **1995,** 3, 489-495.

Balkus, K. J., Jr.; Shepelev, S., *Microporous Mater.* **1993,** 1, 393-391.

Baughman, T. W.; Wagener, K. B., *Adv. Polym. Sci.* **2005,** 176, 1-42.

Begtrup, M., *Acta Chem. Scand.* **1971,** 25, 249-259.

Begtrup, M., *Bull. Soc. Chim. Belg.* **1988,** 97, 573-597.

Begtrup, M.; Larsen, P., *Acta Chem. Scand.* **1990,** 44, 1050-1057.

Bini, R.; Bortolini, O.; Chiappe, C.; Pieraccini, D.; Siciliano, T., *J. Phys. Chem. B* **2007,** 111, 598-604.

Bloch, D., *Polymer Handbook*. 4 ed.; Wiley-Interscience: **1999**

Bonhote, P.; Dias, A.-P.; Papageorgiou, N.; Kalyanasundaram, K.; Gratzel, M., *Inorg. Chem.* **1996,** 35, 1168-1178.

Borsato, G.; De Lucchi, O.; Fabris, F.; Groppo, L.; Lucchini, V.; Zambon, A., *J. Org. Chem.* **2002,** 67, 7894-7897.

Bozkurt, A.; Meyer, W. H., *Solid State Ionics* **2001,** 138, 259-265.

Britz, J.; Meyer, W. H.; Wegner, G., *Macromolecules* **2007,** 40, 7558-7565.

Bruce, P. G., *Polymer Electrolyte Reviews*. 1 ed.; Elsevier Applied Science: New York, **1987**; Vol. 1, pp 237-274.

Brunklaus, G.; Schauff, S.; Markova, D.; Klapper, M.; Mullen, K.; Spiess, H.-W., *J. Phys. Chem. B.* **2009,** 113, 6674-6681.

Bureekaew, S.; Horike, S.; Higuchi, M.; Mizuno, M.; Kawamura, T.; Tanaka, D.; Yanai, N.;

Kitagawa, S., *Nat. Mater.* **2009,** 8, 831-836.

Buriez, O.; Han, Y. B.; Hou, J.; Kerr, J. B.; Qiao, J.; Sloop, S. E.; Tian, M.; Wang, S., *J. Power Sources* **2000,** 89, 149-155.

Carrette, L.; Friedrich, K. A.; Stimming, U., *Fuel Cells* **2001,** 1, 5-39.

Celik, S. U.; Akbey, U.; Graf, R.; Bozkurt, A.; Spiess, H. W., *Phys. Chem. Chem. Phys.* **2008,** 10, 6058-6066.

Celik, S. U.; Aslan, A.; Bozkurt, A., *Solid State Ionics* **2008,** 179, 683-688.

Chalk, A. J.; Harrod, J. F., *J. Am. Chem. Soc.* **1965,** 87, 16-21.

Chen, H.; Palmese, G. R.; Elabd, Y. A., *Chem. Mater.* **2006,** 18, 4875-4881.

Chu, B.; Hsiao, B. S., *Chem. Rev.* **2001,** 101, 1727-1762.

Clark, T. J.; Robertson, N. J.; Kostalik Iv, H. A.; Lobkovsky, E. B.; Mutolo, P. F.; Abruña, H. c. D.; Coates, G. W., *J. Am. Chem. Soc.* **2009,** 131, 12888-12889.

Colomban, P., *Proton Conductors: Solids, Membranes and Gels--Materials and Devices*.

Cambridge University Press: Cambridge, **1992**; Vol. 2, pp 311.

Cramer, N. B.; Scott, J. P.; Bowman, C. N., *Macromolecules* **2002,** 35, 5361-5365.

Croce, F.; Appetecchi, G. B.; Persi, L.; Scrosati, B., *Nature* **1998,** 394, 456-458.

Cuadrado, I.; Casado, C. M.; Lobete, F.; Alonso, B.; Gonzalez, B.; Losada, J.; Amador, U., *Organometallics* **1999,** 18, 4960-4969.

Danks, T. N.; Slade, R. C. T.; Varcoe, J. R., *J. Mater. Chem.* **2003,** 13, 712.

Davide, T.; Stefano, P.; Joachim, L.; Alexander, A., *Macromolecules* **2007,** 40, 1259-1267.

de Grotthuss, C. J. T., *Ann. Chim.* **1806,** LVIII, 54-74.

Deluca, N. W.; Elabd, Y. A., *J. Polym. Sci. Pol. Phys.* **2006,** 44, 2201-2225.

Domanska, U., *Ionic Liq. Chem. Anal.* **2009,** 1, 1-72.

Dueno, E. E.; Chu, F.; Kim, S.-I.; Jung, K. W., *Tetrahedron Lett.* **1999,** 40, 1843-1846.

Egashira, M.; Todo, H.; Yoshimoto, N.; Morita, M., *J. Power Sources* **2008,** 178, 729-735.

Einsla, B. R.; Chempath, S.; Pratt, L. R.; Boncella, J. M.; Rau, J.; Macomber, C.; Pivovar, B. S., *ECS Trans.* **2007,** 11, 1173-1180.

Elabd, Y. A.; Hickner, M. A., *Macromolecules* **2011,** 44, 1-11.

Elabd, Y. A.; Napadensky, E.; Sloan, J. M.; Crawford, D. M.; Walker, C. W., *J. Membr. Sci.* **2003,** 217, 227-242.

Elabd, Y. A.; Walker, C. W.; Beyer, F. L., *J. Membr. Sci.* **2004,** 231, 181-188.

Fauteux, D.; McCabe, P., *Polym. Advan. Technol.* **1995,** 6, 83-90.

Finkelstein, H., *Chem. Ber.* **1910,** 43, 1528-1532.

Fischbach, I.; Spiess, H. W.; Saalwachter, K.; Goward, G. R., *J. Phys. Chem. B* **2004,** 108, 18500-18508.

Fletcher, J. T.; Keeney, M. E.; Walz, S. E., *Synthesis* **2010**, 3339-3345.

Forsyth, S. A.; MacFarlane, D. R., *J. Mater. Chem.* **2003,** 13, 2451-2456.

Fraser, K. J.; MacFarlane, D. R., *Aust. J. Chem.* **2009,** 62, 309-321.

Fringuelli, F.; Pizzo, F.; Taticchi, A.; Wenkert, E., *J. Org. Chem.* **1983,** 48, 2802-2808.

Gierke, T. D.; Munn, G. E.; Wilson, F. C., *J. Polym. Sci. Polym. Phys.* **1981,** 19, 1687-1704.

Golden, J. H.; Chew, B. G. M.; Zax, D. B.; DiSalvo, F. J.; Frechet, J. M. J.; Tarascon, J.-M., *Macromolecules* **1995,** 28, 3468-3470.

Goward, G. R.; Schuster, M. F. H.; Sebastiani, D.; Schnell, I.; Spiess, H. W., *J. Phys. Chem. B* **2002,** 106, 9322-9334.

Gozzo, F. C.; Santos, L. S.; Augusti, R.; Consorti, C. S.; Dupont, J.; Eberlin, M. N., *Chem. Eur. J.* **2004,** 10, 6187-6193.

Graf, R. http://www.mpip-mainz.mpg.de/~graf/documents/research.html (accessed April 30, 2011).

Graf, R.; Demco, D. E.; Hafner, S.; Spiess, H. W., *Solid State Nucl. Magn. Reson.* **1998,** 12, 139-152.

Graf, R.; Heuer, A.; Spiess, H. W., *Phys. Rev. Lett.* **1998,** 80, 5738-5741.

Granados-Focil, S.; Woudenberg, R. C.; Yavuzcetin, O.; Tuominen, M. T.; Coughlin, E. B., *Macromolecules* **2007,** 40, 8708-8713.

Green, M.; Pratt, L.; Wilkinson, G., *J. Chem. Soc.* **1959**, 3753

Grubbs, R. H., *Handbook of Metathesis*. Wiley-VCH Weinheim, **2003**; Vol. 3.

Grubbs, R. H., *Handbook of Metathesis*. Wiley-VCH: Weinheim, **2003**; Vol. 2.

Hahn, S. F., *J. Polym. Sci., Part A Polym. Chem.* **1992,** 30, 397-408.

Hamrock, S. J.; Yandrasits, M. A., *J. Macromol. Sci., Part C: Polym. Rev.* **2006,** 46, 219-244.

Herz, H. G.; Kreuer, K. D.; Maier, J.; Scharfenberger, G.; Schuster, M. F. H.; Meyer, W. H., *Electrochim. Acta* **2003,** 48, 2165-2171.

Hibbs, M. R.; Fujimoto, C. H.; Cornelius, C. J., *Macromolecules* **2009,** 42, 8316-8321.

Hickman, B. S.; Mascal, M.; Titman, J. J.; Wood, I. G., *J. Am. Chem. Soc.* **1999,** 121, 11486-11490.

Hickner, M.; Ghassemi, H.; Kim, Y.; Einsla, B.; McGrath, J., *Chem. Rev.* **2004,** 104, 4587-4612.

Higami, M.; Woudenberg, R. C.; Granados-Focil, S.; Yavuzcetin, O.; Tuominen, M. T.; Coughlin, E. B. PMSE Preprints, **2007**; 97 pp 551-552.

Hino, T.; Inoue, N.; Endo, T., *Macromolecules* **2004,** 37, 9660-9663.

Hooper, R.; Lyons, L. J.; Moline, D. A.; West, R., *Organometallics* **1999,** 18, 3249-3251.

Hoyle, C. E.; Bowman, C. N., *Angew. Chem., Int. Ed.* **2010,** 49, 1540-1573.

Hoyle, C. E.; Lee, T. Y.; Roper, T., *J. Polym. Sci., Part A Polym. Chem.* **2004,** 42, 5301-5338.

Hubner, G.; Roduner, E., *J. Mater. Chem.* **1999,** 9, 409.

Hwang, Y. K.; Lee, J.-M.; Sathaye, S. D.; Cho, G.; Hwang, J.-S.; Chang, J.-S., *J. Nanosci. Nanotechnol.* **2006,** 6, 1850-1853.

In http://howstuffworks.com (accessed March 14, 2011).

Instruments, G. Electrochemical Impedance Spectroscopy Primer.

http://gamry.com/App_Notes/EIS_Primer/Basics_Of_EIS.pdf (accessed May 5, 2011).

Ito, T.; Kenjo, T., *Bull. Chem. Soc. Japan* **1968,** 41, 614-619.

Ivashkevich, O. A.; Matulis, V. E.; Lyakhov, A. S.; Grigorieva, I. N.; Gaponik, P. N.; Sukhanov, G. T.; Filippova, Y. V.; Sukhanova, A. G., *Chem. Heterocycl. Compd.* **2009,** 45, 1218-1225.

Jensen, M. O.; Rothlisberger, U.; Rovira, C., *Biophys. J.* **2005,** 89, 1744-1759.

Jeong, J.-R.; Choi, M. C.; Im, M.-Y.; Kim, M. W.; Shin, S.-C. Magnetics Conference,

INTERMAG, IEEE International, 28 March-3 April **2003**; pp GC-10.

Jeong, Y.; Ryu, J.-S., *J. Org. Chem.* **2010,** 75, 4183-4191.

Jeong, Y.-K.; Kim, D.-Y.; Choi, Y.-S.; Ryu, J.-S., *Org. Biomol. Chem.* **2011,** 9, 374-378.

Kang, K.; Meng, Y. S.; Breger, J.; Grey, C. P.; Ceder, G., *Science* **2006,** 311, 977-980.

Kaplan, M. L.; Rietman, E. A.; Cava, R. J.; Holt, L. K.; Chandross, E. A., *Solid State Ionics* **1987,** 25, 37-40.

Kerr, J. B.; Liu, G.; Curtiss, L. A.; Redfern, P. C., *Electrochim. Acta* **2003,** 48, 2305-2309.

Khan, S. S.; Hanelt, S.; Liebscher, J., *ARKIVOC (Gainesville, FL, U. S.)* **2009**, 193-208.

Kihara, N.; Hara, N.; Endo, T., *J. Org. Chem.* **1993,** 58, 6198-6202.

Kim, J.; Mori, T.; Hayashi, S.; Honma I., *J. Electrochem. Soc.* **2007,** 154, A290-A294.

Knauth, P.; Schoonman, J., *Nanocomposites: Ionic Conducting Materials and Structural Spectroscopies*. 1st ed.; Springer: **2007**; pp 111.

Koh, J. H.; Lee, K. J.; Seo, J. A.; Kim, J. H., *J. Polym. Sci., Part B: Polym. Phys.* **2009,** 47, 1443-1451.

Kondo, M.; Hayakawa, Y.; Miyazawa, M.; Oyama, A.; Unoura, K.; Kawaguchi, H.; Naito, T.; Maeda, K.; Uchida, F., *Inorg. Chem.* **2004,** 43, 5801-5803.

Kostalik, H. A.; Clark, T. J.; Robertson, N. J.; Mutolo, P. F.; Longo, J. M.; Abruña, H. c. D.; Coates, G. W., *Macromolecules* **2010,** 43, 7147-7150.

Kranenburg, J. M.; Tweedie, C. A.; Vliet, K. J. v.; Schubert, U. S., *Adv. Mater.* **2009,** 21, 3551-3561.

Kreuer, K. D., *J. Membr. Sci.* **2001,** 185, 29-39.

Kreuer, K.-D., *Chem. Mater.* **1996,** 8, 610-641.

Kundu, S.; Simon, L. C.; Fowler, M.; Grot, S., *Polymer* **2005,** 46, 11707-11715.

Kwart, H.; Vosburgh, W. G., *J. Am. Chem. Soc.* **1954,** 76, 5400-5403.

Li, Q.; He, R.; Jensen, J. O.; Bjerrum, N. J., *Chem. Mater.* **2003,** 15, 4896-4915.

Li, S.; Zhou, Z.; Abernathy, H.; Liu, M.; Li, W.; Ukai, J.; Hase, K.; Nakanishi, M., *J. Mater. Chem.* **2006,** 16, 858.

Li, S.; Zhou, Z.; Liu, M.; Li, W.; Ukai, J.; Hase, K.; Nakanishi, M., *Electrochim. Acta* **2006,** 51, 1351-1358.

Li, S.; Zhou, Z.; Zhang, Y.; Liu, M.; Li, W., *Chem. Mater.* **2005,** 17, 5884-5886.

Li, X.; Goh, S. H.; Lai, Y. H.; Wee, A. T. S., *Polymer* **2001,** 42, 5463-5469.

Liebscher, J.; Shah, J.; Yacob, Z.; Sadiq, S.; Hanelt, S.; Blumenthal, H., *J. Phys. Conf. Ser.* **2009,** 182.

Liu, W.; Zuckerbrod, D., *J. Electrochem. Soc.* **2005,** 152, A1165-A1170.

Lobaugh, J.; Voth, G. A., *J. Chem. Phys.* **1996,** 104, 2056-2069

Loren, J. C.; Krasinski, A.; Fokin, V. V.; Sharpless, K. B., *Synlett* **2005**, 2847-2850.

Love, J. A.; Morgan, J. P.; Trnka, T. M.; Grubbs, R. H., *Angew. Chem., Int. Ed.* **2002,** 41, 4035-4037.

Lu, J. Q., *J. Phys. Chem. C* **2008,** 112, 10344-10351.

Macdonald, B., *Impedance Spectroscopy: Theory, Experiment, and Applications*. 2 ed.; Wiley-Interscience: **2005**.

Macomber, C. S.; Boncella, J. M.; Pivovar, B. S.; Rau, J. A., *J. Therm. Anal. Calorim.* **2008,** 93, 225-229.

Marko, I. E.; Sterin, S.; Buisine, O.; Mignani, G.; Branlard, P.; Tinant, B.; Declercq, J.-P., *Science* **2002,** 298, 204-206.

Martwiset, S.; Woudenberg, R. C.; Granados-Focil, S.; Yavuzcetin, O.; Tuominen, M. T.; Coughlin, E. B., *Solid State Ionics* **2007,** 178, 1398-1403.

Martwiset, S.; Yavuzcetin, O.; Thorn, M.; Versek, C.; Tuominen, M.; Coughlin, E. B., *J. Polym. Sci.,Part A: Polym. Chem.* **2009,** 47, 188-196.

Matsubara, K.; Kaneuchi, R.; Maekita, N., *J. Chem. Soc., Faraday Trans.* **1998,** 94, 3601-3605.

Mayer, U. F. J.; Gilroy, J. B.; O'Hare, D.; Manners, I., *J. Am. Chem. Soc.* **2009,** 131, 10382-10383.

Meyer, W. H., *Adv. Mater.* **1998,** 10, 439-448.

Moad, G.; Chiefari, J.; Chong, Y. K.; Krstina, J.; Mayadunne, T. A.; Postma, A.; Rizzardo, E.; Thang, S. H., *Polym. Int.* **2000,** 49, 993-1001.

Münch, W.; Kreuer, K. D.; Silvestri, W.; Maier, J.; Seifert, G., *Solid State Ionics* **2001,** 145, 437-443.

Nazri, G.-A.; Pistoia, G., *Lithium Batteries:Science and Technology*. 1 ed.; Springer: **2004**.

Noda, A.; Watanabe, M., *Electrochim. Acta* **2000,** 45, 1265-1270.

Ochiai, B.; Ootani, Y.; Maruyama, T.; Endo, T., *J. Poly. Sci., Part A: Polym. Chem.* **2007,** 45, 5781-5789.

Oliver, W. C.; Pharr, G. M., *J. Mater. Res.* **1992,** 7, 1564-1583.

Page, J. A.; Wilkinson, G., *J. Am. Chem. Soc.* **1952,** 74, 6149-6150.

Peckham, T. J.; Holdcroft, S., *Adv. Mater.* **2010,** 22, 4667-4690.

Persson, J. C.; Jannasch, P., *Macromolecules* **2005,** 38, 3283-3289.

Persson, J. C.; Jannasch, P., *Solid State Ionics* **2006,** 177, 653-658.

Persson, J. C.; Josefsson, K.; Jannasch, P., *Polymer* **2006,** 47, 991-998.

Ren, L.; Hardy, C. G.; Tang, C., *J. Am. Chem. Soc.* **2010,** 132, 8874-8875.

Ren, L.; Hardy, C. G.; Tang, S.; Doxie, D. B.; Hamidi, N.; Tang, C., *Macromolecules* **2010,** 43, 9304-9310.

Rikukawa, M.; Sanui, K., *Prog. Polym. Sci.* **2000,** 25, 1463-1502.

Robertson, N. J.; Kostalik, H. A.; Clark, T. J.; Mutolo, P. F.; Abruña, H. c. D.; Coates, G. W., *J. Am. Chem. Soc.* **2010,** 132, 3400-3404.

Rokicki, G.; Pawlicki, J.; Kuran, W., *J. Prakt. Chem.* **1985,** 327, 718-722.

Roscioli, J. R.; McCunn, L. R.; Johnson, M. A., *Science* **2007,** 316, 249-254.

Rostovtsev, V. V.; Green, L. G.; Fokin, V. V.; Sharpless, K. B., *Angew. Chem., Int. Ed.* **2002,** 41, 2596-2599.

Russell, G. A.; Schmitt, K. D.; Mattox, J., *J. Am. Chem. Soc.* **1975,** 97, 1882-1891.

Scharfenberger, G.; Meyer, W. H.; Wegner, G.; Schuster, M.; Kreuer, K. D.; Maier, J., *Fuel Cells* **2006,** 6, 237-250.

Schmidt-Rohr, K.; Chen, Q., *Nat. Mater.* **2008,** 7, 75-83.

Schmitt, U. W.; Voth, G. A., *J. Chem. Phys.* **1999,** 111, 9361-9381.

Schnell, I.; Spiess, H. W., *J. Magn. Reson.* **2001,** 151, 153.

Schuster, M. F. H.; Meyer, W. H., *Annu. Rev. Mater. Res.* **2003,** 33, 233-261.

Schuster, M. F. H.; Meyer, W. H.; Schuster, M.; Kreuer, K. D., *Chem. Mater.* **2004,** 16, 329-337.

Schuster, M.; Meyer, W. H.; Wegner, G.; Herz, H. G.; Ise, M.; Schuster, M.; Kreuer, K. D.; Maier, J., *Solid State Ionics* **2001,** 145, 85-92.

Shah, J.; Khan, S. S.; Blumenthal, H.; Liebscher, J., *Synthesis* **2009**, 3975-3982.

Sheats, J. E., *J. Organomet. Chem. Libr.* **1979,** 7, 461-521.

Sheats, J. E.; Hlatky, G., *J. Chem. Edu.* **1983,** 60, 1015.

Sheats, J. E.; Kirsch, T., *Syn. Inorg. Metal-Org. Chem.* **1973,** 3, 59.

Sheats, J. E.; Miller, W.; Kirsch, T., *J. Organomet. Chem.* **1975,** 91, 97-104.

Sheats, J. E.; Rausch, M. D., *J. Org. Chem.* **1970,** 35, 3245-3249.

Shen, P. K.; Xu, C.; Meng, H.; Zeng, R., *Adv. Fuel Cells* **2005**, 149-179.

Shuang, G.; Rui, C.; Ting, L.; Zhongwei, C.; Minwei, S.; Yan, L.; Gaohong, H.; Yushan, Y., *Angew. Chem. Int. Ed.* **2009,** 48, 6499-6502.

Shukla, A. K.; Kumar, T. P., *Curr. Sci. India* **2008,** 94, 314-331.

Sirisopanaporn, C.; Fernicola, A.; Scrosati, B., *J. Power Sources* **2009,** 186, 490-495.

Slade, R. C. T.; Varcoe, J. R., *Solid State Ionics* **2005,** 176, 585-597.

Sleightholme, A. E. S.; Varcoe, J. R.; Kucernak, A. R., *Electrochem. Commun.* **2008,** 10, 151-155.

Smitha, B.; Sridhar, S.; Khan, A. A., *J. Membr. Sci.* **2005,** 259, 10-26.

Solasi, R.; Zou, Y.; Huang, X.; Reifsnider, K.; Condit, D., *J. Power Sources* **2007,** 167, 366-377.

Song, J. Y.; Wang, Y. Y.; Wan, C. C., *J. Power Sources* **1999,** 77, 183-197.

Stefan, M. C.; Javier, A. E.; Osaka, I.; McCullough, R. D., *Macromolecules* **2008,** 42, 30-32.

Stokes, K. K.; Orlicki, J. A.; Beyer, F. L., *Polym. Chem.* **2011,** 2, 80-82.

Strehmel, V.; Reynaud, E.; Wetzel, H.; Görnitz, E.; Laschewsky, A., *Macromol. Symp.* **2009,** 275-276, 242-249.

Subbaraman, R.; Ghassemi, H.; Zawodzinski Jr, T., *Solid State Ionics* **2009,** 180, 1143-1150.

Subbaraman, R.; Ghassemi, H.; Zawodzinski, T. A. J., *J. Am. Chem. Soc.* **2007,** 129, 2238-2239.

Sun, J.; Forsyth, M.; MacFarlane, D. R., *J. Phys. Chem. B* **1998,** 102, 8858-8864.

Sun, J.; Jordan, L. R.; Forsyth, M.; MacFarlane, D. R., *Electrochim. Acta* **2001,** 46, 1703-1708.

Swanson, J. M. J.; Maupin, C. M.; Chen, H.; Petersen, M. K.; Xu, J.; Wu, Y.; Voth, G. A., *J. Phys. Chem. B* **2007,** 111, 4300-4314.

Takada, K.; Díaz, D. J.; Abruña, H. D.; Cuadrado, I.; González, B.; Casado, C. M.; Alonso, B.; Morán, M.; Losada, J., *Chem. Eur. J.* **2001,** 7, 1109-1117.

Takeoka, S.; Ohno, H.; Tsuchida, E., *Polym. Advan. Technol.* **1993,** 4, 53-73.

Takizawa, K.; Nulwala, H.; Thibault, R. J.; Lowenhielm, P.; Yoshinaga, K.; Wooley, K. L.; Hawker, C. J., *J. Polym. Sci.,Part A: Polym. Chem.* **2008,** 46, 2897-2912.

Tanaka, M.; Koike, M.; Miyatake, K.; Watanabe, M., *Macromolecules* **2010,** 43, 2657-2659.

Tarascon, J. M.; Armand, M., *Nature* **2001,** 414, 359-367.

Tezuka, T.; Tadanaga, K.; Hayashi, A.; Tatsumisago, M., *J. Am. Chem. Soc.* **2006,** 128, 16470-16471.

Tezuka, T.; Tadanaga, K.; Hayashi, A.; Tatsumisago, M., *Solid State Ionics* **2008,** 179, 1151-1154.

Thibault, R. J.; Takizawa, K.; Lowenheilm, P.; Helms, B.; Mynar, J. L.; Frechet, J.; Hawker, C. J., *J. Am. Chem. Soc.* **2006,** 128, 12084-12085.

Tokuda, H.; Hayamizu, K.; Ishii, K.; Susan, M.; Watanabe, M., *J. Phys. Chem. B* **2005,** 109, 6103-6110.

Toppet, S.; Wouters, G.; Smets, G., *J. Polym. Sci. Pol. Lett.* **1976,** 14, 389-394.

Tuckerman, M. E.; Laasonen, K.; Sprik, M.; Parrinello, M., *J. Chem. Phys.* **1995,** 103, 150-161.

Ümit, A.; Robert, G.; Peng, Y. G.; Chu, P. P.; Spiess, H. W., *J. Polym. Sci., Polym. Phys.* **2009,** 47, 138-155.

University of Cambridge, Teaching and Learning Packages - Fuel Cells.

http://www.doitpoms.ac.uk/tlplib/fuel-cells/types.php (accessed March 14, 2011).

Ünügür-Celik, S.; Akbey, Ü.; Bozkurt, A.; Graf, R.; Spiess, H. W., *Macromol. Chem. Phys.* **2008,** 209, 593-603.

VanLandingham, M. R.; Villarrubia, J. S.; Guthrie, W. F.; Meyers, G. F., *Macromol. Symp.* **2001,** 167, 15-43.

Varcoe, J. R.; Slade, R. C. T., *Fuel Cells* **2005,** 5, 187-200.

Vila, J.; Varela, L. M.; Cabeza, O., *Electrochim. Acta* **2007,** 52, 7413-7417.

Voth, G. A., *Acc. Chem. Res.* **2006,** 39, 143-150.

Wainright, J. S.; Wang, J. T.; Weng, D.; Savinell, R. F.; Litt, M., *J. Electrochem. Soc.* **1995,** 142, L121-L123.

Wakihara, M., *Mater. Sci. Eng.* **2001,** R33, 109-134.

Wang, J. H.; Li, S. H.; Zhang, S. B., *Macromolecules* **2010,** 43, 3890-3896.

Wang, W.; Liang, H.; Favis, B. D.; Schreiber, H. P., *J. Appl. Polym. Sci.* **2001,** 81, 1891-1901.

Wang, Y.; Nakamura, S.; Tasaki, K.; Balbuena, P. B., *J. Am. Chem. Soc.* **2002,** 124, 4408-4421.

Wasserscheid, P.; Welton, T., *Ionic Liquids in Synthesis.* Wiley-VCH: Weinheim, **2002**; pp 41-118.

Wei, X.; Shriver, D. F., *Chem. Mater.* **1998,** 10, 2307-2308.

Wilderbeek, H. T. A.; van der Meer, M. G. M.; Bastiaansen, C. W. M.; Broer, D. J., *J. Phys. Chem. B* **2002,** 106, 12874-12883.

Wilkinson, G., *J. Am. Chem. Soc.* **1952,** 74, 6148-6149.

Wilkinson, G.; Cotton, F. A., *Prog. Inorg. Chem.* Interscience Publishers, Inc: New York, **1959**; Vol. 1.

Winter, M.; Brodd, R. J., *Chem. Rev.* **2004,** 104, 4245-4269.

Woudenberg, R. C., Jr. Anhydrous proton conducting materials for use in high temperature polymer electrolyte membrane fuel cells. PhD Thesis, University of Massachusetts, Amherst, **2007**

Woudenberg, R. C.; Yavuzcetin, O.; Tuominen, M. T.; Coughlin, E. B., *Solid State Ionics* **2007,** 178, 1135-1141.

Wouters, G.; Smets, G., *Makromol. Chem.* **1982,** 183, 1861-1868.

Wright, J. D.; Sommerdijk, N. A. J. M., *Sol-Gel Materials: Chemistry and Applications*. CRC Press: London, **2001**; pp 15.

Wu, Y.; Chen, H.; Wang, F.; Paesani, F.; Voth, G. A., *J. Phys. Chem. B* **2008,** 112, 467-482.

Xiao, L.; Zhang, H.; Jana, T.; Scanlon, E.; Chen, R.; Choe, E.-W.; Ramanathan, L. S.; Yu, S.; Benicewicz, B. C., *Fuel Cells* **2005,** 5, 287-295.

Xiao, L.; Zhang, H.; Scanlon, E.; Ramanathan, L. S.; Choe, E.-W.; Rogers, D.; Apple, T.; Benicewicz, B. C., *Chem. Mater.* **2005,** 17, 5328-5333.

Yamaguchi, D.; Hasegawa, H.; Hashimoto, T., *Macromolecules* **2001,** 34, 6506-6518.

Yan, J.; Hickner, M. A., *Macromolecules* **2010,** 43, 2349-2356.

Yang, Z.; Han, C. D., *Polymer* **2008,** 49, 5128-5136.

Yu, J.; Yi, B.; Xing, D.; Liu, F.; Shao, Z.; Fu, Y.; Zhang, H., *Phys. Chem. Chem. Phys.* **2003,** 5, 611.

Zech, O.; Stoppa, A.; Buchner, R.; Kunz, W., *J. Chem. Eng. Data* **2010,** 55, 1774-1778.

Zhang, Q.; Liu, S.; Li, Z.; Li, J.; Chen, Z.; Wang, R.; Lu, L.; Deng, Y., *Chem. Eur. J.* **2009,** 15, 765-778.

Zhang, S. J.; Sun, N.; He, X. Z.; Lu, X. M.; Zhang, X. P., *J. Phys. Chem. Ref. Data* **2006,** 35, 1475-1517.

Zhang, S. S., *J. Power Sources* **2007,** 164, 351-364.

Zhao, F. Q.; Xue, L.; Xing, X. L.; Hu, R. Z.; Zhou, Z. M.; Gao, H. X.; Yi, J. H.; Xu, S. Y.; Pei, Q., *Sci. China Chem.* **2011,** 54, 461-474.

Zhou, Z.; Li, S.; Zhang, Y.; Liu, M.; Li, W., *J. Am. Chem. Soc.* **2005,** 127, 10824-10825.

Zhou, Z.; Liu, R.; Wang, J.; Li, S.; Liu, M.; Bredas, J.-L., *J. Phys. Chem. A* **2006,** 110, 2322-2324.

Zhou, Z.-B.; Matsumoto, H.; Tatsumi, K., *Chem. Eur. J.* **2004,** 10, 6581-6591.

Zhou, Z.-B.; Matsumoto, H.; Tatsumi, K., *Chem. Eur. J.* **2005,** 11, 752-766.

Zhou, Z.-B.; Matsumoto, H.; Tatsumi, K., *Chem. Eur. J.* **2006,** 12, 2196-2212.

Zhu, Z.; Einset, A. G.; Yang, C.-Y.; Chen, W.-X.; Wnek, G. E., *Macromolecules* **1994,** 27, 4076-4079